Faculty of Aerospace Engineering

Design, Identification and Implementation of a High-Fidelity Cessna Citation II Flight Simulation Model

M.A. van den Hoek

August 9, 2016

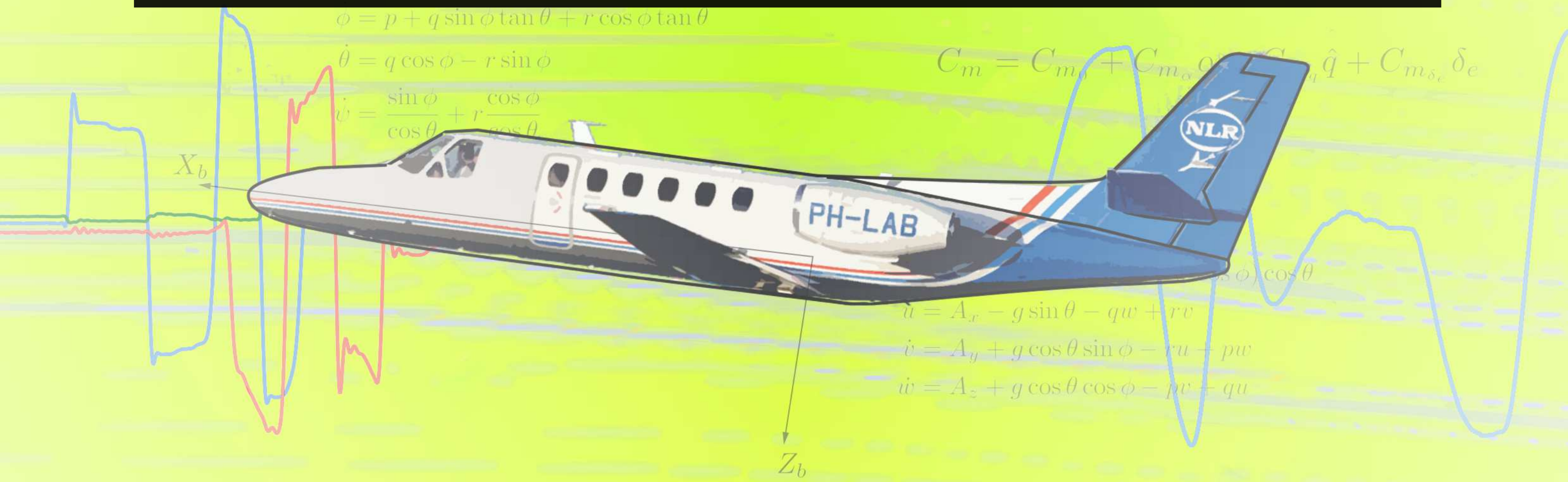

Design, Identification and Implementation of a High-Fidelity Cessna Citation II Flight Simulation Model

Master of Science Thesis

For obtaining the degree of Master of Science in Aerospace Engineering
at Delft University of Technology

M.A. van den Hoek

August 9, 2016

Faculty of Aerospace Engineering · Delft University of Technology

Delft University of Technology

Delft University Of Technology
Department Of
Control and Simulation

The undersigned hereby certify that they have read and recommend to the Faculty of Aerospace Engineering for acceptance a thesis entitled **"Design, Identification and Implementation of a High-Fidelity Cessna Citation II Flight Simulation Model"** by **M.A. van den Hoek** in partial fulfillment of the requirements for the degree of **Master of Science**.

Dated: August 9, 2016

Readers:

Prof.dr.ir. M. Mulder

Dr.ir. C. C. de Visser

Dr.ir. D. M. Pool

Dr.ir. M. M. van Paassen

Dr.ir. H. G. Visser

Summary

As a result of new aviation legislation, from 2019 on all air-carrier pilots are obliged to go through flight simulator-based stall recovery training (Federal Aviation Administration, 2013). This implies that all aircraft dynamics models driving flight simulators must be updated to include accurate pre-stall, stall, and post-stall dynamics. For this reason, the Control and Simulation (C&S) division at the Faculty of Aerospace Engineering, Delft University of Technology, has set up a task force to develop a new methodology for high-fidelity aircraft stall behavior modeling and simulation. This research effort is twofold. First, the current simulation framework is to be upgraded together with the implementation of a newly developed aerodynamic model identified from flight test data obtained from TU Delft's Cessna Citation II laboratory aircraft. In addition, the upgraded simulation framework will be tested and run on the SIMONA research simulator, a 6 degree-of-freedom flight simulator. As second part of this effort, a parallel MSc research effort will focus on the identification of an aerodynamic stall model for the Citation II based on flight test data will be integrated into the upgraded simulation framework(Van Horssen, 2016).

At this moment, the C&S division uses a simulation framework known as the Delft University Aircraft Simulation Model and Analysis Tool (DASMAT) (Van Der Linden, 1998) as its baseline model. This simulation framework was designed as standard Flight CAD package for control and design purposes. The aerodynamic model integrated into the DASMAT simulation framework is the result of an extensive flight test program(Mulder et al., 1987) and is based on the Cessna Citation I. The DASMAT simulation framework, together with the Cessna Citation I aerodynamic model, is known for a number of deficiencies. Most significantly, the aerodynamic model does not match to the dynamics of the current laboratory aircraft, i.e. the Cessna Citation II.

The main aim of this MSc research project is the identification, validation and integration of a new high-fidelity aerodynamic model for the normal, pre-stall flight regime using flight test data from the Cessna Citation II laboratory aircraft. In addition, as part of this thesis work, this newly developed aerodynamic model is integrated into the upgraded simulation framework, such that it will act as the new baseline model with a more accurate representation of the Cessna Citation II's dynamics. This framework also provides an interface for the stall and post-stall models, resulting from a parallel MSc research project. Altogether, the upgraded high-fidelity modular aircraft simulation framework will be used in future research into (1) the investigation of pilot behavior during aerodynamic stall, and (2) the design of advanced control algorithms.

This report is structure as follows. In Part I the final paper is presented. In this paper, the results regarding the identification of a new high-fidelity aerodynamic model are presented. This includes an overview of the determined model structure, the estimated model parameters and a validation and comparison of the DASMAT simulation model and the new aerodynamic model. In Part II the preliminary thesis is presented containing an explanation of the theoretical constructs and some initial off-line simulations together with a comparison of different Kalman filter types. The appendices of the preliminary thesis can be found in Part III. Lastly, paper appendices are included in Part IV.

Acronyms

AFM	Aerodynamic Forces and Moments
AHRS	Attitude and Heading Reference System
BLUE	Best Linear Unbiased Estimator
C&S	Control & Simulation
CG	Center of Gravity
DASMAT	Delft University Aircraft Simulation Model And Analysis Tool
DUT	Delft University of Technology
ECEF	Earth-Centered Earth-Fixed reference frame
EFM	Engine Forces and Moments
EKF	Extended Kalman Filter
EQM	Equations of Motion
FBKS	Forward-backward Kalman Smoother
GLS	Generalized Least Squares
IEKF	Iterated Extended Kalman Filter
IMU	Inertial Measurement Unit
KF	Kalman Filter
MRIEKF	Multi-Rate Iterated Extended Kalman Filter
MSE	Mean Squared Error
NED	North-East-Down reference frame
OLS	Ordinary Least Squares
PCR	Principal Components Regression
PSE	Predicted Square Error
RMS	Root Mean Square
RTS	Rauch-Tung-Striebel
RTSS	Rauch-Tung-Striebel Smoother
SDE	Stochastic Differential Equation
SRS	SIMONA Research Simulator

SRUKF	Square-Root Unscented Kalman Filter
TSM	Two-Step Method
UKF	Unscented Kalman Filter
URTS	Extended Rauch-Tung-Striebel Smoother
URTS	Unscented Rauch-Tung-Striebel Smoother

List of Symbols

Greek Symbols

α	Angle of attack
β	Angle of sideslip
δ_f	Flap deflection
δ_t	Trim tab deflection
$\boldsymbol{\Gamma}$	Discretized stochastic input distribution matrix
λ	Measurement signal bias
Ω_t	Rotational velocity of the central body
$\boldsymbol{\Phi}$	Discretized state transition matrix
ϕ	Roll angle
ψ	Yaw angle
ρ	Density
σ	Standard deviation
$\sigma^2\left\{\cdot\right\}$	Variance of stochastic variable
$\varepsilon,\ \boldsymbol{\varepsilon}$	Scalar or vector-valued model residuals
$\theta,\ \boldsymbol{\theta}$	Scalar or vector-valued set of model parameters
θ	Pitch angle

Roman Symbols

A_x	Acceleration in the x-body axis
A_y	Acceleration in the y-body axis
A_z	Acceleration in the z-body axis

$\bar{c}$	Mean aerodynamic chord
C_l	Non-dimensional moment around the x-body axis
C_L	Lift Coefficient
C_m	Non-dimensional moment around the y-body axis
C_n	Non-dimensional moment around the z-body axis
$\mathbf{Cov}\{\cdot\}$	Covariance operator
C_X	Non-dimensional force in the x-body axis
C_Y	Non-dimensional force in the y-body axis
C_Z	Non-dimensional force in the z-body axis
$\mathbb{E}\{\cdot\}$	Expectation operator
$\mathbf{f}[\cdot]$	Vector-valued state transition function
F_I	Inertial frame
F_b	Aircraft body frame
F_C	Earth-Centered Earth-Fixed frame
F_E	Navigation frame, North-East-Down frame
$\mathbf{F}_{ext}$	External force vector
g	Gravitational acceleration (= 9.80665 m/s^2)
$\mathbf{h}[\cdot]$	Vector-valued measurement equation
$\mathbb{L}(x\|y)$	Value of the likelihood function for x given y
$\mathbf{P}$	Covariance matrix
p	Rotational rate around the x-body axis
$\mathbf{P_0}$	Initial estimation of the covariance matrix
$\mathbf{Q}$	Process noise covariance matrix
q	Rotational rate around the y-body axis
$\mathbf{R}$	Measurement noise covariance matrix
r	Rotational rate around the z-body axis
$\hat{\mathcal{R}}_{xy}$	Estimated correlation of stochastic variable x w.r.t. stochastic variable y
$s\{\cdot\}$	Standard deviation of the stochastic variable
$\mathbb{T}_{Eb}$	Transformation matrix relating a vector in the body axes to the NED frame
u	Longitudinal body velocity
$v_{(\cdot)}$	Measurement noise of the subscripted variable
$V_{\mathbf{TAS}}$	True airspeed
v	Lateral body velocity

$w_{(\cdot)}$	Process noise of the subscripted variable
w	Normal body velocity
W_{x_E}	Wind velocity in the direction of the x-axis in the ECEF frame
W_{y_E}	Wind velocity in the direction of the y-axis in the ECEF frame
W_{z_E}	Wind velocity in the direction of the z-axis in the ECEF frame
$\mathcal{X}$	Set of sigma points
$\mathbf{x}$	State vector
x_E	x-position in the ECEF frame
$\mathbf{X}$	Regression matrix
y_E	y-position in the ECEF frame
z_E	z-position in the ECEF frame
$\dot{(\cdot)}$	Time derivative
$(\cdot)_{\mathbf{gps}}$	Scalar or vector-valued variable expressed in the navigation frame
$\hat{(\cdot)}$	Non-dimensional rotational acceleration
$(\cdot)_s$	Size-varying vector or matrix valued quantity

Contents

Part I

Paper

Identification and Implementation of a High-Fidelity Cessna Citation II Simulation Model Based on Flight Test Data

M.A. van den Hoek* , D.M. Pool† , C.C. de Visser†
and M. Mulder‡

Delft University of Technology, P.O. Box 5058, 2600GB Delft, The Netherlands

As a result of new aviation legislation, from 2019 on all air-carrier pilots are obliged to go through flight simulator-based stall recovery training. For this reason the Control and Simulation division at Delft University of Technology has set up a task force to develop a new methodology for high-fidelity aircraft stall behavior modeling and simulation. As part of this research endeavor, the development of a new high-fidelity Cessna Citation II simulation model, valid throughout the normal, pre-stall flight envelope, is presented in this paper. The new simulation model will replace the current baseline model, which is based on the Cessna Citation I, for an increased fidelity and representation of the dynamics of the current laboratory aircraft, the Cessna Citation II. Aerodynamic model identification was done by employing the Two-Step Method. New in this approach is the use of the Unscented Kalman Filter for an improved accuracy and robustness of the state estimates. For the first time, an explicit model structure is presented for the Citation II. Model structure selection by an orthogonal regression scheme has indicated that most of the six non-dimensional forces and moments can be parametrized sufficiently by a linear model structure. It was shown that only the C_Y and C_X models would benefit from the addition of higher order terms relating to the aerodynamic angles. On balance, the models for the non-dimensional forces were improved marginally in comparison to the existing simulation model. Major improvements were made to the moment models, with an increase of the explained variance of at least 35%.

Nomenclature

$a_x,\ a_y,\ a_z$	Linear accelerations, m/s^2
b	Wing span, m
$\bar{c}$	Mean aerodynamic chord, m
$\mathbb{E}\{\cdot\}$	Expectation operator
$\mathbf{f}[\cdot]$	Vector-valued non-linear state transition function
$\mathbf{h}[\cdot]$	Vector-valued non-linear observation function
h	Altitude, m
$I_{xx},\ I_{yy},\ I_{zz}$	Moments of inertia around body axes, kg m^2
I_{xz}	Cross-moment of inertia between X_b- and Z_b-axis, kg m^2
$\boldsymbol{\mathcal{K}}$	Kalman gain matrix
M	Mach number
m	Aircraft mass, kg
$p,\ q,\ r$	Rotational rates around the body axes, rad/s
$\dot{p},\ \dot{q},\ \dot{r}$	Rotational accelerations around the body axes, rad/s
$\hat{p},\ \hat{q},\ \hat{r}$	Dimensionless rotational rates around the body axes, rad/s

*M.Sc. student, Department of Control and Simulation, Faculty of Aerospace Engineering.
†Assistant Professor, Department of Control and Simulation, Faculty of Aerospace Engineering.
‡Full professor, Department of Control and Simulation, Faculty of Aerospace Engineering.

$\mathbf{Q}$	Process noise variance-covariance matrix
$\mathbf{R}$	Measurement noise variance-covariance matrix
S	Wing surface area, m^2
$u,\ v,\ w$	Velocity components in the body-fixed reference frame, m/s
V_{TAS}	True airspeed, m/s
$x,\ y,\ z$	Position in the Earth-Centered Earth-Fixed reference frame, m

Subscripts

E	Variable expressed in the ECEF frame
m	Measured value

Symbols

α	Angle of attack, rad
β	Angle of sideslip, rad
$\delta_e, \delta_a, \delta_r$	Elevator, aileron and rudder deflections, rad
δ_f	flap deflection, rad
$\hat{\sigma}\left(\cdot\right)$	Estimated variance
λ	Signal bias
ϕ, θ, ψ	Euler angles, rad

I. Introduction

As a result of new aviation legislation, from 2019 on all air-carrier pilots are obliged to go through flight simulator-based stall recovery training.[1] This implies that all aircraft dynamics models driving flight simulators must be updated to include accurate pre-stall, stall, and post-stall dynamics. For this reason, the Control and Simulation (C&S) division at Delft University of Technology has set up a task force to develop a new methodology for high-fidelity aircraft stall behavior modeling and simulation. This research effort is twofold. First, the current simulation framework is to be updated together with the implementation of a newly developed aerodynamic model identified from flight test data obtained from TU Delft's Cessna Citation II laboratory aircraft. In addition, the upgraded simulation framework will be tested and run on the SIMONA research simulator, a 6 degree-of-freedom flight simulator.[2] As second part of this research effort, an aerodynamic stall model for the Citation II based on flight test data will be developed and integrated into the upgraded simulation framework.[3] Note that only the first part is presented in this paper.

At this moment, the C&S division uses a simulation model of the Cessna Citation I, known as the Delft University Aircraft Simulation Model and Analysis Tool (DASMAT)[4] as its baseline model. This simulation model was designed as standard Flight CAD package for control and design purposes within the C&S division of the Faculty of Aerospace Engineering, Delft University of Technology. DASMAT is known for a number of deficiencies; most significantly is its unsatisfactory match with the current laboratory aircrafts flight dynamics. The Citation I model is the result of a flight test program executed for the development of mathematical models describing the aerodynamic forces and moments, engine performance characteristics, flight control systems and landing gear.[5] Earlier attempts at modeling the longitudinal forces and the pitching moment were made by Oliveira et al.[6] However, parameter estimates were only obtained for a limited range of flight conditions with a very limited set of measurements. In addition, in the same paper the authors state that dependency of the aerodynamic model from higher order terms, such as α^2 and terms relating to the time rate of change of the aerodynamic angles, such as $\dot{\alpha}$, are yet to be investigated.[6]

The estimation of stability and control derivatives from flight test data can be formulated in the framework of maximum likelihood estimation.[7] In the context of this paper, aerodynamic model identification will be done by employing the Two-Step Method (TSM).[8,9] This method effectively decomposes the non-linear model identification problem into a non-linear flight path reconstruction problem and linear parameter estimation problem, allowing the use of linear parameter estimation techniques for a significant simplification of the latter procedure. This decomposition can be made under certain conditions concerning accuracy and type of the in-flight measurements.[9] New to the TSM approach is the use of the Unscented Kalman Filter[10] (UKF) for an improved accuracy and robustness of the state estimates in the first step. The latter can be seen as an elaboration to the work of Oliveira et al.,[6] who stated that further improvements in the quality of the parameter estimates obtained from the Two-Step Method can be achieved by improving the accuracy of the state estimation procedure. Methods for even further improving the state estimate obtained from a KF approach exist in the form of Kalman smoothers.[11,12] However, these methods were not employed in the context of this research.

In this paper, the methodology regarding the identification of the aerodynamic model of the Cessna Citation II is presented. This identification procedure is twofold. First, in Section III, the methods used for flight path reconstruction are presented. Subsequently, in Section IV, the general methodology for model structure selection and parameter estimation are outlined. For the first time, an explicit model structure is presented for the Cessna Citation II together with the estimated parameters of the six non-dimensional models. The results for the flight path reconstruction, model structure selection and parameter estimation are given in Section V. The same section also features a model validation by applying the identified models to validation data and a time-domain comparison between the measured data, the identified model and DASMAT. In addition, a comparison between parameter estimates obtained from Koehler (3-2-1-1) and Hardover maneuvers is presented. As a general introduction to the experimental vehicle, the Cessna Citation II and the experimental procedures are first described in Section II.

II. Research Vehicle and Flight Data

In this paper, aerodynamic model identification was applied to the Cessna Citation II laboratory aircraft, model 550, which is co-owned by Delft University of Technology (DUT) and the Netherlands Aerospace Center (NLR). The Citation II is a twin-jet business aircraft, with two Pratt & Whitney JT15D-4 turbofan engines. Both engines deliver a maximum thrust of 11.1 kN each. The maximum operating speed is limited at 198.6 m/s, with a maximum operating altitude of approximately 13 km.[13]

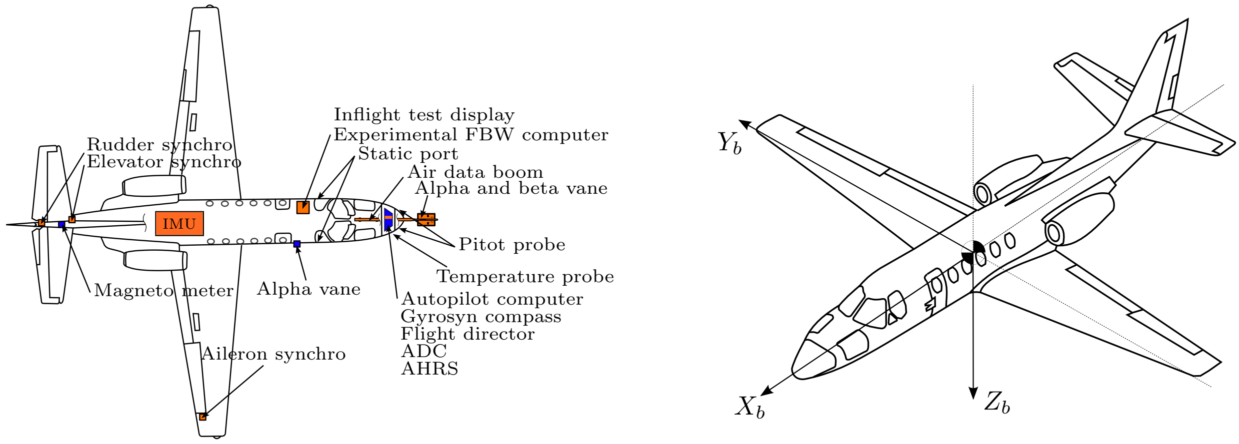

(a) Overview of the aircraft instrumentation systems

(b) Definition of the aircraft body-fixed reference frame or coordinate system $\mathbb{F}_b$

Figure 1. Aircraft instrumentation systems and reference frame

A. Dimensions and mass properties

The Cessna Citation II has a total length of 14.4 m and the outer fuselage diameter is 1.63 m. The sweepback of the main wings at 25% chord is 1.4 degrees, and it has a 4.0 degrees dihedral. The aircraft basic empty weight (BEW) mass and elements of the inertia tensor are summarized in Table 1. Furthermore, the distance between the angle of attack vane and the aircraft nose is approximately 4 meters. The Attitude and Heading Reference System (AHRS) is located beneath the floor of the nose baggage compartment, in front of the forward pressure bulkhead. The distance between the AHRS system, and the nose is approximately 1.9 m. Furthermore, for most of the flights the aircraft was equipped with a highly accurate Inertial Measurement Unit (IMU).

Table 1. Dimensions and mass properties of the aircraft

Dimensions	
b	15.90 m
$\bar{c}$	2.06 m
S	30.00 m^2
Mass properties	
m	4,157 kg
I_{xx}	12,392 kg m^2
I_{yy}	31,501 kg m^2
I_{zz}	41,908 kg m^2
I_{xz}	2,252 kg m^2

All values correspond to the basic empty weight.

B. Instrumentation

The Flight Test Instrumentation System (FTIS) of the Cessna Citation II laboratory aircraft combines the sensor measurements from a variety of instrumentation systems. Recently, this aircraft has been equipped with a new FTIS system replacing the old one. Over the years, flight data from different experiments was collected in a database. The contribution of this work comes in the form of a small set of dynamic maneuvers, in addition to the existing collection, for the identification of a new aerodynamic model. For this reason, the work presented in this paper combines the flight test data originating from the two different FTIS systems. An overview of the instrumentation systems is highlighted in Figure 1(a) and summarized as follows:

- Most of the data that was obtained from previous experimental flights contains a highly accurate measurement of both the linear accelerations ($a_x,\ a_y,\ a_z$) and rotational rates ($p,\ q,\ r$) obtained from the Inertial Measurement Unit (IMU) at a rate of 100 Hz. However, since the upgrade of the FTIS system one has to resort to the AHRS for the previously mentioned measurements. The AHRS system, located below the nose baggage compartment, combines the linear accelerometer measurements and rotational rates around the body-axes to obtain accurate attitude information, represented by the set of Euler angles ($\phi,\ \theta$). In addition, the true heading, denoted by ψ, was processed and obtained from the Flight Management System (FMS). By default, the linear accelerations in y_b and z_b were not corrected for the gravity component. This correction can easily be applied by addition of the gravity component expressed in $\mathbb{F}_b$, i.e. $\mathbb{T}_{bE}\ \mathbf{g}$. The AHRS also suffers from its displacement with respect to the center of gravity for which a correction is required. AHRS measurements were obtained at a variable sampling rate, averaged at 50 Hz.
- Altitude information h, the climb rate $\dot{h}$ and true airspeed V_{TAS} were obtained from the Digital Air Data Computer (DADC) at a sampling frequency of 16.67 Hz.
- Position estimates ($x_E,\ y_E,\ z_E$) together with the estimates of the time rate of change($\dot{x}_E,\ \dot{y}_E,\ \dot{z}_E$) were provided by a Differential Global Positioning System (DGPS). The position vector originating from this series of measurements, expressed in longitude, latitude and altitude, was transformed to a vector expressed in the ECEF frame under the assumption of a locally flat and non-rotating earth. The DGPS system provides data at a rate of 1 Hz.
- Most of the measurements were obtained by making use of an air data boom, combining a set of two synchros for an accurate and undisturbed measurement of the aerodynamic angles, i.e. the angle of attack α and the sideslip angle β. In the absence of such a measurement device, use can be made of the angle of attack vane located on the fuselage in front of the main wing. Its measurement should be used with caution since it suffers from an upwash in the flow directly ahead of the leading edge of the wing. Both devices sample at a frequency of 1000 Hz.
- Control surface deflections ($\delta_e,\ \delta_a,\ \delta_r$) were obtained from a set of synchros sampled at a rate of 100 Hz.

C. Experimental Flight Data

In this paper, the identification of the aerodynamic model was done by combining the data from different series of flight test measurements obtained over a time span of several years (2006-2016). Only a selection of the total data collection was specifically obtained for the purpose of system identification. Some of these measurements originate from flight tests to investigate the worst case scenarios for autopilot failures. During the latter tests, a maximum control surface deflection was commanded resulting in a so-called hardover maneuver[14,15] (see Figure 4). These maneuvers have been proven to be of a specific interest because of their ability to provide sufficient excitation of the aircraft's dynamics.[16] For this reason it was decided to investigate their applicability in the framework of system identification. In addition, a large part of the total data collection originates from demonstration flight tests for Aerospace Engineering students. Typically, these sets contain time traces of the longitudinal and lateral dynamic eigenmodes of the aircraft.

The study into optimal inputs for aerodynamic model identification is a whole field of research standing on its own.[17,18] In the context of this research, it was chosen to employ a set of longitudinally and laterally induced 3-2-1-1 maneuvers, also known as Koehler maneuvers, for a proper excitation of the Citation II's frequency band spanning the dynamic eigenmodes of the aircraft. This 3-2-1-1 input consists of 4 consecutive steps in alternating directions. In addition to a proper excitation of the aircraft's dynamics, the latter type of maneuver also allows for relatively straightforward application at different test points within a limited amount of time. An example of a longitudinally induces 3-2-1-1 dynamic maneuver is depicted in Figure 3.

A proper selection of the test points, i.e. the conditions under which the identification maneuvers will be performed, is essential to guarantee the widest possible coverage of the flight envelope. The design of dynamic input maneuvers is specifically aimed at excitation of the variables belonging to the symmetric or asymmetric state-planes under the assumption that both can be decoupled effectively. Because of the limited non-linearity in the (M, h) state-plane, only few test points are required along the whole span of the plane, removing the requirement to perform dynamic maneuvers at high altitude or velocity.[19]

As depicted in Figure 2, the current collection of test points for both longitudinally and laterally induced dynamic maneuvers covers the flight envelope over the complete range of velocities while limited observations at different altitude levels are available. At a total of 212 test points, more than 400 dynamic maneuvers were performed.

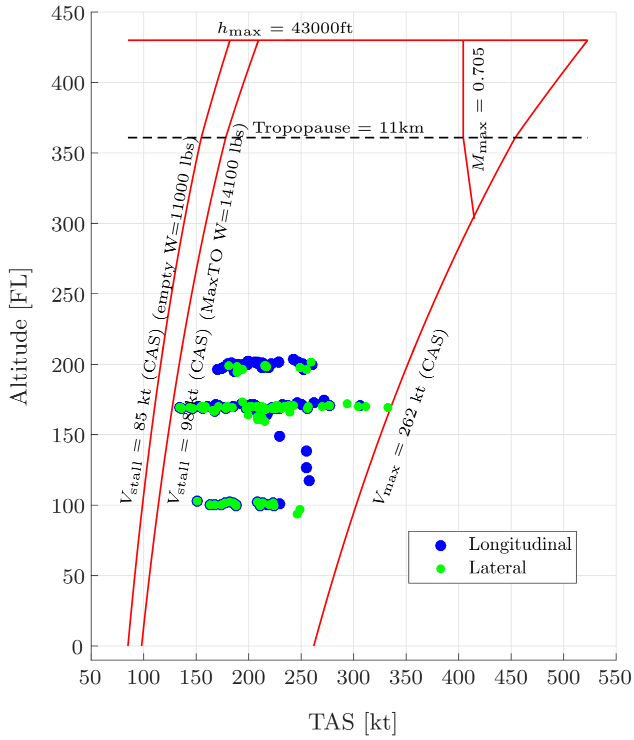

Figure 2. Overview of the location of the longitudinal and lateral test points inside the flight envelope.

III. Flight Path Reconstruction

In this section, the methodology for the flight path reconstruction procedure is presented. First, the data preparation and filtering preliminaries are presented followed by a theoretical overview and motivation for the use of the Unscented Kalman Filter.

A. Data Preparation

Prior to the Kalman filtering procedure, the collected flight data was pre-processed by applying a sequence of corrections and conversions. Because of the inherent difference in sampling rates, a unification through re-sampling is required before running the data through a Kalman filter (KF). Alternatively, multi-rate implementations of the KF are available.[20,21] However, application of this type of KF to simulated data have indicated equivalent performance of the single-rate implementation on re-sampled data in an off-line identification framework. For this reason, unification to a sampling rate of 100 Hz was performed.

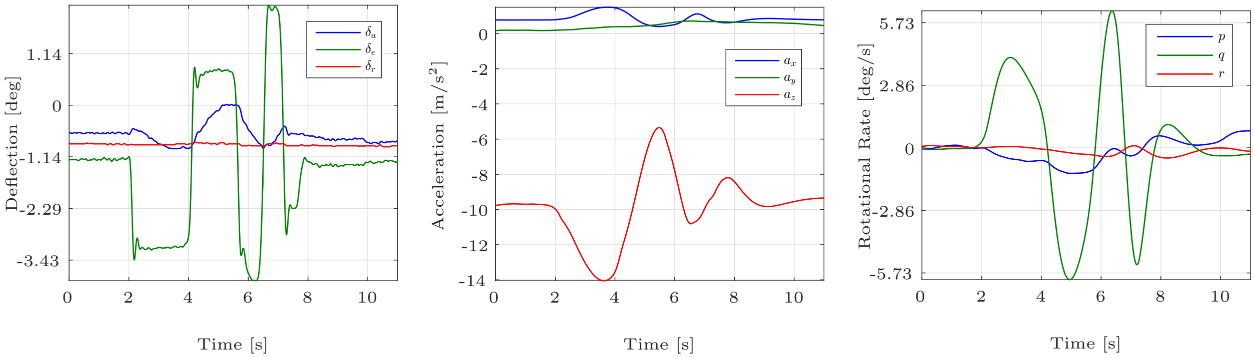

(a) Control surface deflections (b) Linear accelerations (c) Rotational rates

Figure 3. Typical control surface deflections, linear accelerations and rotational rates during a longitudinally induced 3-2-1-1 dynamic maneuver in δ_e

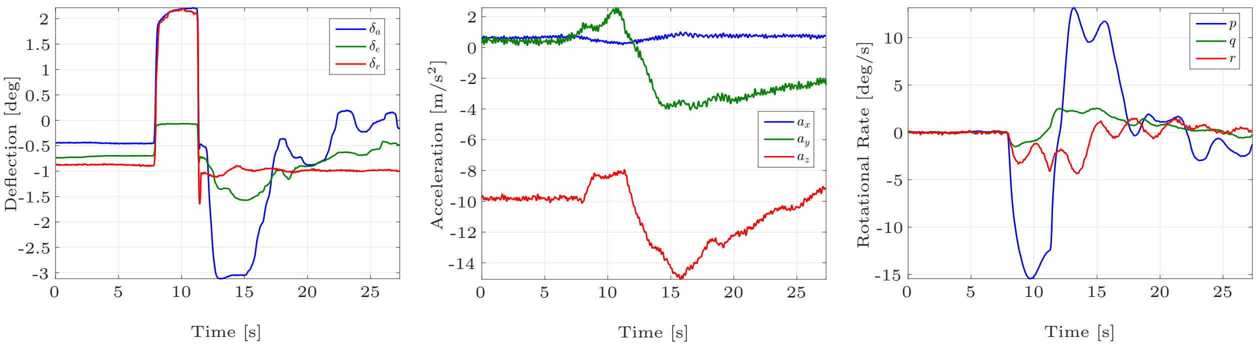

(a) Control surface deflections (b) Linear accelerations (c) Rotational rates

Figure 4. Typical control surface deflections, linear accelerations and rotational rates during a coupled hardover maneuver

Estimates of the elements of the inertia tensor (I_{xx}, I_{yy}, I_{zz} and I_{xz}) aircraft mass m (for basis empty weight values see Table 1) and fuel burn $\dot{m}$ at every time step k were provided by an aircraft mass model based on splines [19, Ch. 5.4.6]. This mass model takes into account the geometry of the fuel tank, remaining fuel weight and weights and moments caused by the passengers and baggage. In addition, GNSS coordinates were converted to their counterpart in the Earth-Centered-Earth-Fixed $\mathbb{F}_E$-frame.

As more extensively described in Section B, measurements were obtained from in-flight data collection equipment.[14–16] An a priori estimation of the sensor characteristics is tabulated in Table 2. In order to reduce noise levels on the measurements, the linear and rotational accelerations were filtered through a simple low-pass filter with a cutoff frequency of 6 Hz.

Table 2. Flight Test Instrumentation System sensor variables used in flight path reconstruction with their associated 1σ standard deviation and sampling rate F_s.

Parameter	Unit	1σ std	F_s [Hz] *	Source
Altitude	m	3.00×10^{-1}	16.67	Static probe
X_b-axis rotation	rad	8.70×10^{-3}	50	Sperry vertical gyro
Y_b-axis rotation	rad	8.70×10^{-3}	50	Sperry vertical gyro
Z_b-axis rotation	rad	1.73×10^{-2}	10	Gyrosyn compass
True airspeed	m/s	1.00×10^{-1}	16.67	Pitot-static probe
Angle of attack	rad	3.50×10^{-3}	1000	Alpha vane
Angle of sideslip	rad	3.50×10^{-3}	1000	Beta vane
X_b-axis linear acceleration	m/s^2	2.00×10^{-2}	100	Q-Flex 3100 accelerometer
Y_b-axis linear acceleration	m/s^2	2.00×10^{-2}	100	Q-Flex 3100 accelerometer
Z_b-axis linear acceleration	m/s^2	3.00×10^{-2}	100	Q-Flex 3100 accelerometer
X_b-axis rotational rate	rad/s	2.00×10^{-3}	100	LITEF μFORS rate gyro
Y_b-axis rotational rate	rad/s	2.00×10^{-3}	100	LITEF μFORS rate gyro
Z_b-axis rotational rate	rad/s	5.00×10^{-3}	100	LITEF μFORS rate gyro

* Sampling rate values correspond to the new FTIS. Data obtained from the old FTIS have different sampling rates.

B. Kalman Filtering Preliminaries

1. *State transition function and navigation equations*

The set of stochastic differential equations, in the context of aircraft dynamics, can in general be described by:

$$\begin{aligned} \dot{\mathbf{x}}(t) &= \mathbf{f}\left[\mathbf{x}(t), \mathbf{u}(t), t\right] + \mathbf{G}(\mathbf{x}(t), t)\mathbf{w}(t) \\ \mathbf{z}_n(t) &= \mathbf{h}\left[\mathbf{x}(t), \mathbf{u}(t), t\right] \\ \mathbf{z}(t) &= \mathbf{z}_n(t) + \mathbf{v}(t) \end{aligned} \tag{1}$$

where $\mathbf{f}[\cdot]$ is the non-linear state transition function and $\mathbf{h}[\cdot]$ the non-linear measurement function. The process noise and (output) measurement noise are assumed to be zero-mean, white and uncorrelated and can be parametrized by:

$$\mathbb{E}\left\{\mathbf{v}\mathbf{v}^{\intercal}\right\} = \mathbf{Q} \qquad \mathbb{E}\left\{\mathbf{w}\mathbf{w}^{\intercal}\right\} = \mathbf{R} \qquad \mathbb{E}\left\{\mathbf{w}\mathbf{v}^{\intercal}\right\} = 0 \tag{2}$$

where the diagonal elements of the process and measurement noise covariance matrices are composed of the squared standard deviation as given in Table 2. The full kinematic model is given by combining the differential equations for the flat earth position, body velocity components and the equations of rotational motion. The whole set of differential equations is then given by:

$$\dot{z}_E = -u\sin\theta + (v\sin\phi + w\cos\phi)\cos\theta \qquad \dot{\phi} = p + q\sin\phi\tan\theta + r\cos\phi\tan\theta$$
$$\dot{u} = a_x - g\sin\theta - qw + rv \qquad \dot{\theta} = q\cos\phi - r\sin\phi \tag{3}$$
$$\dot{v} = a_y + g\cos\theta\sin\phi - ru + pw \qquad \dot{\psi} = \frac{\sin\phi}{\cos\theta} + r\frac{\cos\phi}{\cos\theta}$$
$$\dot{w} = a_z + g\cos\theta\cos\phi - pv + qu$$

In this set of kinematic equations, the IMU measurements are used as system input. In order to model the noise characteristics and bias of the IMU signals, these were modeled as:

$$a_{x_m} = a_x + \lambda_{a_x} + w_x \qquad p_m = p + \lambda_p + w_p$$
$$a_{y_m} = a_y + \lambda_{a_y} + w_y \qquad q_m = q + \lambda_q + w_q \tag{4}$$
$$a_{z_m} = a_z + \lambda_{a_z} + w_z \qquad r_m = r + \lambda_r + w_r$$

where λ indicates the bias of the associated signal and w indicates the process noise of the subscripted variable.

In the context of this paper, some of the measurements regarding the linear accelerations were obtained from the AHRS located in the nose section of the aircraft, at an offset location from the center of gravity (see section B). Laban[22] derived a model for the transformation of the linear accelerations to obtain the true linear accelerations at the cg. The latter equation involves the derivatives of the rotational rates which, in turn, contain a small bias: e.g. $\dot{p}_m = \frac{d}{dt}(p - \lambda_p)$. By safely assuming a time-invariant bias term of the rotational rates in the calculation of the derivative term, a significant simplification can be made to the filter structure. The kinematic relations for the time derivative of the body velocities can now be replaced by:

$$\begin{aligned}
\dot{u} &= (a_x - \lambda_{a_x}) + (x_{cg} - x)\left\{(q-\lambda_q)^2 + (r-\lambda_r)^2\right\} - (y_{cg} - y)\left\{(p-\lambda_p)(q-\lambda_q) - \dot{r}_m\right\} - \\
&\quad (z_{cg} - z)\left\{(p-\lambda_p)(r-\lambda_r) + \dot{q}_m\right\} - g\sin\theta - (q-\lambda_q)\,w + rv \\
\dot{v} &= \left(a_y - \lambda_{a_y}\right) + (y_{cg} - y)\left\{(r-\lambda_r)^2 + (p-\lambda_p)^2\right\} - (z_{cg} - z)\left\{(q-\lambda_q)(r-\lambda_r) - \dot{p}_m\right\} \\
&\quad (x_{cg} - x)\left\{(q-\lambda_q)(p-\lambda_p) + \dot{r}_m\right\} + g\cos\theta\sin\phi - (r-\lambda_r)\,u + (p-\lambda_p)\,w \\
\dot{w} &= (a_z - \lambda_{a_z}) + (z_{cg} - z)\left\{(p-\lambda_p)^2 + (q-\lambda_q)^2\right\} - (x_{cg} - x)\left\{(r-\lambda_r)(p-\lambda_p) - \dot{r}_m\right\} \\
&\quad (y_{cg} - y)\left\{(r-\lambda_r)(q-\lambda_q) + \dot{p}_m\right\} + g\cos\theta\cos\phi - (p-\lambda_p)\,v + (q-\lambda_q)\,u
\end{aligned} \tag{5}$$

in which the time derivatives of the rotational rates can be obtained prior to filtering by a numerical differentiation scheme capable of accounting for mediocre noise levels.

In the context of this paper, angle of attack and angle of sideslip measurements were primarily obtained through the use of an intrusive nose boom (see Figure 1(a)). To this end, the set of observation equations was extended by including the equation for the angle of attack and angle of sideslip as measured by the boom[22] including the sensor biases.[19] This model contains an unknown fuselage-upwash coefficient $C_{\alpha_{\text{up}}}$ together with a kinematically induced angle of attack and angle of sideslip, under the assumption of a zero vertical wind component and alignment of the boom with the X_b-axis. The complete set of observation equations, or the navigation model, is given by:

$$h_m = h + v_h \qquad V_{\text{TAS}_m} = \sqrt{u^2 + v^2 + w^2} + v_{V_{\text{TAS}}}$$
$$\phi_m = \phi + v_\phi \qquad \alpha_v = (1 + C_{\alpha_{\text{up}}})\tan^{-1}\frac{w}{u} + \frac{(q-\lambda_q)x_{v_\alpha}}{\sqrt{u^2+v^2+w^2}} + v_\alpha \tag{6}$$
$$\theta_m = \theta + v_\theta \qquad \beta = \tan^{-1}\frac{v}{\sqrt{u^2+w^2}} - \frac{(r-\lambda_r)x_{v_\beta}}{\sqrt{u^2+v^2+w^2}} + v_\beta$$
$$\psi_m = \psi + v_\psi$$

where v is the standard notation for the measurement noise of the subscripted variable and x_v denotes the location of the boom along the X_b-axis for the alpha and beta vane.

For use in flight path reconstruction with a Kalman filter, the set of equations in Eq. (3) was extended with the time derivatives of additional states that require reconstruction, i.e. sensor biases. Commonly, the state transition function is simply assumed to be zero since the bias is constant in reality. For increased excitation of the sensor bias state, the state transition function for the linear accelerations and fuselage-upwash coefficient was modeled as zero-mean unit-variance random walk scaled by a factor k, as earlier applied in the work of Mulder et al.:[14]

$$\dot{\lambda} \sim k \cdot \mathcal{N}(0, 1) \tag{7}$$

The bias state transition function for the rotational rates was assumed to be zero for its usually very small bias. On balance, the state vector together with the augmented bias terms is given by:

$$\mathbf{x} = \begin{bmatrix} h & u & v & w & \phi & \theta & \psi & \lambda_{a_x} & \lambda_{a_y} & \lambda_{a_z} & \lambda_p & \lambda_q & \lambda_r & C_{\alpha_{\text{up}}} \end{bmatrix}^{\mathsf{T}} \tag{8}$$

2. State Reconstructability

In the definition of non-linear observability, a distinction is made between local non-linear observability and global non-linear observability. The first definition refers to the ability to observe a non-linear state from a local Taylor expansion.[23] Generalizing to non-linear systems, different methods to estimate the non-linear observability exist, however, Walcott, Corless & Zak recommended the Lie-algebraic method under the assumption that a priori knowledge about the dynamics of the system is precise.[24] By applying the arithmetic of the Lie dervative, an iterative procedure can be used to estimate the non-linear state observability. If the observability matrix $\mathbf{O}$ reaches full rank within the first $n-1$ Lie derivatives, non-linear observability is guaranteed. If full rank is achieved within the first iteration, the system can also be considered as locally observable. If additional iterations are required, local non-linear observability deteriorates. In this context, reconstructability is directly related to the ability to observe the state vector in a Kalman filter procedure. Rank deficiency in the observability matrix may directly result in the inability to reconstruct the state vector from the sequence of measurement data. The presented state vector in Eq. (8) was confirmed to obtain full rank within two iterations, confirming non-linear observability.

3. Additional non-linear air data observation equations

As stated before, the angle of attack in some of the measurement sequences was obtained from the alpha vane - located alongside the aircraft fuselage - in the absence of more accurate measurement devices such as the air data boom. To this end, Bennis developed an additional non-linear air data observation model compensating for the viscous damper-mechanisms of the alpha vane.[25] Augmentation of this model to the non-linear state transition function should improve the filter's innovation sequence and consistency

$$\frac{d\alpha_v}{dt} = \frac{1}{\tau}\left[\left\{\tan^{-1}\left(\frac{w - x_{\alpha_v}(q - \lambda_q)}{u}\right) + C_{\alpha_{\text{up}}} \tan^{-1}\left(\frac{w}{u}\right)\right\} - \alpha_v\right] \tag{9}$$

where τ indicates a time constant and α_v the angle of attack as measured by the vane alongside the aircraft fuselage.

C. Kalman Filtering Procedure

The application of the Kalman filter, which was originally designated for linear state-space,[26] to systems with non-linear dynamics can be enabled by linearization around state $\mathbf{x}$ for every time step k. Further improvement can be reached by employing a local iteration scheme, effectively reducing the difference between the reference trajectory and the estimate. However, for dynamic systems with moderate to severe non-linearities, the use of this class of filters may expose the shortcomings of the linearization technique. Elaborating on the latter statement, Julier & Uhlmann[10] argue that the two major drawbacks of the (Iterated) Extended Kalman Filter (IEKF) are related to this linearization:[27]

1. If the system demonstrates moderately to highly non-linear behavior within the time scale of the time step, $[t_k, t_{k+1}]$, the system cannot be assumed to show locally linear behavior.
2. The implementation of the Jacobian matrices is somewhat cumbersome and is error-prone as most formulation errors originate from a wrongly defined Jacobian matrix.

To effectively address these flaws, Julier & Uhlmann introduced an improved class of Kalman filters known as the Unscented Kalman Filter (UKF).[10] This class of filters is, instead of a linearization around a set point, based on the unscented transform for calculating the statistics of a random variable undergoing a non-linear transformation. In the same paper, the authors show that when using a state linearization approach, only the second order statistical measures can be approximated whilst in many practical situations higher order terms might be required to prevent the introduction of significant biases or errors. Additionally, Chowdhary & Jategaonkar conclude from their research effort that the augmented version of the UKF for parameter estimation is the fastest in terms of convergence at the cost of additional computational burden.[28]

The definition of the UKF begins with the selection of a so-called set of sigma points. These points can be obtained from the unscented transformation of the augmented state vector and covariance matrix. In the original definition of the UKF, the state vector and covariance matrix were only augmented with the process noise.[10] Hence, hereby it was also assumed that the states and corresponding errors are propagated linearly through the measurement equations. In most cases, such an approximation is tolerated. However, since the computational burden of an increased augmented state vector and covariance matrix is limited, it was chosen to also augment the latter two quantities with the measurement noise characteristics.[27,29]

To begin with the formulation of the augmented UKF, the augmented state vector and covariance matrix are defined as:

$$\hat{\mathbf{x}}^a(k) = [\hat{\mathbf{x}}(k|k)^\intercal \; \mathbf{v}(k)^\intercal \; \mathbf{w}(k)^\intercal]^\intercal \tag{10}$$

$$\mathbf{P}^a(k) = \begin{bmatrix} \mathbf{P}(k) & 0 & 0 \\ 0 & \mathbf{Q} & 0 \\ 0 & 0 & \mathbf{R} \end{bmatrix} \tag{11}$$

where $\mathbf{v}$ and $\mathbf{w}$ in the augmented state vector represent the means of the process and measurement noise; these can therefore be assumed to have zero mean, hence their values will be zero. The augmented state vector and covariance matrix can then easily be transformed to the unscented domain by:

$$\begin{aligned} \boldsymbol{\mathcal{X}}_i^a(k) &= \left[\hat{\mathbf{x}}^a(k) + \sqrt{(L+\lambda)\mathbf{P}^a(k)}\right] \quad & i = 1, 2, \dots, L \\ \boldsymbol{\mathcal{X}}_i^a(k) &= \left[\hat{\mathbf{x}}^a(k) - \sqrt{(L+\lambda)\mathbf{P}^a(k)}\right] \quad & i = L+1, L+2, \dots, 2L \end{aligned} \tag{12}$$

This set of transformed points, indicated by $\boldsymbol{\mathcal{X}}^a$, is referred to as the set of sigma points. Parameters L and λ are, respectively, the dimensionality of the state vector and a scaling factor defined as $\lambda = \alpha^2(L+\kappa) - L$. α is a parameter to reflect the spread of the sigma points around its mean, state vector $\hat{\mathbf{x}}$, and β is a factor to account for any prior knowledge. The latter is set to a value of 2 for Gaussian distributions. κ is an extra scaling factor which is usually set to zero. Subsequently, the weights for the set of transformed means and covariances are defined as follows:

$$\begin{aligned} W_0^{(m)} &= \frac{\lambda}{L+\lambda} \\ W_0^{(c)} &= \frac{\lambda}{L+\lambda} + (1 - \alpha^2 + \beta) \\ W_i^{(m)} = W_i^{(c)} &= \frac{1}{2(L+\lambda)} \qquad i = 1, 2, \dots, 2L \end{aligned} \tag{13}$$

From this point, the equations of the UKF become more trivial. Analogously to the EKF, the state vector which is now expressed as sigma points are propagated through the system's dynamics:

$$\boldsymbol{\mathcal{X}}^a(k+1|k) = \boldsymbol{\mathcal{X}}^a\,(k|k) + \int_{t_k}^{t_{k+1}} \mathbf{f}\left[\boldsymbol{\mathcal{X}}^{a,x}(k|k), \mathbf{u}(k), \boldsymbol{\mathcal{X}}^{a,v}(k|k), \tau\right] d\tau \tag{14}$$

where $\boldsymbol{\mathcal{X}}^{a,x}$ refers to the columns of the sigma points matrix related to the state and superscript v refers to the sigma points related to the process noise. The one step ahead state estimation can be calculated by:

$$\hat{\mathbf{x}}\,(k+1|k) = \sum_{i=0}^{2L} W_i^{(m)} \boldsymbol{\mathcal{X}}^a\,(k+1|k) \tag{15}$$

and the one step ahead covariance matrix by:

$$\mathbf{P}\left(k+1|k\right)=\sum_{i=0}^{2L}W_i^{(c)}\left(\boldsymbol{\mathcal{X}}_i^{a,x}-\hat{\mathbf{x}}(k|k)\right)\left(\boldsymbol{\mathcal{X}}_i^{a,x}-\hat{\mathbf{x}}(k|k)\right)^{\intercal} \tag{16}$$

Again, similarly to the EKF, the sigma points representing the state vector and measurement noise are propagated through the measurement equations and subsequently the transformed means for the measurements are calculated:

$$\boldsymbol{\mathcal{Y}}(k+1|k)=\mathbf{h}\left[\boldsymbol{\mathcal{X}}^{a,x}(k+1|k),\boldsymbol{\mathcal{X}}^{a,w}(k+1|k)\right] \tag{17}$$

with the transformed measurements given by taking the mean of the transformed sigma points:

$$\hat{\mathbf{y}}=\sum_{i=0}^{2L}W_i^{(m)}\boldsymbol{\mathcal{Y}}_i(k+1|k) \tag{18}$$

The measurement covariance and measurement-state cross-covariance can be calculated by:

$$\mathbf{P_{yy}}=\sum_{i=0}^{2L}W_i^{(c)}\left(\boldsymbol{\mathcal{Y}}_i(k+1|k)-\hat{\mathbf{y}}(k|k)\right)\left(\boldsymbol{\mathcal{Y}}_i(k+1|k)-\hat{\mathbf{y}}(k|k)\right)^{\intercal} \tag{19}$$

$$\mathbf{P_{xy}}=\sum_{i=0}^{2L}W_i^{(c)}\left(\boldsymbol{\mathcal{X}}_i^{a,x}-\hat{\mathbf{x}}(k|k)\right)\left(\boldsymbol{\mathcal{Y}}_i-\hat{\mathbf{y}}(k|k)\right)^{\intercal} \tag{20}$$

Finally, to complete the definition of the augmented UKF, gain matrix $\boldsymbol{\mathcal{K}}$, corrected state estimation $\hat{\mathbf{x}}(k+1|k+1)$ and corrected covariance matrix estimation $\mathbf{P}(k+1|k+1)$ are expressed as:

$$\boldsymbol{\mathcal{K}}(k+1)=\mathbf{P_{xy}}\mathbf{P_{yy}}^{-1} \tag{21}$$

$$\hat{\mathbf{x}}(k+1|k+1)=\hat{\mathbf{x}}(k+1|k)+\boldsymbol{\mathcal{K}}\left\{\mathbf{y}(k+1)-\hat{\mathbf{y}}(k+1|k)\right\} \tag{22}$$

$$\mathbf{P}(k+1|k+1)=\mathbf{P}(k+1|k)-\boldsymbol{\mathcal{K}}(k+1)\mathbf{P_{yy}}\boldsymbol{\mathcal{K}}^{\intercal}(k+1) \tag{23}$$

For additional numerical stability and guaranteed semi-definite state covariance matrix, the square-root implementation of the UKF can be used.[30] This type uses the Cholesky decomposition to address certain numerical advantages in the calculation of the transformed statistical properties. Further extensions to the UKF, e.g. the Sigma-Point Kalman Filter[31] and its iterative counterpart[32] were introduced later. However, these filters populate the whole state-space with sigma points instead of only a selected optimal range. Therefore, the computational burden of such filters do not outweigh the advantages and their application is restricted.[33]

IV. Aerodynamic Model Identification

Different researches suggest the use of subspaces in the identification of multiple locally defined aerodynamic models.[34,35] These methods allow identification from several large-amplitude maneuvers, effectively organizing the whole data set in subspaces of the dominant aerodynamic variable (α or β). By also applying model structure selection to every subspace, any non-linearity in the horizontal or lateral state-plane can be approximated by a set of ordinary polynomials. Despite this advantage, a requirement for this method is to have sufficient data in every subspace. In addition, since the identification in this paper is applied to the normal, pre-stall regime, most of the dynamics are sufficiently approximated by assuming linear dependence of the model parameters with respect to the angle of attack or the sideslip angle. In the context of this paper, a per-maneuver model identification scheme was applied followed by post-smoothing of the locally identified models through regression of the identified parameters versus the Mach number and altitude.

A. Preliminaries

If it is assumed that the aerodynamic force and moment coefficients are analytic functions of the corresponding independent variables, they can be expressed in the form of a Taylor series.[9] For the longitudinal state-plane, there is a general consensus that the dependency of the model coefficients[16,17] can be expressed as:

$$C_a = C_a(\alpha,\ \dot{\alpha},\ q,\ \delta_e,\ \delta_f,\ \delta_{t_e},\ T_e,\ M,\ h)\ \in \mathbb{R}^8 \quad \text{for} \quad a = X,\ Z,\ m \tag{24}$$

Analogously, the assumption can be made that the lateral non-dimensional forces and moments can be parametrized as follows:

$$C_a = C_a(\beta,\ \dot{\beta},\ p,\ r,\ \delta_a,\ \delta_r,\ \delta_{t_a},\ \delta_{t_r},\ M,\ h)\ \in \mathbb{R}^{10} \quad \text{for} \quad a = Y,\ l,\ n \tag{25}$$

Because of the absence of flap and trim tab measurements, dependency of the model coefficients on the corresponding variables cannot be assessed. For this reason, flap and trim tab deflection and their effect on the non-dimensional forces and moments are neglected. The six non-dimensional forces and moments can be calculated by:

$$C_X = \frac{m\left(a_x - \lambda_{a_x}\right) - T_x}{\overline{q}S} \tag{26}$$

$$C_Y = \frac{m\left(a_y - \lambda_{a_y}\right)}{\overline{q}S} \tag{27}$$

$$C_Z = \frac{m\left(a_x - \lambda_{a_z}\right)}{\overline{q}S} \tag{28}$$

$$C_l = \frac{I_{xx}}{\overline{q}Sb}\left(\dot{p} - \frac{I_{xz}}{I_{xx}}\left(\left(p-\lambda_p\right)\left(q-\lambda_q\right) + \dot{r}\right) + \frac{I_{zz}-I_{yy}}{I_{xx}}\left(q-\lambda_q\right)\left(r-\lambda_r\right)\right) \tag{29}$$

$$C_m = \frac{I_{yy}}{\overline{q}S\overline{c}}\left(\dot{q} - \frac{I_{xx}-I_{zz}}{I_{yy}}\left(p-\lambda_p\right)\left(r-\lambda_r\right) + \frac{I_{xz}}{I_{yy}}\left(\left(p-\lambda_p\right)^2 - \left(r-\lambda_r\right)^2\right) - M_T\right) \tag{30}$$

$$C_n = \frac{I_{zz}}{\overline{q}Sb}\left(\dot{r} - \frac{I_{xz}}{I_{zz}}\left(\dot{p} - \left(q-\lambda_q\right)\left(r-\lambda_r\right)\right) + \frac{I_{yy}-I_{xx}}{I_{zz}}\left(p-\lambda_p\right)\left(q-\lambda_q\right)\right) \tag{31}$$

where λ denotes the bias obtained from the flight path reconstruction procedure for each of the accelerations and rotational rates. Since the derivatives of the rotational rates are not measured directly, these can be obtained by numerical differentiation. Corrections to the non-dimensional force in X_b and the non-dimensional pitch rate were made by making use of an engine model. The engine-produced thrust in Z_b was neglected and assumed to be approximately zero.

B. Parameter Estimation

The principles of regression analysis are well known and previously applied in many different researches in the framework of aerodynamic system identification.[35–37] The ordinary least squares (OLS) estimator, defined as the minimum residual

$$\mathbf{\Theta}_{\text{OLS}} = \min_{\Theta\in\mathbb{R}} \left\|\mathbf{X}\cdot\mathbf{\Theta} - \mathbf{y}\right\| \tag{32}$$

where $\|\cdot\|$ denotes the L^2 norm in Euclidean space $\mathbb{R}^n$. The well-known solution in terms of linear operations is given by:

$$\hat{\mathbf{\Theta}}_{\text{OLS}} = \left(\mathbf{X}^{\intercal}\mathbf{X}\right)^{-1}\mathbf{X}^{\intercal}\mathbf{y} \tag{33}$$

According to the Gauss-Markov theorem, the OLS estimator is the best linear unbiased estimator under the assumption that the variance of the residuals should be homoscedastic and the correlation terms should vanish.[38] In addition, under the assumption of a normally distributed residuals vector the OLS estimator is identical to the maximum likelihood estimator, effectively attaining the Cramér-Rao lower bounds (CRLB).[39]

The standard bounds of the parameter estimates are given by the diagonal elements of the variance-covariance matrix:

$$\mathrm{Cov}\left\{\mathbf{\Theta}\right\} = \mathbb{E}\left\{\left(\hat{\mathbf{\Theta}} - \mathbf{\Theta}\right)^{\intercal}\left(\hat{\mathbf{\Theta}} - \mathbf{\Theta}\right)\right\} = \sigma^2\left(\mathbf{X}^{\intercal}\mathbf{X}\right)^{-1} \tag{34}$$

where σ^2 can be approximated by the mean squared error of the residuals. Using the estimated covariance, pair-wise correlation of the estimated parameters can be assessed by:

$$\mathrm{Corr}\left\{\hat{\mathbf{\Theta}}\right\} = \begin{pmatrix} \frac{1}{\sigma(\hat{\Theta}_1)} & 0 & \dots & 0 \\ 0 & \frac{1}{\sigma(\hat{\Theta}_2)} & \dots & 0 \\ \vdots & \vdots & \ddots & \vdots \\ 0 & 0 & \dots & \frac{1}{\sigma(\hat{\Theta}_p)} \end{pmatrix} \mathrm{Cov}\left\{\hat{\mathbf{\Theta}}\right\} \begin{pmatrix} \frac{1}{\sigma(\hat{\Theta}_1)} & 0 & \dots & 0 \\ 0 & \frac{1}{\sigma(\hat{\Theta}_2)} & \dots & 0 \\ \vdots & \vdots & \ddots & \vdots \\ 0 & 0 & \dots & \frac{1}{\sigma(\hat{\Theta}_p)} \end{pmatrix} \tag{35}$$

Because aircraft parameter estimation is often associated with data collinearity,[40] a biased parameter estimation technique known as Principal Components Regression (PRC) was used. PCR is able to increase the accuracy of the parameter estimates in case of multi-collinearity among the predictor variables.[35]

C. Model Structure Selection

Aerodynamic model structure selection is a non-trivial process. A literature study reveals an abundance of different techniques, all arriving at a postulated aerodynamic model structure for the six non-dimensional forces and moments. In the aerospace community there is a general consensus about the linear model structure, formed by a linear combination of the independent variables in Eq. (24) and Eq. (25). However, model structure selection remains an important step in order to capture second and higher order non-linearities, including interaction of the independent variables.[41]

Stepwise regression[34] is a method specifically aimed at data-driven selection of an appropriate model structure from a set of candidate regressors. Later modifications to this approach restricted the selection of candidate regressors to higher order terms, starting at a fixed linear model structure.[41] The pool of candidate regressors is to be formed by single terms, cross-interactions and higher order terms corresponding to the independent variables in Eq. (24) and Eq. (25). The downside of the stepwise regression method is that it includes addition and elimination criteria.[42] In addition, regressors cannot be evaluated independently because of their interaction with other regressors in the selected model structure.

More recently, Morelli[36,43] and Grauer[44] applied a multi-variate polynomial model obtained from an orthogonal model structure selection to various aircraft. The latter model structure selection technique transforms the full set of candidate regressors to the orthogonal domain in order to test the significance of each parameter. By defining a predicted square error (PSE),[44] selection of the orthogonal basis functions can be done by minimization of the latter metric. Terms contributing less than a certain threshold value can also be removed from the model structure.

The process of orthogonal basis functions model structure selection begins with the orthogonalization process of the set of candidate regressors:

$$\mathbf{p}_0 = 1, \quad \mathbf{p}_j = \mathbf{x}_j - \sum_{k=0}^{j-1}\gamma_{kj}\mathbf{p}_k \quad \text{for} \quad j = 1, 2, \dots, n \tag{36}$$

where $\mathbf{x}_j$ is the j^{th} vector of independent variables and coefficient γ_{kj} is defined as:

$$\gamma_{kj} = \frac{\mathbf{p}_k^{\intercal}\mathbf{x}_j}{\mathbf{p}_k^{\intercal}\mathbf{p}_k} \quad \text{for} \quad k = 0, 1, \dots, j-1 \tag{37}$$

Orthogonal vectors $\mathbf{p}_0, \mathbf{p}_1, \dots, \mathbf{p}_n$ now form the columns of orthogonal regression matrix $\mathbf{P}$. The parameter estimate can now be obtained by the least squares estimator in Eq. (33). This can be done by subsequently calculating the contribution to the total least-squares cost independently for each candidate regressor with:

$$J(\hat{\mathbf{a}}_j) = \frac{\left(\mathbf{p}_j^{\intercal}\mathbf{y}\right)^2}{\mathbf{p}_j^{\intercal}\mathbf{p}_j} \tag{38}$$

a selection can be made based on the PSE, which is defined as:

$$\text{PSE} = \frac{1}{N}(\mathbf{y} - \hat{\mathbf{y}})^{\intercal}(\mathbf{y} - \hat{\mathbf{y}}) + \sigma_{\max}^2 \frac{n}{N} \tag{39}$$

The maximum model fit error variance can be obtained from:

$$\sigma_{\max}^2 = \frac{1}{N-1} \sum_{i=1}^{N} (y_i - \overline{\mathbf{y}})^2 \tag{40}$$

In the context of efficiency, model structure selection by use of either orthogonal basis function or a stepwise regression scheme allows the modeling of non-linearities in the horizontal and longitudinal state-planes by including higher-order terms and cross-term interactions. It was chosen to generalize this scheme to per-maneuver identification which can later be regressed versus the Mach number and altitude.

Collinearity amongst the regressors should be avoided at all costs when averaging the set of estimated parameters over the $(M-h)$ range. Correlation coefficients of over 0.9 should be avoided.[35] However, in aircraft problems correlation cannot always be avoided since, amongst others, control surface deflections are closely related with their induced rotational velocities. Including highly correlated terms in the model will induce relatively large variations of the estimated parameters, leading to difficulties in the generalization over the Mach and altitude domain. For this reason, highly correlated terms should be removed from the final model structure. Current model structure selection procedures do not account for high pairwise collinearity, therefore manual analysis is required.

D. Model Parameter $(M-h)$ fit

After obtaining the appropriate model structure selection and removing highly correlated terms, the estimated parameters can be regressed with respect to the Mach number and altitude. By doing so, every identified parameter will be made a function of the Mach number and altitude. Because of the expected limited non-linearities in the $(M-h)$ state-plane, a linear regression function should provide adequate approximation power. Identification in subspaces of the Mach number and altitude reduces the model dependency by removing the corresponding terms from Eq. (24) and Eq. (25). Alternatively, regression of the estimated parameters versus the angle of attack or sideslip angle allows the estimated parameters to be described as a function of the corresponding aerodynamic angle. However, because of the rather high excursion of the aerodynamic angles, the latter variables cannot be assumed constant for the duration of the maneuver.

In order to allow regression of the Mach number and altitude versus the value or the corresponding parameter, it was assumed that the Mach number and altitude are constant for the duration of the complete dynamic maneuver. In order to obtain a smoothed relation of the model parameters with respect to the Mach number and altitude, a robust least-squares fit routine was employed. By doing so, outliers in the sets of estimated parameters can be eliminated. The resulting $(M-h)$ plane fit will be used to describe the parameters of the six dimensionless models in a look-up table.

V. Results

In this section the results of the flight path reconstruction, model structure selection and parameter estimation procedure are presented. In addition, a comparison between parameter estimates by Koehler and Hardover maneuvers is presented, followed by post identification smoothing of the locally identified models.

A. Flight Path Reconstruction

The results for the flight path reconstruction procedure comprises a total of more than 200 individually reconstructed dynamic maneuvers, both longitudinally and laterally induced. For this reason, only a selection of results is shown in this paper. For a typical 3-2-1-1 dynamic maneuver in elevator, the results are depicted in Figure 5. In this figure, the state estimate by the UKF together with the bias estimate, innovation sequences, filtered and reconstructed measurements and the control surface deflections during the maneuver are shown. Innovation sequences are shown to confirm filter consistency.

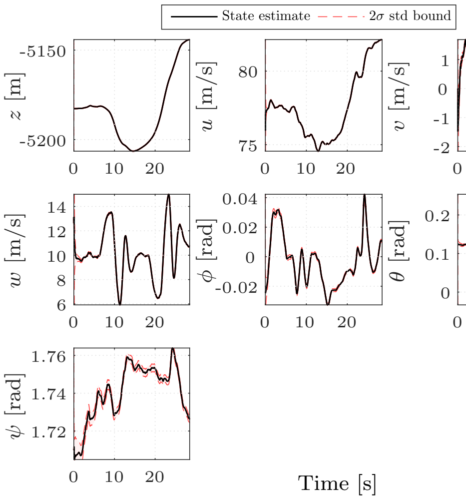

(a) UKF state estimate sequences

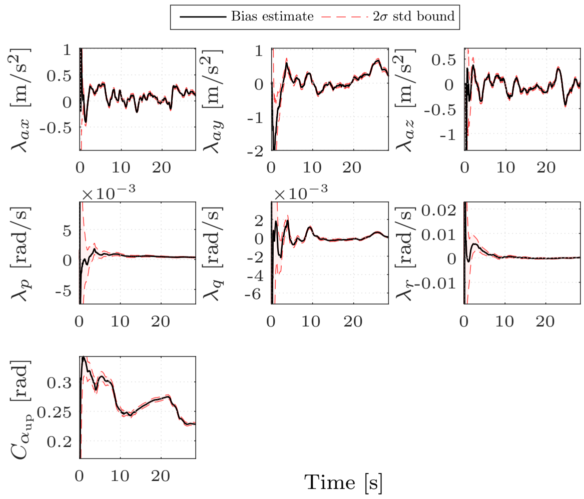

(b) UKF bias estimate sequences

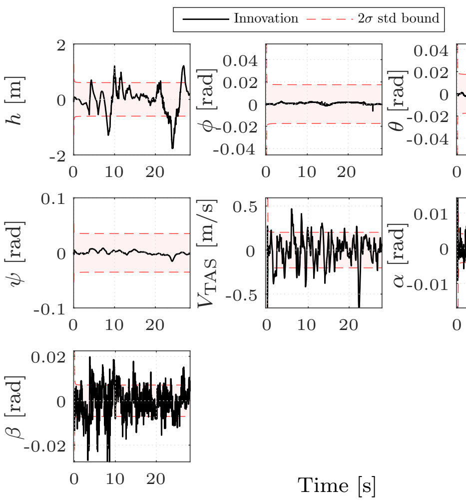

(d) UKF filter innovation sequences

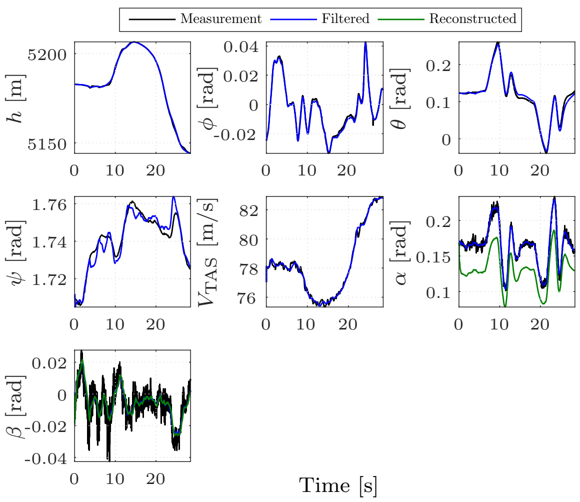

(e) Measurement values together with filtered and reconstructed measurement sequences

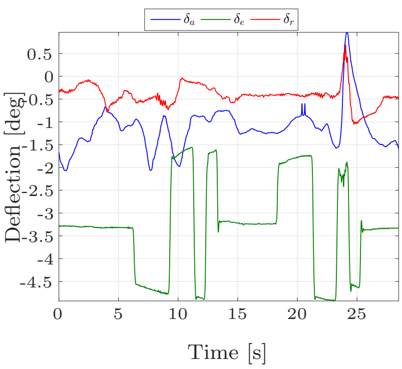

(g) Control surface deflections

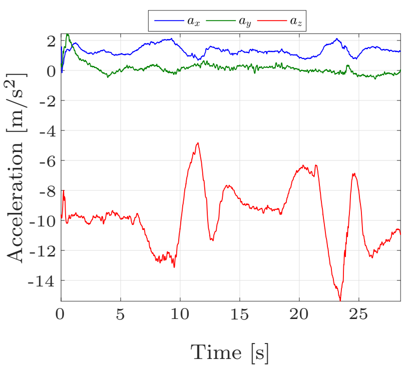

(h) Measured accelerations

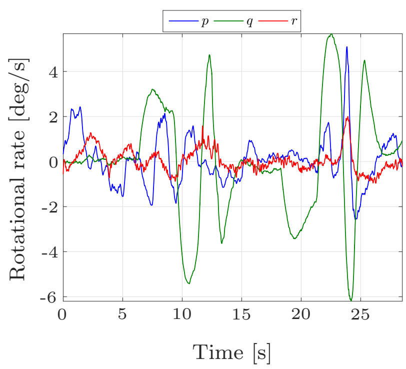

(i) Measured rotational rates

Figure 5. The state and bias estimate together with the innovation sequences, the reconstructed measurements and control surface deflections for a typical δ_e induced longitudinal 3-2-1-1 dynamic maneuver obtained from a flight path reconstruction procedure with the UKF.

B. Aerodynamic Model Identification

The results from the model structure selection procedure and parameter estimation are presented in this section together with a model validation by applying the identified least squares model to flight derived non-dimensional forces and moments together with a comparison versus the currently implemented aerodynamic model in the DASMAT simulation framework.

1. *Model Structure Selection*

By populating a pool of candidate regressors, up to and including degree 2 (e.g. α^2) with first order cross-interactions between different model parameters (e.g. $\alpha\delta_e$), the orthogonal least squares model structure determination routine resulted in the model terms presented in Figure 6. As clearly indicated by the red line, the threshold for including model terms was set at a percentage of 50. Note that model structure selection for each of the six models was applied to a subset of the total number of data sets, selected on basis of sufficient excitation of the corresponding state plane. In addition to selecting the model structure with the lowest PSE, model terms in the final model contributing less than 1% in reduction of the root mean square error were removed.

Candidate pools for the lateral models contain a larger set of candidate regressors because of their extended basis with respect to the longitudinal basis (see Eq. (24) and Eq. (25)). Note that the currently selected candidate pool did not include terms related to the time rate of change of the angle of attack and angle of sideslip. These terms were removed because of their high pair-wise correlation with rotational rates around the body axis, an effect of multi-collinearity in the regression matrix. In effect, the estimated coefficients for the pitch rate and yaw rate can be considered to also include the effects of the time rate of change of the angle of attack and sideslip angle. For the same reason, candidate regressors with degree 3 or higher were neglected.

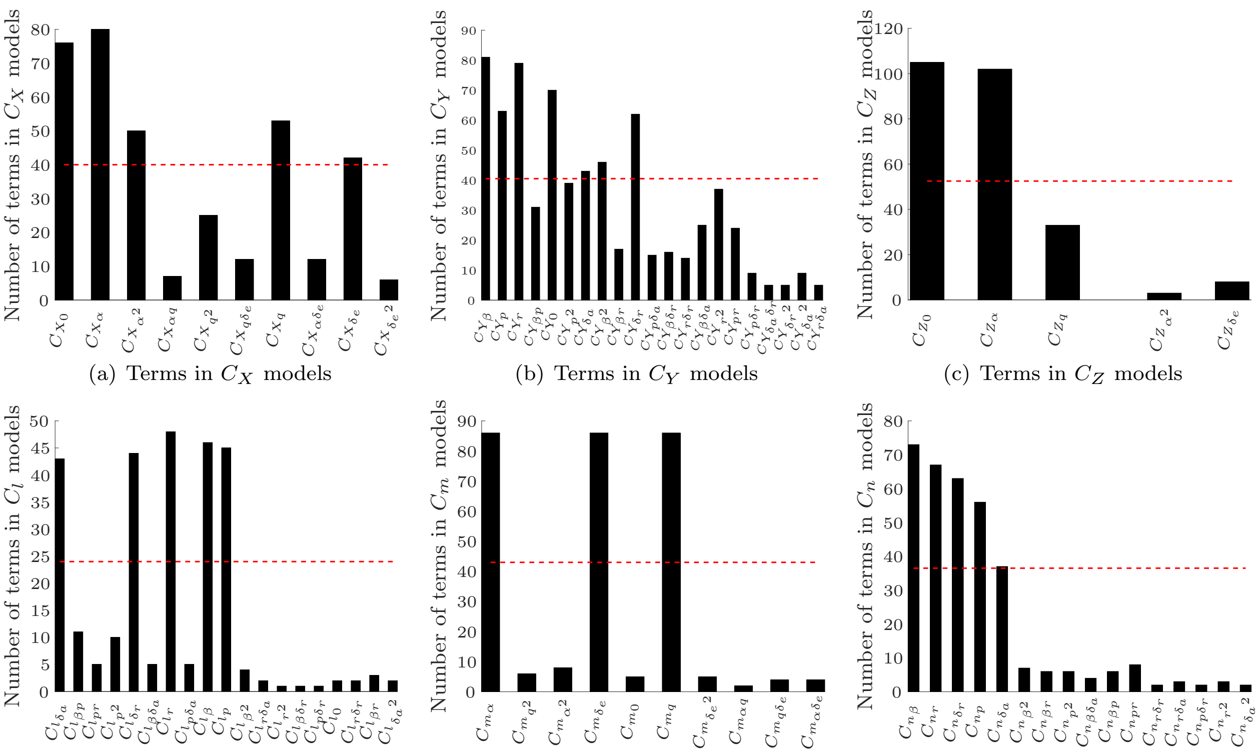

(a) Terms in C_X models (b) Terms in C_Y models (c) Terms in C_Z models

(d) Terms in C_l models (e) Terms in C_m models (f) Terms in C_n models

Figure 6. Absolute number of model terms selected in the longitudinal and lateral models obtained from an orthogonal least squares model structure selection procedure.

2. Model Parameter Identification

The final model structure of the non-dimensional forces and moments in X_b, obtained from an orthogonal least squares model selection scheme, consisted of a total of 5 terms, i.e. C_{X_0}, C_{X_α}, C_{X_q}, $C_{X_{\delta_e}}$, $C_{X_{\alpha^2}}$. However, the term related to the squared angle of attack was removed from the model for its high pair-wise correlation with the angle of attack term. Identified values for the parameters as tabulated in Table 3. Tabulated values represent the parameters in the total number of locally identified models. The minimum, maximum and mean values for the estimated parameters and corresponding variance were included as performance measure to indicate consistence of the estimates.

Model estimates for the C_Y model, presented in Table 4, do contain all linear terms from the earlier proposed model structure. In addition, the squared angle of sideslip was indicated as final model regressor from the model selection procedure. Identification of this parameter was successful because of the limited correlation with the remaining model terms. However, from Table 4 it also becomes apparent that the estimate of $C_{Y_{\beta}^2}$ lacks in accuracy, reflected by the its high variance.

In relation to the other longitudinal models, a deviation from the model terms obtained from model structure selection procedure was made for the C_Z (Table 5) and C_m (Table 7) models. In order to align the model structures of the longitudinal models, same model terms were assumed as earlier determined for the C_X model. In general, the intercept term was assumed to be included in all models for its ability to act as bin for any variance in the dependent variable that cannot be described by the selected set of independent variables.

Selection of the model terms for the non-dimensional roll and yaw moment proved simple and straight-forward: both models can sufficiently be parametrized by a model structure containing linear terms for the lateral variables (see Table 6 and Table 8). On balance, the models for the 6 dimensionless forces and moments resulting from the model structure selection procedure and parameter estimation were parametrized as follows:

$$C_X = C_{X_0} + C_{X_\alpha}\alpha + \cancel{C_{X_{\alpha^2}}\alpha^2} + C_{X_q}\hat{q} + C_{X_{\delta_e}}\delta_e \tag{41}$$

$$C_Y = C_{Y_0} + C_{Y_\beta}\beta + C_{Y_p}\hat{p} + C_{Y_r}\hat{r} + C_{Y_{\delta_a}}\delta_a + C_{Y_{\delta_r}}\delta_r + C_{Y_{\beta^2}}\beta^2 \tag{42}$$

$$C_Z = C_{Z_0} + C_{Z_\alpha}\alpha + C_{Z_q}\hat{q} + C_{Z_{\delta_e}}\delta_e \tag{43}$$

$$C_l = C_{l_0} + C_{l_\beta}\beta + C_{l_p}\hat{p} + C_{l_r}\hat{r} + C_{l_{\delta_a}}\delta_a + C_{l_{\delta_r}}\delta_r \tag{44}$$

$$C_m = C_{m_0} + C_{m_\alpha}\alpha + C_{m_q}\hat{q} + C_{m_{\delta_e}}\delta_e \tag{45}$$

$$C_n = C_{n_0} + C_{n_\beta}\beta + C_{n_p}\hat{p} + C_{n_r}\hat{r} + C_{n_{\delta_a}}\delta_a + C_{n_{\delta_r}}\delta_r \tag{46}$$

Table 3. Estimated parameters mean variance, minimum variance and maximum variance for the C_X model, obtained from an orthogonal least squares model structure selection approach.

	$\overline{\theta}$	θ_{min}	θ_{max}	$\overline{\sigma}(\theta)$	$\sigma(\theta)_{min}$	$\sigma(\theta)_{max}$
C_{X_0}	-0.051	-0.594	0.019	1.553×10^{-5}	4.134×10^{-8}	4.710×10^{-4}
C_{X_α}	0.862	-0.213	12.733	1.115×10^{-3}	2.059×10^{-5}	5.349×10^{-2}
C_{X_q}	-4.465	-100.213	17.117	8.591×10^{-1}	1.296×10^{-2}	8.320
$C_{X_{\delta_e}}$	-0.172	-3.602	0.842	2.572×10^{-3}	3.688×10^{-5}	2.736×10^{-2}

Table 4. **Estimated parameters mean variance, minimum variance and maximum variance for the C_Y model, obtained from an orthogonal least squares model structure selection approach.**

	$\overline{\theta}$	θ_{min}	θ_{max}	$\overline{\sigma}(\theta)$	$\sigma(\theta)_{min}$	$\sigma(\theta)_{max}$
C_{Y_0}	0.004	-0.056	0.059	8.638×10^{-8}	3.190×10^{-10}	8.079×10^{-7}
C_{Y_β}	-0.794	-2.258	-0.169	4.389×10^{-4}	1.362×10^{-6}	4.080×10^{-3}
C_{Y_p}	-0.159	-4.163	2.583	1.403×10^{-2}	3.772×10^{-5}	1.152×10^{-1}
C_{Y_r}	1.958	-1.813	13.569	2.199×10^{-2}	3.163×10^{-5}	1.496×10^{-1}
$C_{Y_{\delta_a}}$	-0.180	-4.305	1.397	2.083×10^{-3}	1.548×10^{-6}	2.282×10^{-2}
$C_{Y_{\delta_r}}$	0.839	-1.988	26.784	4.846×10^{-2}	1.152×10^{-6}	1.427
$C_{Y_{\beta^2}}$	2.754	-14.888	48.476	1.028	2.795×10^{-5}	9.398

Table 5. **Estimated parameters mean variance, minimum variance and maximum variance for the C_Z model, obtained from an orthogonal least squares model structure selection approach.**

	$\overline{\theta}$	θ_{min}	θ_{max}	$\overline{\sigma}(\theta)$	$\sigma(\theta)_{min}$	$\sigma(\theta)_{max}$
C_{Z_0}	-0.213	-0.941	0.025	1.575×10^{-4}	1.075×10^{-6}	5.183×10^{-3}
C_{Z_α}	-4.037	-8.231	2.868	8.074×10^{-3}	2.369×10^{-4}	4.290×10^{-1}
C_{Z_q}	-57.766	-267.955	189.902	1.320×10^{1}	2.363×10^{-1}	1.979×10^{2}
$C_{Z_{\delta_e}}$	-0.836	-6.355	25.163	4.456×10^{-2}	7.952×10^{-4}	6.847×10^{-1}

Table 6. **Estimated parameters mean variance, minimum variance and maximum variance for the C_l model, obtained from an orthogonal least squares model structure selection approach.**

	$\overline{\theta}$	θ_{min}	θ_{max}	$\overline{\sigma}(\theta)$	$\sigma(\theta)_{min}$	$\sigma(\theta)_{max}$
C_{l_0}	-0.002	-0.020	0.010	1.826×10^{-8}	1.182×10^{-10}	3.285×10^{-7}
C_{l_β}	-0.073	-0.143	-0.006	1.407×10^{-6}	9.575×10^{-8}	1.490×10^{-5}
C_{l_p}	-0.494	-0.710	0.056	2.656×10^{-5}	1.727×10^{-6}	1.508×10^{-4}
C_{l_r}	0.376	0.024	0.785	6.498×10^{-5}	4.639×10^{-7}	4.298×10^{-4}
$C_{l_{\delta_a}}$	-0.178	-0.276	0.121	6.081×10^{-6}	1.585×10^{-7}	9.996×10^{-5}
$C_{l_{\delta_r}}$	0.102	-1.309	2.314	6.865×10^{-4}	2.784×10^{-8}	1.619×10^{-2}

Table 7. **Estimated parameters mean variance, minimum variance and maximum variance for the C_m model, obtained from an orthogonal least squares model structure selection approach.**

	$\overline{\theta}$	θ_{min}	θ_{max}	$\overline{\sigma}(\theta)$	$\sigma(\theta)_{min}$	$\sigma(\theta)_{max}$
C_{m_0}	0.021	-0.022	0.089	4.918×10^{-7}	1.252×10^{-8}	5.698×10^{-6}
C_{m_α}	-0.488	-0.855	-0.253	2.509×10^{-5}	2.856×10^{-6}	1.904×10^{-4}
C_{m_q}	-11.935	-22.066	-1.489	3.466×10^{-2}	2.968×10^{-3}	2.920×10^{-1}
$C_{m_{\delta_e}}$	-1.250	-1.508	-0.351	1.204×10^{-4}	9.907×10^{-6}	1.097×10^{-3}

Table 8. **Estimated parameters mean variance, minimum variance and maximum variance for the C_n model, obtained from an orthogonal least squares model structure selection approach.**

	$\overline{\theta}$	θ_{min}	θ_{max}	$\overline{\sigma}(\theta)$	$\sigma(\theta)_{min}$	$\sigma(\theta)_{max}$
C_{n_0}	0.000	-0.002	0.002	1.158×10^{-8}	2.084×10^{-10}	1.326×10^{-7}
C_{n_β}	0.079	-0.056	0.145	3.689×10^{-6}	1.548×10^{-7}	5.965×10^{-5}
C_{n_p}	-0.142	-0.677	0.284	1.307×10^{-4}	5.361×10^{-6}	3.267×10^{-3}
C_{n_r}	-0.295	-0.474	0.374	1.005×10^{-4}	3.055×10^{-6}	5.440×10^{-4}
$C_{n_{\delta_a}}$	-0.025	-0.155	0.073	4.720×10^{-5}	5.616×10^{-7}	1.049×10^{-3}
$C_{n_{\delta_r}}$	-0.065	-0.611	0.578	7.338×10^{-4}	1.783×10^{-7}	1.770×10^{-2}

3. *Identification with Hardover Control Inputs*

As already stated in Section C, a part of the experimental flight test data consists of the time traces of coupled Hardover maneuvers. In order to assess the usefulness of these maneuvers in the framework of aerodynamic model identification, a comparison between parameter estimates for all six non-dimensional models obtained from Koehler (3-2-1-1) maneuvers and Hardover maneuvers is presented in Figure 7. The estimates in this figure were obtained from averaging estimates from a set of Koehler and Hardover input maneuvers at approximately the same flight conditions, where the error bars indicate 1σ standard deviation of the averaged parameters.

In general it can be stated that parameter estimates for the longitudinal and lateral moments obtained from a Hardover input are in agreement with estimates obtained from a Koehler input. Average values of the parameter estimates obtained from both maneuvers only differ slightly.

In contrast to the moment model parameters, larger differences between the estimates obtained from both maneuvers are observed. In particular for C_Z, in Figure 7(c), where all of the estimates, except for the bias term, differ in sign. For almost all of the parameters, estimates obtained from Koehler inputs show smaller confidence intervals indicative of a higher accuracy.

C. Model Parameter $(M - h)$ fit

After separate model parameter estimation for each of the 212 indicated test points, the obtained model parameters were generalized as function of the Mach number and the altitude. The resulting robust least square estimate for the $(M - h)$-plane fit of the C_m model is presented in Figure 8. Note that the Mach number and altitude were assumed to be constant for the duration each maneuver such that the parameters can be plotted versus the latter two variables. Plane fits for the parameters of the other five non-dimensional models can be found in Appendix A. The plane fits are presented as curve fit as a function of the Mach number and altitude at, respectively, the average altitude and average Mach number.

From Figure 8 it becomes evident that due to the rather large spread of the identified parameters of the local models, indicated by the red cross symbol together with its confidence bounds, the prediction interval of the obtained plane fit is also rather large. A cause for this large spread can be found by considering the origin of the different measurements as most of the measurements originate from different flights, obtained under different atmospheric conditions. Nevertheless, it is clear that a relationship between the estimated parameters and the Mach number is present.

The same cannot be said for almost all of the estimated parameters with respect to the altitude (also see Appendix A). Considering the relatively small slope of these estimates, a sufficient approximation can also be given by assuming a constant parameter value. Also notice that the low information content, especially for the lateral models, makes it hard to estimate dependency of the model parameters on the altitude which can be seen from the limited number of locally identified models at different altitude ranges. Furthermore, the linear trends of the longitudinal parameters show a clearer dependence on the Mach number in comparison to the lateral model parameters. The convex hull, indicating the validity region of the models, of the (M, h) plane together with the convex hull of some other parameters relating to the identified models can be found in Appendix B.

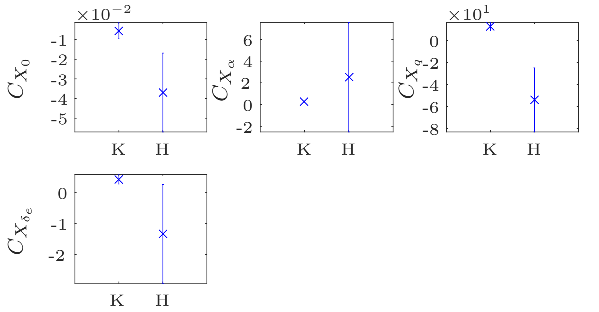

(a) Parameter estimates of the C_X model terms at $M =$ 0.32 to 0.36 and $h = 5100$ to 5200 m

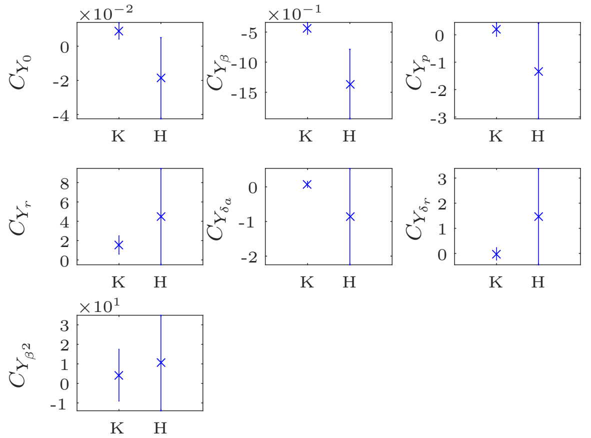

(b) Parameter estimates of the C_Y model terms at $M =$ 0.35 to 0.40 and $h = 5100$ to 5200 m

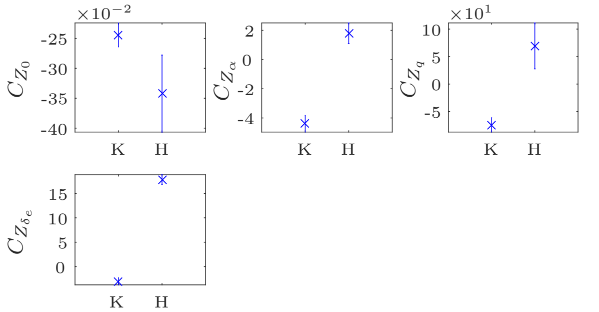

(c) Parameter estimates of the C_Z model terms at $M =$ 0.32 to 0.37 and $h = 5100$ to 5200 m

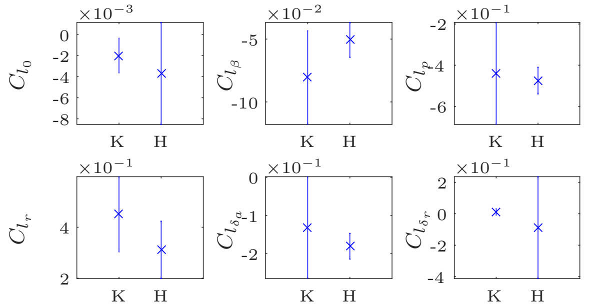

(d) Parameter estimates of the C_l model terms at $M = 0.32$ to 0.37 and $h = 5100$ to 5200 m

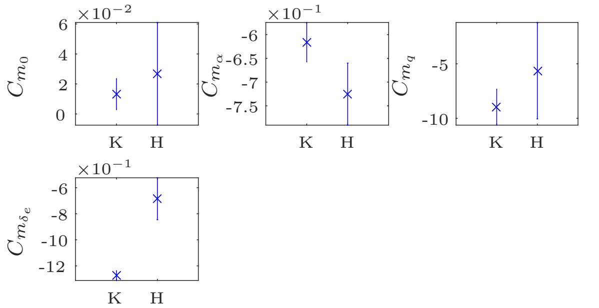

(e) Parameter estimates of the C_m model terms at $M =$ 0.20 to 0.25 and $h = 5100$ to 5200 m

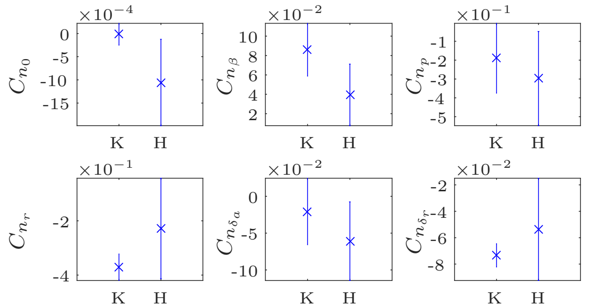

(f) Parameter estimates of the C_n model terms at $M = 0.31$ to 0.36 and $h = 5100$ to 5200 m

Figure 7. Comparison of the identified parameters for the six non-dimensional forces and moments by using a 3-2-1-1 Koehler (K) input or Hardover (H) input on the control surfaces. The mean of the estimated parameter, obtained from averaging a set of Koehler and Hardover maneuvers, is indicated by the x. The error bars indicate the 1σ standard deviation of the averaged estimates.

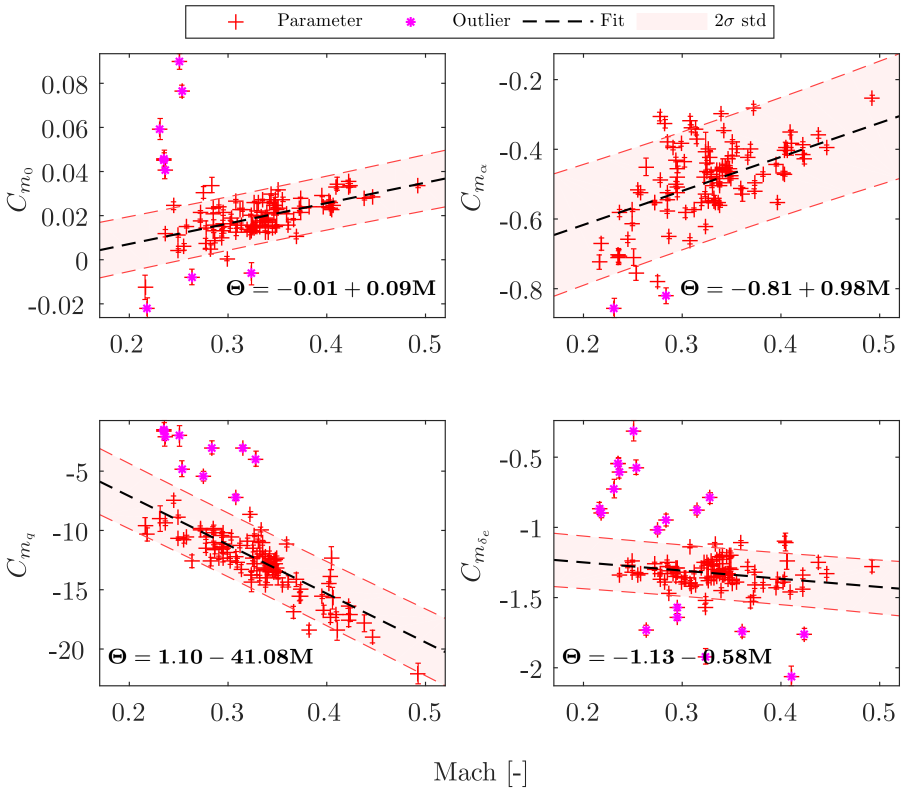

(a) C_m parameters versus M at an average altitude of 4900 m

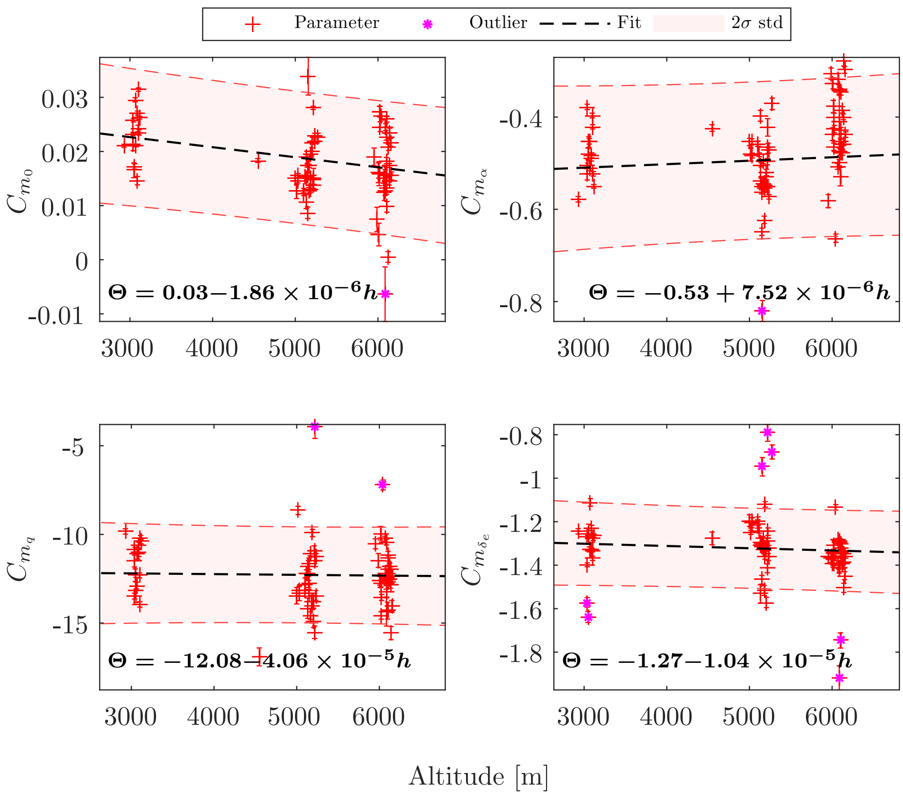

(b) C_m parameters versus h at an average Mach number of 0.31

Figure 8. Estimated parameters of the pitch rate C_m model, obtained from a collection 106 of longitudinally induced δ_e 3-2-1-1 and hardover maneuvers with the error bars indicating the uncertainty of the estimate, plotted versus the Mach number M and altitude h together with the robust least squares fit and its corresponding 2σ confidence bounds on the predicted output.

D. Model Validation

The identified models for all six non-dimensional forces and moments were applied to an independent validation data set consisting of 20% of the total data set. A comparison between the aircraft derived forces and moments, the least squares model and the DASMAT model which is currently implemented in the simulation framework is shown in Figure 9. In addition, fit statistics in terms of the coefficient of determination and the relative root mean square error (RRMSE) are tabulated in Table 9.

The identified model for C_X predicts the magnitude of the force more closely to the measured value than the DASMAT model for all of the validation sets. Worst performance of the least-squares model is observed during very large excitation of the C_X force as can be seen from close-up one in Figure 9(a). The same observation can be made for the C_Z and C_m models, also indicated in the first close-up of Figure 9(c) and Figure 9(e). In addition, the newly identified C_m model clearly performs better in terms of model bias.

Performance of the newly identified C_Y model and the DASMAT version is on par. However, the new least-squares model performs slightly better in the presence of large excitations. The same can be said about the C_l model. However, the new model performs better in predicting the bias of the output. On average, the C_n model was increased significantly when considering the coefficient of determination in Table 9. This is mainly reflected by the increased ability to predict the yaw moment in the absence of large excitation, especially because the current DASMAT model is well capable of predicting the magnitude of the non-dimensional yaw moment in case of large excitation.

A time-domain comparison between the new least-squares model and DASMAT for a longitudinally induced 3-2-1-1 maneuver is presented in Figure 10. The same can be found for a coupled Hardover maneuver in Figure 11. Both figures indicate an increased fidelity of the predicted aircraft states by the new least-squares model in comparison to the DASMAT model. Most significant is the better fit of the new model for the velocity in the direction of the X_b axis and the Euler angles.

Table 9. Fit statistics for the least squares model and the existing DASMAT (D) model averaged over all validation sets.

	C_X	C_Y	C_Z	C_l	C_m	C_n
R^2	0.76	0.77	0.77	0.75	0.76	0.85
R^2_D	0.60	0.55	0.64	0.25	0.00	0.50
RRMSE (%)	6.76	5.32	6.38	4.96	5.8	4.72
RRMSE_D (%)	8.79	7.34	7.97	8.65	12.65	8.50

VI. Discussion

In this paper a new high-fidelity aerodynamic model for the Cessna Citation II was identified using flight test data. For the first time, an explicit model structure was formulated by employing an orthogonal least squares model structure selection routine. Model identification was done by using the Two-Step Method. New in this method is the use of the Unscented Kalman Filter for an improved accuracy of the state estimates. After separate parameter estimation on more than 200 locally defined models, the resulting parameters were smoothed by using a plane fit, such that the estimated parameters can be described as a function of the Mach number and altitude. In addition, a comparison between the use of Koehler and Hardover control inputs in the framework of aerodynamic model identification was presented.

The flight path reconstruction procedure was applied to a total of more than 200 individual dynamic maneuvers. In general, the results obtained from the UKF in the framework of flight path reconstruction are in good agreement with the presented raw data. As discussed in previous sections, the choice for the UKF was made based on the ability of the UKF to cope with non-Gaussian noise in a better way than the EKF by employing a set of sample points to represent the state mean and covariance. Standard bounds for the state estimates show steady convergence, indicating high accuracy of the final estimate. Similarly, the bias estimates achieve steady-state values together with converged confidence bounds. Consistency of the filter estimates can be confirmed by the innovation sequences and their standard bounds. As observed, most innovation sequences stay within the confidence bounds with the exception of the altitude. The latter

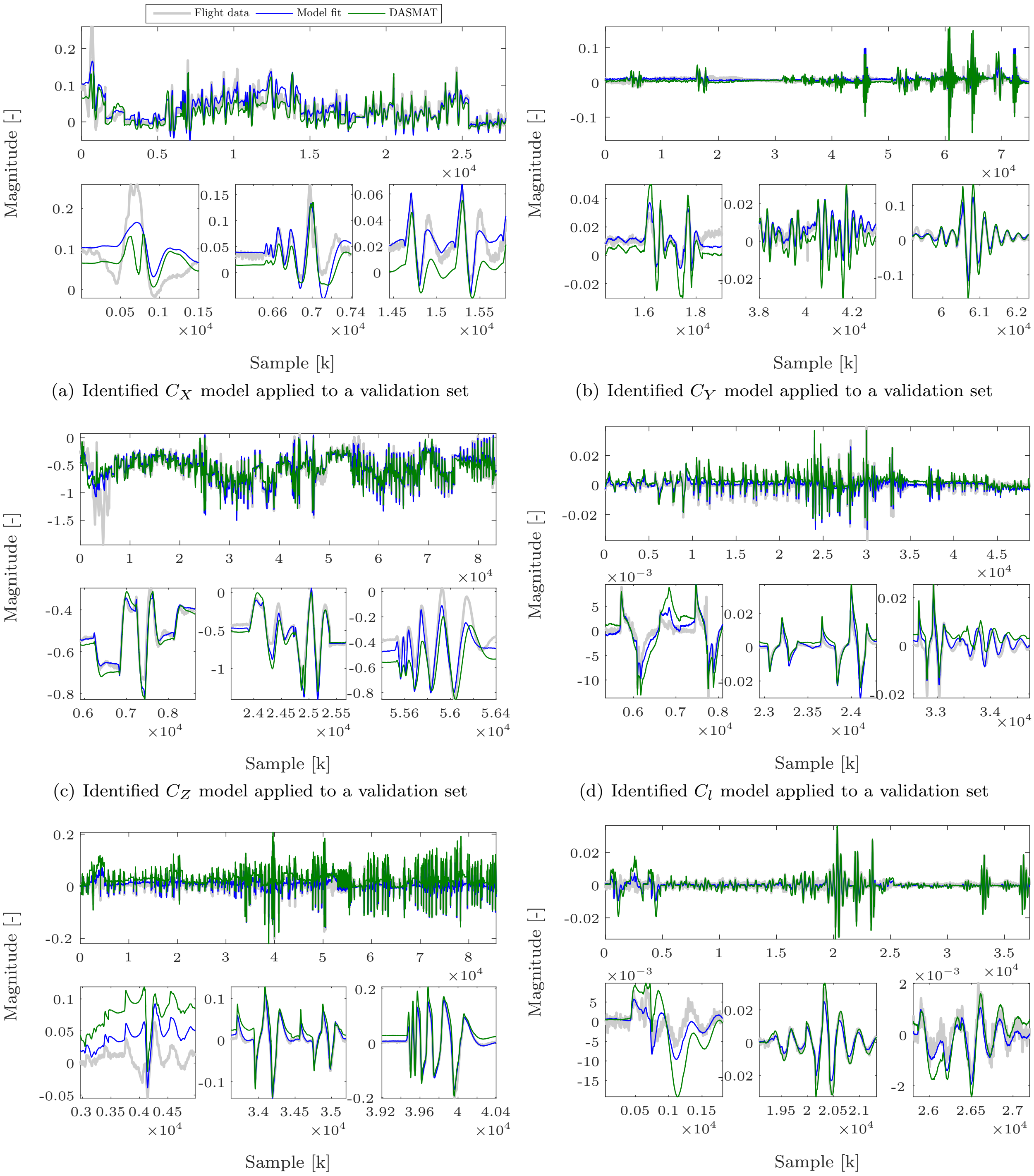

(a) Identified C_X model applied to a validation set

(b) Identified C_Y model applied to a validation set

(c) Identified C_Z model applied to a validation set

(d) Identified C_l model applied to a validation set

(e) Identified C_m model applied to a validation set

(f) Identified C_n model applied to a validation set

Figure 9. The identified models for the six non-dimensional forces and moments (blue) applied to validation data, consisting of 20% of the total data collection, in comparison with the currently implemented aerodynamic model in the DASMAT simulation framework (green) and the flight derived non-dimensional forces and moments (grey). For every model, three close-ups of interesting portions of the complete validation set are presented below each subplot.

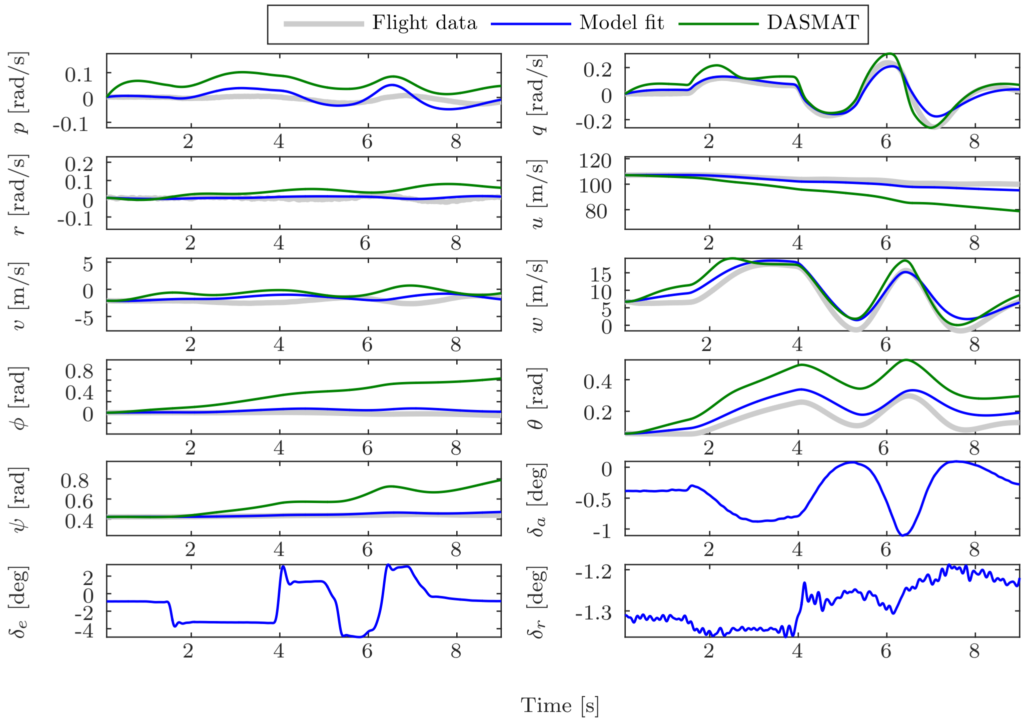

Figure 10. Time domain response of the newly implemented aerodynamic model together with the currently implemented aerodynamic model in the DASMAT simulation framework and the flight derived aircraft states and control surface deflections for a longitudinally induced δ_e 3-2-1-1 maneuver.

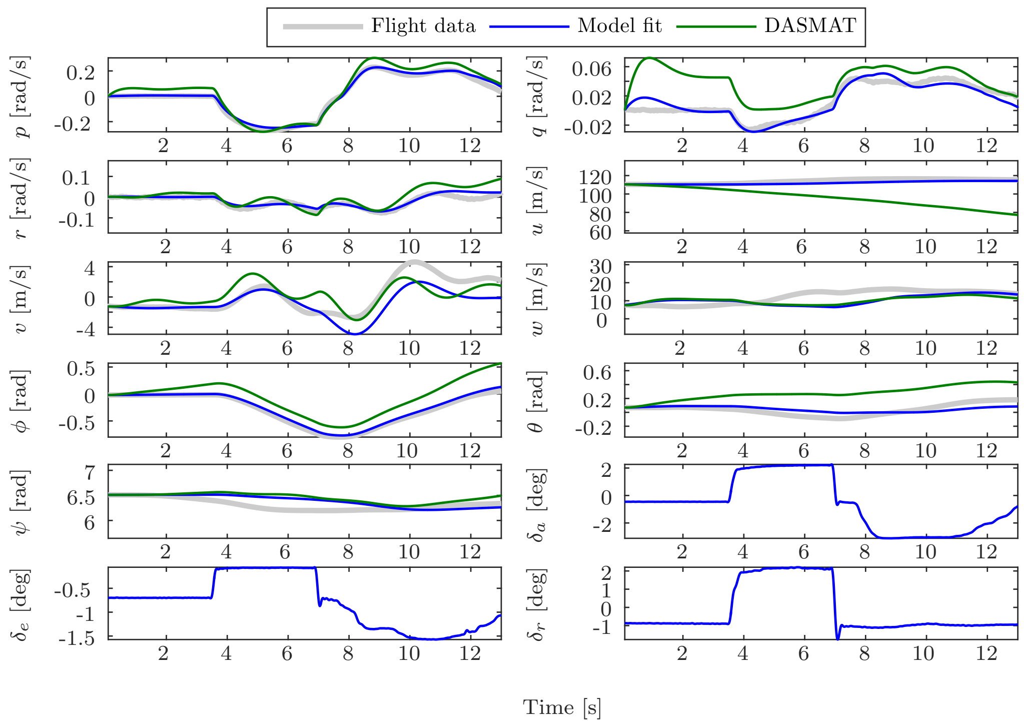

Figure 11. Time domain response of the newly implemented aerodynamic model together with the currently implemented aerodynamic model in the DASMAT simulation framework and the flight derived aircraft states and control surface deflections for a coupled δ_a, δ_e, δ_r Hardover maneuver.

is caused by the rather high uncertainty of the altitude measurement.

The model terms obtained from the orthogonal least squares model structure selection procedure confirm the earlier predicted non-linearities in the state-plane for longitudinal motion which are clearly more present in the model for the non-dimensional X_b force in the form of a term relating to α^2. Despite its clear presence in the majority of all locally defined models, identification of such a parameter has been proven impossible in terms of model parsimony. Due to collinearity of the squared regressor with its linear counterpart, which results in a high pair-wise correlation (over 0.9 in terms of the correlation coefficient, see Eq. (35)), a consistent identification of both parameters was impossible. This is a problem fully attributed to model parameter estimation with least squares. From the perspective of the goodness of fit, this parameter should be included as it marginally increased the fit statistic. However, from the perspective of parsimony, this term should not be included because of its high variance, indicative of a low accuracy parameter estimate. For the same reason, terms relating to the time rate of change of the angle of attack and the angle of sideslip ($\dot{\alpha}$ and $\dot{\beta}$) were not included in the model selection and parameter estimation procedures.

Similar observations can be made for the side force model C_Y. In contrast to the C_Z and C_m models, the C_X, C_Y and, to a lesser extent, the C_l and C_n models all contain non-linear terms and cross-interactions for some of the locally identified models. The latter observation confirms that significant non-linearities are present for the earlier mentioned models. In this context, generalization by assuming a fixed model structure for all locally defined models is not an appropriate measure in order to model small-scale dynamics requiring a more refined model structure capable of capturing all higher order non-linear dynamics. However, in the scope of this report and in the framework of aircraft simulation, the identification of a generalized baseline aerodynamic model governs. For this reason, consistency of the model parameter estimates is more important. In order to capture the higher order non-linearities more effectively, other modeling methods such as model identification by multi-variate splines, might offer a solution.

The approach that was used in this paper provides an adequate engineering solution to aerodynamic model identification from a series of flight test data. In addition, a form of continuity between the multiple locally identified models was created by regressing the coefficients versus the Mach number and altitude. It is important to realize that such an approach can only be used when the expected non-linearities in the corresponding state-plane are limited. In addition, the variation in the Mach number and altitude per identified local model should also be restricted in order to obtain valid results over the (M, h) range. Most of the plane fits showed rather large prediction intervals and the slope of the trend w.r.t. the altitude indicated that most of the parameters remain almost constant over altitude. However, drawing this conclusion might be premature because of the absence of sufficient measurements at different altitudes for the lateral models. These models can be improved by performing measurements at altitudes different than the ones presented in this paper. Nevertheless, a clear dependence of the parameters on the Mach number was observed.

Hardover maneuvers are maneuvers that are not specifically designed nor performed for the purpose of aerodynamic model identification. However, because of their large excitation of the aircraft's dynamics these maneuvers have potential to be used in the identification of a new model. Comparison of the estimated set of parameters by Koehler and Hardover maneuvers has indicated that the latter maneuvers can be used in an approach such as presented in this paper, i.e. a separate per maneuver identification followed by $(M - h)$ plane fit, because the average values of the Hardover maneuvers are close to the parameter estimates by Koehler control inputs. Note however that the estimates obtained from the Hardover maneuvers for the non-dimensional body forces show larger differences w.r.t. the estimates obtained from Koehler maneuvers with, in some cases, even a difference in sign. Overall, estimates obtained from Hardover inputs show a much larger uncertainty than their Koehler counterparts.

The main aim of this research project was to identify a new aerodynamic model for the Cessna Citation II laboratory aircraft. At the same time, the applicability of the high-fidelity aerodynamic model implemented in the existing simulation framework (Cessna Citation I) was investigated. Small differences between the DASMAT model and the newly identified model were observed for the representation of the non-dimensional body forces. The explained variance of these models was improved by at least 13%. More significant improvements, in terms of the coefficient of determination, were made to the model representing the moments around the body axes. These models were improved by an increase in the explained variance of at least 35%. Despite these clear improvements, it has also become evident that the available data is concentrated around a limited number of altitudes. This becomes especially clear when considering the lateral models, as data sets with sufficient excitation for aerodynamic model identification are focused around one altitude range. In order to improve these models and increase the region of validity, data collection at altitudes other than the ones presented in this paper should be given priority in future work. In addition, trim tab measurements should be performed during flight tests and parameters related to this measurement should be investigation for identifiability in order to further increase the fidelity of the simulation model. The simulation model presented in this paper will be used together with a stall and post-stall model, the result from a parallel research project,[3] in future research efforts into, e.g., pilot behavior during aerodynamic stall and the development of new control algorithms.

VII. Conclusion

As a result of new aviation legislation, from 2019 on all air-carrier pilots are obliged to go through flight simulator-based stall recovery training. For this reason, the C&S division set up a task force for the development of a new methodology for high-fidelity stall behavior and modeling. As part of this research effort, the current simulation framework and baseline model are to be updated with new models for the regular flight envelope and the stall and post-stall flight regimes for an increased fidelity and representation of the Cessna Citation II laboratory aircraft.

In this paper, the methodology regarding the identification of an aerodynamic model for flight simulation training from flight test data was developed for the normal post-stall flight envelope. By employing the Two-Step Method (TSM), the Unscented Kalman Filter (UKF) was used in cooperation with linear parameter estimation techniques. Results indicate that the state estimates and measurement reconstructions by the UKF are in good agreement with the presented data.

This research effort results in a simple and parsimonious set of aerodynamic models describing the 6 non-dimensional forces and moments. The model presented in this paper outperforms the current aerodynamic model implemented in the DASMAT framework in terms of goodness of fit, in all 6 degrees of freedom, when compared to the recorded forces and moments of the Cessna Citation II laboratory aircraft. The explained variance of the non-dimensional forces was increased with at least 13%. More significant improvements were made to the non-dimensional moments; an increase of the explained variance of at least 35% was achieved.

The work presented in this paper, together with the results from a parallel research project into the identification of a stall and post-stall model, will be used in future research into, e.g., the behavior of pilots during aerodynamic stall and the development of new control algorithms.

References

[1]Federal Aviation Administration, "Qualification, Service, and Use of Crewmembers and Aircraft Dispatchers," Tech. rep., U.S. Department of Transportation, 2013.

[2]Stroosma, O., van Paassen, M. M., and Mulder, M., "Using the SIMONA Research Simulator for Human-machine Interaction Research," *AIAA Modeling and Simulation Technologies Conference and Exhibit*, , No. August, 2003, pp. 5525–5525.

[3]van Horssen, L. J., *Aerodynamic Stall Modeling for the Cessna Citation II based on Flight Test Data*, Master's thesis, Delft University of Technology, 2016.

[4]van der Linden, C. A. A. M., *DASMAT - Delft University Aircraft Simulation Model and Analysis Tool*, Delft University Press, Delft, 1998.

[5]Mulder, J. A., Baarspul, M., Breeman, J. H., Nieuwpoort, A. M. H., Verbaak, J. P. F., and Steeman, P. S. J. M., "Determination of the mathematical model for the new Dutch government civil aviation flying school flight simulator," *Society of Flight Test Engineers, 18th Annual symposium*, Delft University of Technology, Amsterdam, 1987.

[6]Oliveira, J., Chu, Q. P., Mulder, J. A., Balini, H. M. N. K., and Vos, W. G. M., "Output error method and two step method for aerodynamic model identification," *AIAA Guidance, Navigation, and Control Conference and Exhibit*, , No. August, 2005, pp. 1–9.

[7]Nahi, N. E., *Estimation theory and applications*, John Wiley & Sons, 1969.

[8]Mulder, J. A., Chu, Q. P., Sridhar, J. K., Breeman, J. H., and Laban, M., "Non-linear aircraft flight path reconstruction review and new advances," *Progress in Aerospace Sciences*, Vol. 35, No. 7, 1999, pp. 673–726.

[9]Mulder, J. A., Sridhar, J. K., and Breeman, J. H., *Identification of Dynamic Systems- Applications to Aircraft Part 2: Nonlinear Analysis and Manoeuvre Design*, Vol. 3, North Atlantic Treaty Organisation, Neuilly Sur Seine, 1994.

[10]Julier, S. J. and Uhlmann, J. K., "A New Extension of the Kalman Filter to Nonlinear Systems," *International Symposium for Aerospace Defense Sensing Simulutation and Controls*, Vol. 3, No. 2, 1997, pp. 26.

[11]Höhndorf, L., Siegel, J., Sembiring, J., Koppitz, P., and Holzapfel, F., "Reconstruction of Aircraft Trajectories during Landing using a Rauch-Tung-Striebel Smoother, Instrument Landing System Deviation Information, and Taxiway Locations," *AIAA Atmospheric Flight Mechanics Conference*, , No. June, 2016, pp. 1–14.

[12]Teixeira, B. O. S., Tôrres, L. A. B., Iscold, P., and Aguirre, L. A., "Flight path reconstruction - A comparison of nonlinear Kalman filter and smoother algorithms," *Aerospace Science and Technology*, Vol. 15, No. 1, 2011, pp. 60–71.

[13]Cessna Aircraft Company, "Operating Manual Model 550 Citation II, Unit -0627 And On," Tech. rep., Wichita, Kansas, USA, 1990.

[14]Mulder, M., Lubbers, B., Zaal, P. M. T., van Paassen, M. M., and Mulder, J. A., "Aerodynamic Hinge Moment Coefficient Estimation Using Automatic Fly-by-Wire Control Inputs," *Proceedings of the AIAA Modeling and Simulation Technologies Conference and Exhibit, Chicago (IL)*, No. AIAA-2009-5692, 2009.

[15]Zaal, P. M. T., Pool, D. M., Postema, F. N., in 't Veld, A. C., Mulder, M., van Paassen, M. M., and Mulder, J. A., "Design and Certification of a Fly-By-Wire System with Minimal Impact on the Original Flight Controls," *Proceedings of the AIAA Guidance, Navigation, and Control Conference and Exhibit, Chicago (IL)*, No. AIAA-2009-5985, 2009.

[16]de Visser, C. C., Mulder, J. A., and Chu, Q. P., "Global Nonlinear Aerodynamic Model Identification with Multivariate Splines," *AIAA Atmospheric Flight Mechanics Conference*, AIAA, 2009.

[17]Klein, V. and Morelli, E. A., *Aircraft System Identification: Theory and Practice*, AIAA Education Series, Reston, VA, 2nd ed., 2006.

[18]Mulder, J. A., *Design and evaluation of dynamic flight test manoeuvres*, Ph.D. thesis, Delft, 1986.

[19]de Visser, C. C., *Global Nonlinear Model Identification with Multivariate Splines*, Ph.D. thesis, Delft University of Technology, Delft, 2011.

[20]Smyth, A. and Wu, M., "Multi-rate Kalman filtering for the data fusion of displacement and acceleration response measurements in dynamic system monitoring," *Mechanical Systems and Signal Processing*, Vol. 21, No. 2, 2007, pp. 706–723.

[21]Armesto, L., Chroust, S., Vincze, M., and Tornero, J., "Multi-rate fusion with vision and inertial sensors," *IEEE International Conference on Robotics and Automation, 2004. Proceedings. ICRA '04. 2004*, Vol. 1, 2004, pp. 193–199.

[22]Laban, M., *On-Line Aircraft Aerodynamic Model Identification*, Ph.d. thesis, Delft University of Technology, Delft, 1994.

[23]Sontag, E. D., "A concept of local observability," *Systems and Control Letters*, Vol. 5, No. 1, 1984, pp. 41–47.

[24]Walcott, B. L., Corless, M. J., and Zak, S. H., "Comparative study of non-linear state-observation techniques," *International Journal of Control*, Vol. 45, No. 6, 1987, pp. 2109–2132.

[25]Bennis, R. J. M., *Non-linear State Estimation Techniques with Application to Dynamic Modelling of Angle of Attack Vane from Cessna Citation II Flight Data*, Master's thesis, Delft University of Technology, Delft, 1998.

[26]Kalman, R. E., "A New Approach to Linear Filtering and Prediction Problems," *American Society of Mechanical Engineering - Journal of Basic Engineering*, Vol. 82, No. Series D, 1960, pp. 35–45.

[27]Julier, S. J. and Uhlmann, J. K., "Unscented filtering and nonlinear estimation," *Proceedings of the IEEE*, Vol. 92, No. 3, 2004, pp. 401–422.

[28]Chowdhary, G. and Jategaonkar, R., "Aerodynamic parameter estimation from flight data applying extended and unscented Kalman filter," *Aerospace Science and Technology*, Vol. 14, No. 2, 2010, pp. 106–117.

[29]Wan, E. A. and Van Der Merwe, R., "The unscented Kalman filter for nonlinear estimation," *Adaptive Systems for Signal Processing, Communications, and Control Symposium 2000. AS-SPCC. The IEEE 2000*, 2002, pp. 153–158.

[30]Van Der Merwe, R. and Wan, E. A., "The square-root unscented Kalman filter for state and parameter-estimation," *Acoustics, Speech, and Signal Processing, 2001. Proceedings. (ICASSP '01). 2001 IEEE International Conference on*, Vol. 6, 2001, pp. 3461–3464 vol.6.

[31]van der Merwe, R. and Wan, E. A., "Sigma-Point Kalman Filters for Integrated Navigation," *Proceedings of the 60th Annual Meeting of the Institute of Navigation (ION)*, 2004, pp. 641–654.

[32]Sibley, G., Sukhatme, G. S., and Matthies, L. H., "The Iterated Sigma Point Kalman Filter with Applications to Long Range Stereo," *Rss*, 2006.

[33]Armesto, L., Tornero, J., and Vincze, M., "On multi-rate fusion for non-linear sampled-data systems: Application to a 6D tracking system," *Robotics and Autonomous Systems*, Vol. 56, No. 8, 2008, pp. 706–715.

[34]Batterson, J. G. and Klein, V., "Partitioning of flight data for aerodynamic modeling of aircraft at high angles of attack," *Journal of Aircraft*, Vol. 26, No. 4, apr 1989, pp. 334–339.

[35]Klein, V., "Estimation of aircraft aerodynamic parameters from flight data," *Progress in Aerospace Sciences*, Vol. 26, No. 1, 1989, pp. 1–77.

[36]Morelli, E. A., "Global nonlinear parametric modelling with application to F-16 aerodynamics," *American Control Conference, 1998. Proceedings of the 1998*, Vol. 2, jun 1998, pp. 997–1001 vol.2.

[37]Morelli, E. and Derry, S. D., "Aerodynamic Parameter Estimation for the X-43A (Hyper-X) from Flight Data," *AIAA Atmosperic FlightMechanics Conference and Exhibit*, , No. August, 2005.

[38]Goldberg, M. A. and Cho, H. A., *Introduction to Regression Analysis*, WIT Press, Southampton, UK, 2003.

[39]Watson, P. K. and Teelucksingh, S. S., *A Practical Introduction to Econometric Methods: Classical and Modern*, University of the West Indies Press, 2002.

[40]Morelli, E. A., "Practical Aspects of the Equation-Error Method for Aircraft Parameter Estimation," *AIAA Atmospheric Flight Mechanics Conference*, , No. 6114, 2006, pp. 1–18.

[41]Klein, V., Batterson, J. G., and Murphy, P. C., "Determination of airplane model structure from flight data by using modified stepwise regression," Tech. rep., NASA Langley Research Center, Hampton, 1981.

[42]Lombaerts, T., Oort, E. V., Chu, Q. P., Mulder, J. A., and Joosten, D., "Online Aerodynamic Model Structure Selection and Parameter Estimation for Fault Tolerant Control," *Journal of Guidance, Control, and Dynamics*, Vol. 33, No. 3, 2010, pp. 707–723.

[43]Morelli, E., "Efficient Global Aerodynamic Modeling from Flight Data," *50th AIAA Aerospace Sciences Meeting including the New Horizons Forum and Aerospace Exposition*, Aerospace Sciences Meetings, American Institute of Aeronautics and Astronautics, jan 2012.

[44]Grauer, J. A. and Morelli, E. A., "Generic Global Aerodynamic Model for Aircraft," *Journal of Aircraft*, Vol. 52, No. 1, jul 2014, pp. 13–20.

Part II

Preliminary Thesis

Chapter 1

Introduction

As a result of new aviation legislation, from 2019 on all air-carrier pilots are obliged to go through flight simulator-based stall recovery training (Federal Aviation Administration, 2013). This implies that all aircraft dynamics models driving flight simulators must be updated to include accurate pre-stall, stall and post-stall dynamics. For this reason, the division of Control and Simulation has recently set up a task force to develop a new methodology for high-fidelity aircraft stall behavior modeling and simulation. This data is to be derived from flight test data from our Cessna Citation II laboratory aircraft and tested in our SIMONA simulator. At this moment, the C&S division uses a simulator model of the Cessna Citation known as the Delft University Aircraft Simulation and Analysis Tool (DASMAT) model as its baseline Citation aircraft model. This model does not include an accurate model for the aircrafts stall behavior. As part of this stall modeling research, a new high-fidelity flight simulation model of the Cessna Citation II laboratory aircraft will be developed, which will replace the current DASMAT model as baseline model.

1-1 Flight Simulation

Since the early beginnings of aviation and the successful construction of the first fixed-wing aircraft by the Wright brothers, the idea of learning to fly while remaining safely on the ground existed. Especially in the early beginnings, while most aircraft did not show the expected reliability, flight was a dangerous undertaking only reserved for true daredevils. The pilots of the first powered aircraft were trained by a series of exercises on real aircraft (Baarspul, 1990). While gradually proceeding to higher powered aircraft and while gradually gaining more control over the vehicle, one would ultimately become proficient in the art of flight. It was not long before the first ground based training devices were introduced. In contrast to the hydraulically driven full motion simulators these days, the first synthetic training devices were driven manually by the muscle force of the instructors to generate the required roll, pitch and yaw motion. After the beginning of the information age and with the availability of more advanced and powerful computer systems, flight simulation really took off and the modern simulator took form.

Nowadays, flight simulation is one of the major means in the training of pilots. Subjective fidelity, in other words, the sense of realism that is experienced by the subject, i.e. the pilot, is essential in that matter (Baarspul, 1990). In general, the following main areas of flight simulator applications can be identified (Baarspul, 1990; Allerton, 2010): (1) flight crew training, (2) research on the human-machine interface, (3) aircraft and equipment design, development, test and evaluation and (4) licensing, certification and accident investigation.

The replication of flight conditions in a simulator and the creation of subjective fidelity requires the simulator to be able to accurately simulate certain components of the aircraft. At the heart of every simulation are the equations of motion. These equations describe the aircraft's linear movement, rotations and orientation. The equations of motion are driven by the forces and moments created by the aircraft's aerodynamics, propulsion and inertia characteristics. These three components are represented by, respectively, the aerodynamic model, engine model and inertia characteristics of the aircraft which are determined by the structural properties of the aircraft and the gravitation of the central body. The importance of these models also stipulates the importance of aircraft model identification in the process of designing high-fidelity flight simulations.

In general, the design of a simulation model can be divided into a couple of phases. Roughly, these phases can be identified as: (1) simulation framework design, (2) identification and integration of the aerodynamic model into the framework and (3) extension of the simulation model by, e.g., an engine model and landing gear model. In the late 90s a similar flight simulation model was developed by Delft University of Technology to provide a high-fidelity representation of the Cessna Citation I (Van Der Linden, 1998). Since the upgrade of TU Delft's Cessna Citation I laboratory aircraft to the Citation II, the simulation model that was setup by Van der Linden became outdated. Fortunately, the simulation framework is modular, to a certain degree, and therefore allows for an easy upgrade of certain components such as the aerodynamic model. The main objective of this research is to provide a high-fidelity representation of the Citation II dynamics.

For this reason, the main contents of this report will be about the identification of a new aerodynamic model which is valid over the whole flight envelope. From an academic point of view, research into the aircraft dynamics is well-founded and therefore not interesting. New challenges arise from the integration of a stall model into the identified regular flight envelope aerodynamic model and the creation of a global, non-linear model.

1-2 Aircraft System Identification

The development of mathematical models for physical systems is of essential importance if we want to analyse and improve the performance of these systems. Mostly, these mathematical models are based on a limited number of observations. Experimental data is generally noisy and thus presents a challenging problem. The development of mathematical systems from input-output data is called system identification.

System identification, together with flight simulation and flight control, form the three general problems in aerospace flight dynamics and control (Klein & Morelli, 2006). The set of identification techniques available today can be used to characterize the aerospace vehicle's dynamics. The outcome of this identification process can be used for many ends, some of them include: verification of theoretical prediction and the development of much more accurate and comprehensive models for e.g. flight simulators which require extra accuracy or expansion of the flight envelope. Many advanced modern day flight control and stability augmentation techniques, such as fault-tolerant control (FTC) methods use system identification to estimate the parameters of a mathematical model and update the on-board model during flight. Hence, system identification can be considered as a very important in the branch of aircraft control & simulation.

System identification basically consists of three parts: (1) state estimation, (2) model structure selection and (3) parameter estimation. In flight it is essential to know the current state of the aircraft. State estimation is concerned with getting accurate estimates for the states. However, in some cases direct measurement of some states is difficult or even impossible. Reconstruction of these states from other sensor sources might provide a solution is such cases, i.e. sensor fusion. State estimation might also provide a more accurate and less biased estimate of the state vector and accompanying sensor biases.

Every mathematical models consists of a certain number of parameters. Parameter estimation techniques assume a fixed (mathematical) model structure, the process now consists of finding the unknown model parameters. This is done by estimators, functions of random variables that produce an estimate of the parameter(s). Many different ways of organizing the search for the best parameter exist. Difficulties that are encountered can include: evaluation of proper model structure and candidate models, accuracy of the model, computational efficiency. The first of these difficulties relates to the second general step of system identification: model structure selection. A proper selection of the model structure leads to the definition of model parameters, as used during the parameter estimation procedure.

Over the last decades, system identification has gained a lot of interest from industry and many advanced methods have been developed, ranging from model identification with Kalman filters (Klein & Schiess, 1977), maximum likelihood estimation (Klein, 1989) and stepwise regression (Klein, Batterson, & Murphy, 1981). The latter three methods as mentioned above have proven to be successful, however, these methods present the user with a complex non-linear optimization problem potentially with many local optima. Delft University of Technology made a major contribution to the collection of system identification methodology by developing the Two-Step Method (TSM). This method effectively reduced the the system identification problem into a non-linear state estimation problem and parameter estimation problem (Mulder, Chu, Sridhar, Breeman, & Laban, 1999). The first step of TSM consists of a flight path reconstruction by employing a Kalman filter. Since the introduction of the Kalman filter in the late 60s by Kalman (1960), the application became widespread and many new extensions were developed, e.g. (Julier & Uhlmann, 1997, 2004; Zhan & Wan, 2007; Armesto, Chroust, Vincze, & Tornero, 2004).

In first instance, when thinking of model identification, one would think of a process that is applied once. That is during the design of a mathematical model for any application. However, more recently system identification has also become a major part of aircraft control by utilizing recursive system identification methods such that the control system of the vehicle is able to cope with changes in, for example, geometry (Lombaerts, Oort, Chu, Mulder, & Joosten, 2010; Söderström, Ljung, & Gustavsson, 1978). The goal of system identification in this scope is to identify an (aerodynamic) model that is able to predict the forces and moments acting on the vehicle which can be used to define control laws. The application of system identification in recursive methods is not relevant to the research topic in this literature review and can therefore be ignored in the remainder of this document. Nevertheless, the theoretical constructs for both online and offline flight path reconstruction and parameter estimation are similar.

In the remaining step, using the output of the flight path reconstruction, the parameters of a model, whose structure is to be defined, are estimated. The latter procedure can be done by using one of the many available parameter estimation methods. Many linear methods, such as least-squares methods (Strejc, 1983), are available. However, these methods cannot always be applied. In the case of large uncertainties in the measurement vector it might be better to resort to methods which take the stochastic nature and accompanying probability density of the measurement and uncertainty of the dynamics into account, such as maximum likelihood methods (Lichota & Lasek, 2013; Klein, 1989).

In addition, the identification of a global aerodynamic model can be done by either (1) partitioning the whole flight envelope into smaller subspaces and by organizing the local models in look-up tables or by blending these subspaces together using, for example, spline interpolation (Van Oort, Sonneveldt, Chu, & Mulder, 2010; Klein, 1989). Or by (2) the more recently introduced global identification using multivariate splines (De Visser, Mulder, & Chu, 2009).

1-3 Research aims and objectives

In this section the research aims and objectives for the work that is to be performed as part of this thesis are presented. Additionally, the feasibility of this project within the given time frame is discussed.

1-3-1 Project Aims

The aim of this graduation project is to provide an upgraded high-fidelity modular aircraft simulation framework that can be used in future research to (1) investigate pilot behavior over the whole flight envelope including the stall and post-stall regime, and (2) design new advanced control algorithms. The development of the stall dynamics is part of another MSc research project and out of the scope of this project. However, during the execution of this project, the aim is provide an interface to fully integrate the post-stall dynamics from the other research project into the simulation framework that will be setup. An existing simulation framework for the Cessna Citation I aircraft was already designed in the late 90s (DASMAT) (Van Der Linden, 1998). This project aims to use the existing framework and upgrade or replace the individual components of the simulation program where necessary while preserving the modularity of the current implementation.

1-3-2 Objectives

In order to design a high-fidelity simulation model of the Cessna Citation II a couple of steps are required. As stipulated in Section 1, most research uses the so called Two-Step Method (TSM). The same method will be used in this research, implying that a flight path reconstruction and parameter estimation procedure will be executed. At a later stage the aerodynamic model must be integrated into the upgraded simulation framework together with the stall and post-stall dynamics. In short, the objective and sub-objectives can be stated as:

- **Design a high-fidelity simulation model of the Cessna Citation II aircraft, by validation of the existing aerodynamic model and identification of an upgraded aerodynamic model from the provided experimental flight data, which is valid over the normal, pre-stall flight envelope and integrate this model into the (upgraded/extended) DASMAT framework**.

    1. Perform flight path reconstruction (FPR) using the provided experimental data of the Cessna Citation II lab aircraft. For the FRP procedure, appropriate methods should be selected for the data preparation and the filtering itself.
    2. By selecting an appropriate model structure, the model parameters should be estimated by using an appropriate model parameter estimation method and by using the outcome of the flight path reconstruction procedure.
    3. Upgrade the existing DASMAT simulation framework by upgrading the individual components of the simulation framework such as the the equations of motion, engine model, mass model (see Chapter 2).
    4. Provide an interface for the extension of the baseline aerodynamic model with the stall and post-stall aerodynamics to obtain an accurate aerodynamic model that is able to simulate the stall and post-stall behavior.
    5. By performing a validation of the DASMAT simulation model with Citation II flight test data, the predictive capability of DASMAT w.r.t. the Citation II dynamics can be evaluated. Model components can be upgraded or replaced based on the outcome of this procedure.

1-3-3 Motivation & Feasibility

Currently, the Control & Simulation department of Delft University of Technology uses DASMAT as baseline simulation tool for the Cessna Citation I. The replacement of the Citation I by the Citation II has rendered the DASMAT simulation model inaccurate for the prediction of forces and moments, among others the suspected discrepancy between the predicted drag and actual drag of the Citation II. In addition to the mismatch w.r.t. the laboratory aircraft's dynamics, the current model does not contain a stall and post-stall model nor the interface to integrate such models into the simulation framework. The development of such stall models is out of the scope of this thesis, however, an interface for the integration of these models should be provided. For this reason, the current simulation framework is to be updated.

The motivation for the development of a high-fidelity Cessna Citation II simulation model is given by the requirement to being able to accurately reproduce the aircraft's dynamics over the full flight envelope for future research into, for example, pilot behavior during stall maneuvers and the design of advanced control algorithms. Up to this date, there is no (non-commercial) high-fidelity simulation of the Cessna Citation II that is able to accurately reproduce post-stall dynamics for the use in other research. Any stall model that is to be integrated into the updated framework will rely on a baseline model. A new aerodynamic model, representing the Citation II's dynamics is to be identified and validated by using flight test data. At the same time, this new model will act as baseline model in the upgraded simulation framework.

Research into the modeling of the whole flight envelope and post-stall dynamics has been a hot topic over the last few year, e.g. (Dias, 2015). With the availability of experimental data from previously recorded flights, the data required for system identification was already obtained. In addition, the existence of a simulation framework (DASMAT) should provide feasibility to successfully perform the project in the given time-frame. This framework will be discussed in more detail in Chapter 2.

Challenges that could affect the feasibility of this project concern the absence of flight test data in certain parts of the flight envelope. Currently, recordings of the aerodynamic angles are available within older data sets. However, large parts of the total data collection do not include recordings of the aerodynamic angles. It should be investigated if this data is usable for the purpose of aerodynamic model identification. In addition, recordings at only a few discrete locations in the flight envelope are available. Data acquisition in parts of the flight envelope with no previous recordings will aid in increasing the region of validity of any identified model. At later stages during the project the possibility to collect new data exists, however it is still unknown if there is enough budget to perform expensive and time consuming experimental flights.

Chapter 2

Simulation Framework - DASMAT

Currently, the baseline simulation framework that is being used in the Control & Simulation (C&S) department of the faculty of Aerospace Engineering, Delft University of Technology (DUT), is the Delft University Aircraft Simulation Model And Analysis Tool (DASMAT) (Van Der Linden, 1998). As part of this thesis, a validation and upgrade of the existing simulation framework will be performed. Mostly, this upgrade involves conversion of the old Simulink model block structure to a more contemporary and clearer format. In this chapter the current Simulation framework will be discussed together with a preliminary analysis of the problems associated with this model structure.

2-1 Current Structure DASMAT

The DASMAT software package was introduced in 1996 as the baseline simulation model of the C&S department of the faculty of Aerospace Engineering. While originally formulated as a generic non-linear aircraft simulation model, extension with the aerodynamic model of the Cessna Citation Ce500 and corresponding engine model allowed DASMAT to be used for the analysis and design of new control algorithms. Despite originally being developed with a Cessna Citation Ce500 aerodynamic model, DASMAT was intended to be extended with a Cessna Citation II model (Van Der Linden, 1998). However, up to date this upgrade has not been performed yet. The current Citation I model is the result of a flight test program executed for the development of mathematical models describing the aerodynamic forces and moments, engine performance characteristics, flight control systems and landing gear (Mulder et al., 1987).

Currently, DASMAT roughly consists of 8 blocks, divided as follows: (1) Airdata, (2) Wind model, (3) Aerodynamic Forces and Moments (AFM), (4) Engine Forces and Moments (EFM), (5) Gravity, (6) Landing Gear, (7) Equations of Motion (EQM) and (8) Observation model. An overview[1] of the current structure of DASMAT can be found in Figure 2-1. In this figure,

[1] For a more thorough overview of the overall structure of the simulation models and its individual components, the author suggests (Van Der Linden, 1998).

the output of the model are denoted by y, where y_{atm} and y_{ad} refer to outputs of the airdata model containing information about the atmospheric conditions, y_{wind} is the output of the wind model containing the wind direction and velocities defined in the Earth-Centered Earth-Fixed reference frame (ECEF) frame and y_{obs} is the output vector of the observation model. The state vector and its derivative are indicated by, respectively, x and $\dot{x}$ Most notably is the absence of a mass model, as currently DASMAT does not feature an accurate simulation of the mass and inertia properties. Mass properties, denoted by m and I, are currently used as constant input to the simulation model.

In addition to the lack of an accurate mass model, DASMAT suffers from the following deficiencies:

1. Most importantly, there is a mismatch with the laboratory aircraft dynamics, i.e. Citation I versus Citation II.
2. The current model assumes constant mass and inertia properties.
3. Initial analysis has indicated problems with the lateral acceleration in coordinated turns (see Section 2-2).
4. The model does not feature an accurate landing gear model and ground interaction model.
5. Overall, the model structure is obscure and the structure of the individual components, i.e. block-in-block, is outdated. Since its release in 1996, new functionality has been added to Simulink, allowing for the design of clearer simulation model components.
6. Initial analysis has shown a mismatch of the aircraft engine model with respect to the engine specification (see Section 2-3).
7. The drag model of the aerodynamic model incorporated into DASMAT is suspected to not accurately resemble the Citation II drag well enough.

Despite these deficiencies, DASMAT provides an excellent base for any simulation model. The general layout of the simulation framework is in agreement with standard conventions and allows for modularity up to a certain degree. The latter property is an important requirement that must be retained and possibly extended during the upgrade to a new framework.

In the following sections some of the deficiencies as listed above will be elaborated. In addition, an overview of the current aerodynamic model will be presented in Section 2-4.

2-2 Gravitation and Accelerations

In order to assess discrepancies in the accelerometer readings, as outputted by the DASMAT simulation model, an analysis of the accelerations is presented in this section. Currently DASMAT contains three outputs giving the accelerometer read-off in the x, y and z body-axis. The basic principle used in all accelerometers stems from the ability of the device to

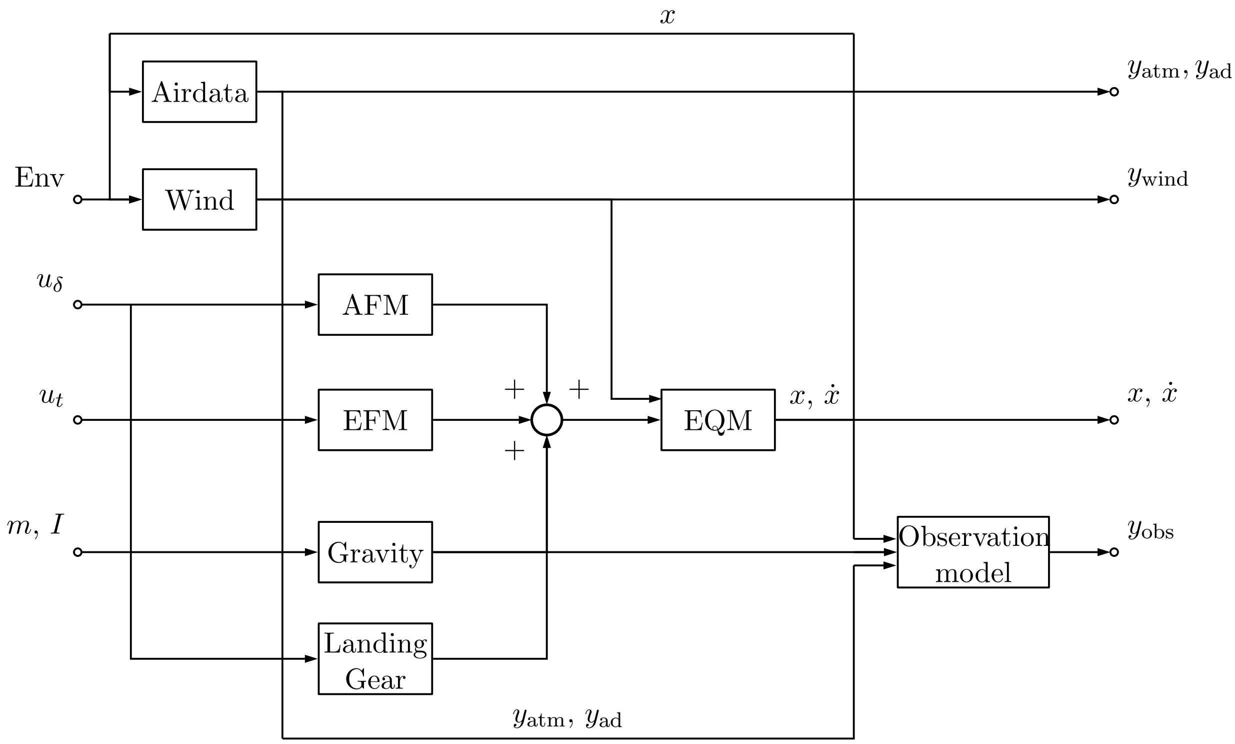

Figure 2-1: The current structure of the DASMAT simulation framework.

measure a force F required for preventing a proof mass from accelerating with respect to its carrier. This can either be done mechanically or by means of a magnetic or electrostatic field.

According to classical Newtonian mechanics, the acceleration is given as the sum of the acceleration of the proof mass and the gravitational force:

$$\mathbf{a} = \frac{\mathbf{F}}{m} + \mathbf{g} \equiv \mathbf{f} + \mathbf{g} \tag{2-1}$$

in which $\mathbf{f}$ indicates the specific force. Note that in Eq. (2-1) $\mathbf{g}$ is the component of the gravitational force. It now becomes evident that, in fact, accelerometers measure the specific force or proper acceleration, i.e. the acceleration w.r.t. free-fall $\mathbf{f}$ (Stevens & Lewis, 2003):

$$s\mathbf{f} = s\left(\mathbf{a} - \mathbf{g}\right) \tag{2-2}$$

where s is some scaling factor which can be ignored for now.

Analysis of the current DASMAT model has indicated discrepancies in the output of the accelerometer reading of the y-body axis, in other words, the specific force in y-body axis shows errors. The following situations[2] were identified:

1. When the aircraft is trimmed in a level turn, indicating non-wings-level constant-turn-rate flight at a load factor larger than one, the accelerometer indicated a zero-g reading

[2]Both situations were identified at an altitude of 2000 meters with a true airspeed of 90 m/s and an aircraft weight of 4500 kg.

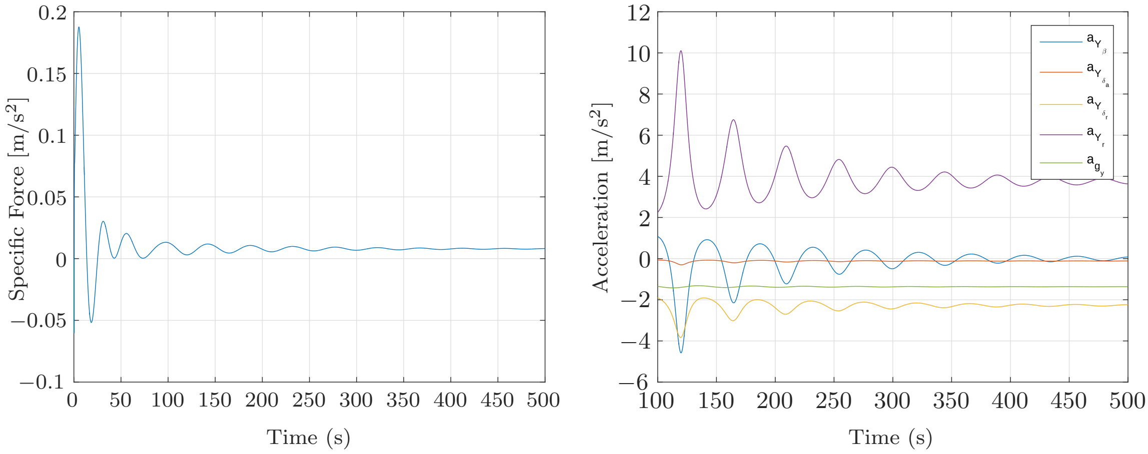

(a) Total specific force as measured by the accelerometer in the y-body axis.

(b) Components of the body acceleration and the gravitational acceleration in the y-body axis.

Figure 2-2: The time history of the specific force as output of the DASMAT simulation

in the y-body direction. The occurrence of this situation may be correct in case the acceleration caused by the body forces approximately equals the lateral component of the gravitational force. However, given the fact that the sideslip angle is not zero and by considering force equilibrium conditions it becomes apparent that such a situation cannot occur.

2. When steering the aircraft into a coordinated, zero-sideslip turn and while keeping the sideslip at zero the specific force indicated by the accelerometer in the y-body axis attains a non-zero value. By considering Eq. (2-2) it is expected for the accelerometer to show a zero reading since the aerodynamic force and lateral component of the gravitational force will cancel each other out. However, in reality `anyb` remains at an offset.

A coordinated turn is defined as a zero lateral acceleration turn. In the case of a symmetric aircraft this also implies zero sideslip angle. In the asymmetric case, the sideslip may not be exactly zero because of asymmetric thrust and the effects of angular momentum of spinning rotors (Stevens & Lewis, 2003). However, it can be verified that DASMAT simulates a perfectly symmetrical aircraft such that the latter case can be ignored.

Knowing that the sideslip angle goes to zero, it is possible to write Eq. (2-1) by writing a_y in components that contribute to the total acceleration. By assuming that the contribution of the aileron deflection to the accelerometer measurement in y_b is approximately zero and that the contribution of β goes to zero, the following equation is obtained:

$$f_y = \cancel{\frac{C_{Y_\beta}\beta}{m}}qS + \cancel{\frac{C_{Y_{\delta_a}}\delta_a}{m}}qS + \frac{C_{Y_{\delta_r}}\delta_r}{m}qS + \frac{C_{Y_r}r}{m}qS - g\sin\phi \tag{2-3}$$

By plotting the total specific force in Figure 2-2a and the individual components of the body acceleration in the Y-axis and the lateral component of the gravitational force, given by the terms from Eq. (2-3), in Figure 2-2b it becomes evident that the total specific force is not zero while maintaining a zero-sideslip coordinated-turn. In general, it can be stated that either the magnitude of the contribution of the rudder deflection to the y-body acceleration remains too small or the magnitude of the contribution of the yaw rate remains too large. Hence, the error causing the non-zero body acceleration is caused by a discrepancy in the model parameters $C_{Y_{\delta_r}}$ and C_{Y_r}.

2-3 Engine Model

The original DASMAT simulation model features an aircraft specific engine model in combination with a generic engine model extending the aircraft specific engine model with an atmospheric model (Van Der Linden, 1998). The aircraft at the heart of this report, the Cessna Citation II, is equipped with two small JT-15D turbofan engines built by the Pratt & Whitney corporation.

The engine state is determined by the aircraft specific engine model and usually contains the rotational rates of the fans and gas turbine. Inputs to the engine model are given by the full aircraft state vector $\mathbf{x}$ and the power lever setting (angle).

After initialization of the full aircraft model a trim procedure is required. In DASMAT this routine is performed by `trim_citation.m` and receives as input the desired aircraft's altitude, true airspeed or Mach number, desired flight path angle and other trim defining constraints such as the initial mass and trim tab deflections. By using a minimization heuristic which minimizes the value of the trim cost function, the final trim is obtained. During this procedure a separate engine trim is performed giving, as output, the engine state, thrust setting and thrust limit.

By defining a range of airspeeds and performing the exact same routine at different altitude settings, the trim procedure was repeated with a step size of 0.5 Mach. Initially, it was investigated if the trim procedure would choose an engine trim point below the maximum available thrust at the current altitude. The Matlab function was designed in such a way that any thrust demand above the maximum available thrust would result in a `NaN` return indicating that the demanded setting is not available. Figure 2-3 shows the required thrust T_{req}, following from the general aircraft trim, and the thrust limit as returned from the engine trim routine T_{lim}. In the same figure, the chosen engine trim point, i.e. the highest available thrust setting at the specific altitude, is indicated by the 'O' marker. Note that due to the limited resolution, for most entries this point lies well before the crossing point of the T_{req} and T_{lim} lines. The indication as given by Figure 2-3 shows that the engine trim procedure chooses the correct values of the thrust trim setting in terms of not returning values beyond the engine's limits.

Secondly, the thrust limit as returned by the engine trim procedure was compared with the theoretically available thrust from the engine manufacturer's specification (Pratt & Whitney Canada Incorporated, 1996). A comparison between the latter two indicated relatively large discrepancies. By evaluating Figure 2-4, the difference between the engine specification limit, indicated by T_{th}, and the thrust limit from the engine model, indicated by T_{lim}, becomes apparent. At all altitudes, except FL330, the maximum thrust produced by the engine model lies well below the thrust limit as indicated by the engine specification. Note that specifically

FL330 was included because problems were indicated at this flight level. Figure 2-4 indicates that the actual available thrust exceeds the specified limit.

The latter conclusion is indicative of shortcomings with the internal engine model structure. The identification of a new engine and propulsion model lies beyond the scope of this research. In practice however, it should be relatively straightforward to quickly implement an improved version of the engine model by using the data provided in (Pratt & Whitney Canada Incorporated, 1996).

2-4 General Aerodynamic Model

Currently, the aerodynamic model incorporated into the DASMAT simulation framework is a high-fidelity representation of the Cessna Citation I dynamics. A complete overview of this aerodynamic model and its parameters is given in Table 2-1 and continued in Table 2-2. It should be noted that the set of parameters is given in the wind axis reference frame. Hence, the general formulation of the aerodynamic model can be expressed as follows:

$$\mathbf{FM}_{ae} = \begin{bmatrix} C_D(\mathbf{x}_\mathrm{p}) & C_Y(\mathbf{x}_\mathrm{p}) & C_L(\mathbf{x}_\mathrm{p}) & C_l(\mathbf{x}_\mathrm{p}) & C_m(\mathbf{x}_\mathrm{p}) & C_n(\mathbf{x}_\mathrm{p}) \end{bmatrix} \tag{2-4}$$

where $\mathbf{x}_\mathrm{p}$ is a predefined state vector combining the individual elements that are required as input to the aerodynamic model. In DASMAT, this state vector required for the calculation of the individual parameters is defined as:

$$\begin{aligned} \mathbf{x}_\mathrm{p} = [&p \quad q \quad r \quad \alpha \quad \beta \quad h_E \quad h_{cg} \quad \delta_e \quad \delta_a \quad \delta_r \\ &\delta_{t_e} \quad \delta_{t_a} \quad \delta_{t_r} \quad \delta_{flap} \quad \text{gear} \quad x_{cg} \quad M \quad V_{eas}] \in \mathbb{R}^{18} \end{aligned} \tag{2-5}$$

where h_{cg} indicates the altitude of the center of gravity above the local surface, this is also referred to as the radio altitude. Furthermore, the state vector also contains more conventional variables such as the vector of rotational rates, aerodynamic angles, pressure altitude and Mach number. It is important to realize that the state vector required for the calculation of the parameters, i.e. interpolation from a set of look-up tables, differs from the general state vector, which is denoted by:

$$\mathbf{x} = \begin{bmatrix} p & q & r & V_\mathrm{TAS} & \alpha & \beta & h_E & x_E & y_E \end{bmatrix} \tag{2-6}$$

The drag model incorporates a total of 9 aerodynamic derivatives, each of these parameters is a function of the indicated variables in the Dependency column. The Multiplier column in Table 2-1 indicates the variable to multiply the parameter in order to obtain the non-dimensional force or moment contribution. In addition, sometimes the parameter receives a correction, for e.g. the ground effect, in such cases the name or value of these additional multipliers are shown in the same column. In general, for the non-dimensional forces, KBASD is a multiplier factor to account for the presence of the ground effect below a certain threshold altitude in the intercept term of the model. KGEHDR applies the same correction to the flap effectiveness at near ground altitudes. KUUT is a correction factor to incorporate the effect of a gear extension.

These correction factors can also be used to correct other parameters, as indicated in Table 2-1. The model parameters for the non-dimensional pitching moment, C_m as indicated in Table 2-2, have three more correction factors in addition to the earlier presented ones. AELPHA is a correction factor to the elevator effectiveness to incorporate for mixed angle of attack and flap effects. KEMEAS and KQXM are correction factors for, respectively, the equivalent airspeed and changes in CG position.

From Table 2-1 and Table 2-2 it also becomes apparent that the current model structure has been referred to as obscure and obsolete. In addition to multiple parameters that can effectively be organized in single look-up tables, the aerodynamic model also features a series of corrections. The use of the current model for the analysis of control algorithms is possible, however, when considering the internal mechanics of the model, overview is quickly lost. In addition, extensions to the current model structure are harder to incorporate.

2-5 DASMAT Upgrade

As part of this thesis work, a feasibility study was performed concerning the upgrade possibilities of the DASMAT simulation framework. Despite the possibilities that come with model development from scratch, such as a complete overhaul of the model's internal mechanics, trim procedure etc., this approach will also consume a large amount of time. In addition, such an approach should also be questioned because it might not be necessary to completely overhaul the given model. Given the limited time frame, upgrades of individual components of the existing simulation framework seems like a more plausible option. Despite its obscurity at some points, the overall structure of the model agrees with the general aerospace conventions. In addition, the current structure allows for modularity, enabling the future integration of additional components such as the post-stall aerodynamic model.

In order to facilitate the upgrade of the individual simulation framework components, a classification was made based on the amount of work and importance of each block. An overview of this classification is presented in Figure 2-5. Red indicates a high priority upgrade and green a lower priority upgrade. Blue is the classification for a normal priority upgrade.

As mentioned before, DASMAT currently features a Cessna Citation I aerodynamic model. In order to math the laboratory aircraft's dynamics, an upgrade will be made to the existing aerodynamic model using system identification techniques. The remain of this report will elaborate on that subject. This upgrade must be considered as the most comprehensive part of the upgrade process. For this reason, the AFM block is shown in red, indicating a high priority upgrade.

Deficiencies with the EFM block were found in the analysis presented in the previous section. However, the engine block forms it own set of subsystems and corresponding engine model. A complete overhaul of this subsystem is therefore excluded from this thesis. In addition to the upgrade of the general structure of some blocks, the same can be done for the engine block allowing easier future upgrades of its subsystems. At the same time, if some spare time is available, any improvements to the engine block would be welcome. The other blocks that have received the normal priority upgrade label are the airdata, gravity, observation model and EQM blocks. In most cases, these blocks will only receive an upgrade to the new embedded Matlab function block format. Re-routing of the wind data streams might be a possibility when changing the aerodynamic model incorporated in DASMAT, since the current AFM block requires inputs from the wind and turbulence models in the calculation of gust derivatives.

In addition to the changes presented above, a readily-available mass model based on splines (De Visser et al., 2009) will be integrated in the simulation framework. This upgrade deprecates the mass and inertia input port of the current model. The addition of an output port enables the ouput of mass properties. The ouput of the mass model should also be redirected to the AFM, EFM, Gravity and Landing gear blocks, since these block require mass properties for the calculation of forces and moments. The latter changes have also been depicted in Figure 2-5.

The low-priority upgrade label, indicated in green, is given to the Wind and Landing Gear blocks. The upgrade of the first block can be done parallel to any other upgrade process due to its simplicity while the landing gear forms its own set of systems and subsystems and can therefore be considered as out of the scope.

2-6 Conclusion

In this chapter an overview of the DASMAT simulation framework was presented. This framework is currently being used at the C&S department of the faculty of Aerospace Engineering as the baseline simulation model. This model is governed by a set of model parameters which closely resemble the Cessna Citation I dynamics. Since the upgrade of the laboratory aircraft, now a Cessna Citation II, there is a mismatch between the laboratory aircraft's dynamics and the model incorporated in DASMAT. For this reason an upgrade of the existing simulation framework is required.

In order to facilitate the upgrade of the aerodynamic model and to make the simulation framework future-proof, an overall upgrade of the framework is desired. As part of this thesis, a feasibility study was performed into the possibilities for this upgrade. In addition, early analysis has indicated problems with several components of the current framework. Where the aerodynamic force and moments block requires a complete overhaul and newly identified model, the engine forces and moments form its own set of systems and subsystems. Any upgrades to the latter set of routines are out of the scope of this report, however, they do require attention in future upgrades. Most importantly, as part of this thesis, all simulation subsystems are planned to be converted to the new embedded Matlab function block format, allowing for simple upgrades and greatly enhancing the general overview of the model. Currently, DASMAT forms a set of complex systems and subsystems, in particular the structure of the aerodynamic model is obscure and outdated.

Optionally, the state representation of the model will be changed as it is currently represented by the true airspeed and the aerodynamic angles. The upgrade of the landing gear model itself is considered out of the scope of this thesis, however, if any improved model is available, integration of such a block will be included.

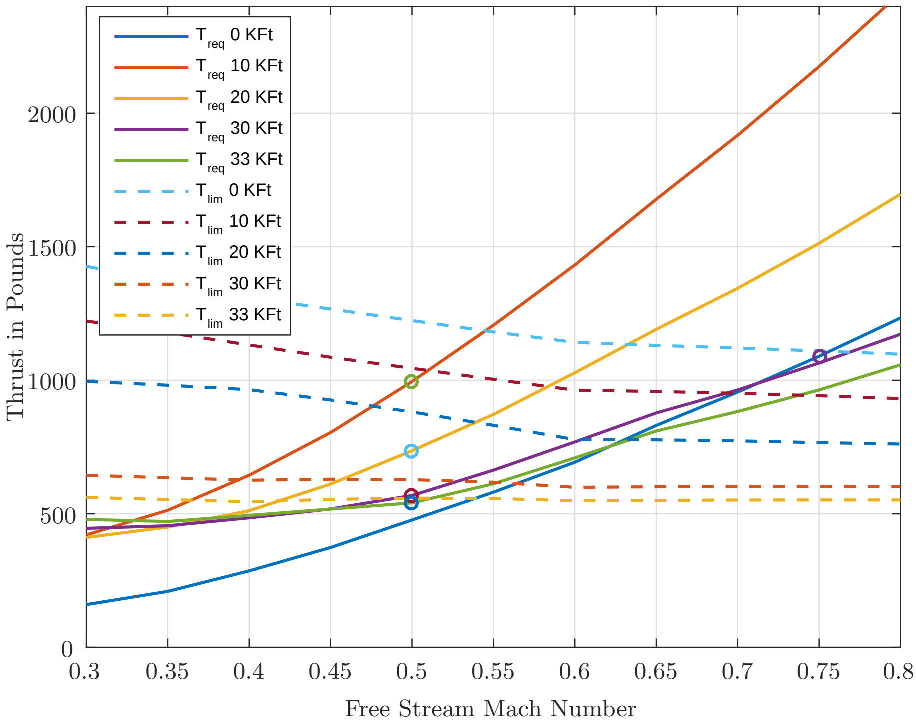

Figure 2-3: The required thrust T_{req} and thrust limits T_{lim} obtained from the aircraft and engine trim routine for different altitudes. The 'O' marker indicates the actual thrust setting.

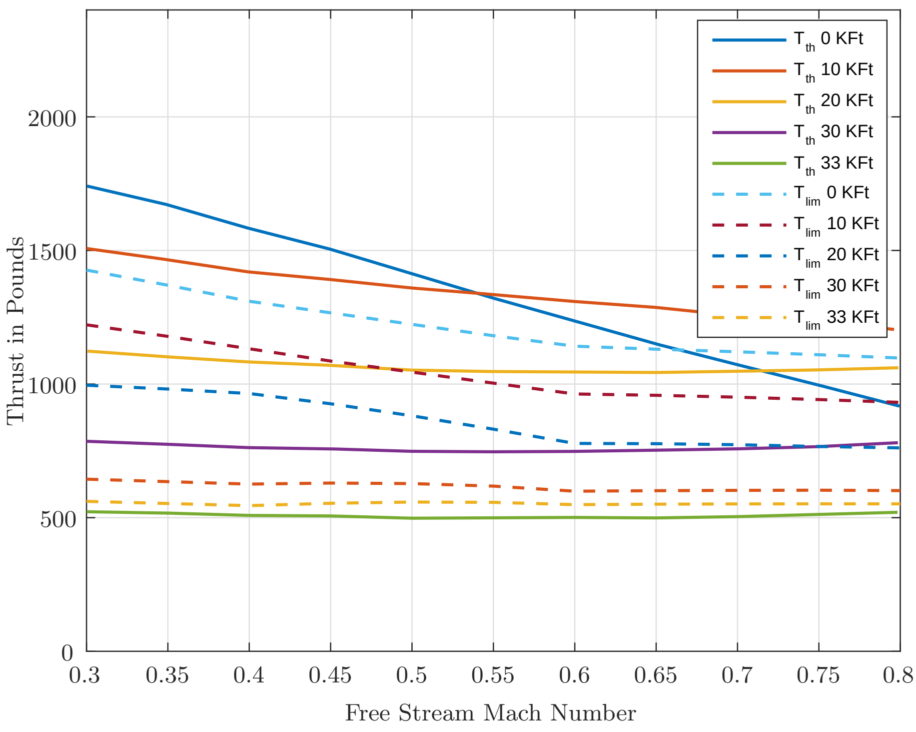

Figure 2-4: The thrust limits obtained from the engine trim routine T_{lim} versus the theoretical thrust limits as indicated in the engine specification manual T_{th}

Estimator	Parameter	DASMAT ID	Dependency	Multiplier	Comments
C_D	$C_{D_{\alpha,M}}$	CDAM	α, M	-	Base drag coefficient
	$C_{D_{\alpha,\delta_{flap}}}$	CDAF	α, δ_{flap}	KBASD	Base drag coefficient
	$C_{D_{\delta_e}}$	CDEAF	α, δ_{flap}	δ_e	Elevator effectiveness
	$C_{D_{\alpha,\delta_a}}$	CDWAW	α, δ_a	-	Constant
	$C_{D_{\beta,\delta_{flap}}}$	CDBBF	β, δ_{flap}	-	Constant
	C_{D_q}	CDQAF	α, δ_{flap}	$\frac{q\bar{c}}{V}$	
	$C_{D_{r^2}}$	CDRUAF	α, δ_{flap}	$\frac{rb}{2V}^2$	
	$C_{D_{gear}}$	CDUAF	α, δ_{flap}	$[0,1]$ (KUUT) gear	Gear parameter
	$C_{D_{ground}}$	CDGAF	α, δ_{flap}	h_{radio} (KGEHDR)	Ground effect
C_Y	$C_{Y_{\beta_{\alpha,\delta_{flap}}}}$	CYBAF	α, δ_{flap}	β	
	$C_{Y_{\beta_{\alpha,\beta}}}$	CYBAB	α, β	β	
	$C_{Y_{\delta_a}}$	CYWAF	α, δ_{flap}	δ_a	Aileron effectiveness
	$C_{Y_{\delta_r}}$	CYRUAF	α, δ_{flap}	δ_r	
		LSFACT	δ_r	δ_r	
	C_{Y_r}	CYRAF	α, δ_{flap}	$\frac{rb}{2V}$	
	$C_{Y_{gear}}$	CYBUAF	α, δ_{flap}	$[0,1]$ KUUT gear	Gear parameter
C_L	$C_{L_{\alpha,M}}$	CLAM	α, M	-	Base lift coefficient
	$C_{L_{\alpha,\delta_{flap}}}$	CLAF	α, δ_{flap}	-	Base lift coefficient
	$C_{L_{\delta_{e_{\alpha,M}}}}$	CLEAM	α, M	δ_e	
	$C_{L_{\delta_{e_{\alpha,\delta_{flap}}}}}$	CLEAF	α, δ_{flap}	δ_e	
	$C_{L_{q_{\alpha,\delta_{flap}}}}$	CLQAF	α, δ_{flap}	$\frac{q\bar{c}}{V}$	
		KQXL	x_{cg}	$\frac{q\bar{c}}{V}$	
	$C_{L_{gear}}$	CLUAF	α, δ_{flap}	$[0,1]$ (KUUT)	Gear parameter
	$C_{L_{q_{gear}}}$	CLQUAF	α, δ_{flap}	$\frac{q\bar{c}}{V} \cdot [0,1]$ (KUUT)	Gear parameter, pitch
	$C_{L_{ground}}$	CLGAF	α, δ_{flap}	h_{radio}	Ground effect
		CLGEAF	α, δ_{flap}	h_{radio}	Ground effect
C_l	$C_{l_{\beta_{\alpha,\delta_{flap}}}}$	CIBAF	α, δ_{flap}	β	
	$C_{l_{\beta_{M,h_e}}}$	CIBMH	M, h_e	β	
	$C_{l_{\beta_{\alpha,\beta}}}$	CIBAB	α, β, δ_{flap}	β	
	$C_{l_{\delta_a}}$	CIWAF	α, δ_{flap}	δ_a	
	$C_{l_{\delta_{r_{\alpha,\delta_{flap}}}}}$	CIRUAF	α, δ_{flap}	δ_r	
	$C_{l_{\delta_{r_{M,h_e}}}}$	CIRUMH	M, h_e	δ_r	
	$C_{l_{trim}}$	CIWTAM	α, M	δ_{t_a}	Aileron trim tab
	$C_{l_{p_{\alpha,\delta_{flap}}}}$	CIPAF	α, δ_{flap}	$\frac{pb}{2V}$	
	$C_{l_{p_{M,h_e}}}$	CIPMH	M, h_e	$\frac{pb}{2V}$	
	C_{l_r}	CIRAF	α, δ_{flap}	$\frac{rb}{2V}$	
	$C_{l_{ground}}$	LROLL	δ_{flap}	$\beta \cdot h_e$	Ground effect

Table 2-1: DASMAT aerodynamic model parameters

Estimator	Parameter	DASMAT ID	Dependency	Multiplier	Comments
C_m	$C_{m_{\alpha,M}}$	`CMAM`	α, M	-	Base moment
	C_{m_α}	`CMAF`	α, δ_{flap}	-	Base moment
	$C_{m_{\delta_{e_{\alpha,M}}}}$	`CMEAM`	α, M	$\delta_e \cdot \text{EALPHA} \cdot \text{KEMEAS}$	
	$C_{m_{\delta_{e_{\alpha,\delta_{flap}}}}}$	`CMEAF`	α, δ_{flap}	$\delta_e \cdot \text{EALPHA} \cdot \text{KEMEAS}$	
	$C_{m_{\delta_{r,\beta}}}$	`CMRBR`	β, δ_r	-	Constant
	$C_{m_{\delta_{t_e}}}$	`CMETAM`	α, M	δ_{t_e}	
	$C_{m_{\beta,\delta_{flap}}}$	`CMBBF`	β, δ_{flap}	-	Constant
	C_{m_q}	`CMQAF`	α, δ_{flap}	$\frac{q\bar{c}}{V} \cdot \text{KQXM}$	CG correction
	$C_{m_{q_{\alpha,\delta_{flap}}}}$	`CMQUAF`	α, δ_{flap}	$\frac{q\bar{c}}{V} \cdot \text{KUUT}$	Gear parameter
	$C_{m_{\delta_{e_{\alpha,\delta_{flap}}}}}$	`CMEUAF`	α, δ_{flap}	$\delta_e \cdot \text{KUUT}$	Gear parameter
	$C_{m_{ground}}$	`CMGAF`	α, δ_{flap}	h_{cg}	Ground effect
	$C_{m_{ground}}$	`VDOMMYR38`	δ_{flap}	$\alpha \cdot h_{cg}$	Ground effect
	$C_{m_{ground}}$	`LFCMEGAF`	α	$\delta_e \cdot h_{cg}$	Ground effect
	$C_{m_{ground}}$	`KGEMEAS`	V_{EAS}	$\delta_e \cdot h_{cg}$	Ground effect
C_n	$C_{n_{\beta_{\alpha,\delta_{flap}}}}$	`CNBAF`	α, δ_{flap}	β	
	$C_{n_{\beta_{M,h_e}}}$	`CNBMH`	M, h_e	β	
	$C_{n_{\beta_{\alpha,\beta}}}$	`CNBAB`	α, β	β	
	$C_{n_{\delta_{a_{\alpha,\delta_{flap}}}}}$	`CNWAF`	α, δ_{flap}	δ_a	
	$C_{n_{\delta_{a_{M,h_e}}}}$	`CNWMH`	M, h_e	δ_a	
	$C_{n_{\delta_r}}$	`CNRUAF`	α, δ_{flap}	δ_r	
	$C_{n_{\delta_{t_r}}}$	`CNRTAM`	α, M	δ_{t_r}	
	$C_{n_{p_{\alpha,\delta_{flap}}}}$	`CNPAF`	α, δ_{flap}	$\frac{pb}{2V}$	
	$C_{n_{p_{M,h_e}}}$	`CNPMH`	M, h_e	$\frac{pb}{2V}$	
	C_{n_r}	`CNRAF`	α, δ_{flap}	$\frac{rb}{2V}$	

Table 2-2: DASMAT aerodynamic model parameters - Continued

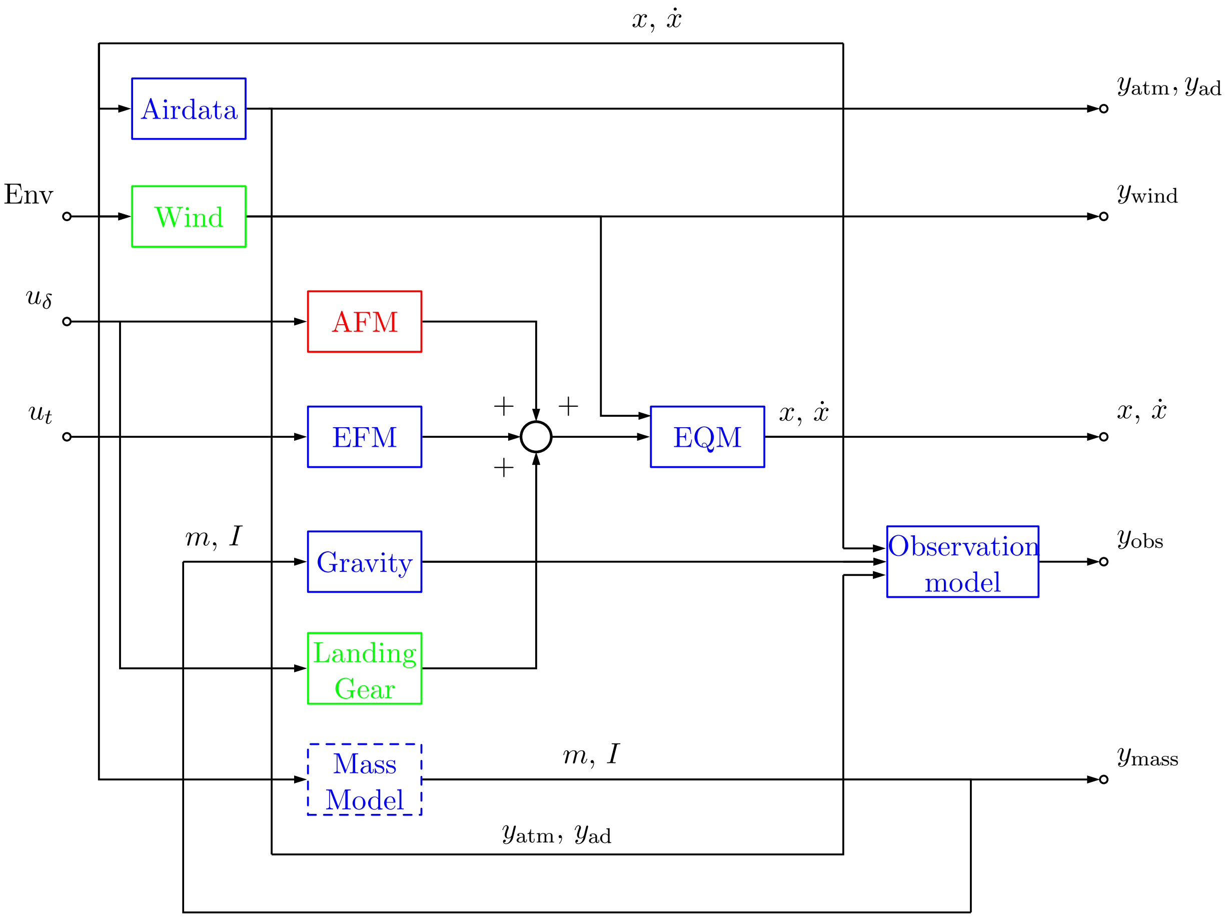

Figure 2-5: The structure of the current simulation framework DASMAT together with the upgrade classification indicates per block, where red indicated a high priority upgrade, blue a normal priority upgrade and green a low priority upgrade.

Chapter 3

Equations of Motion

3-1 Introduction

The equations of motion form the heart of any simulation. These equations, describing the vehicle's motion with respect to any given reference frame, are subdivided into three smaller sets of equations describing, respectively, (1) the translational motion, (2) the rotational motion and (3) the attitude of the local frame with respect to the central frame. These frames can be oriented in any given direction. However, for uniformity and simplicity it is common to only use conventional aerospace reference frames. An overview of these frames is presented in Appendix III, this provides a simplified derivation of the equations of translational motion, rotational motion and the attitude equations.

3-2 Equations of Translational Motion

Starting with Newton's laws of motion, the motion of a mass-varying non-rigid body can be described as (Mulder, Van Staveren, & Van der Vaart, 2000):

$$\mathbf{F}^I_{\text{ext}} = m\frac{d^2\mathbf{r}^I_{\text{cm}}}{dt^2} + 2\boldsymbol{\Omega}^I_{bI} \times \int\limits_m \frac{\delta\tilde{\mathbf{r}}}{\delta t}dm + \int\limits_m \frac{\delta^2\tilde{\mathbf{r}}}{\delta t^2}dm \tag{3-1}$$

where $\frac{\delta}{\delta t}(\cdot)$ denotes a derivative of a vector quantity taken in the local frame, in contrast to $\frac{d}{dt}(\cdot)$, which expresses the derivative of a vector quantity in inertial space F_I. **tilder** is the location of the mass element w.r.t. the center of mass and $\mathbf{r}^{\text{I}}_{\text{cm}}$ the location of the center of mass with respect to the inertial frame. Note that vector quantities are indicated by bold typesetting. The individual components of Eq. (3-1) can be identified as the total of the external forces, the acceleration of the center of mass, the contribution of the Coriolis force due to time variations in the mass distribution and the relative force.

Eq. (3-1) gives the external force produced by the individual components of the force equation with respect to inertial space. By considering a vehicle with a fixed mass, moving with velocity $\mathbf{V}_C$ with respect to the ECEF, denoted by F_C, and at a distance $\mathbf{r}_{cm}^C$ from the origin of the reference frame, i.e. the center of the rotating body, the translational motion of a point mass with respect to rotating frame F_C is given by:

$$\mathbf{F}_{\text{ext}}^C = m\frac{d^2\mathbf{r}_{\text{cm}}^C}{dt^2} + 2m\mathbf{\Omega}_{CI}^C \times \frac{d\mathbf{r}_{cm}^C}{dt} + m\mathbf{\Omega}_{CI}^C \times \left(\mathbf{\Omega}_{CI}^C \times \mathbf{r}_{cm}^C\right) \tag{3-2}$$

The position of the aircraft with respect to F_C can easily be obtained by using the following kinematic relationship:

$$\frac{d\mathbf{r}_{cm}^C}{dt} = \mathbf{V}_C \tag{3-3}$$

After reformulation and expressing the velocity vector, position vector, rotation vector and external forces with respect to the navigation frame or North-East-Down reference frame (NED) F_E, the dynamic equations of translation motion are given by:

$$\begin{aligned}
\dot{V}_N &= \frac{F_x^E}{m} - 2\Omega_t V_E \sin\delta - \Omega_t^2 R \sin\delta\cos\delta - \frac{V_E^2\tan\delta - V_N V_D}{R} \\
\dot{V}_E &= \frac{F_y^E}{m} + 2\Omega_t\left(V_D\cos\delta + V_N\sin\delta\right) + \frac{V_E}{R}\left(V_N\tan\delta + V_D\right) \\
\dot{V}_D &= \frac{F_z^E}{m} + 2\Omega_t V_E\cos\delta - \Omega_t^2 R\cos^2\delta - \frac{V_E^2 + V_N^2}{R}
\end{aligned} \tag{3-4}$$

where Ω_t denotes the angular velocity of the central body with respect to inertial space. In this case the central body referred to is Earth which rotates with approximately 7.29×10^{-5} radians per second. The location of the aircraft center of gravity relative to earth is expressed in spherical polar coordinates with δ denoting the latitude.

By expressing the equations of translational motion in the body frame and using the identity in Eq. (3-5) to express the time-rate of change of the velocity in the body frame

$$\left.\frac{d\mathbf{V}_G}{dt}\right|_E^b = \left.\frac{d\mathbf{V}_G}{dt}\right|_b^b + \mathbf{\Omega}_{bE}^b \times \mathbf{V}_b \tag{3-5}$$

where $\mathbf{V}_b$ is defined as $(u, v, w)^T$, i.e. the aerodynamic velocity components expressed in the body frame. Expansion and simplification of Eq. (3-5) finally results in the the set of equations relation the force components in the body frame to the rotational rates and angular orientation of the body. This set of equations is given by:

$$\begin{aligned}
X &= m\left(\dot{u} + qw - rv\right) + mg\sin\theta \\
Y &= m\left(\dot{v} + ru - pw\right) - mg\cos\theta\sin\phi \\
Z &= m\left(\dot{w} + pv - qu\right) - mg\cos\theta\cos\phi
\end{aligned} \tag{3-6}$$

3-3 Equations of Rotational Motion

The general formulation of the equations of rotational motion, for a vehicle which is moving w.r.t. to an inertial frame, is given by (Mulder et al., 2000):

$$\begin{aligned}\mathbf{M}^b_{\mathrm{cm}} = \int\limits_m \tilde{\mathbf{r}} \times \left(\frac{d\boldsymbol{\Omega}^b_{bI}}{dt} \times \tilde{\mathbf{r}}\right) dm + \int\limits_m \tilde{\mathbf{r}} \times \left[\boldsymbol{\Omega}^b_{bI} \times \left(\boldsymbol{\Omega}^b_{bI} \times \tilde{\mathbf{r}}\right)\right] dm + \\ 2\int\limits_m \tilde{\mathbf{r}} \times \left(\boldsymbol{\Omega}^b_{bI} \times \frac{\delta\tilde{\mathbf{r}}}{\delta t}\right) dm + \int\limits_m \tilde{\mathbf{r}} \times \frac{\delta^2\tilde{\mathbf{r}}}{\delta t^2} dm\end{aligned} \tag{3-7}$$

Knowing that the angular momentum for a rigid body around the center of mass can also be written as:

$$\mathbf{B_{cm}} = \mathbf{I} \cdot \boldsymbol{\Omega} \tag{3-8}$$

the time-derivative of Eq. (3-8) then gives the rotational motion vector

$$\mathbf{M_{cm}} = \frac{\delta \mathbf{B_{cm}}}{\delta t} + \boldsymbol{\Omega} \times \mathbf{B_{cm}} \tag{3-9}$$

Expansion of the first term on the right-hand side of Eq. (3-9) results in

$$\frac{\delta \mathbf{B_{cm}}}{\delta t} = \frac{\delta \mathbf{I}}{\delta t} \cdot \boldsymbol{\Omega} + \mathbf{I} \cdot \frac{\delta \boldsymbol{\Omega}}{\delta t} = \mathbf{I} \cdot \frac{\delta \boldsymbol{\Omega}}{\delta t} \tag{3-10}$$

and by substituting Eq. (3-10) into Eq. (3-9) and reapplying the equation for angular momentum in Eq. (3-8), finally, the equation of rotational motion for a mass-varying rigid body is obtained and is written as:

$$\mathbf{M_{cm}} = \mathbf{I} \cdot \dot{\boldsymbol{\Omega}} + \boldsymbol{\Omega} \times \mathbf{I} \cdot \boldsymbol{\Omega} \tag{3-11}$$

According to the Principle of Solidification, Eq. (3-11) can also be used to describe the rotational motion of a non-rigid body. By re-writing the general formulation in Eq. (3-11) and expressing the components in the body-axis, the full set of non-linear equations is obtained as:

$$\dot{\boldsymbol{\Omega}}^{\mathbf{b}}_{\mathbf{bI}} = \mathbf{I}^{-1}\left(\mathbf{M}^{\mathbf{b}}_{\mathbf{cm}} - \boldsymbol{\Omega}^{\mathbf{b}}_{\mathbf{bI}} \times \mathbf{I} \cdot \boldsymbol{\Omega}^{\mathbf{b}}_{\mathbf{bI}}\right) \tag{3-12}$$

With the Euler equations, the external moments are related to the inertial angular accelerations. By expressing the variables in Eq. (3-12) as vectors in the body frame F_b and by assuming that the aircraft has a plane of symmetry aligned with the X_b-Z_b plane such that these cross-products of inertia drop, the Euler equations simplify to:

$$\begin{pmatrix}\dot{p}\\ \dot{q}\\ \dot{r}\end{pmatrix} = \begin{pmatrix} I_{xx} & 0 & -I_{xz}\\ 0 & I_{yy} & 0\\ -I_{xz} & 0 & I_{zz}\end{pmatrix}^{-1} \left\{\begin{pmatrix}L\\ M\\ N\end{pmatrix} - \begin{pmatrix}p\\ q\\ r\end{pmatrix} \times \begin{pmatrix} I_{xx} & 0 & -I_{xz}\\ 0 & I_{yy} & 0\\ -I_{xz} & 0 & I_{zz}\end{pmatrix}\begin{pmatrix}p\\ q\\ r\end{pmatrix}\right\} \tag{3-13}$$

The set of first-order differential equation rotational dynamics for an aircraft with a geometrical plane of symmetry are given by solving Eq. (3-13) for the vector of total aerodynamic moments. This operation results in the following simplification of the equations of rotational motion which will be used throughout the remainder of this report:

$$\begin{aligned} L &= I_x\dot{p} - (I_y - I_z)\,qr - I_{xz}\,(\dot{r} + pq) \\ M &= I_y\dot{q} - (I_z - I_x)\,rp - I_{zx}\left(r^2 - p^2\right) \\ N &= I_z\dot{r} - (I_x - I_y)\,pq - I_{zx}\,(\dot{p} - qr) \end{aligned} \tag{3-14}$$

Note that from this point the notation of the products of inertia with a single subscript for non-cross products has been adopted for simplicity.

3-4 Attitude Equations

The Euler angles, i.e. roll angle ϕ, pitch angle θ and yaw angle ψ, are used to define the orientation of the body frame F_b with respect to the navigation frame F_E. The three Euler angles arise from three successive rotations of the NED frame to the body frame. By using this procedure on the angular velocity vector, the angular velocity vector of the body frame w.r.t. the NED frame can be found by subtracting the rotation of NED frame with respect to the inertial frame from the rotation of the body frame with respect to the inertial frame. Without further elaboration, the non-linear kinematic relations for an aircraft navigating on a spherical, rotating earth are given by (Mulder et al., 1999):

$$\begin{aligned} \dot{\phi} &= p + q\sin\phi\tan\theta + r\cos\phi\tan\theta - \left(\frac{V_E}{R} + \Omega_t\cos\delta\right)\frac{\cos\psi}{\cos\theta} + \frac{V_N\sin\psi}{R\cos\theta} \\ \dot{\theta} &= q\cos\phi - r\sin\phi + \left(\frac{V_E}{R} + \Omega_t\cos\delta\right)\sin\psi + \frac{V_N\cos\psi}{R} \\ \dot{\psi} &= q\frac{\sin\phi}{\cos\theta} + r\frac{\cos\phi}{\cos\theta} + \left(\frac{V_E}{R} + \Omega_t\cos\delta\right)\tan\theta\cos\psi + \frac{V_N\tan\theta\sin\psi}{R} + \\ &\qquad \frac{V_E\tan\delta}{R} + \Omega_t\sin\delta \end{aligned} \tag{3-15}$$

A full derivation of these equations is given in (Mulder et al., 2000). By neglecting the rotation of the earth and using a flat earth approximation, the full set of non-linear equations of rotational motion reduces to the well-known set of first-order differential equations for the Euler angles, i.e. ϕ, θ and ψ. By assuming two planes of symmetry, these equations are given by:

$$\begin{aligned} \dot{\phi} &= p + q\sin\phi\tan\theta + r\cos\phi\tan\theta \\ \dot{\theta} &= q\cos\phi - r\sin\phi \\ \dot{\psi} &= \frac{\sin\phi}{\cos\theta} + r\frac{\cos\phi}{\cos\theta} \end{aligned} \tag{3-16}$$

These equations are also referred to as the attitude equations. Despite the radical assumptions, such as flat and non-rotating earth, these simplified equations can still be used for most applications of flight simulation (Baarspul, 1990).

3-5 Non-linear Kinematic Model

Kinematic models of aircraft motion consist of a set of first order ordinary differential equations in which not the physical inputs (e.g. control surface deflections, engine thrust) but rather measured variables such as body accelerations and body rotation rates appear as forcing functions (Mulder, Sridhar, & Breeman, 1994). The body accelerations in this context are the accelerations measured by accelerometers with respect to the body's center of gravity, i.e. A_x, A_y and A_z which denote the components of the acceleration in the x, y and z body axis. Using Newton's second law of motion, the body accelerations can be related to the body forces by:

$$
\begin{aligned}
X &= mA_x \\
Y &= mA_y \\
Z &= mA_z
\end{aligned}
\tag{3-17}
$$

It is important to realize that although the physical inputs are not distinctively shown in Eq. (3-17), these quantities do serve as input to the set of kinematic equations since they are included as independent variables in the aerodynamic model, relating the control surface inputs and engine thrust to the produced aerodynamic forces and moments. Substitution of the formulation of the body forces in Eq. (3-17) into the derived equations relating the body forces to the rotational rates and orientation of the body in Eq. (3-6) results in the following formulation that will be used throughout the flight-path reconstruction procedure:

$$
\begin{aligned}
\dot{u} &= A_x - g\sin\theta - qw + rv \\
\dot{v} &= A_y + g\cos\theta\sin\phi - ru + pw \\
\dot{w} &= A_z + g\cos\theta\cos\phi - pv + qu
\end{aligned}
\tag{3-18}
$$

If the body accelerations and angular rates are known from, e.g., measurements from an Inertial Measurement Unit (IMU), the kinematic equation can be solved numerically resulting in the time histories of the translational velocity components and the body orientation angles.

The velocity of the aircraft's center of gravity w.r.t. the navigation frame can be found by rotating the body velocities using rotation matrix $\mathbb{T}_{Eb}$ which is defined as:

$$
\mathbb{T}_{Eb} = \begin{pmatrix}
\cos\theta\cos\psi & \sin\phi\sin\theta\cos\psi - \cos\phi\sin\psi & \cos\phi\sin\theta\cos\psi + \sin\phi\sin\psi \\
\cos\theta\cos\psi & \sin\phi\sin\theta\sin\psi + \cos\phi\cos\psi & \cos\phi\sin\theta\sin\psi - \sin\phi\cos\psi \\
-\sin\theta & \sin\phi\cos\theta & \cos\phi\cos\theta
\end{pmatrix}
\tag{3-19}
$$

The velocity components in the navigation frame are then found by adding the atmospheric wind components expressed along the axes of F_E:

$$\begin{pmatrix} \dot{x}_E \\ \dot{y}_E \\ \dot{z}_E \end{pmatrix} = \mathbb{T}_{Eb} \begin{pmatrix} u \\ v \\ w \end{pmatrix} + \begin{pmatrix} W_{xE} \\ W_{yE} \\ W_{zE} \end{pmatrix} \tag{3-20}$$

Note that the position of the center of gravity relative to the local earth frame and the body velocities can be found by, respectively, numerical integration of Eq. (3-18) and Eq. (3-20).

Chapter 4

Flight Path Reconstruction

In this chapter the methodology for the reconstruction of a flight path from a recorded series of measurements is presented. This is the first step of the TSM. Most often, these measurements originate from different sources and therefore, inherently, possess different noise characteristics. Kalman filters have been used extensively, in the past and present, as navigation filter. These can effectively combine information from different sources, i.e. sensor fusion, and make an accurate state estimation by comparing the actual and estimated measurement. Over the years many different types of Kalman filters have been presented. In this chapter, an overview of the most important types of Kalman filters, applicable to off-line flight path reconstruction has been presented together with a comparison of the different types obtained from application to the DASMAT simulation framework. In addition to the analysis of different Kalman filter types, state reconstructability will be discussed in detail together with an application of different smoother types to the filtered simulation data.

4-1 Literature Review

Flight path reconstruction is the process of reconstructing the original sequence of states as a function of time given a series of measurements. These measurements can originate from different sources: (1) computational fluid dynamics (CFD) simulations, (2) wind tunnel measurements and (3) experimental flight test data. These methods do not necessarily have to be used in isolation, a combination of methods is also possible. In industry it is usual practice to make an initial model using CFD and wind tunnel data. This model can then be refined by using data originating from experimental flights. However, in practice, the first two methods have major shortcomings. While wind tunnel experiments are very expensive to perform and do not have to ability to reach certain states, CFD does often not have enough approximation power in non-linear regions of the flight envelope. To this extent, model identification by using flight test data has been used predominantly. Due to process and measurement noise inherently associated with flight test data, the use of the Kalman filter was introduced for use in the flight path reconstruction problem.

Since the introduction of the Kalman filter in the late 60s by Kalman (1960), the application became widespread and many new extensions were developed, e.g. (Julier & Uhlmann, 1997, 2004; Zhan & Wan, 2007; Armesto et al., 2004; Sarkka, 2008). In the original paper by Kalman (1960) a new look at optimal estimation and models for random processes was presented. In this paper Kalman stated that a Gaussian signal will not lose its properties by propagation through a linear system. By inverse logic, it would then also become evident that a Gaussian observation would be caused by propagation of the Gaussian signal from the source through a linear system. Hence, the system itself would not contribute to the random nature of the signal. Furthermore, Kalman derived its optimal filtering strategy by assuming that the system dynamics are time-invariant and stationary. The assumptions mentioned before allowed for a simplified solutions to the optimal filtering problem, however, at the same time these assumptions also highlight the major downside of this approach. Most systems in real life have a non-linear nature, especially aircraft dynamics, which can be classified as moderately to highly non-linear. Under these circumstances, the filter loses its optimality. Therefore this type of filter will not be applicable to flight path reconstruction with non-linear state transition and observation functions.

For this exact application, an extension to the Kalman filter was developed (Mulder et al., 1999), referred to as the extended Kalman filter (EKF). The working principle of this type of Kalman filter is based on a truncated first order Taylor expansion of the non-linear state transition and observation function, effectively leading to a linearized system. To even further improve the performance of the extended Kalman filter, an iterative procedure with local iterations on an individual time interval. This method is referred to as the iterated extended Kalman filter (IEKF). Due to the linearization of the dynamics in the first few steps of this approach it is directly applicable to non-linear systems. The latter method has been applied, for example, by Chowdhary and Jategaonkar (2010) and Teixeira et al.(2011). When taking a closer look at the exact mechanics behind the Kalman filter, it becomes evident that the IEKF, uses local iterations around a linearized state transition and observation function. The same procedure as in (Kalman, 1960) can then be applied to obtain an estimated state. However, in the latter situation the estimated state cannot be called optimal anymore, at best sub-optimal. This is due to the linearization about a certain set-point. In this case, if the system shows linear to moderately non-linear behavior, the linearization about the set-point does not produce very large errors. In turn, the Kalman filter reaches optimality in the state estimation. However, as described before, most systems are of moderately to highly non-linear nature and do therefore not allow for linearization about any point in the state-space. These arguments were also given in (Julier & Uhlmann, 2004) to plead for the use of a more robust approach. Since aircraft dynamic are usually moderately non-linear, a more robust approach to Kalman filtering might be beneficial for a more accurate state estimation, ultimately leading to a more accurate model.

It was much later when a new extension to the existing Kalman filtering techniques was proposed by Julier and Uhlmann (1997). Instead of making use of a linearization of the system's dynamics, a set of discretely sampled points was used to represent the mean and covariance of the state. Above all, in theory, this method should have the advantage over the previously mentioned methods for being able to work with non-Gaussian distributions. The latter might be especially useful when working with data of unknown distribution. In this specific research, state reconstruction will be done by using experimental flight test data. While in theory this data will be normally distributed, in practice it will often contains noise of unknown source and can therefore not be treated as Gaussian anymore. Later work by Julier and Uhlmann (2004) revealed that, after a thorough analysis of the IEKF, the standard IEKF implementation has some benefits over other filters. The most important finding was that the EKF forms a successful compromise between computational complexity and applicability. However, at the same time it was also found that the approximation of a non-linear system by linearization is only reliable if the error-in-error-out relationship is also linear. In addition, for large systems the calculation of the Jacobian can be a difficult and error-prone operation. To address these deficiencies Julier and Uhlmann developed the Unscented Kalman Filter (UKF). The basic idea behind the UKF is that the approximation of Gaussian distribution is easier than the approximation of a non-linear function (Julier & Uhlmann, 1997, p. 5). With this approach, a set of so-called sigma points are chosen around the current state representing the state's mean and covariance. Subsequently, all these points are propagated through the systems dynamics to estimate the predicted mean and covariance of the one-step-ahead state. The UKF uses a deterministic approach to select appropriate points around the current state to represent the mean and covariance. From this point it is easy to arrive at methods taking into account the statistical properties of the whole state-space. In fact, the UKF was derived from the Sigma-Point Kalman Filter (SPKF), which populates the whole state-space with sigma points before propagation through the system's dynamics (Van Der Merwe & Wan, 2004). Despite the improved representation of the mean and covariance, the computational burden of such a method would not weigh against its advantages because the number of computational operations per time step increases dramatically. The nature of the problems itself is also of a different order. Due to the high uncertainties in the measurement of a GPS signal, as presented in the paper of Van der Merwe and Wan (2004), population of samples over the whole state-space can be beneficial. This in contrast to the problem presented in this work, where sensor measurements are assumed to have a relatively high accuracy.

A comparative study between the (I)EKF and UKF was performed in many researches. A comparison for the application in flight path reconstruction was performed by Chowdhary and Jategaonkar (2010) and later by Teixeira et al. (2011). The concluding remarks of the last paper were that a significant increase of performance, in terms of mean squared error, was not observed by using the UKF instead of the EKF while computational costs were much higher. Furthermore, Chowdhary and Jategaonkar applied the filter-before-estimation method and argued that the UKF shows faster convergence which, in this specific case did not come at much higher computational costs. However, the simplified set of kinematic equations used in (Chowdhary & Jategaonkar, 2010) reveals why this conclusion was drawn. This in contrast to the set of equations that was used in (Teixeira et al., 2011). The latter will also be used in this research. It should be noted however that both papers do not discuss the influence of body induced velocities on the aerodynamic angles. The validity of this assumption does not hold at higher angles of attack, i.e. stall model identification, something that is not very relevant to this research.

The analysis of flight test data is often subjected to working with data from different sources sampled at different rates. These systems are called multi-rate systems. Adapted versions of the IEKF and UKF have both been employed to directly use this data. This so-called multi-rate Kalman filter (MR-KF) was first introduced by Armesto et al. (2004) and later applied in many different application (Smyth & Wu, 2007; Armesto, Tornero, & Vincze, 2008). To overcome the problems associated with multi-rate data, this type of filter can directly be applied in the flight path reconstruction problem for this research. However, direct interpolation of this data and the use of a regular Kalman filter might suffice. The fact that the multi-rate implementation of the Kalman filter comes without extra computational costs might be a reason for the preference of such a filter. In the work by Armesto, the MR-KF was applied for different ends than earlier presented works. However, its application has successfully shown the applicability of such a filter.

The following sections will elaborate on the elements that were discussed in this introduction. To start off, the definition of a general linear and non-linear set of stochastic differential equations is given in Section 4-2. Subsequently an overview of the kinematic equations and observation model is given in Section 4-3 followed by the introduction of different types of Kalman filters. These concepts will be applied to a non-linear simulation model of the Cessna Citation II to show the performance of the different theoretical constructs in a flight path reconstruction problem.

4-2 Stochastic Differential Equations

The basic linear Kalman filter (Kalman, 1960) is based on a set of linear, Stochastic Differential Equations (SDEs) given by:

$$\begin{aligned} \dot{\mathbf{x}}(t) &= \mathbf{A}\mathbf{x}(t) + \mathbf{B}\mathbf{u}(t) + \mathbf{G}\mathbf{w}(t) \\ \mathbf{z}_n(t) &= \mathbf{C}\mathbf{x}(t) + \mathbf{D}\mathbf{u}(t) + \mathbf{v}(t) \\ \mathbf{z}(t_k) &= \mathbf{z}_n(t_k) + \mathbf{v}(t_k) \qquad k = 1, 2, \ldots \end{aligned} \tag{4-1}$$

with $\mathbf{A}$ the state transition matrix, $\mathbf{B}$ the deterministic input distribution matrix and $\mathbf{G}$ the stochastic input distribution matrix. The observation or measurement $\mathbf{z}$ is a linear combination of output matrix $\mathbf{C}$, feedforward matrix $\mathbf{D}$ and process noise vector $\mathbf{v}(t)$. Vector-valued and matrix-valued quantities are indicated by a boldface typesetting. The initial state of the state space model in Eq. (4-1) is given by $\mathbf{x}(t_0) = \mathbf{x}_0$ and is a random vector with a known mean value of $\mu_0 = \mathbb{E}\{\mathbf{x}_0\}$ and covariance matrix $\mathbf{P}_0 = \mathbb{E}\{(\mathbf{x}_0 - \mu_0)(\mathbf{x}_0 - \mu_0)^\intercal\}$.

The stochastic differential equations presented in Eq. (4-1) describe a linear system. However, in most cases the system and measurement equations are of non-linear nature. In addition, in Eq. (4-1) it was assumed for the system noise to be purely additive whilst in reality noise can also be propagated through the system's dynamics. The set of stochastic differential equations for a general non-linear system is given by:

$$\begin{aligned} \dot{\mathbf{x}}(t) &= \mathbf{f}\left[\mathbf{x}(t), \mathbf{u}(t), t\right] + \mathbf{G}(\mathbf{x}(t), t)\mathbf{w}(t) \\ \mathbf{z}_n(t) &= \mathbf{h}\left[\mathbf{x}(t), \mathbf{u}(t), t\right] \\ \mathbf{z}(t_k) &= \mathbf{z}_n(t_k) + \mathbf{v}(t_k) \end{aligned} \tag{4-2}$$

where $\mathbf{f}[\cdot]$ is the non-linear state transition function and $\mathbf{h}[\cdot]$ the non-linear measurement function. The process noise and (output) measurement noise are assumed to be zero-mean, white and uncorrelated and can be parametrized by:

$$\mathbb{E}\{\mathbf{v}\mathbf{v}^\intercal\} = \mathbf{Q} \qquad \mathbb{E}\{\mathbf{w}\mathbf{w}^\intercal\} = \mathbf{R} \qquad \mathbb{E}\{\mathbf{w}\mathbf{v}^\intercal\} = 0 \tag{4-3}$$

4-3 Kinematic and Navigation Model

The full kinematic model is given by combining the differential equations for the flat earth position in Eq. (3-20), body velocity components in Eq. (3-18) and the equations of rotational motion Eq. (3-16). The whole set of differential equations is then given by:

$$
\begin{aligned}
\dot{x}_E &= (u\cos\theta + (v\sin\phi + w\cos\phi)\sin\theta)\cos\psi - (v\cos\phi - w\sin\phi)\sin\psi + W_{x_E} \\
\dot{y}_E &= (u\cos\theta + (v\sin\phi + w\cos\phi)\sin\theta)\sin\psi + (v\cos\phi - w\sin\phi)\cos\psi + W_{y_E} \\
\dot{z}_E &= -u\sin\theta + (v\sin\phi + w\cos\phi)\cos\theta + W_{z_E} \\
\dot{u} &= A_x - g\sin\theta - qw + rv \\
\dot{v} &= A_y + g\cos\theta\sin\phi - ru + pw \\
\dot{w} &= A_z + g\cos\theta\cos\phi - pv + qu \\
\dot{\phi} &= p + q\sin\phi\tan\theta + r\cos\phi\tan\theta \\
\dot{\theta} &= q\cos\phi - r\sin\phi \\
\dot{\psi} &= \frac{\sin\phi}{\cos\theta} + r\frac{\cos\phi}{\cos\theta}
\end{aligned}
\tag{4-4}
$$

In this set of kinematic equations, the IMU measurements are used as system input. In order to model the noise characteristics and bias of the IMU signals, these were modeled as:

$$
\begin{aligned}
A_{x_m} &= A_x + \lambda_{A_x} + w_x \\
A_{y_m} &= A_y + \lambda_{A_y} + w_y \\
A_{z_m} &= A_z + \lambda_{A_z} + w_z \\
p_m &= p + \lambda_p + w_p \\
q_m &= q + \lambda_q + w_q \\
r_m &= r + \lambda_r + w_r
\end{aligned}
\tag{4-5}
$$

where λ indicates the bias of the associated signal and $w_{(\cdot)}$ indicates the process noise of the subscripted variable. For use in flight path reconstruction with a Kalman filter, the set of equations in Eq. (4-4) needs to be extended with the time derivatives of any additional states that required reconstruction, e.g. the sensor biases. In this case, the state transition function can simple be assumed to be zero since the bias is constant in reality. Alternatively, as Lubbers applied in his work (Lubbers, 2009), sensor biases can be modeled as random walk for an increased state excitation and, theoretically, better convergence to the true state. In either of the two cases, the augmented state vector then becomes:

$$
\mathbf{x}_{\text{aug}} = [\mathbf{x} \quad \lambda]^{\mathsf{T}} \in \mathbb{R}^n \tag{4-6}
$$

where n indicates the dimensionality of the system. Note that in this context, the λ only indicates the augmented states related to the sensor biases, however, these can be any additional states.

Observation data can be acquired from different sources. In general, the position and velocities in F_E are acquired from GPS measurements. In addition, the aircraft's attitude can also be acquired from GPS measurements but a more common source would be the Attitude and Heading Reference System (AHRS). The complete set of observation equations, or the navigation model, is given by:

$$
\begin{aligned}
x_{\mathrm{gps}_m} &= x + v_x \\
y_{\mathrm{gps}_m} &= y + v_y \\
z_{\mathrm{gps}_m} &= z + v_z \\
u_{\mathrm{gps}_m} &= [u\cos\theta + (v\sin\phi + w\cos\phi)\sin\theta]\cos\psi - (v\cos\phi - w\sin\phi)\sin\psi + W_{x_E} + v_u \\
v_{\mathrm{gps}_m} &= [u\cos\theta + (v\sin\phi + w\cos\phi)\sin\theta]\sin\psi + (v\cos\phi - w\sin\phi)\cos\psi + W_{y_E} + v_v \\
w_{\mathrm{gps}_m} &= -u\sin\theta + (v\sin\phi + w\cos\phi)\cos\theta + W_{z_E} + v_w \\
\phi_m &= \phi + v_\phi \\
\theta_m &= \theta + v_\theta \\
\psi_m &= \psi + v_\psi \\
V_{\mathrm{TAS}_m} &= \sqrt{u^2 + v^2 + w^2} + v_{V_{TAS}} \\
\alpha &= \tan^{-1}\frac{w}{u} + v_\alpha \\
\beta &= \tan^{-1}\frac{v}{\sqrt{u^2 + w^2}} + v_\beta
\end{aligned}
\tag{4-7}
$$

where $v_{(\cdot)}$ is the standard notation for the measurement noise of the subscripted variable. Note that in Eq. (4-7), the set of equations depends on the velocity components expressed in the body frame F_b, however, the resulting velocity components are expressed in the navigation frame F_E, emphasized by the $(\cdot)_{\mathrm{gps}}$ subscript.

4-4 Extended Kalman Filter

As already stated before, many different types of Kalman filters exist. The original Kalman filter as introduced by Kalman (Kalman, 1960) was designated for linear systems. A simple extension to allow this type of filter, defined in linear state-space, to work with non-linear equations was introduced by local linearizations of the non-linear state transition function and measurement equations around the set-point defined by the state k, where k is the current time step. The latter extension became a widespread application and is known as the Extended Kalman Filter (EKF) (Mulder et al., 1999).

A high level overview of the Kalman filtering procedure is given in Figure 4-1. From this figure it becomes apparent that the Kalman filter works by (1) making an estimation of the dynamic system's current state $\hat{\mathbf{x}}(k+1|k)$ by a predication step performed with an internal model of the system's dynamics and (2) comparison of the predicted measurements vector $\hat{y}$ with the actual measurements vector. The difference between the latter two vectors is referred to as the innovation of step k and is subsequently used as input to the estimator where the

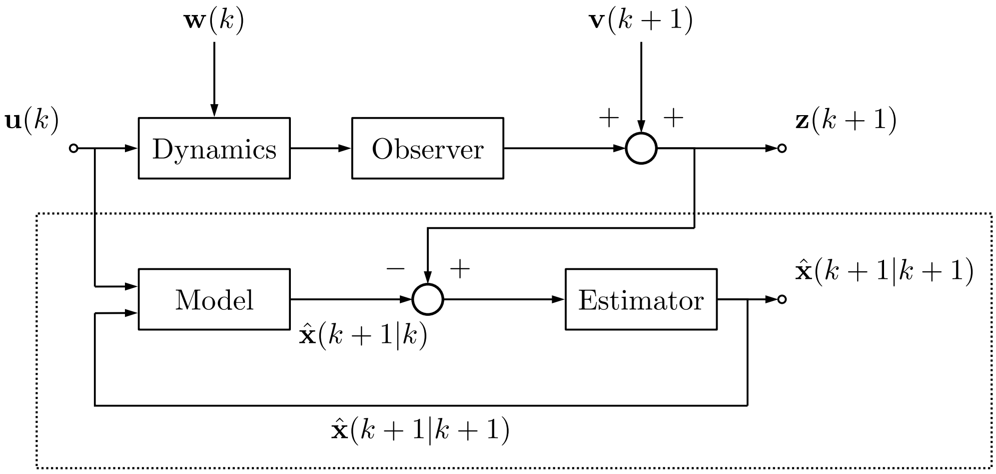

Figure 4-1: High level overview of the general Kalman filtering sequence.

vector of innovations is weighted with the Kalman gain K to arrive at the state estimate $\hat{\mathbf{x}}(k+1|k+1)$.

The complete set of equations for state estimation with the EKF are summarized in Eqs.(4-8)-(4-12). All classes of Kalman filters require some a priori information about the state and state covariance vector known as the initial state $\mathbf{x}_0$ and initial covariance matrix $\mathbf{P}_0$. In addition, sensor noise characteristics are parametrized by the process noise covariance matrix $\mathbf{R}$, containing the IMU or equivalent linear and rotational acceleration measurement device's variances on the diagonal. Equivalently, the noise characteristics of the measurement sensors, such as the airdata systems and GPS, are parametrized by $\mathbf{Q}$. It should be noted that these quantities are to be provided a priori, this means that appropriate values should either be provided in the form of a sensor noise specification of they should be estimated from stationary measurements.

To briefly elaborate on the functions of the specific EKF filter equations, Eq. (4-8) is at the basis of all classes of Kalman filters as it defines the one step ahead prediction of the state variables using previous state $\hat{\mathbf{x}}(k)$ that is either obtained from the previous filter step or defined as the initial state.

$$\hat{\mathbf{x}}(k+1|k) = \hat{\mathbf{x}}(k|k) + \int_{t_k}^{t_{k+1}} \mathbf{f}\left[\hat{\mathbf{x}}(k|k), \mathbf{u}(k), \mathbf{v}(k), \tau\right]\, d\tau \tag{4-8}$$

An initial estimate of the covariance matrix of the step ahead can then be made by using Eq. (4-9). Similarly, the Kalman filter gain can be calculated by Eq. (4-10), this quantity is only calculated once and not updated recursively, hence the notation only includes the current step.

$$\mathbf{P}(k+1|k) = \mathbf{\Phi}(k+1|k) \cdot \mathbf{P}(k|k) \cdot \mathbf{\Phi}^{\mathsf{T}}(k+1|k) + \mathbf{\Gamma}(k+1|k) \cdot \mathbf{Q}(k) \cdot \mathbf{\Gamma}(k+1|k) \tag{4-9}$$

$$\mathbf{K}(k+1) = \mathbf{P}(k+1|k) \cdot \nabla\mathbf{h}_{\mathbf{x}}^{\mathsf{T}} \cdot \left(\nabla\mathbf{h}_{\mathbf{x}} \cdot \mathbf{P}(k+1|k) \cdot \nabla\mathbf{h}_{\mathbf{x}}^{\mathsf{T}} + \mathbf{R}(k+1)\right)^{-1} \tag{4-10}$$

Finally, Eqs.(4-11)-(4-12) describe the recursive update to the state estimate and covariance matrix estimate for the step ahead.

$$\hat{\mathbf{x}}(k+1|k+1) = \hat{\mathbf{x}}(k+1|k) + \mathbf{K}(k+1)\cdot(\mathbf{z}(k+1) - \mathbf{h}\left[\hat{\mathbf{x}}(k+1|k), \mathbf{u}(k+1)\right]) \tag{4-11}$$

$$\mathbf{P}(k+1|k+1) = \mathbf{P}(k+1|k) - \mathbf{K}(k+1)\cdot\nabla\mathbf{h}_{\mathbf{x}}\cdot\mathbf{P}(k+1|k) \tag{4-12}$$

where $\nabla\mathbf{f}_{\mathbf{x}}$ and $\nabla\mathbf{h}_{\mathbf{x}}$ are the Jacobian matrices of the state transition and measurement function with respect to state estimate $\hat{\mathbf{x}}$ at time-instant k, which are functions of the current state and input, defined as:

$$\nabla\mathbf{f}_{\mathbf{x}} = \frac{\partial}{\partial\mathbf{x}} f\left(\mathbf{x}(t), \mathbf{u}(t), t\right) \equiv \begin{bmatrix} \frac{\partial f_1}{\partial x_1} & \cdots & \frac{\partial f_1}{\partial x_n} \\ \vdots & \ddots & \vdots \\ \frac{\partial f_n}{\partial x_1} & \cdots & \frac{\partial f_n}{\partial x_n} \end{bmatrix} \tag{4-13}$$

in which the number of states is equal to the number of state transition functions per definition. Similarly, the Jacobian matrix for the measurement equations can be formed by applying Eq. (4-13) to a system of n states and m equations. Note that in Eq. (4-10), $\mathbf{\Phi}$ and $\mathbf{\Gamma}$ are the discretized state transition matrix, earlier found by $\nabla\mathbf{f}_{\mathbf{x}}$, and the discretized stochastic input distribution matrix $\mathbf{G}$. These quantities can be found by:

$$\mathbf{\Phi}(k) = \mathbf{I} + \sum_{n=1}^{\infty} \nabla\mathbf{f}_{\mathbf{x}}^{n} \frac{1}{n!}\left(t_k - t_{k-1}\right)^n \tag{4-14}$$

$$\mathbf{\Gamma}(k) \cong \left[\frac{1}{(n+1)!}\cdot\mathbf{I} + \sum_{n=1}^{\infty} \nabla\mathbf{f}_{\mathbf{x}}^{n}\left(t_k - t_{k-1}\right)^n\right] \times \mathbf{G}(t_k - t_{k-1}) \tag{4-15}$$

Together, these steps, when used in recursive fashion, formalize the definition of the EKF.

4-5 Iterated Extended Kalman Filter

Despite its simplicity and effective local linearization of the non-linear state transition functions, the EKF lacks from poor performance in the presence of significant non-linearities in the system's dynamics. In addition to the recursive prediction and update of the state vector and covariance matrix, the introduction of a local iteration scheme provides a better approximation of the non-linear equations. As Mulder et al. argues in (Mulder et al., 1999), the purpose of these iterations is to improve the reference trajectory and with that also the final estimate of the state vector.

In comparison to the standard implementation of the EKF, the Iterated Extended Kalman Filter (IEKF) iteratively determines the one step ahead prediction of the state vector by re-evaluating the linearized measurement equations and gain matrix. The following scheme can be used for the local iteration when integrated in an EKF framework:

$$\begin{aligned}\boldsymbol{\zeta}_{i+1} = \hat{\mathbf{x}}(k+1|k) + \mathbf{K}(\boldsymbol{\zeta}_i) \cdot \left\{\mathbf{z}(k+1) - \mathbf{h}\left[\boldsymbol{\zeta}_i, \mathbf{u}(k+1)\right] - \nabla\mathbf{h}_{\boldsymbol{\zeta}_i} \cdot (\hat{\mathbf{x}}(k+1|k) - \boldsymbol{\zeta}_i)\right\} \\ i = 1, 2, \ldots, l \qquad \boldsymbol{\zeta}_1 = \hat{\mathbf{x}}(k+1|k)\end{aligned} \tag{4-16}$$

where $\nabla\mathbf{h}_{\boldsymbol{\zeta}_i}$ denotes the matrix of linearized measurement equations expressed at iteration i as Jacobian matrix obtained from partial derivatives of the measurement equations with respect to the elements of the temporal state vector $\boldsymbol{\zeta}_i$. Note that this quantity is required to be determined for every iteration, the same holds for the measurement equations and the gain matrix. The number of maximum iterations l can be chosen depending on the type of application.

4-6 Unscented Kalman Filter

As argued in the previous subsections, the application of the Kalman filter, which was originally designated for linear state-space (Kalman, 1960), to systems with non-linear dynamics can be enabled by linearization around state $\mathbf{x}$ for every time step k. Further improvement can be reached by employing a local iteration scheme, effectively reducing the difference between the reference trajectory and the estimate. However, for dynamic systems with moderate to high non-linearities, the use of this class of filters may expose the shortcomings of the linearization technique. In addition, Julier & Uhlmann argue that the use of the EKF class of Kalman filters has led to the general concensus that the filter is difficult to implement and difficult to tune (Julier & Uhlmann, 1997). Elaborating to the latter statement, Julier & Uhlmann argue that the two major drawbacks of the EKF/IEKF are related to this linearization, these are (Julier & Uhlmann, 2004):

1. If the system demonstrates moderately to highly non-linear behavior within the time scale of the time step, $[t_k, t_{k+1}]$, the system cannot be assumed to show locally linear behavior.
2. The implementation of the Jacobian matrices is somewhat cumbersome and is error-prone as most formulation errors originate from a wrongly defined Jacobian matrix.

To effectively address these flaws, Julier & Uhlmann introduced an improved class of Kalman filters known as the Unscented Kalman Filter (UKF) (Julier & Uhlmann, 1997). This class of filters is, instead of a linearization around a set point, based on the unscented transform for calculating the statistics of a random variable undergoing a non-linear transformation. In the same paper, the authors show that when using a state linearization approach, only the second order statistical measures can be approximated whilst in many practical situation higher order terms might be required to prevent the introduction of significant biases or errors.

Additionally, Chowdhary & Jategaonkar conclude from their research effort that the augmented version of the UKF for parameter estimation is the fastest in terms of convergence at the cost of additional computational burden (Chowdhary & Jategaonkar, 2010).

The definition of the UKF begins with the selection of a so-called set of sigma points. These points can be obtained from the unscented transformation of the augmented state vector and covariance matrix. In the original definition of the UKF, the state vector and covariance matrix were only augmented with the process noise (Julier & Uhlmann, 1997). Hence, hereby it was also assumed that the states and corresponding errors are propagated linearly through the measurement equations. In most cases, such an approximation is tolerated. However, since the computational burden of an increased augmented state vector and covariance matrix is limited, it was chosen to also augment the latter two quantities with the measurement noise characteristics (Julier & Uhlmann, 2004; Wan & Van Der Merwe, 2002). This UKF filter is, hereafter, referred to as the augmented UKF.

To begin with the formulation of the augmented UKF, the augmented state vector and covariance matrix are defined as:

$$\hat{\mathbf{x}}^a(k) = [\hat{\mathbf{x}}(k|k)^\intercal \ \mathbf{v}(k)^\intercal \ \mathbf{w}(k)^\intercal]^\intercal \tag{4-17}$$

$$\mathbf{P}^a(k) = \begin{bmatrix} \mathbf{P}(k) & 0 & 0 \\ 0 & \mathbf{Q} & 0 \\ 0 & 0 & \mathbf{R} \end{bmatrix} \tag{4-18}$$

where $\mathbf{v}$ and $\mathbf{w}$ in the augmented state vector represent the means of the process and measurement noise, these can therefore be assumed to have zero mean, hence their values will be zero. The augmented state vector and covariance matrix can then easily be transformed to the unscented domain by:

$$\begin{aligned} \boldsymbol{\mathcal{X}}_i^a(k) &= \left[\hat{\mathbf{x}}^a(k) + \sqrt{(L+\lambda)\mathbf{P}^a(k)}\right] \qquad i = 1, 2, \ldots, L \\ \boldsymbol{\mathcal{X}}_i^a(k) &= \left[\hat{\mathbf{x}}^a(k) - \sqrt{(L+\lambda)\mathbf{P}^a(k)}\right] \qquad i = L+1, L+2, \ldots, 2L \end{aligned} \tag{4-19}$$

This set of transformed points, indicated by $\boldsymbol{\mathcal{X}}^a$, is referred to as the set of sigma points. Parameters L and λ are, respectively, the dimensionality of the state vector and a scaling factor defined as $\lambda = \alpha^2(L+\kappa) - L$. α is a parameter to reflect the spread of the sigma points around its mean, state vector $\hat{\mathbf{x}}$, and β is a factor to account for any prior knowledge. The latter is set to a value of 2 for Gaussian distributions. κ is an extra scaling factor which is usually set to zero. Subsequently, the weights for the set of transformed means and covariances are defined as follows:

$$\begin{aligned} W_0^{(m)} &= \frac{\lambda}{L+\lambda} \\ W_0^{(c)} &= \frac{\lambda}{L+\lambda} + (1 - \alpha^2 + \beta) \\ W_i^{(m)} = W_i^{(c)} &= \frac{1}{2(L+\lambda)} \qquad i = 1, 2, \ldots, 2L \end{aligned} \tag{4-20}$$

From this point, the equations of the UKF become more trivial. Analogously to the EKF, the state vector which is now expressed as sigma points are propagated through the system's dynamics:

$$\boldsymbol{\mathcal{X}}^a(k+1|k) = \boldsymbol{\mathcal{X}}^a\,(k|k) + \int_{t_k}^{t_{k+1}} \mathbf{f}\left[\boldsymbol{\mathcal{X}}^{a,x}(k|k), \mathbf{u}(k), \boldsymbol{\mathcal{X}}^{a,v}(k|k), \tau\right] d\tau \tag{4-21}$$

where $\boldsymbol{\mathcal{X}}^{a,x}$ refers to the columns of the sigma points matrix related to the state and superscript v refers to the sigma points related to the process noise. The one step ahead state estimation can be calculated by:

$$\hat{\mathbf{x}}\,(k+1|k) = \sum_{i=0}^{2L} W_i^{(m)} \boldsymbol{\mathcal{X}}^a\,(k+1|k) \tag{4-22}$$

and the one step ahead covariance matrix by:

$$\mathbf{P}\,(k+1|k) = \sum_{i=0}^{2L} W_i^{(c)} \left(\boldsymbol{\mathcal{X}}_i^{a,x} - \hat{\mathbf{x}}(k|k)\right) \left(\boldsymbol{\mathcal{X}}_i^{a,x} - \hat{\mathbf{x}}(k|k)\right)^{\intercal} \tag{4-23}$$

Again, similarly to the EKF, the sigma points representing the state vector and measurement noise are propagated through the measurement equations and subsequently the transformed means for the measurements are calculated:

$$\boldsymbol{\mathcal{Y}}(k+1|k) = \mathbf{h}\left[\boldsymbol{\mathcal{X}}^{a,x}(k+1|k), \boldsymbol{\mathcal{X}}^{a,w}(k+1|k)\right] \tag{4-24}$$

with the transformed measurements given by taking the mean of the transformed sigma points:

$$\hat{\mathbf{y}} = \sum_{i=0}^{2L} W_i^{(m)} \boldsymbol{\mathcal{Y}}_i(k+1|k) \tag{4-25}$$

The measurement covariance and measurement-state cross-covariance can be calculated by:

$$\mathbf{P_{yy}} = \sum_{i=0}^{2L} W_i^{(c)} \left(\boldsymbol{\mathcal{Y}}_i(k+1|k) - \hat{\mathbf{y}}(k|k)\right) \left(\boldsymbol{\mathcal{Y}}_i(k+1|k) - \hat{\mathbf{y}}(k|k)\right)^{\intercal} \tag{4-26}$$

$$\mathbf{P_{xy}} = \sum_{i=0}^{2L} W_i^{(c)} \left(\boldsymbol{\mathcal{X}}_i^{a,x} - \hat{\mathbf{x}}(k|k)\right) \left(\boldsymbol{\mathcal{Y}}_i - \hat{\mathbf{y}}(k|k)\right)^{\intercal} \tag{4-27}$$

Finally, to complete the definition of the augmented UKF, gain matrix $\boldsymbol{\mathcal{K}}$, corrected state estimation $\hat{\mathbf{x}}(k+1|k+1)$ and corrected covariance matrix estimation $\mathbf{P}(k+1|k+1)$ are expressed as:

$$\boldsymbol{\mathcal{K}}(k+1) = \mathbf{P_{xy}} \mathbf{P_{yy}}^{-1} \tag{4-28}$$

$$\hat{\mathbf{x}}(k+1|k+1) = \hat{\mathbf{x}}(k+1|k) + \boldsymbol{\mathcal{K}}\left(\mathbf{y}(k+1) - \hat{\mathbf{y}}(k+1|k)\right) \tag{4-29}$$

$$\mathbf{P}(k+1|k+1) = \mathbf{P}(k+1|k) - \boldsymbol{\mathcal{K}} \mathbf{P_{yy}} \boldsymbol{\mathcal{K}}^{\intercal} \tag{4-30}$$

For additional numerical stability and guaranteed semi-definite state covariance matrix, the Square-Root Unscented Kalman Filter (SRUKF) implementation of the UKF can be used (Van Der Merwe & Wan, 2001). This type uses the Cholesky decomposition to address certain numerical advantages in the calculation of the transformed statistical properties. Further extensions to the UKF, e.g. the Sigma-Point Kalman Filter (Van Der Merwe & Wan, 2004) and its iterative counterpart (Sibley, Sukhatme, & Matthies, 2006), were introduced later. However, these filters populate the whole state-space with sigma points instead of only a selected optimal range. Therefore, the computational burden of such filters do not weight against the advantages and their application is restricted (Armesto et al., 2008).

4-7 Multi-rate systems and Kalman Filtering

The different classes of Kalman filters presented in the previous sections have different internal mechanics, however, it was assumed that the IMU data and measurement data are available at the same base sample rate. In many applications, and more importantly in the identification of aircraft models, data often originates from different equipment devices and can therefore be obtained at different sample rates (Mulder et al., 1994; Smyth & Wu, 2007), hence these kinds of systems are referred to as multi-rate systems. The latter violates the basic assumption of the earlier mentioned classes of Kalman filters. In order for these filters to work with multi-rate samples, a basic interpolation scheme can be set up to re-sample the data. However, for data with an inherently low sample rate, such as GPS measurements which are often obtained with less than 20 samples a second, interpolation might affect the accuracy of the state estimate.

A more structural solution to the problem as presented above is by making use of a multi-rate implementation of the Kalman filter. While firstly introduced to fuse data available from visual and inertial sensors by Armesto et al. (2004), the multi-rate implementation can potentially also be succesfully applied to multi-rate systems in flight path reconstruction problems.

Before the equations of the multi-rate Kalman filte implementation are given, a general multi-rate system is to be defined. A multi-rate stochastic model is given as:

$$\begin{aligned} \dot{\mathbf{x}}\left(k|k\right) &= \mathbf{f}\left[\mathbf{x}\left(k|k\right), \mathbf{u}\left(k\right), \mathbf{w}\left(k\right)\right] \\ \mathbf{y}_s\left(k+1\right) &= \mathbf{h}_s\left[\mathbf{x}(k|k)\right] + \mathbf{v}_s\left(k\right) \end{aligned} \tag{4-31}$$

where $\mathbf{f}\left[\cdot\right]$ is the standard notation for the vector-valued state transition function, equivalent to the state transition matrix in the case of a linear system. Similarly, $\mathbf{h}\left[\cdot\right]$ represents the vector-valued measurement equation. Subscript $\left(\cdot\right)_s$ indicates a time-varying vector or matrix quantity where the size depends on the number of available samples at time-instant k. The formulation of the multi-rate IEKF is analogous to the formulation of the conventional (single-rate) IEKF (Armesto et al., 2008, 2004; Smyth & Wu, 2007) and is given by:

$$\hat{\mathbf{x}}(k+1|k) = \hat{\mathbf{x}}(k|k) + \int_{t_k}^{t_{k+1}} \mathbf{f}\left[\hat{\mathbf{x}}(k|k), \hat{\mathbf{u}}(k), t\right] \, dt \tag{4-32}$$

$$\mathbf{P}(k+1|k) = \nabla\mathbf{f_x} \cdot \mathbf{P}(k|k) \cdot \nabla\mathbf{f_x^\intercal} + \mathbf{G} \cdot \mathbf{Q}(k) \cdot \mathbf{G} \tag{4-33}$$

$$\mathbf{K}_s(k+1) = \mathbf{P}(k+1|k) \cdot \nabla\mathbf{h}^\intercal_{\mathbf{x},s} \cdot \left(\nabla\mathbf{h}_{\mathbf{x},s} \cdot \mathbf{P}(k+1|k) \cdot \nabla\mathbf{h}^\intercal_{\mathbf{x},s} + \mathbf{R}_s(k+1)\right)^{-1} \tag{4-34}$$

$$\hat{\mathbf{x}}(k+1|k+1) = \hat{\mathbf{x}}(k+1|k) + \mathbf{K}_s(k+1) \cdot (\mathbf{z}_s(k+1) - \mathbf{h}_s\left[\hat{\mathbf{x}}(k+1|k), \hat{\mathbf{u}}(k+1)\right]) \tag{4-35}$$

$$\mathbf{P}(k+1|k+1) = \mathbf{P}(k+1|k) - \mathbf{K}_s(k+1) \cdot \nabla\mathbf{h}_{\mathbf{x},s} \cdot \mathbf{P}(k+1|k) \tag{4-36}$$

where $\nabla\mathbf{f_x}$ and $\nabla\mathbf{h}_{\mathbf{x},s}$ are the Jacobian matrices of the state transition function and the size-varying measurement function with respect to state estimate $\hat{\mathbf{x}}$ at time-instant k. The Kalman gain, innovation and covariance of the innovation are time-varying. Hence, the number of elements in these quantities will be given by the number of observations available at the current step.

Multi-rate Kalman filters exist in different forms, including the UKF (Armesto et al., 2004, 2008). In this report, only the multi-rate implementation of the EKF will be shown. Hereby it will be assumed that any increase in filter performance, i.e. the ability of the filter to effectively reduce the difference between the true state and the state estimate, of the multi-rate implementation for, e.g., the IEKF will show a similar increase in performance for other classes of filters.

4-8 Kalman Smoothers

In order to even further improve the accuracy of the state estimate obtained from any class of Kalman filter, the Kalman smoother may be employed in offline state estimation (Teixeira et al., 2011). In contrast to the forward recursive scheme of the earlier presented classes of Kalman filters, Kalman smoothers use future measurements in a backwards recursive scheme.

In this report, three types of Kalman filters are considered. The Rauch-Tung-Striebel Smoother (RTSS), Unscented Rauch-Tung-Striebel Smoother (URTS) (Sarkka, 2008) and Forward-backward Kalman Smoother (FBKS) (Teixeira et al., 2011). The first two can, in terms of internal mechanics, be compared to their forward recursive Kalman filter schemes. The FBKS is a simple forward-backward recursion of the standard implementation of the EKF.

Without going into the derivation of each of these smoother types, it was concluded that filters, in general, can improve the accuracy of the estimate significantly for offline state estimation problems. For a comparison of the different types, the author suggests, e.g., (Teixeira et al., 2011).

However, Mulder et al. argue that the use of these types of algorithms should be limited to systems with serious non-linear behavior (Mulder et al., 1999).

4-9 Additional Non-Linear Air Data Observation Models

In this section additional observation models are presented which can be used in cooperation with the earlier presented observation equations, see Section 4-3. The set of observation equations, see Eq. (4-7), can directly be applied in any aircraft flight path reconstruction problem under the assumption that the aerodynamic angles can be measured directly at the location of the CG. However, in reality this is not possible in most of the cases. Due to the wing-fuselage interaction and changes in the direction of the airflow caused by interaction of the wing with the air, i.e. upwash, sensor readings can be influenced dramatically. For this reason, the angle of attack and sideslip angle are preferred to be measured in front of the aircraft, in undisturbed flow. Since these types of devices do not measure the true geometrical aerodynamic angles but a combination of the true angle, a kinematically induced angle, fuselage induced angle and vertical wind component contribution (De Visser, 2011), the measurement equations need to be extended with the following set of equations for the angle of attack and sideslip angle (Laban, 1994):

$$\alpha_v = \left(1 + C_{\alpha_{\text{up}}}\right)\alpha + \frac{(q-\lambda_q)x_{\text{v}\alpha}}{\sqrt{u^2+v^2+w^2}} + C_{\alpha_0} \tag{4-37}$$

$$\beta_v = \left(1 + C_{\beta_{\text{si}}}\right)\beta - \frac{(r-\lambda_r)x_{\text{v}\beta}}{\sqrt{u^2+v^2+w^2}} + \frac{(p-\lambda_p)z_{\text{v}\beta}}{\sqrt{u^2+v^2+w^2}} + C_{\beta_0} \tag{4-38}$$

where x and z, respectively, denote the position of the corresponding boom-mounted vane. By using these models, the state vector is to be augmented with the coefficients that are to be estimated, i.e. $C_{\alpha_{\text{up}}}$, C_{α_0}, $C_{\beta_{\text{si}}}$ and C_{β_0}.

In some cases, the availability of additional measurement devices, such as the angle of attack and sideslip boom, is unlikely. In these cases, only raw data obtained from the angle of attack or sideslip (boom-mounted) vane can be used. To this end, Bennis developed a model to more accurately compensate for the viscous damper-mechanism of the vanes (Bennis, 1998). This model can be augmented to the state transition function:

$$\frac{d\alpha_v}{dt} = \frac{1}{\tau}\left[\left\{\tan^{-1}\left(\frac{w - x_{\alpha_v}(q-\lambda_q)}{u}\right) + C_{\alpha_{\text{up}}}\tan^{-1}\left(\frac{w}{u}\right) + C_{\alpha_0}\right\} - \alpha_v\right] \tag{4-39}$$

With the introduction of new states and the additional of new state-transition equations, the observability of the dynamic system can be affected. A short investigation into the observability of such systems is presented in Section 4-10.

4-10 State Observability and Reconstructability

Extensions to the most basic formulation of the state-transition and measurement equations sometimes comes at the cost of reduced observability of the dynamic system. Observability, defined as the measure to indicate the ability to observe the internal state of a dynamic system from a series of external measurements, can become even more tedious for systems described by a set of non-linear equations. For linear systems, the observability matrix can easily be obtained (Ljung, 2002), while for non-linear systems use can be made of Lie derivatives.

In the definition of non-linear observability, a distinction is made between local non-linear observability and non-linear observability. The first definition refers to the ability to observe a non-linear state from a local Taylor expansion (Sontag, 1984), such as applied in the IEKF.

Different methods to estimate the non-linear observability exist, however, Walcott, Corless & Zak found the Lie-algebraic method very attractive despite the requirement that a priori knowledge about the dynamics of the system should be precise (Walcott, Corless, & Zak, 1987). The Lie-algebraic method can be summarized as follows:

$$\mathbf{O}(x) = \begin{bmatrix} \nabla \left(L_f^0 \mathbf{h} \right)_{\mathbf{x}} \\ \nabla \left(L_f^1 \mathbf{h} \right)_{\mathbf{x}} \\ \vdots \\ \nabla \left(L_f^{n-1} \mathbf{h} \right)_{\mathbf{x}} \end{bmatrix} \tag{4-40}$$

where n indicates the state vector dimensionality and $L_f\mathbf{h}$ defined as:

$$\begin{aligned} L_f^0 \mathbf{h} &= \nabla \mathbf{h}_{\mathbf{x}} \\ L_f^1 \mathbf{h} &= \nabla \mathbf{h}_{\mathbf{x}} \cdot \mathbf{f} \\ L_f^2 \mathbf{h} &= \nabla \left(L_f^1 \mathbf{h} \right)_{\mathbf{x}} \cdot \mathbf{f} \\ &\vdots \\ L_f^{n-1} \mathbf{h} &= \nabla \left(L_f^{n-2} \mathbf{h} \right)_{\mathbf{x}} \cdot \mathbf{f} \end{aligned} \tag{4-41}$$

By applying the above arithmetic, an iterative procedure can be used to estimate the non-linear state observability. If the observability matrix $\mathbf{O}$ reaches full rank within the first $n-1$ Lie derivatives, non-linear observability is guaranteed. If full rank is achieved within the first iteration, the system can also be considered as locally observable. Any additional iterations deteriorate the local non-linear observability.

In this context, reconstructability is directly related to the ability to observe the state vector in a Kalman filter procedure. Rank deficiency in the observability matrix may directly result in the inability to reconstruct the state vector from the sequence of measurement data.

4-11 Comparison Different KF and KS types

In the previous sections, the theoretical concepts of several types of Kalman filters and smoothers have been elaborated, accompanied by additional theoretical insight into, e.g., non-linear observability and extensions to the collection of non-linear state transition and measurement equations.

A comparative study was performed between the different types of Kalman filters and smoothers in the framework of a non-linear Cessna Citation I simulation model[1]. To this

[1] The DASMAT simulation model, for more information see Section 2 or (Van Der Linden, 1998)

end, an observation model was constructed inside the simulation framework to obtain a set of corrupted measurements for both the IMU and air data systems. In order to realistically mimic the noise characteristics of a real air data system, the following noise characteristics were used:

$$\begin{aligned}
\sigma\left(\lambda_m\right) &= 0.001 \quad [\mathrm{m/s^2}]/[\mathrm{deg}/s] \\
\sigma\left(x_{\mathrm{gps,m}}\right) = s\left(y_{\mathrm{gps,m}}\right) = s\left(z_{\mathrm{gps,m}}\right) &= 10 \quad [\mathrm{m/s}] \\
\sigma\left(V_{x_{\mathrm{gps,m}}}\right) = s\left(V_{y_{\mathrm{gps,m}}}\right) = s\left(V_{z_{\mathrm{gps,m}}}\right) &= 0.1 \quad [\mathrm{m/s}] \\
\sigma\left(\phi_m\right) = s\left(\theta_m\right) = s\left(\psi_m\right) &= 0.1 \quad [\mathrm{deg}] \\
\sigma\left(V_{\mathrm{TAS,m}}\right) &= 0.1 \quad [\mathrm{m/s}] \\
\sigma\left(\alpha_m\right) = s\left(\beta_m\right) &= 0.1 \quad [\mathrm{deg}]
\end{aligned}$$

Additionally, wind speed was initialized at $W_E = \begin{bmatrix}10 & 6 & 1\end{bmatrix}^\intercal$ expressed in the navigation frame and a sensor bias for the IMU measurements was set to the same level as the noise standard deviation.

The state vector for the simulations runs was defined as:

$$\begin{aligned}
\mathbf{x} = [&x_{\mathrm{gps}} \quad y_{\mathrm{gps}} \quad z_{\mathrm{gps}} \quad u \quad v \quad w \quad \phi \quad \theta \quad \psi \\
&W_{x,E} \quad W_{y,E} \quad W_{z,E} \quad \lambda_{A_x} \quad \lambda_{A_y} \quad \lambda_{A_z} \quad \lambda_p \quad \lambda_q \quad \lambda_r]^\intercal \quad \in \mathbb{R}^{18}
\end{aligned} \tag{4-42}$$

Note that the state is augmented with both the sensors biases and wind velocity components. The state transition equation for both quantities was modeled as zero. Furthermore, reconstructability analysis has shown to converge to full rank within two iterations, hence the first degree Lie derivative.

4-11-1 Iterated Extended Kalman Filter

The IEKF was applied to the non-linear simulation model with the state vector and noise levels as indicated. The results for the IEKF are shown in Figures 4-2 to 4-5.

Figure 4-2 shown the state estimate resulting from the Kalman filter recursion together with the real state and the 2 standard deviations bound. As becomes clearly evident from this figure, the estimates of the asymmetrical states suffer from the absence of appropriate excitation in lateral motion. However, the estimates of the lateral states stay within acceptable error margin as is confirmed by Figure 4-6. Similarly, the same conclusion can be drawn for the symmetrical states resulting from an aileron or rudder input, exciting the asymmetrical states.

Similarly, the bias estimates show a more accurate prediction for the symmetrical states which can be explained by the same reasoning. See Figure 4-3 and Figure 4-7.

In addition to the reconstructed states, the filtered measurements can be reconstructed by running the state estimates through the non-linear measurement equations. The resulting filtered measurements are shown in Figure 4-4 along with the raw measurements.

It is common practice to validate the Kalman filter sequence by inspection of the innovation sequences, produced by the differences between predicted and actual measurement for each recursion. These innovation sequences should stay within the 2 sigma bounds while adopting white noise characteristics. From Figure 4-5 it becomes apparent that this Kalman filter recursion clearly stays within the 2 sigma bounds and the innovation signals resemble white noise. To confirm the last statement, the autocorrelation of the innovations clearly indicates an uncorrelated signal, see Figure 4-8. Note that the dirac delta at lag zero, indicative for an uncorrelated signal, is not shown in the figure for practical reasons. Overall, in terms of Root Mean Square (RMS), the IEKF achieved a score of 0.285.

4-11-2 Unscented Kalman Filter

In order to test the performance of the UKF, this class of Kalman filter was also applied to data obtained from a non-linear Cessna Citation I simulation. Again, similar to the IEKF, all states converge to their nominal value. The state estimates for the lateral states suffer from appropriate excitation is lateral direction, however, these states still stay within the 2 sigma standard bounds. In terms of the convergence rate and uncertainty of the state estimate and bias estimate, see Figure 4-9 and Figure 4-10, no clear difference can be UKF and IEKF can be distinguished.

Analogously, as follows from the consistency of the state and bias estimate, no clear difference is visible in terms of the error and its standard bounds for the state and bias estimate, see Figure 4-11 and Figure 4-12. From the autocorrelation of the innovation sequences, it can be stated that the UKF is also consistent.

4-12 Performance of KF and KS types

For a more in depth comparison between the IEKF and the UKF applied to simulation data, the EKF filter was used as reference. In addition to the earlier mentioned filter classes, smoothers were also applied in cooperation with the different Kalman filter types. It should be noted that the smoothers work according to a backwards recursion scheme, hence a forward recursion should first be provided by the Kalman filter. The different types of smoothers can be applied in combination with the forward recursion from any type of Kalman filter. However, for consistency, in this report the different types of smoothers were applied only in combination with their forward recursion Kalman counterpart, e.g. the URTS was applied to data obtained from the forward pass of the UKF. The FBKS combines the forward and backward recursion of the IEKF to obtain a smoother state estimate.

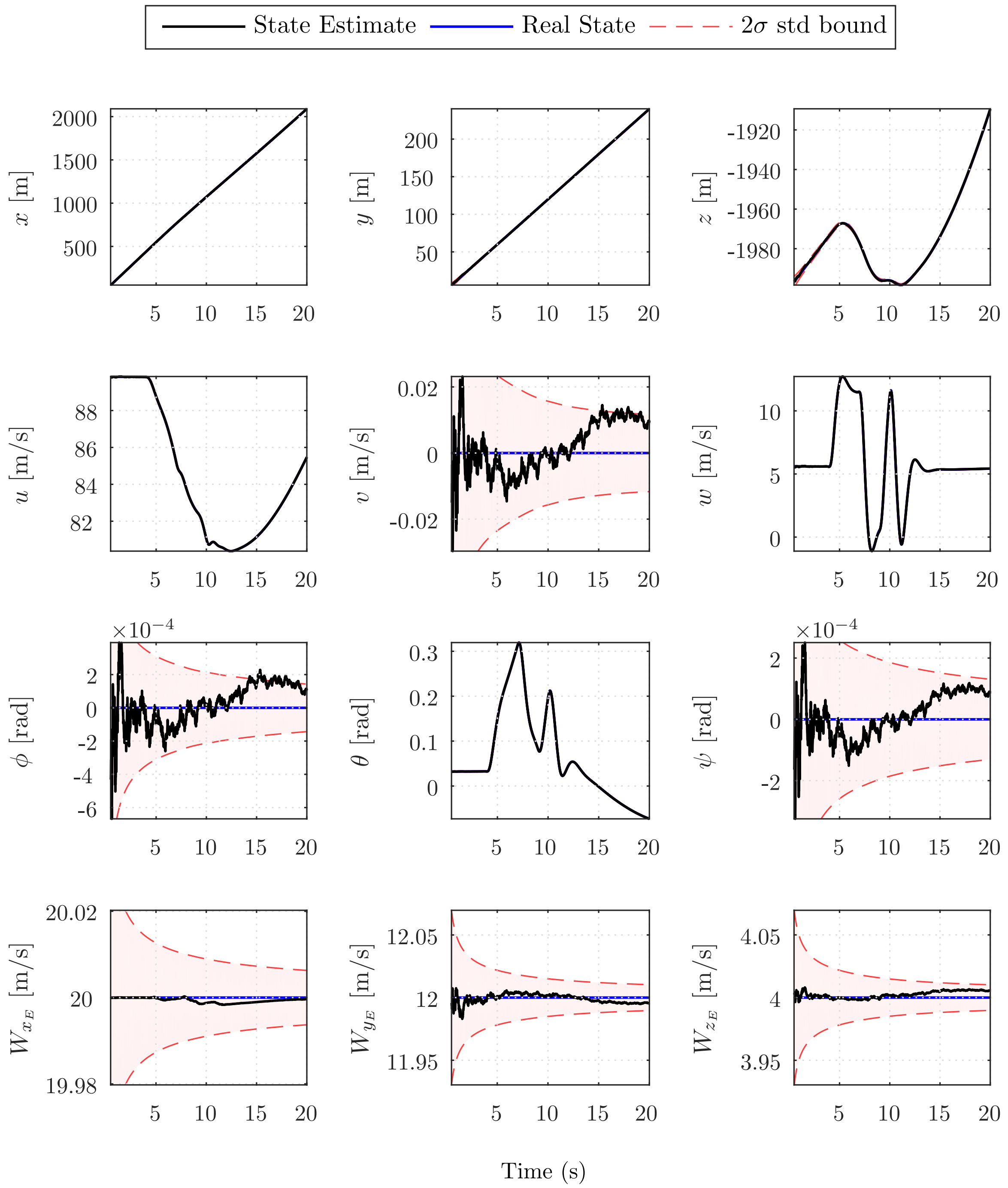

Figure 4-2: IEKF state reconstruction on data obtained from a non-linear Cessna Citation I flight simulation model together with the 2σ confidence bounds (red) and the real aircraft state (blue).

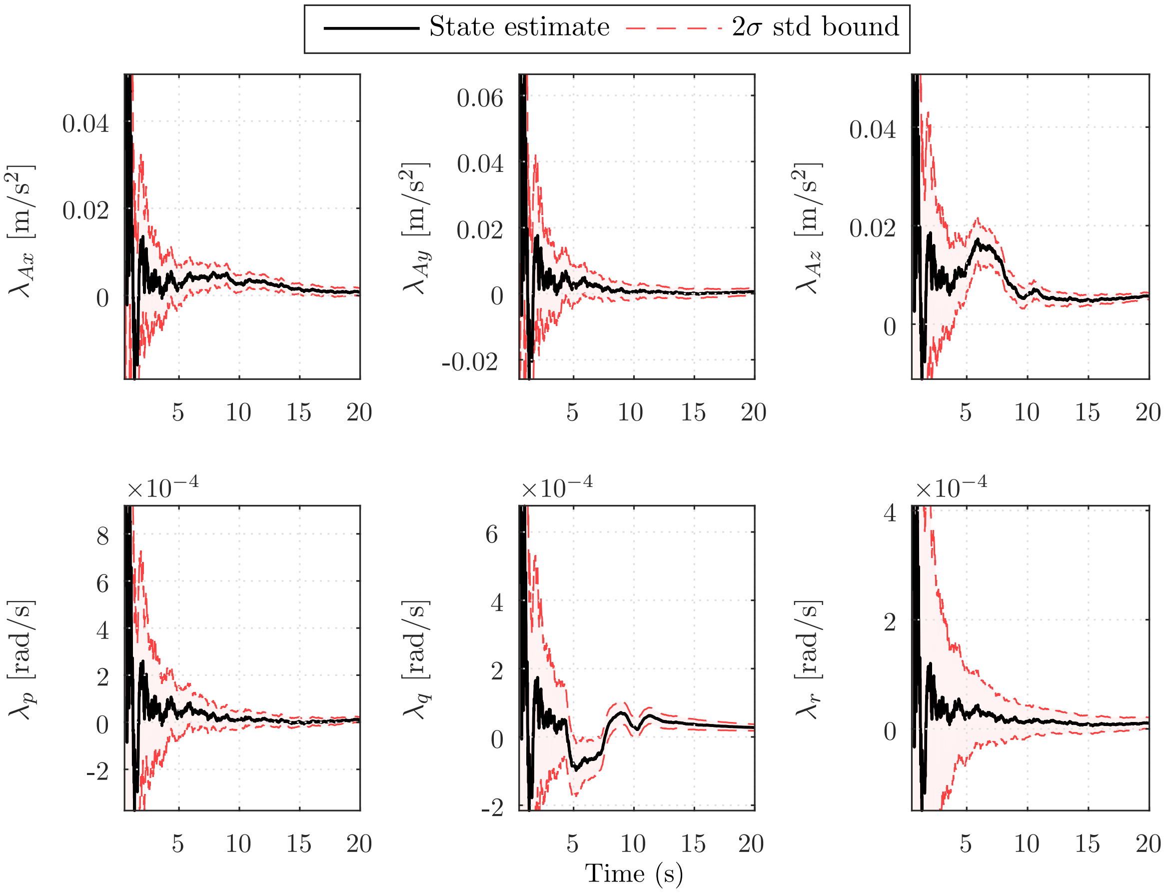

Figure 4-3: Estimated IMU sensor biases obtained with the IEKF on data obtained from a non-linear Cessna Citation I flight simulation model together with the 2σ confidence bounds (red) and the real bias (blue).

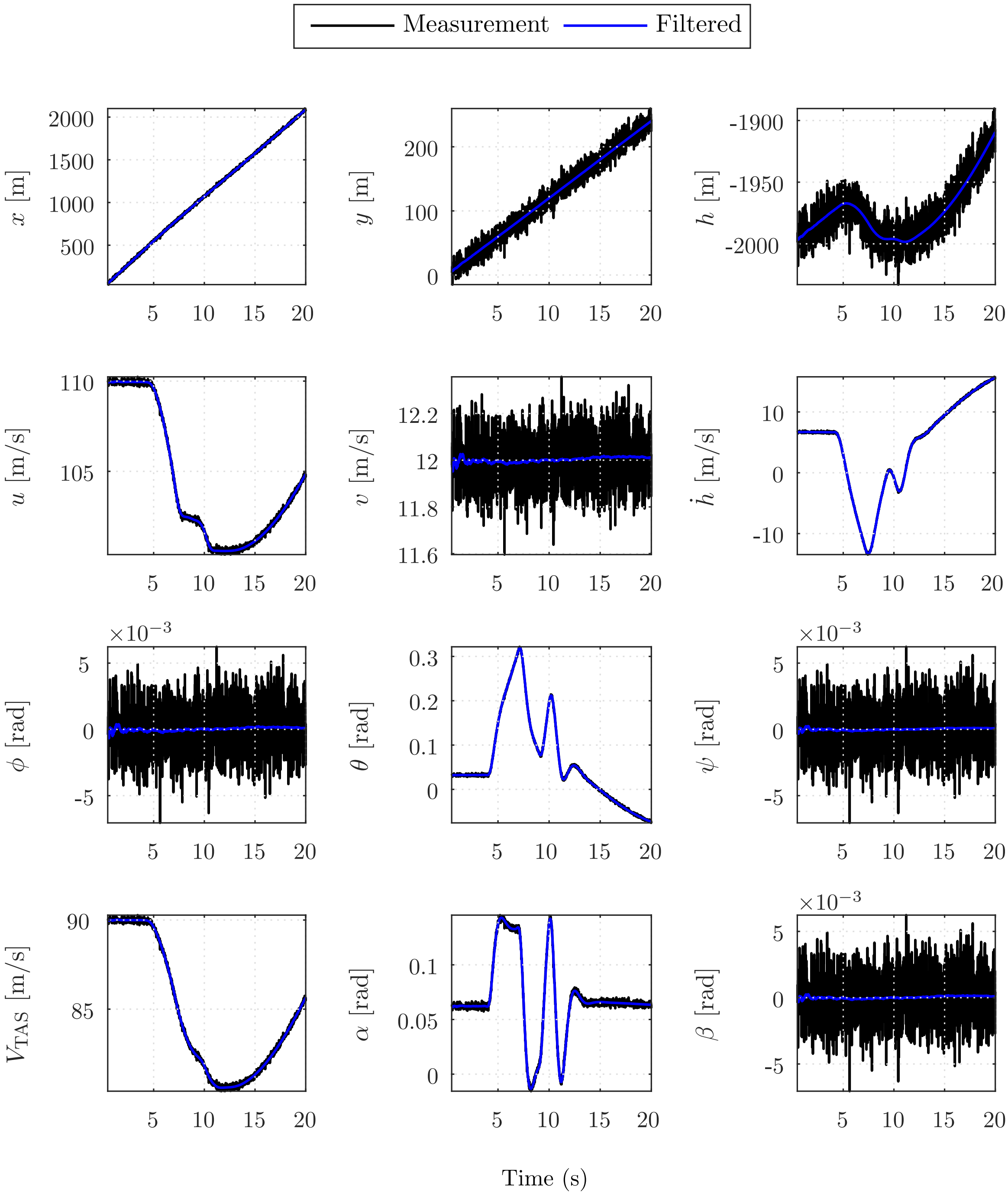

Figure 4-4: Measurement data used in the observation equations together with the measurements reconstructed by using the filtered data (blue).

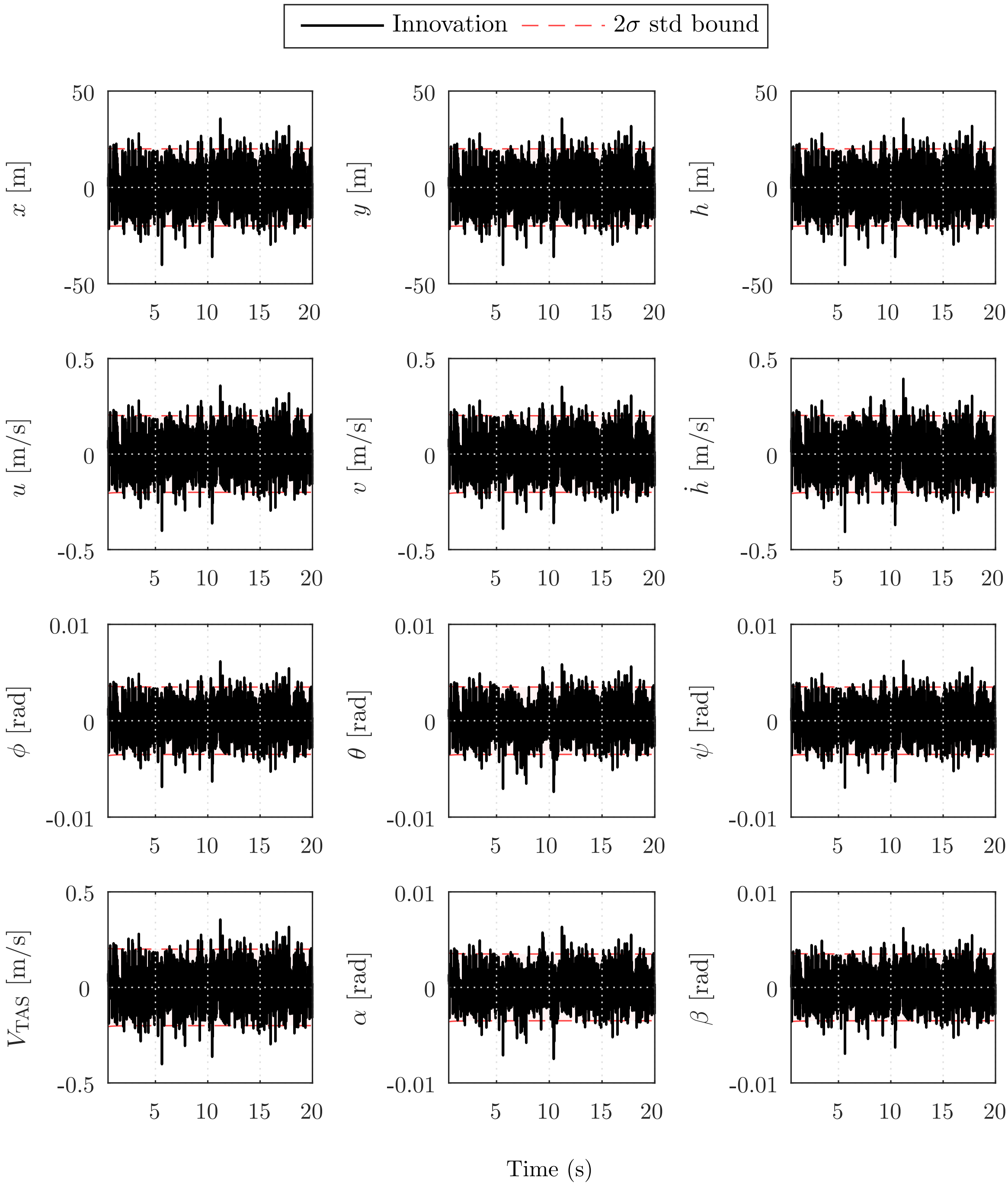

Figure 4-5: The set of innovation sequences of the IEKF when applied on data obtained from a non-linear Cessna Citation I simulation model.

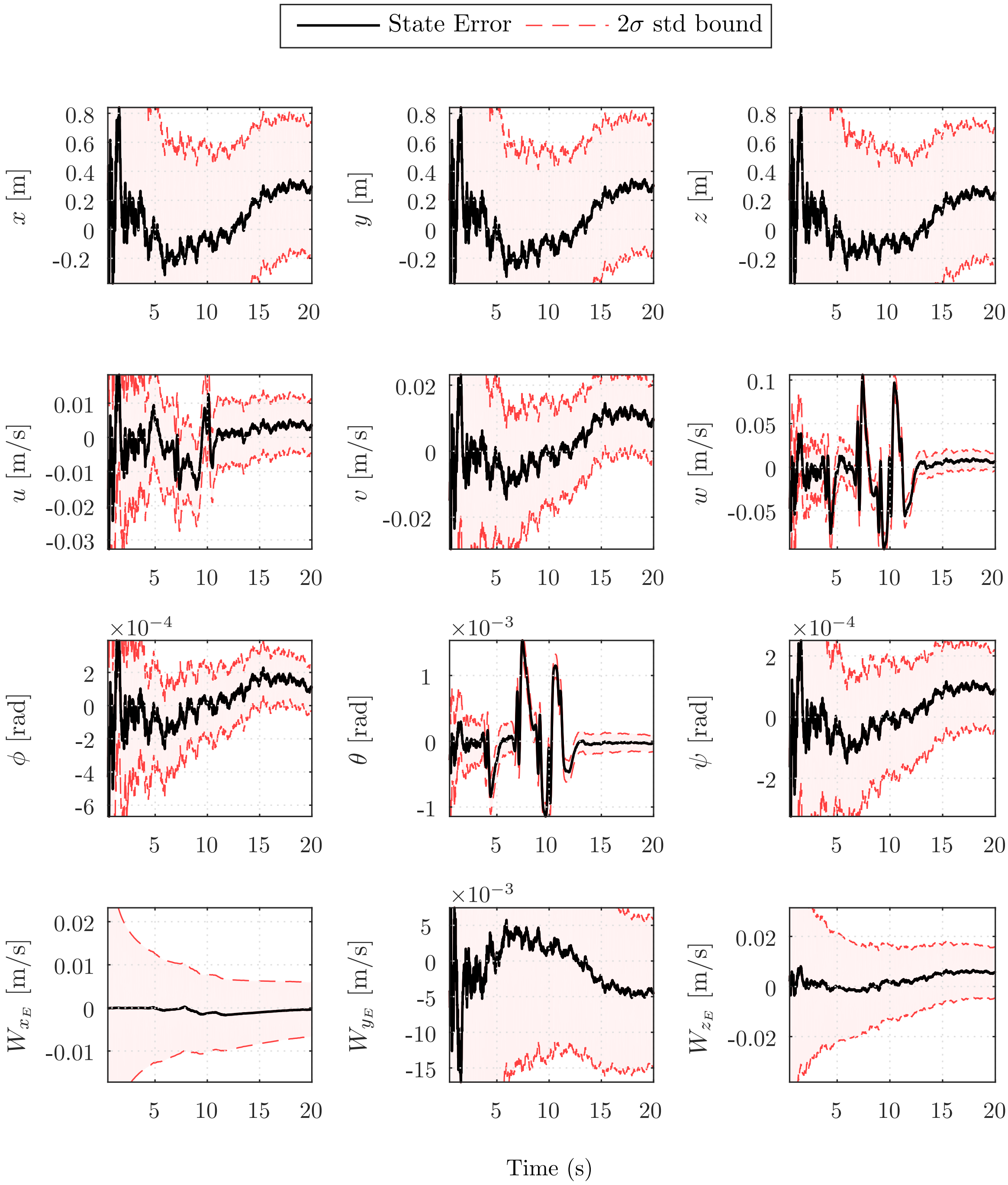

Figure 4-6: Error sequences, defined as the difference between the reconstructed state and the true state, when applying the IEKF to non-linear Cessna Citation I simulation data.

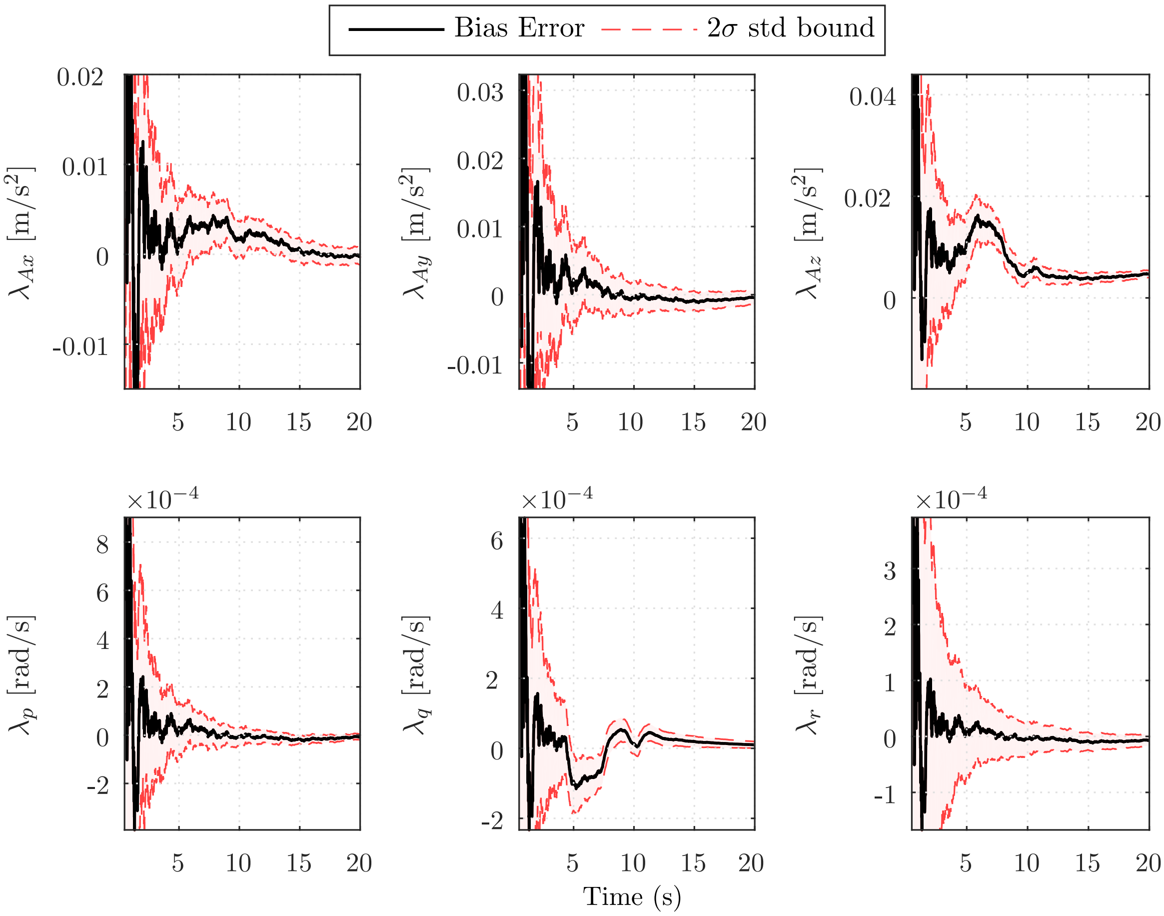

Figure 4-7: Error sequences for the IMU sensor biases, defined as the difference between the reconstructed sensor bias and the true sensor bias, when applying the IEKF to non-linear Cessna Citation I simulation data.

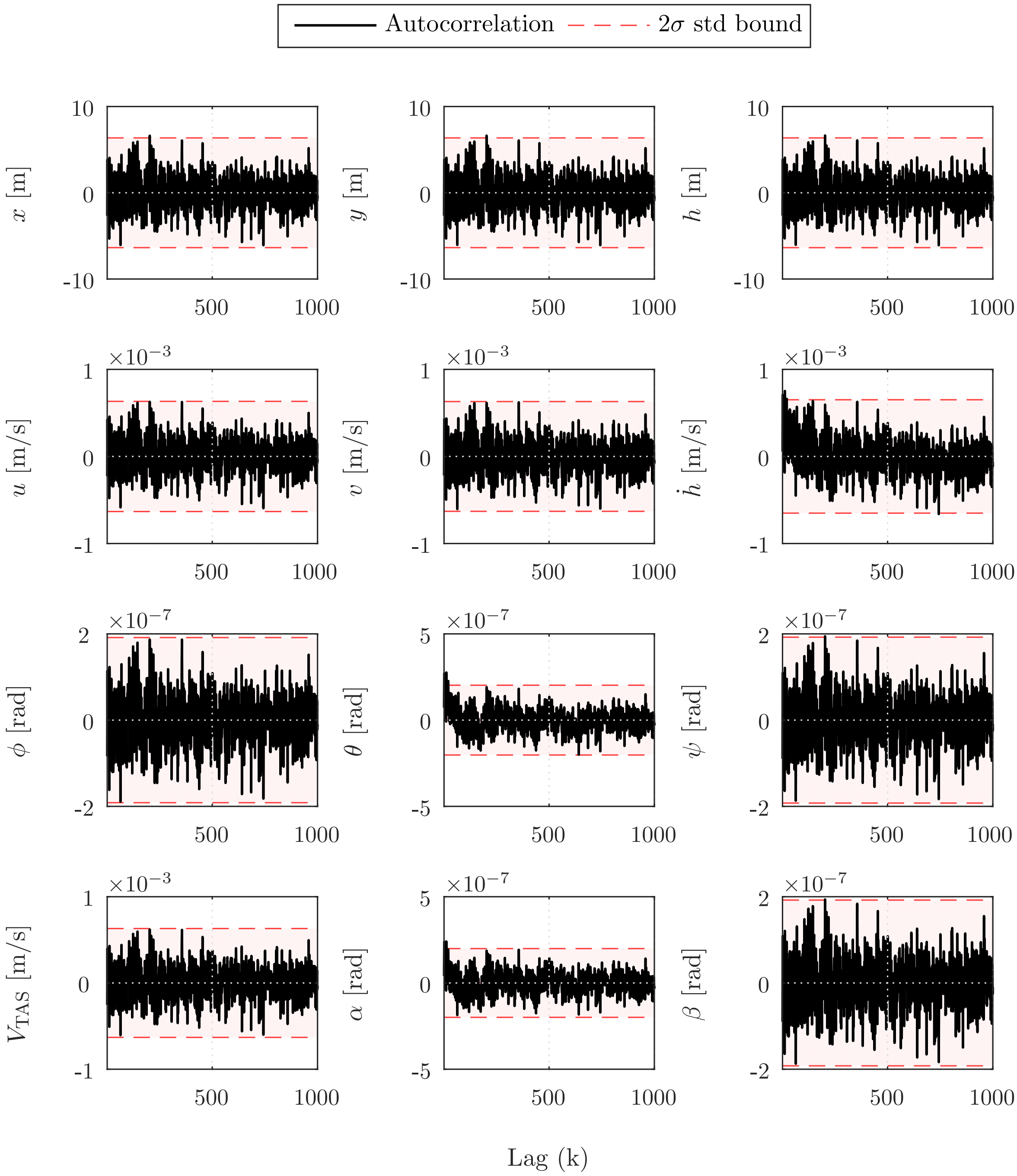

Figure 4-8: The consistency of the IEKF when applied to non-linear Cessna Citation I simulation data in terms of the autocorrelation of the innovation sequences $\mathcal{R}_{ss}$.

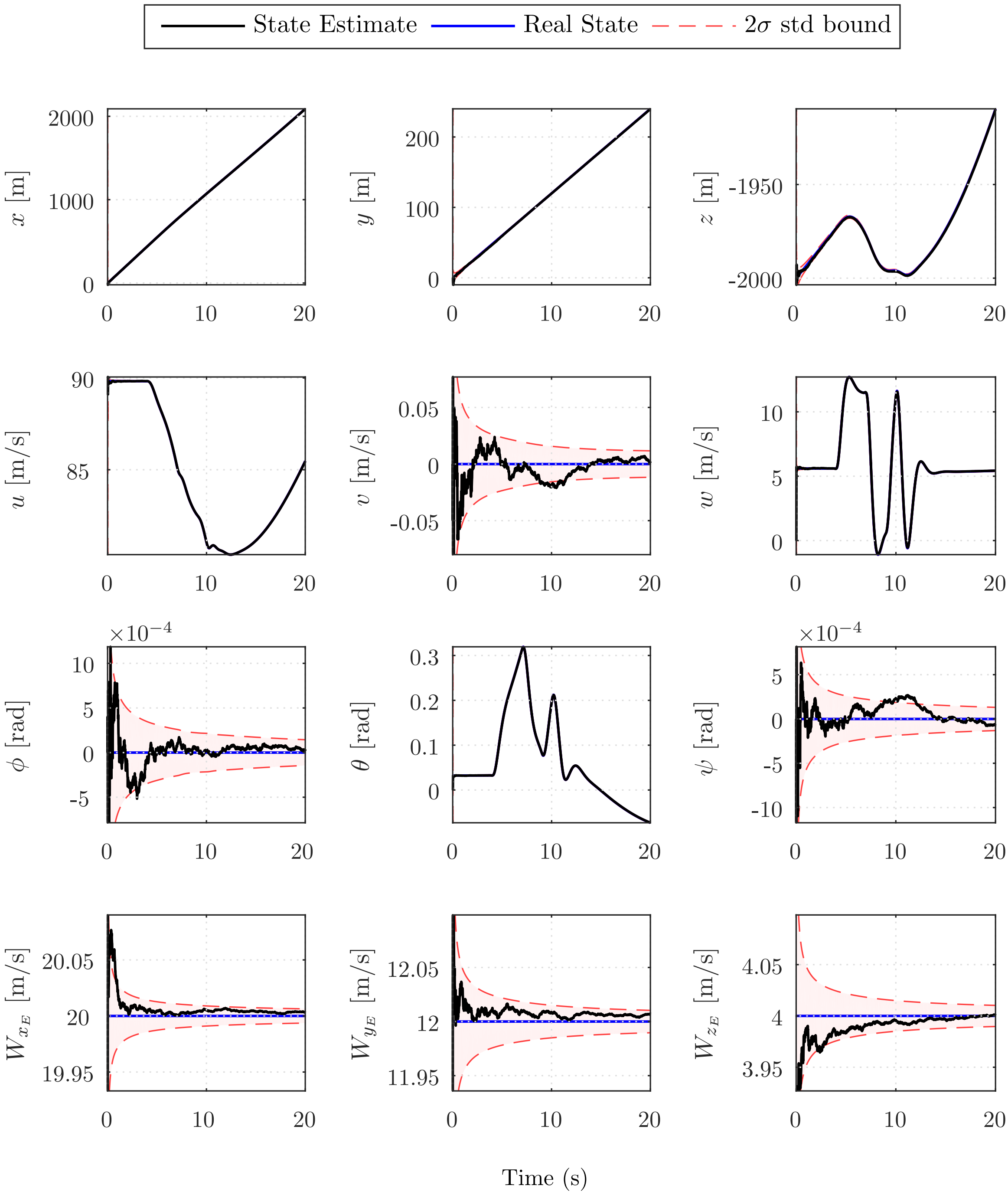

Figure 4-9: UKF state reconstruction on data obtained from a non-linear Cessna Citation I flight simulation model together with the 2σ confidence bounds (red) and the real aircraft state (blue).

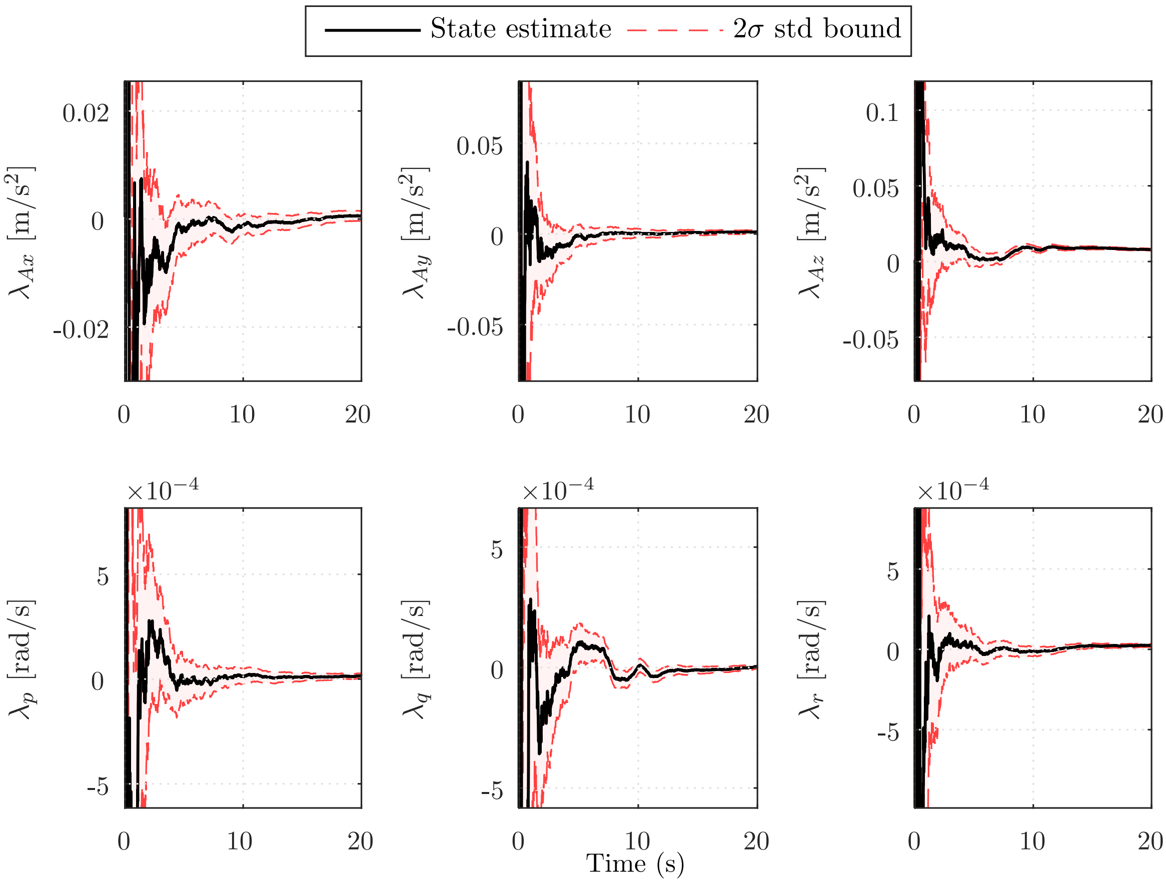

Figure 4-10: Estimated IMU sensor biases obtained with the UKF on data obtained from a non-linear Cessna Citation I flight simulation model together with the 2σ confidence bounds (red) and the real bias (blue).

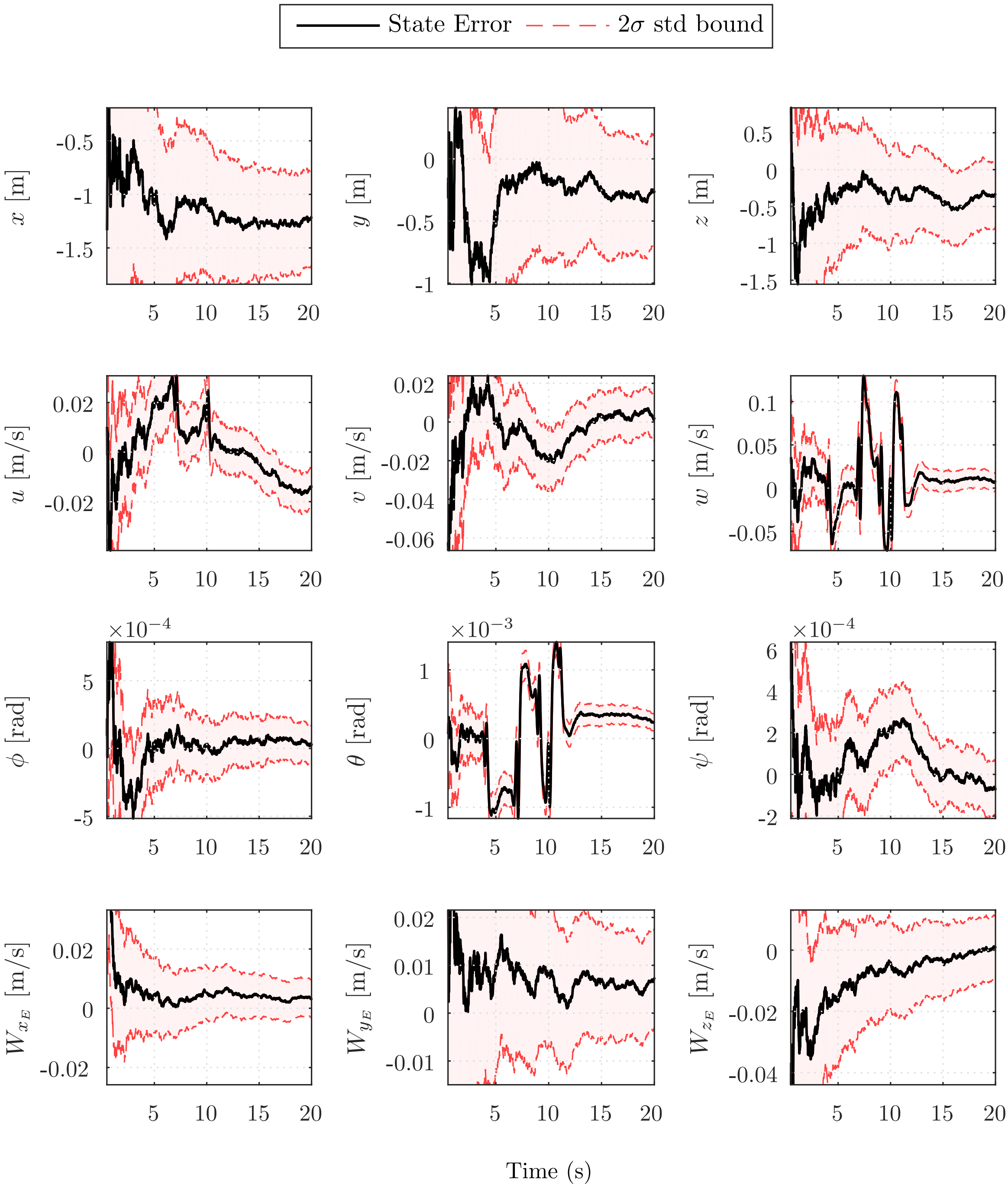

Figure 4-11: Error sequences, defined as the difference between the reconstructed state and the true state, when applying the UKF to non-linear Cessna Citation I simulation data.

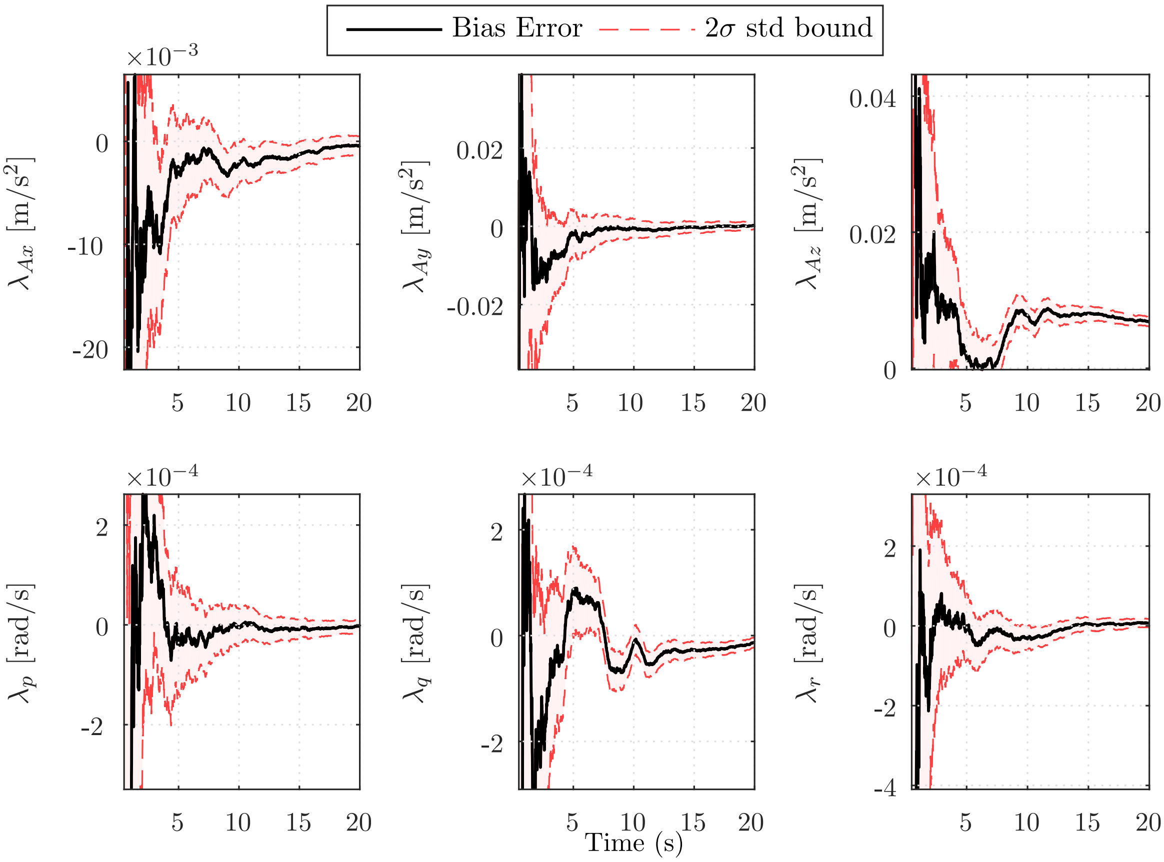

Figure 4-12: Error sequences for the IMU sensor biases, defined as the difference between the reconstructed sensor bias and the true sensor bias, when applying the UKF to non-linear Cessna Citation I simulation data.

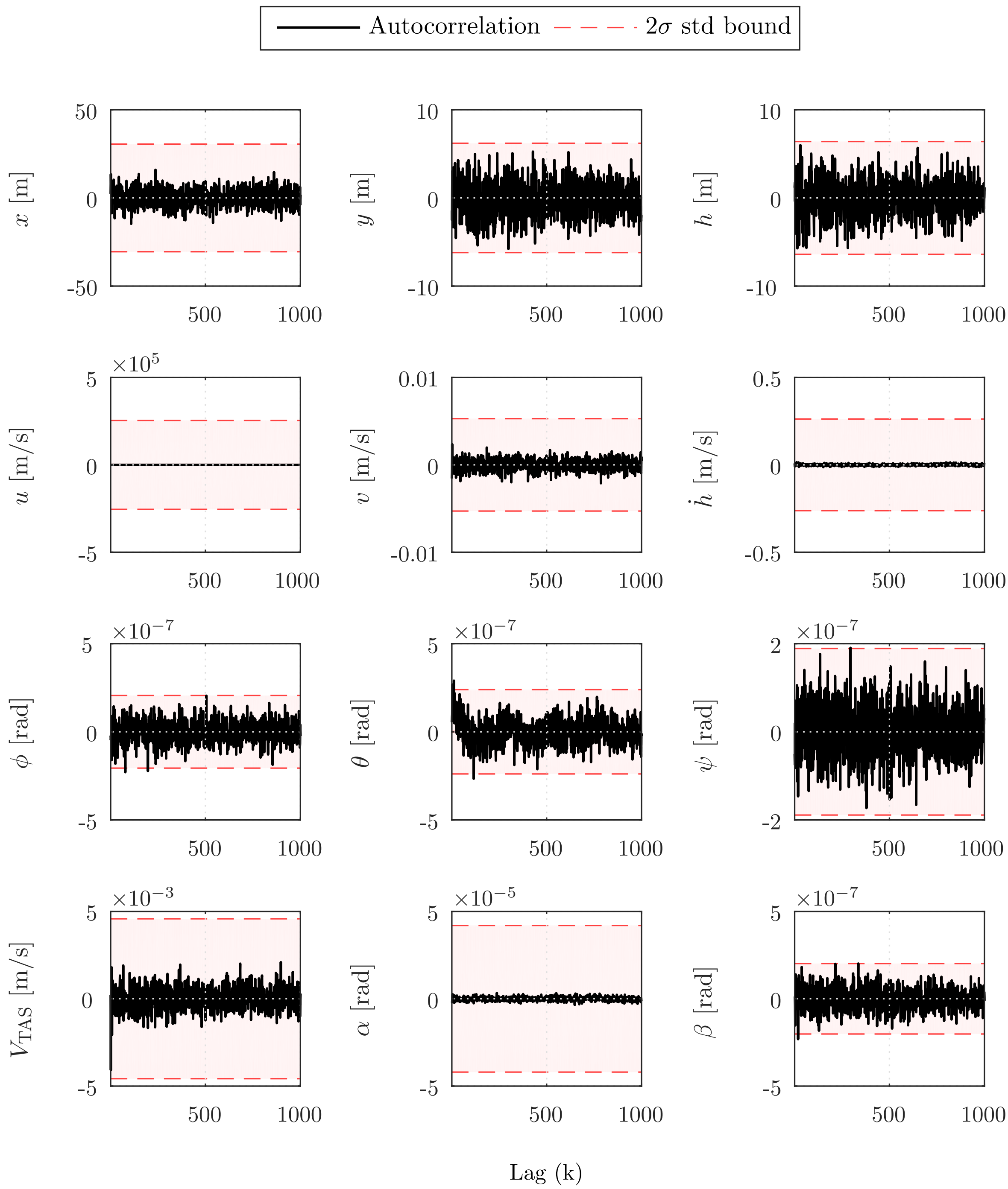

Figure 4-13: The consistency of the UKF when applied to non-linear Cessna Citation I simulation data in terms of the autocorrelation of the innovation sequences $\mathcal{R}_{ss}$.

The performance of the different Kalman filter and smoother types is shown in Figure 4-14 in terms of the magnitude of the RMS of the error indicated per state. As becomes evident from Figure 4-14, the position estimates show the largest RMSE, however, this can directly be related to the high noise intensity of the corrupted signals. For a better comparison of the low RMSE state estimates, Figure 4-15 shows the relative RMSE for each state. The latter figure clearly shows the deterioration in the state estimate by the use of an additional smoother. However, in absolute terms, this increase in RMSE is only marginal and therefore the performance can be said to be approximate the same level. It can be stated though that the additional computational costs of the application of a backward recursion smoother do not weight against the improvement in some state estimates.

For the identification of an aerodynamic model, clearly the position estimates do not play any role of significance. The altitude however is important in the defining the non-dimensional forces and moments. Clearly, the most important states are the body velocity components and the Euler angles. The estimated sensor biases are also important in order to obtain a corrected set of IMU measurements. Focusing on these states, it becomes evident that only in some cases the use of a smoother provides a slightly more accurate state estimate. In most cases, the use of a single-pass IEKF suffices and shows best performance in terms of the RMSE. In some cases, especially for the estimated sensor biases, the UKF provides a slightly better estimate. Overall, the performance of the IEKF and UKF can be considered similar. When applying the UKF to real flight test data, performance metrics might differ from the metrics presented in this work. In fact, results might be pointing towards an increased accuracy of the state estimates as obtained from the UKF. This can be stated by following the earlier presented reasoning and by considering the level of non-linearities in the simulation model. Since the simulation model itself is driven by a series of first order Taylor approximations of the non-dimensional forces and moments, the state estimation procedure does not benefit from any additional capability of approximating non-linearities in the presented data.

4-13 Sensitivity to Initial Conditions

In addition to the performance of the IEKF and UKF on a set of data with different noise realizations, the performance of both filter classes for different random initializations of the state vector was tested and averaged over a series of 50 Monte Carlo simulations. Random initializations points for each state were chosen around the true state with a standard deviation equal to two times the standard deviation of the noise (offset factor of 1). In addition, a deteriorated initialization of 20 standard deviations is shown in Figure 4-18 and Figure 4-19.

From Figure 4-16 and Figure 4-17 it becomes evident that for an offset factor of 1 of the initial state, a difference between the IEKF and UKF cannot be observed as both filters at approximately the same rate to the steady state error of the estimate.

Figure 4-18 and Figure 4-19 show different results for an initialization of the state vector at an offset factor of 10. In these figure, the inability of the IEKF to produce an accurate state estimate at some recursions due to observability problems is not reflected. However, on average the IEKF does show faster convergence to the steady state error. Yet again the

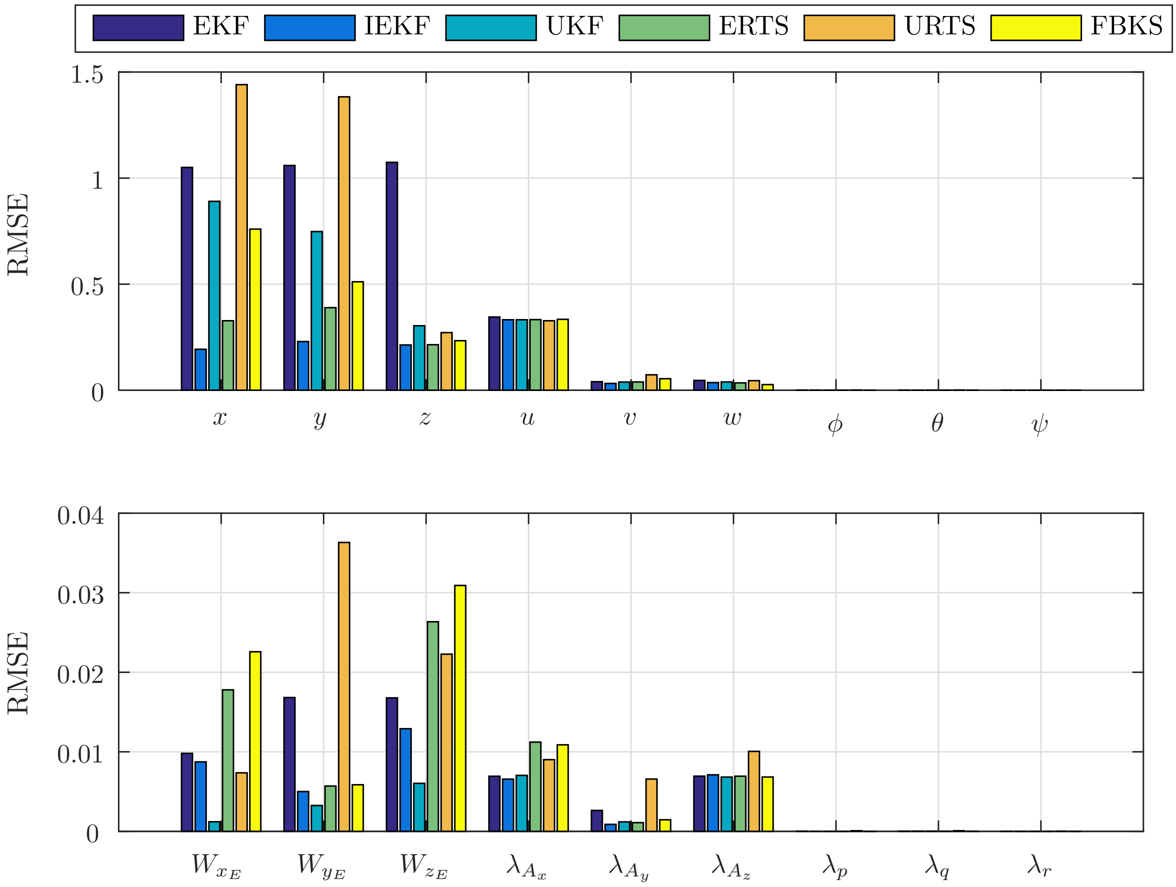

Figure 4-14: Comparison between different types of Kalman filters and smoothers applied to data obtained from a non-linear Cessna Citation I simulation model in terms of the RMSE indicated separately for each estimated state. Each index is the average of a 50 run Monte Carlo simulation.

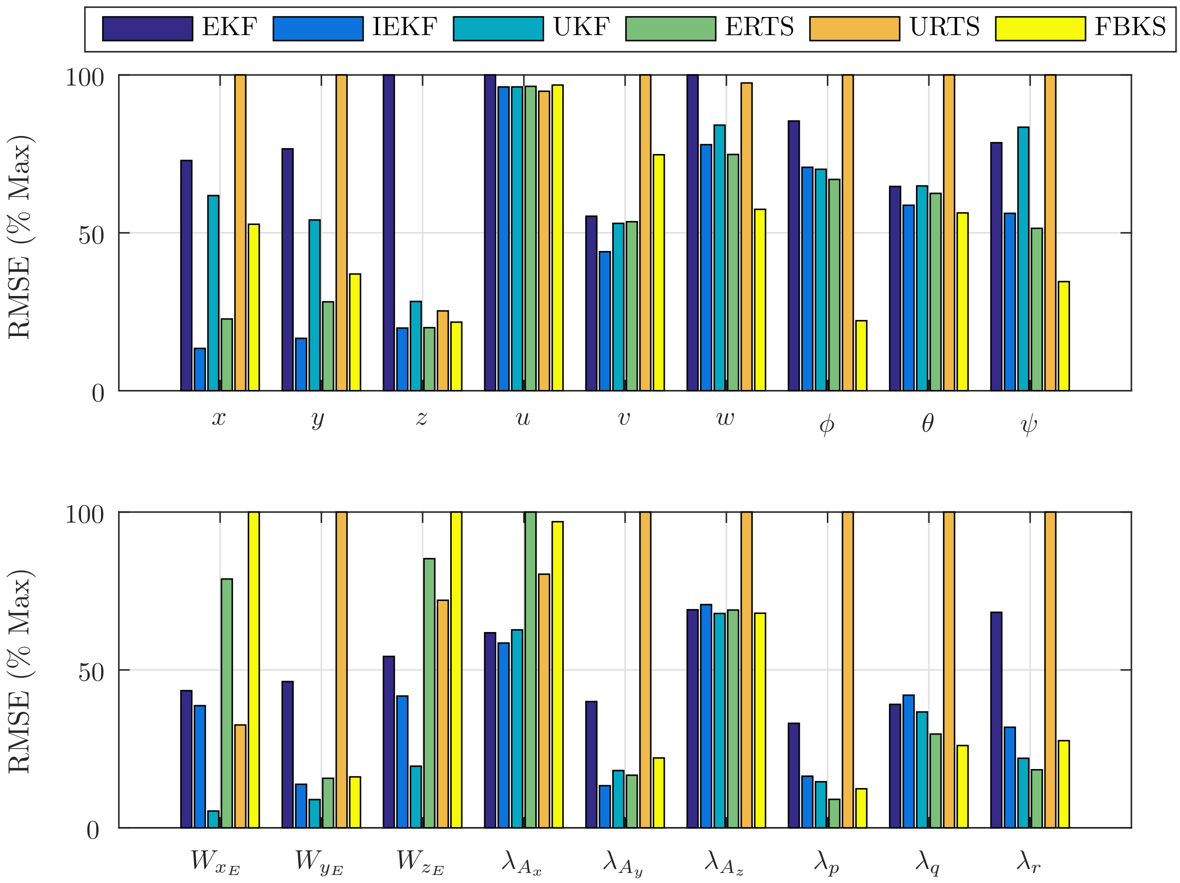

Figure 4-15: Comparison between different types of Kalman filters and smoothers applied to data obtained from a non-linear Cessna Citation I simulation model in terms of the relative RMSE indicated separately for each estimated state. Each index is the average of a 50 run Monte Carlo simulation.

IEKF and UKF converge to the same value after more than 40 iterations except for the state estimate of the x position and v body velocity despite the marginal difference.

4-14 Multi-rate versus Interpolation

The multi-rate implementation of the Kalman filter offers a structural solution if flight data is obtained at different sample rates. However, the data can simply be resampled at a specific rate. In order to investigate the difference between the two methods a comparison was made.

To mimic a multi-rate system, data from different sources, such as AHRS and IMU, was collected at different sample rates from the Citation I simulation. Since in realistic scenarios, elementary data such as the linear and rotational accelerations and body attitude angles are always collected at high sample rates, an investigation into the influence of sensor fusion in a multi-rate Kalman filter is of minor importance since linear interpolation techniques can already give a reasonable estimate because of the small time scale. More realistically, the collected set of measurements suffers from the low update rate of the GPS measurements. For this reason it was chosen to investigate the effect of medium and low sample rate GPS data on the performance of the Multi-Rate Iterated Extended Kalman Filter (MRIEKF) versus the IEKF applied to data obtained from spline interpolation.

When GPS data is obtained at a medium sample rate of 10 Hz, the difference between MR-IEKF and the regular IEKF with interpolation is small for most states. As expected, the MR-IEKF shows a marginal improvement or equal performance to the regular IEKF for the position estimates. More surprisingly, the sensor bias estimates show a relative improvement in performance in terms of the RMSE when the data is first resampled to the same base rate, see Figure 4-20.

In the scenario of the 1 Hz GPS sample rate, it clearly becomes evident that the interpolation approach offers increased accuracy over the multi-rate implementation, see Figure 4-21. This can be explained by the fact that the components of the GPS position can, in most cases, be approximated relatively well by a linear function. Therefore, it can be stated that interpolation techniques are well suited when applied to resample low-rate GPS data. AHRS data and IMU data, in this case study, were considered to have a fixed sample rate. In reality, it is very unlikely that the latter two systems provide samples at low rates.

In terms of overall RMSE, the multi-rate implementation of the IEKF scored slightly better in both cases: 0.72 versus 0.79 at 10 Hz and 1.51 versus 2.06 at 1 Hz.

4-15 Conclusion

In this chapter the theoretical constructs regarding flight path reconstruction were introduced and elaborated. In the context of this work, Kalman filter techniques will be used for flight

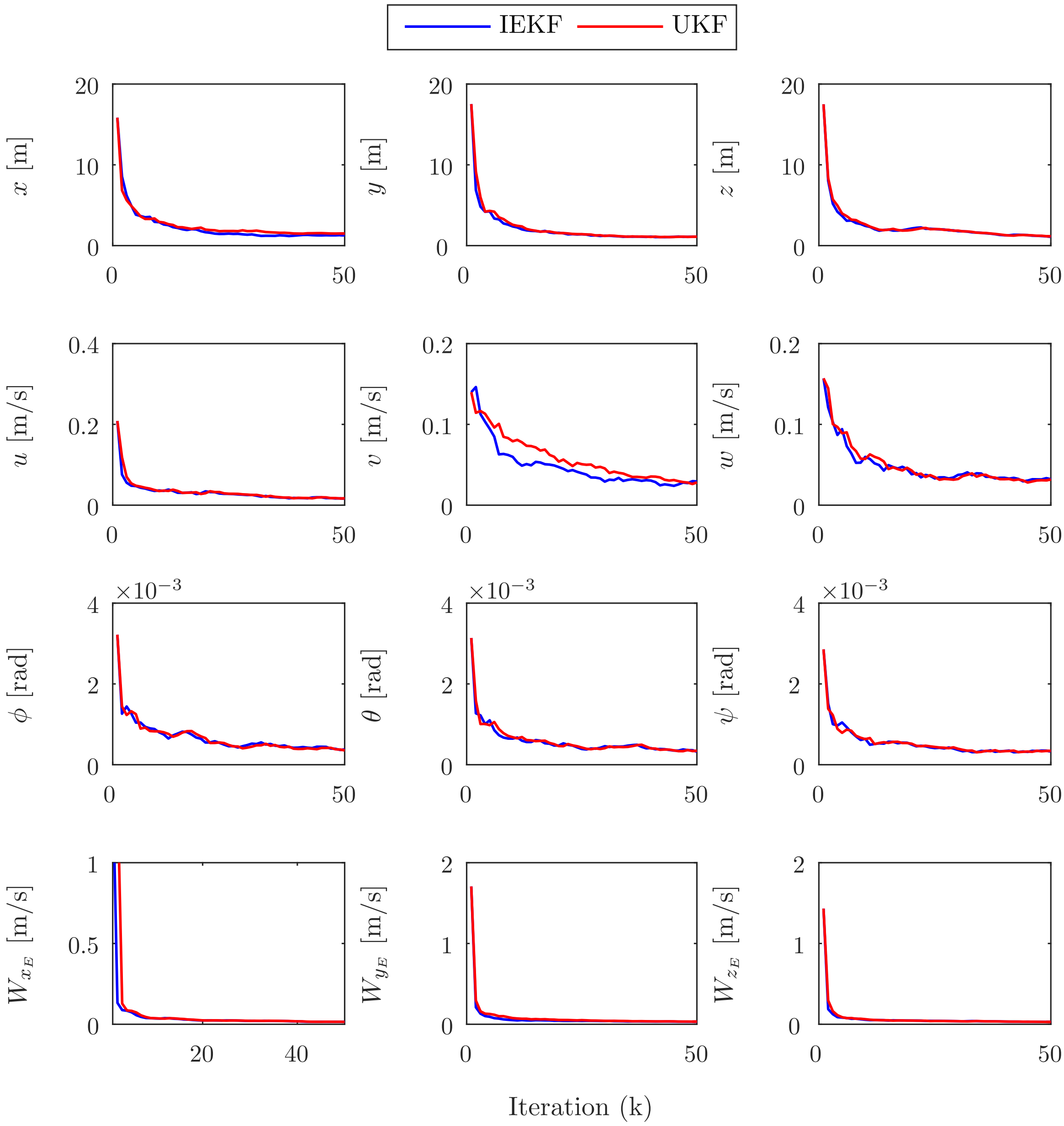

Figure 4-16: Convergence rate of the state estimate, expressed in terms of the error RMS, of the IEKF versus the UKF for $N = 50$ random initializations with an offset factor of 1.

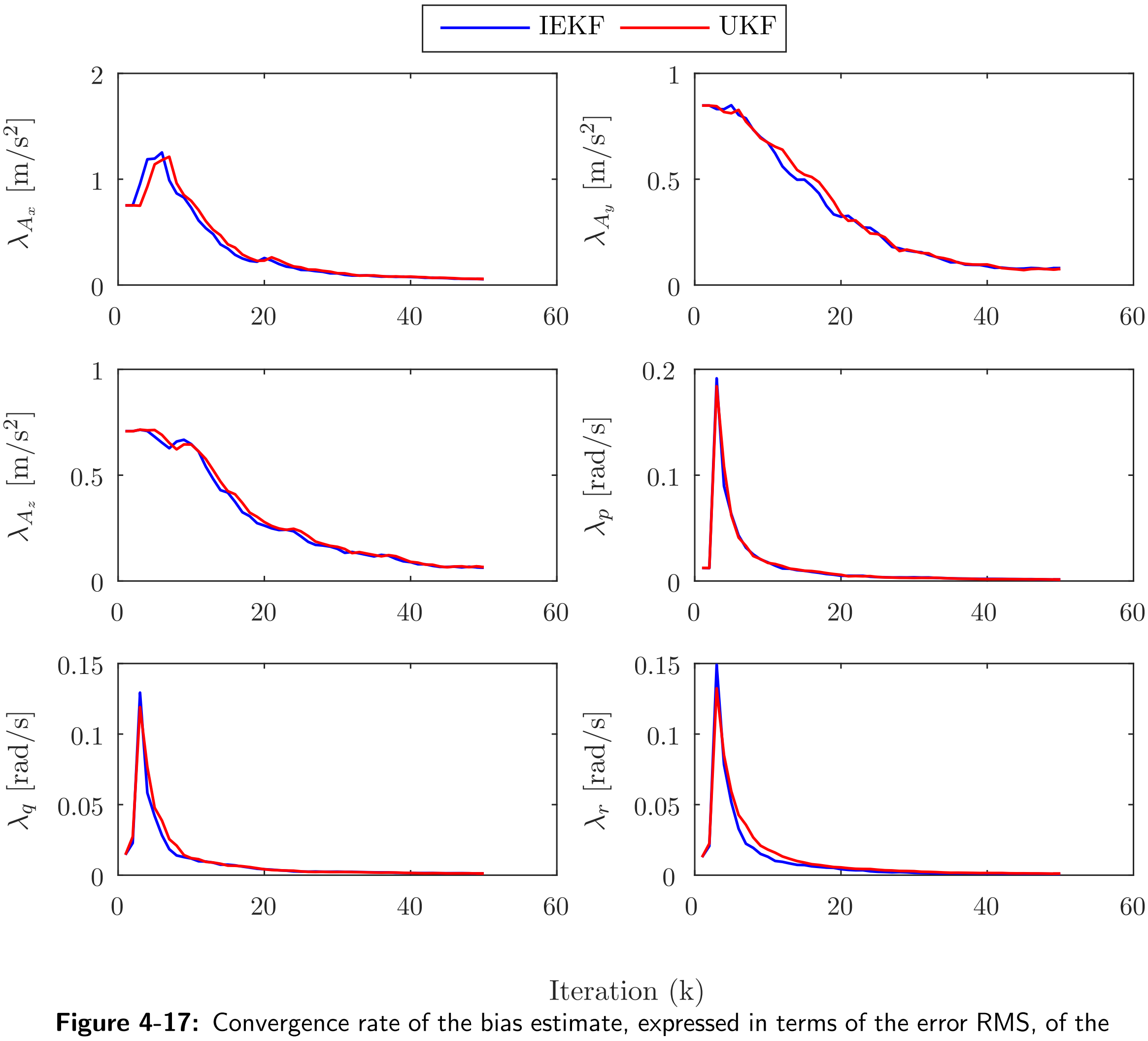

Figure 4-17: Convergence rate of the bias estimate, expressed in terms of the error RMS, of the IEKF versus the UKF for $N = 50$ random initializations with an offset factor of 1.

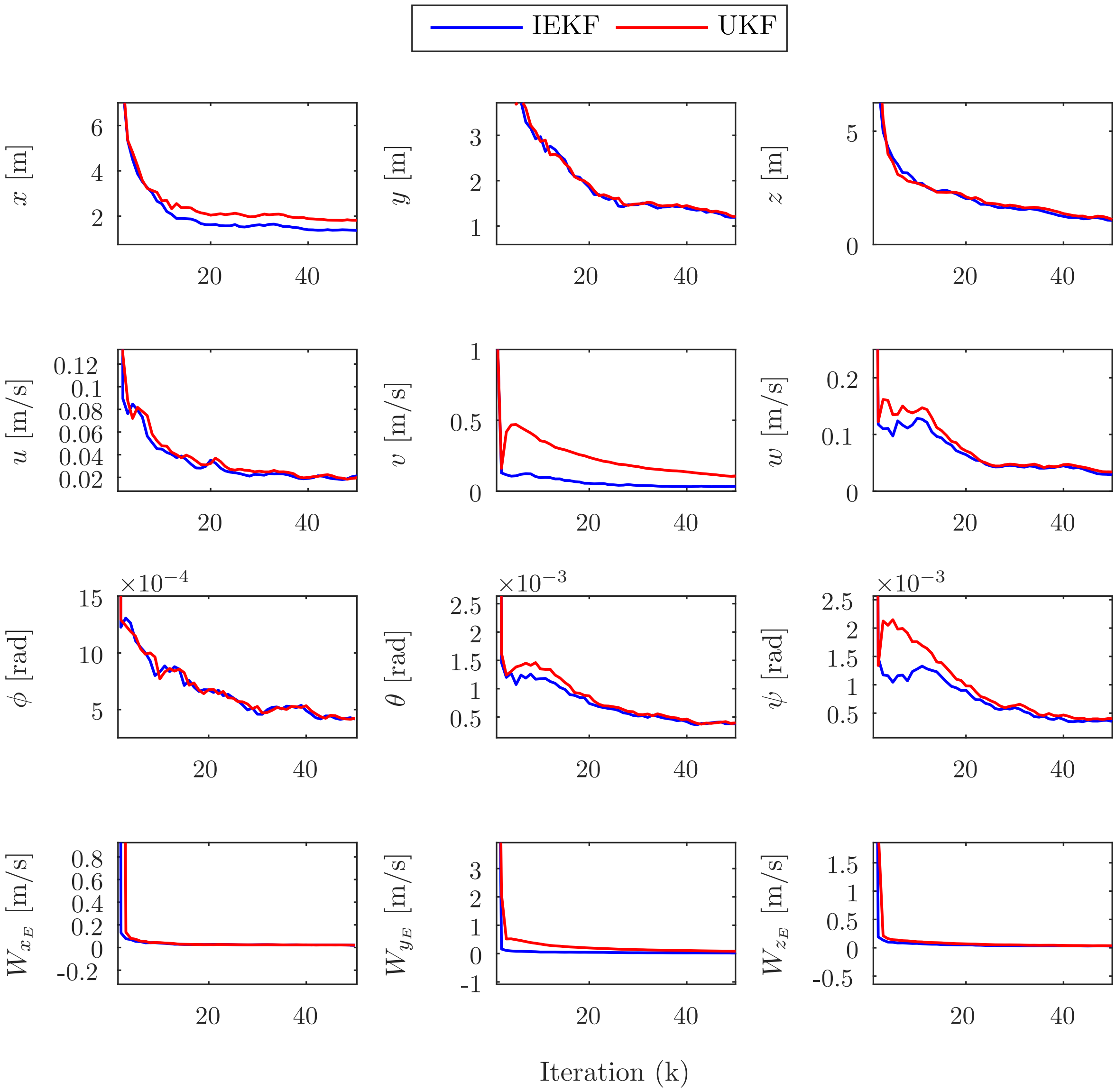

Figure 4-18: Convergence rate of the state estimate, expressed in terms of the error RMS, of the IEKF versus the UKF for $N = 50$ random initializations with an offset factor of 10.

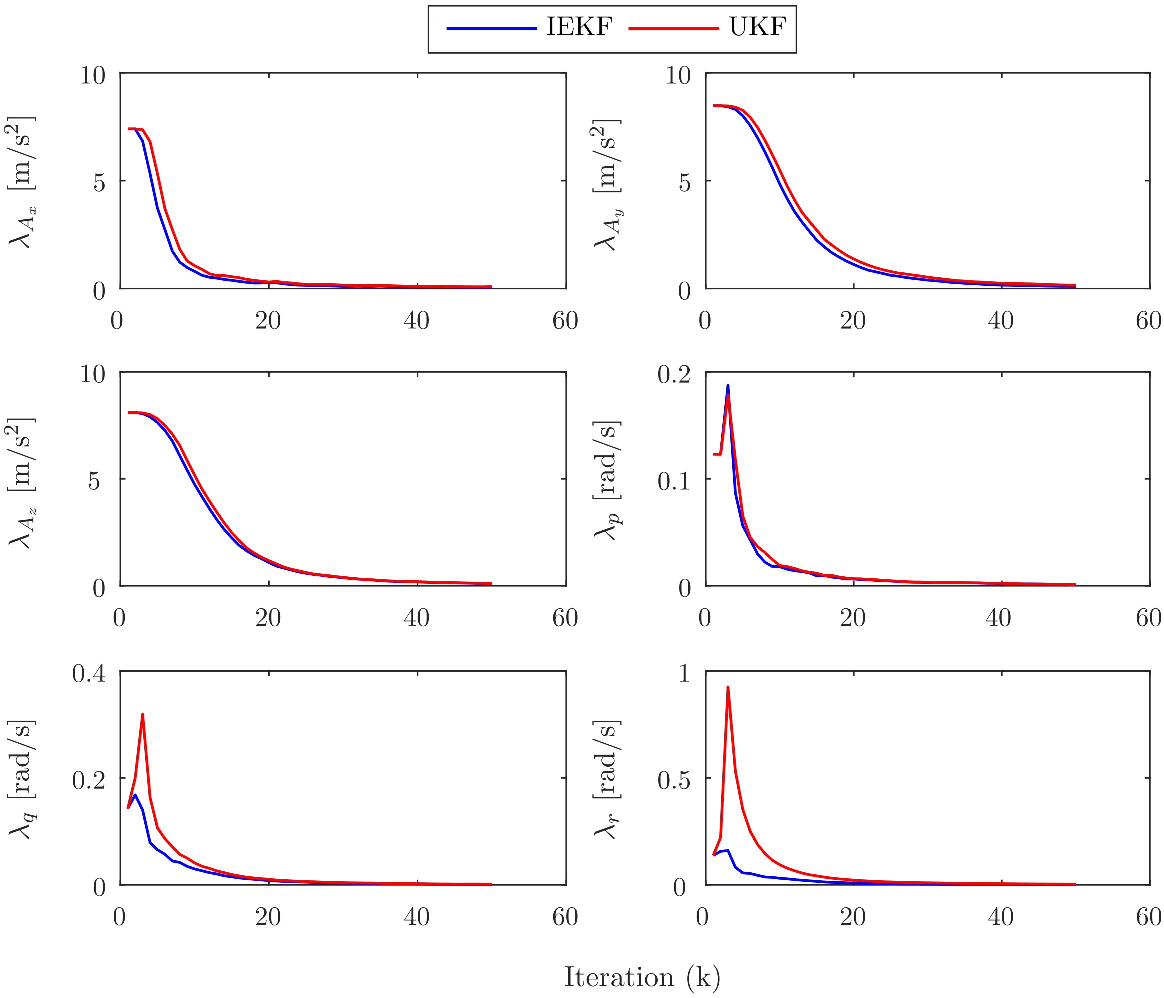

Figure 4-19: Convergence rate of the bias estimate, expressed in terms of the error RMS, of the IEKF versus the UKF for $N = 50$ random initializations with an offset factor of 10.

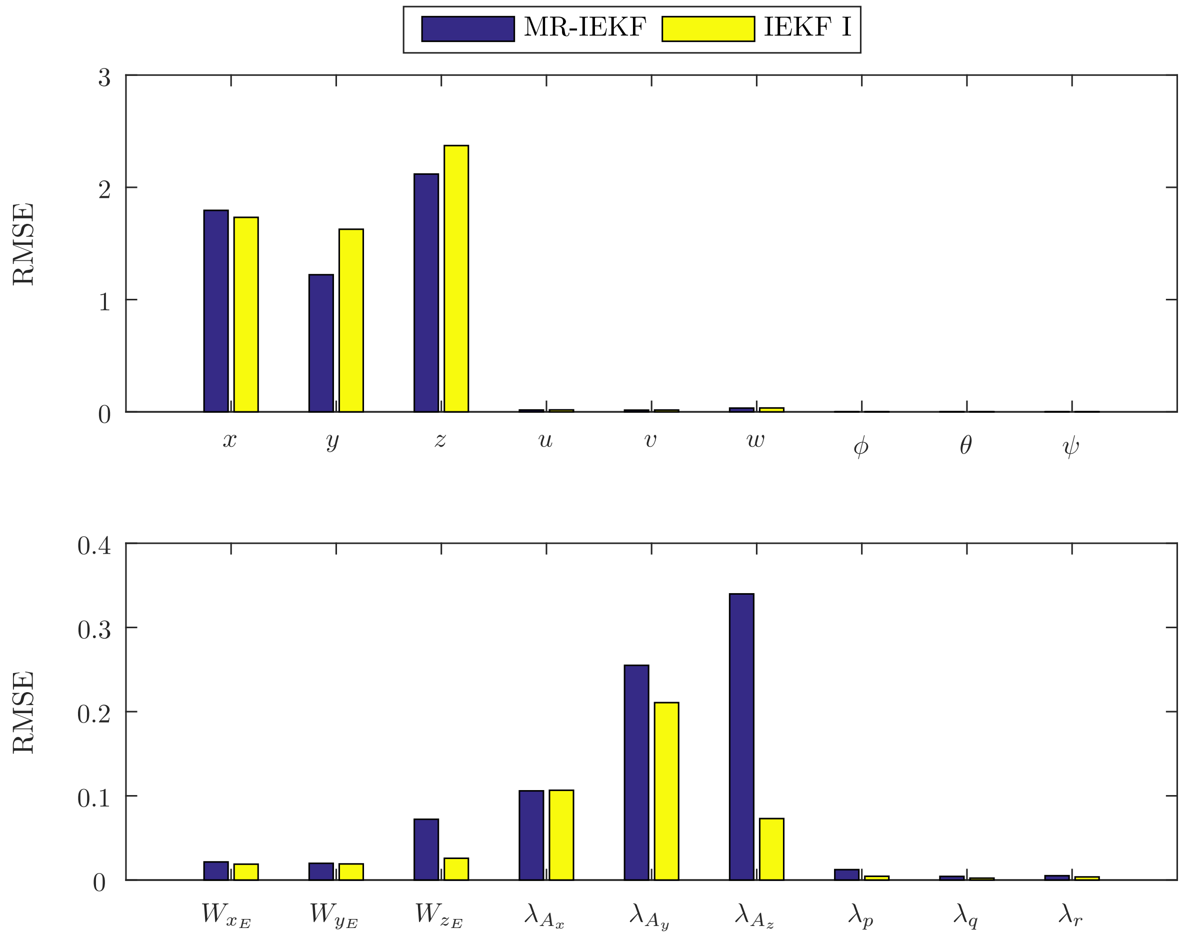

Figure 4-20: Comparison between the performance of the multi-rate IEKF and the regular IEKF with single-rate data obtained from spline interpolation for a GPS sample rate of 10 Hz

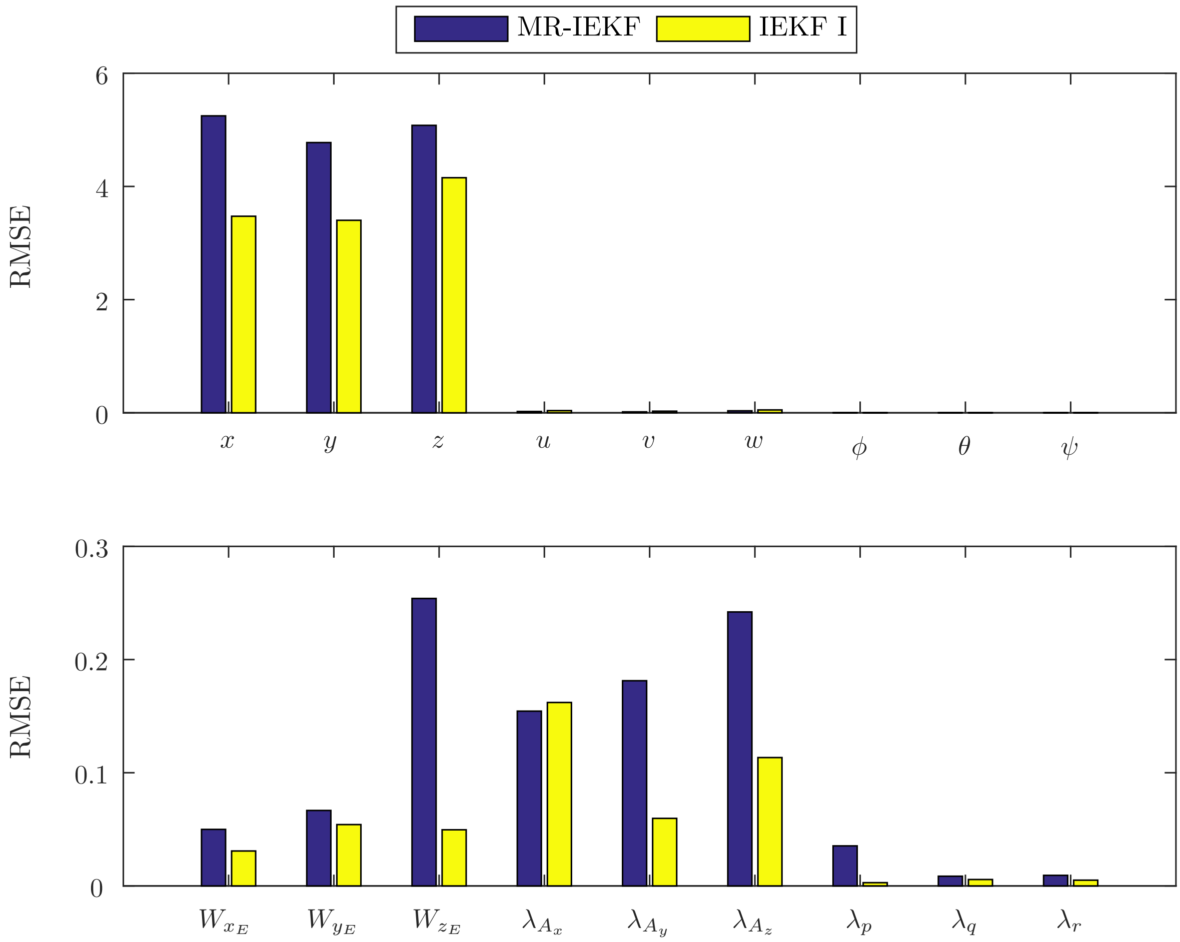

Figure 4-21: Comparison between the performance of the multi-rate IEKF and the regular IEKF with single-rate data obtained from spline interpolation for a GPS sample rate of 1 Hz

path reconstruction and data compatibility checking in order to use a collection of flight path data for the identification of a new aerodynamic model of the Cessna Citation II.

During the years, many different classes of Kalman filter have been developed for different applications. The most used Kalman filter up to date is the extended Kalman filter, which employs a local linearization technique to allow application to non-linear systems. The latter type of filter was improved by a minor extension in the form of local iterations. These iterations reduce the difference between the state estimate and the reference trajectory, hence the IEKF. Despite their sub-optimality in non-linear flight path reconstruction problems, these filters are still widely used for these types of problems.

As a more recent innovation, the UKF was introduced as a new class of Kalman filter with its own internal dynamics. Instead of relying on (iterative) state linearization, the stochastic properties of the underlying dynamics are now represented by a set of sigma points obtained from the unscented transformation of the state vector. In theory, this approach should be able to capture the second and higher order statistical properties of the system with greater accuracy than the traditional approaches. Furthermore, different researches also confirm the superiority of the UKF in terms of convergence rate when applied to non-linear state estimation problems.

The choice of state transition functions and measurement equations plays a significant role in the performance of any type of Kalman filter. Additions to the standard set of equations can improve the performance of the filter in terms of a smaller magnitude of some innovation sequences. Despite these improvements, extensions to the state equations must be made with caution as the set of measurements must provide enough information for a successful reconstruction. Observability is a measure to indicate the ability to obtain information about the internal state from an external set of measurements. For non-linear systems, this is reflected by the Lie derivatives.

In this chapter, an investigation into the performance of different Kalman filter and smoothers was performed in the framework of a non-linear Cessna Citation I simulation model. This investigation reveals no significant improvement in the state estimate by the UKF versus the IEKF. In terms of sensitivity to initial conditions, the IEKF performed slightly better for a large offset from the nominal state. However, this large offset may be considered as unrealistic. In most cases, application of additional Kalman smoothers do not improve the accuracy of the state estimates.

In reality, data is often obtained at different sample rates. A more structural solution to this problem is the use of a multi-rate Kalman filter. Analysis has also indicated that the use of such types of Kalman filters only improve the estimates of certain states. Moreover, in most cases the estimate of the states obtained at higher sample rates deteriorate in comparison to the state estimate obtained from a regular KF with a spline interpolation approach to resample the data.

On balance, the IEKF and UKF show comparable performance when applied to the Cessna Citation I simulation framework. The choice between the two types of filters can therefore be based on the computational efficiency and the theoretical prospects of both filter classes. When considering the, theoretical, improved ability of the UKF to process data corrupted with non-Gaussian noise, the latter class of KF receives slight preference above its counterpart.

Chapter 5

Parameter Estimation

In aerospace system identification, parameter estimation is an essential step in the determination of a model. Often these model parameters are obtained from experimental data, i.e. flight test data. As already mentioned in previous chapters, the TSM was chosen as base method for this work. By effectively decomposing the non-linear identification problem into two steps, linear parameter estimation techniques can be used to identify the parameters of the selected model structure. Therefore, linear parameter estimation techniques will be discussed in particular.

In this chapter, parameter estimation methods and the methodology in model structure selection will be elaborated in a framework applied to the identification of an aerodynamic model from flight test data. In addition, the selected methodology will be applied to data acquired from a non-linear Cessna Citation I simulation model.

5-1 Introduction

Parameter estimation is an essential part in the identification of an aerodynamic model from flight test data. Many different techniques are described in literature, of which the most applied methods in the domain of parameter estimation are the least-squares methods (Strejc, 1983). This collection of methods tries to find the best fit to the presented data by minimizing the sum of squared residuals, the difference between the estimated model output and data. From a theoretical perspective, these methods have efficiently reduced parameter estimation from a non-linear to a linear optimization problem. The assumption that was taken for this approach is that the residuals of the observation should be uncorrelated and that the variance should be stationary. For raw flight data these assumptions do not often hold. Minor extension to the original least-squares approach can help in these cases, however, this requires the covariance matrix to be known beforehand. These methods include weighted least-squares and generalized least-squares (Klein, 1989). In theory, the best possible estimate of the parameters, i.e. the parameters that did most likely produce the set of data presented, is found by application of maximum likelihood estimation. This method was applied in a lot of different research (Lichota & Lasek, 2013; Kumar & Ghosh, 2011; Chu, Mulder, & Van Woerkom, 1995) and many applications were derived from this theory (Chu, Mulder, & Van Woerkom, 1996; Rauch, Striebel, & Tung, 1965). Despite its theoretical estimation of the asymptotic covariance matrix, and therefore also a set of parameters with the least variance, this method also presents a non-linear optimization problem. This in contrast to the least-squares routines. Altogether, maximum likelihood estimation is a more robust method when working with stochastic data. Its application should be preferred when considering the use of the equation-error and filter-error methods. In case of decomposition of the equation-error method into a flight path reconstruction problem and parameter estimation problem (TSM) its usefulness depends on the covariance of the residuals. In the latter case, least squares methods can also give an accurate estimate of the model parameters under the assumption that the residuals of the model are uncorrelated.

Least squares methods exist in many forms, all of which have the Ordinary Least Squares (OLS) method at their basis. Before going into the derivation of the OLS method, it is important to know that all linear least squares methods build upon the assumption that any function can be expressed in terms of an algebraic basis. Given a set of any arbitrary number N of observations of independent variable x and the same number of dependent variable $y = f(x)$, the data can be approximated by a function of the type:

$$\phi(x) = \sum_{i=1}^{m} \theta_i \varphi_i(x) \tag{5-1}$$

where $\varphi(fx)$ denotes any basis function. In least squares, it is common practice to use an algebraic polynomial basis function which, in turn, can be expressed as:

$$\varphi_i(x) = x^{i-1} \tag{5-2}$$

Substitution of Eq. (5-2) into Eq. (5-1) yields univariate polynomial basis $P(x)$:

$$P(x) = \sum_{i=1}^{m} \theta_{i-1} x^{i-1} = \theta_0 + \theta_1 x + \theta_2 x^2 + \ldots + \theta_{m-1} x^{m-1} \tag{5-3}$$

where the degree of the polynomial is denoted by $m-1$. Most frequently, the polynomial basis is a function of more than one variable which can be formulated by superimposing the different independent variables related to the dependent variable. A generalized description of a bi-variate polynomial of degree $m-1=2$ is given as following:

$$P(x_1, x_2) = \theta_0 + \theta_{1,0} x_1 + \theta_{0,1} x_2 + \theta_{2,0} x_1^2 + \theta_{1,1} x_1 x_2 + \ldots = \sum_{i=1}^{n+m=d} \theta_{n,m} \frac{d!}{n!m!} x_1^n x_2^m \tag{5-4}$$

where n and m indicate, respectively, the degree of independent variables x_1 and x_2. The total degree is given by $n+m=d$.

5-2 Principles of Regression Analysis

Usually for regression analysis it is assumed that the model is linear in the parameters. Hence, the parameters of the model only appear in linear fashion, e.g. parameters appear as multiplicative factors for every term or cross-term of independent variables. By having defined a model structure such as described in Section 5-1, it is possible to collect the set of N independently collected observations in regression matrix or design matrix $\mathbf{X}$. For a polynomial of degree m the design matrix is given by:

$$\mathbf{X} = \begin{pmatrix} 1 & x(1) & x^2(1) & \dots & x^m(1) \\ 1 & x(2) & x^2(2) & \dots & x^m(2) \\ \vdots & \vdots & \vdots & \ddots & \vdots \\ 1 & x(N) & x^2(N) & \dots & x^m(N) \end{pmatrix} \tag{5-5}$$

The regression model can now be formulated as follows:

$$\mathbf{y} = \mathbf{X}\boldsymbol{\theta} + \boldsymbol{\varepsilon} \tag{5-6}$$

where $\boldsymbol{\theta}$ is a vector of parameters and $\boldsymbol{\varepsilon}$ the vector of model residuals. The independent variables in the rows of $\mathbf{X}$ are also often referred to as regressors. The least squares estimation of the model parameters is found by, as the name implies, minimizing the sum of squared residuals. By defining a criterion or cost function J as follows:

$$J = \sum_{i=1}^{N} \varepsilon_i = \sum_{i=1}^{N} (y_i - X(x_i)\boldsymbol{\theta}) \tag{5-7}$$

where $X(x_i)$ is the ith row of the design matrix. The convex cost function has a minimum when the partial derivative of the cost function with respect to the parameter vector $\boldsymbol{\theta}$ is zero

$$\frac{\partial J(\mathbf{x}, \boldsymbol{\theta})}{\partial \boldsymbol{\theta}} = \frac{\boldsymbol{\varepsilon}^\intercal \boldsymbol{\varepsilon}}{\partial \boldsymbol{\theta}} = 0 \tag{5-8}$$

The set of parameters for which the convex cost function is minimized is obtained by solving for $\arg\min_\theta J$. Without a full derivation, the least squares estimator for the parameters of a linear in the parameters model is given by (Strejc, 1983; Ljung, 2002):

$$\hat{\boldsymbol{\theta}} = \left(\mathbf{X}^\intercal \mathbf{X}\right)^{-1} \mathbf{X}^\intercal \mathbf{y} \tag{5-9}$$

The predicted outcome of the ordinary least squares estimator is then given by:

$$\hat{\mathbf{y}} = \mathbf{X}\hat{\boldsymbol{\theta}} \tag{5-10}$$

Subsequently, the residuals and Mean Squared Error (MSE) can be defined as:

$$\boldsymbol{\varepsilon} = \mathbf{y} - \hat{\mathbf{y}} \tag{5-11}$$

$$\text{MSE} = \frac{1}{N}\sum_{i=1}^{N}(\mathbf{y}-\hat{\mathbf{y}})^2 \tag{5-12}$$

The OLS estimator is a very simple and straightforward procedure to obtain an estimate of the model parameters, however, it should be used with caution. The OLS estimator was derived with the following assumptions which should also be met for the OLS estimator to be a Best Linear Unbiased Estimator (BLUE):

1. The model is linear in the parameters, i.e. the dependent variable is a function of a set of superimposed independent variables multiplied by their coefficients with, in addition, an error term describing the error of the regression model with respect to the real model.
2. The expected value for the model residuals is equal to zero: $\mathbb{E}\{\varepsilon_i\} = 0$.
3. The variance of the residuals is constant $\text{Var}(\varepsilon_i|x_i) = \sigma^2$. This assumption implies that all diagonal terms of the residuals covariance matrix are equal to each other: $\text{Cov}(\varepsilon_1, \varepsilon_1) = \text{Cov}(\varepsilon_2, \varepsilon_2) = \ldots = \text{Cov}(\varepsilon_N, \varepsilon_N) = \sigma^2$.
4. The last assumption states that the correlation terms in the covariance matrix of the residuals should be equal to zero, these terms correspond to the off-diagonal terms of the residuals covariance matrix: $\mathbb{E}(\varepsilon_i^\intercal \varepsilon_j) = \text{Cov}(\varepsilon_i, \varepsilon_j) = 0 \quad \forall\, i \neq j$.

The latter two conditions imply that the covariance matrix of the residuals should be homoskedastic, i.e. a constant term in the diagonal and all other elements equal to zero. The above mentioned assumptions are the Gauss-Markov assumptions, summarized in the Gauss-Markov theorem.

As already mentioned earlier in previous chapters, the main advantage of the use of the TSM is an effective decomposition of the non-linear parameter estimation problem into a non-linear state estimation or reconstruction problem and a linear parameter estimation problem. For this reason, the use of OLS in the parameter estimation procedure suffices in most cases. However, depending on the performance of the Kalman filter and nature of the system's dynamics, which is always (moderately to highly) non-linear in aircraft state estimation, the residuals resulting from the parameter estimation problem, in the practical case, might be heteroskedastic. In other words, the off-diagonal terms of the residuals covariance matrix are not equal to zero indicating correlation between the residuals. In addition, the variance of the residuals might vary in time resulting in non-homogeneous variance over the residuals covariance matrix. In these cases, the use of a Generalized Least Squares (GLS) method offers a solution.

The fundamental model assumptions for GLS are analogous to the assumptions for the OLS model but differ in the assumption of the residual covariance matrix. In the OLS case, the covariance matrix can simply be written as $\hat{\sigma}^2\mathbf{I}$, where the covariance matrix under GLS differs in terms of non-homogeneous variance on the diagonal and non-zero elements off the main diagonal:

$$\text{Cov}\{\boldsymbol{\varepsilon}\} = \mathbb{E}\{\boldsymbol{\varepsilon}^\intercal\boldsymbol{\varepsilon}\} = \boldsymbol{\Sigma} \tag{5-13}$$

Analogously as in the OLS case, a convex cost function can be defined as:

$$J_{\text{GLS}} = (\mathbf{y} - \mathbf{X}\boldsymbol{\theta})^\mathsf{T}\, \boldsymbol{\Sigma}^{-1}\, (\mathbf{y} - \mathbf{X}\boldsymbol{\theta}) \tag{5-14}$$

Without further derivation, we arrive at the generalized least squares estimate of parameter vector $\boldsymbol{\theta}_{\text{GLS}}$ (Ljung, 2002; Klein & Morelli, 2006):

$$\boldsymbol{\theta}_{\text{GLS}} = \left(\mathbf{X}^\mathsf{T}\boldsymbol{\Sigma}^{-1}\mathbf{X}\right)^{-1} \mathbf{X}^\mathsf{T}\boldsymbol{\Sigma}^{-1}\mathbf{y} \tag{5-15}$$

At this point it also becomes apparent that, for this regression approach, an a priori estimate of the error covariance matrix $\boldsymbol{\Sigma}$ must be available. However, in reality this matrix is often unknown. Many authors, including Klein & Morelli (Klein & Morelli, 2006), suggest the use of a hybrid or two-step approach. This method estimates an a priori residuals covariance matrix with the use of the OLS estimate. This matrix is then estimated as follows:

$$\boldsymbol{\Sigma} = \text{Cov}\left\{\boldsymbol{\varepsilon}\right\} = \mathbb{E}\left\{\boldsymbol{\varepsilon}^\mathsf{T}\boldsymbol{\varepsilon}\right\} = \hat{\mathcal{R}}_{\varepsilon\varepsilon} \tag{5-16}$$

where $\hat{\mathcal{R}}_{\varepsilon\varepsilon}$ indicates the autocorrelation matrix of the residuals. For a zero mean and weakly stationary random process (Klein & Morelli, 2006), the autocorrelation of the residuals can be estimated by:

$$\hat{\mathcal{R}}_{\varepsilon\varepsilon} = \frac{1}{N}\sum_{i=1}^{N-k} = v(i)v(i+k) \qquad k = 0, 1, 2, \ldots, r \tag{5-17}$$

where r indicates the maximum lag index.

The hybrid or two-step GLS method should be used with caution. Maddala argues that in the case where there are no lagged dependent variables used as regressors, the GLS estimate obtained from a covariance estimation by OLS have the same asymptotic distribution as the estimate based on the true residuals covariance matrix (Maddala, 1971). However, if this is not the case, the efficiency of the GLS estimator is lost. In such cases, the OLS estimator would still be more efficient, i.e. estimates from OLS would have a better agreement with the asymptotic lower bounds of the variance.

5-3 Aerodynamic Model Formulation

The general formulation of the aerodynamic model follows from a linearized set of forces and moments. The dependence of the longitudinal coefficients and input variables is expressed as

$$C_a = C_a\left(\alpha, \beta, q, \delta_e\right) \quad \text{a = X, Z or m} \tag{5-18}$$

Similarly, this dependence for the asymmetrical or lateral variables is expressed as

$$C_a = C_a\left(\beta, \alpha, p, r, \delta_a, \delta_r\right) \quad \text{a = Y, l or n} \tag{5-19}$$

Clearly, for large-amplitude deviations and disturbances, it cannot be assumed that the symmetric and asymmetric degrees of freedom are completely decoupled. For this reason, the angle of attack and sideslip angle should be included in both the lateral and longitudinal equations. However, from the perspective of input maneuver design (Mulder, 1986) it can be said that when performing longitudinal maneuvers there is little to no excitation among the lateral states and vice versa. Therefore it is safe to assume that other lateral states do not have to be included in the longitudinal model and longitudinal states in the lateral model.

The model is made independent from mass, velocity and aircraft dimensions by using non-dimensional rotational rates. Different model representations are possible. The stability and control derivatives can be expressed in either the stability frame or body frame. In the context of aerodynamic model identification from flight test data, the use of a representation in the aircrafts body frame is more appropriate (Klein & Morelli, 2006). If it is necessary to compare the estimated set of parameters with an a priori model from windtunnel data, it might be more convenient to express the parameters in the stability frame, however, this approach requires translational accelerations in both X_b and Z_b. The use of the ensemble of noisy measurements for the translational accelerations to calculate the accelerations in the direction of the lift and drag vector can lead to significant amplification of the noise levels (Klein & Morelli, 2006).

Considering the preceding discussion, it was chosen to use the following set of equations to represent the aerodynamic model. Note however that this set is a base model that can later be expanded by including higher order terms.

$$C_X = C_{X_0} + C_{X_\alpha}\alpha + C_{X_\beta}\beta + C_{X_{\hat{q}}}\frac{q\bar{c}}{V} + C_{X_{\delta_e}}\delta_e \tag{5-20}$$

$$C_Y = C_{Y_0} + C_{Y_\beta}\beta + C_{Y_\alpha}\alpha + C_{Y_{\hat{p}}}\frac{pb}{2V} + C_{Y_{\hat{r}}}\frac{rb}{2V} + C_{Y_{\delta_a}}\delta_a + C_{Y_{\delta_r}}\delta_r \tag{5-21}$$

$$C_Z = C_{Z_0} + C_{Z_\alpha}\alpha + C_{Z_\beta}\beta + C_{Z_{\hat{q}}}\frac{q\bar{c}}{V} + C_{Z_{\delta_e}} \tag{5-22}$$

$$C_l = C_{l_0} + C_{l_\beta}\beta + C_{l_\alpha}\alpha + C_{l_{\hat{p}}}\frac{pb}{2V} + C_{l_{\hat{r}}}\frac{rb}{2V} + C_{l_{\delta_a}}\delta_a + C_{l_{\delta_r}}\delta_r \tag{5-23}$$

$$C_m = C_{m_0} + C_{m_\alpha}\alpha + C_{m_\beta}\beta + C_{m_{\hat{q}}}\frac{q\bar{c}}{V} + C_{m_{\delta_e}} \tag{5-24}$$

$$C_n = C_{n_0} + C_{n_\beta}\beta + C_{n_\alpha}\alpha + C_{n_{\hat{p}}}\frac{pb}{2V} + C_{n_{\hat{r}}}\frac{rb}{2V} + C_{n_{\delta_a}}\delta_a + C_{n_{\delta_r}}\delta_r \tag{5-25}$$

where subscript $\hat{(\cdot)}$ relates to the non-dimensional rotational acceleration.

Note that the stability derivatives corresponding to the engine forces and moments are not included in the equations presented above. This will also be reflected in the calculation of the non-dimensional forces and moments from the linear and rotational accelerations, where the thrust components will be subtracted. The latter quantities cannot be measured directly in flight and require to be computed with the help of the following equations (Morelli, 2012):

$$C_X = \frac{mA_x - T_x}{\bar{q}S}, \qquad C_Y = \frac{mA_y}{\bar{q}S}, \qquad C_Z = \frac{mA_z - T_z}{\bar{q}S} \tag{5-26}$$

$$C_l = \frac{I_{xx}}{\overline{q}Sb}\left(\dot{p} - \frac{I_{xz}}{I_{xx}}(pq + \dot{r}) + \frac{I_{zz} - I_{yy}}{I_{xx}}qr\right) \tag{5-27}$$

$$C_m = \frac{I_{yy}}{\overline{q}S\overline{c}}\left(\dot{q} - \frac{I_{xx} - I_{zz}}{I_{yy}}pr + \frac{I_{xz}}{I_{yy}}(p^2 - r^2) - M_T\right) \tag{5-28}$$

$$C_n = \frac{I_{zz}}{\overline{q}Sb}\left(\dot{r} - \frac{I_{xz}}{I_{zz}}(\dot{p} - qr) + \frac{I_{yy} - I_{xx}}{I_{zz}}pq\right) \tag{5-29}$$

The results from Eqs. (5-26)-(5-29) form the set of N dependent variables. Note that the subtraction of the thrust from the force in the X_b axis is straightforward, however, in order to calculate the pitching moment due to thrust, some more accurate information about the positioning of the engines with respect to the center of gravity is required. Most commonly this quantity is assumed to be zero, the same holds for the thrust force along the Z_b axis. The change in rotational rate per unit time can be obtained from smoothed differentiation of the rotational rates when not measured directly (Klein & Morelli, 2006).

5-4 Diagnostic for Regression Analysis

In this section an overview will be given of the methods that will be used during the diagnostic of the selected regression model. First, in Section 5-4-1 methods to determine the goodness of fit in terms of different quantities will be presented and, subsequently, in Section 5-4-2 an overview will be given of a collection of methods to analyze the significance of the overall model and the model parameters independently.

5-4-1 Statistical Measures

In linear regression, the estimated parameter, as mentioned before, is given by:

$$\hat{\boldsymbol{\theta}} = \left(\mathbf{X}^\intercal\mathbf{X}\right)^{-1}\mathbf{X}^\intercal\mathbf{y}$$

The estimated output of the regressor is then given by substituting Eq. (5-4-1) into $\hat{\mathbf{y}} = \mathbf{X}\hat{\beta}$, analogously to Eq. (5-10)

$$\hat{\mathbf{y}} = \underbrace{\mathbf{X}\left(\mathbf{X}^\intercal\mathbf{X}\right)^{-1}\mathbf{X}^\intercal}_{\mathbf{H}}\mathbf{y} \tag{5-30}$$

In the equation above, $\mathbf{H}$ is often referred to as the *hat matrix* and plays an important role in diagnostics for regression analysis. It should be noted that the hat matrix is symmetric and idempotent, implying that $\mathbf{H}^\intercal = \mathbf{H}$ and $\mathbf{H}^2 = \mathbf{H}$, allowing for many simplifications. The error, or residuals, can be expressed by linear combinations of the observed response variable as follows:

$$\boldsymbol{\varepsilon} = \mathbf{y} - \hat{\mathbf{y}} = \mathbf{y} - \mathbf{H}\mathbf{y} = \left(\mathbf{I} - \mathbf{H}\right)\mathbf{y} \tag{5-31}$$

The covariance of the residual can be found by making use of the idempotency property of the hat matrix and by knowing that $\sigma^2\{\mathbf{y}\} = \sigma^2\{\varepsilon\} = \sigma^2\mathbf{I}$:

$$\hat{\sigma}^2\{\boldsymbol{\varepsilon}\} = (\mathbf{I}-\mathbf{H})\,\sigma^2\{\mathbf{y}\}\,(\mathbf{I}-\mathbf{H})^\mathsf{T} = \sigma^2\,(\mathbf{I}-\mathbf{H}) \tag{5-32}$$

in which $\sigma^2\{\cdot\}$ indicates the variance of the stochastic variable. This approach requires the variance of the residual to be known beforehand, however, in most cases this does not apply. An estimation of the variance can be made by making use of the MSE and by knowing that the MSE is the sum of the variance and the squared bias term. Hence, if it is assumed that the bias term is small, it is safe to make an estimation of the residuals variance by using $\sigma^2 \approx \hat{\sigma}^2 = \text{MSE}$. The latter can be done by:

$$\hat{\sigma}^2 = \frac{\boldsymbol{\varepsilon}^\mathsf{T}\boldsymbol{\varepsilon}}{n-p} = \frac{(\mathbf{y}-\mathbf{X}\boldsymbol{\theta})^\mathsf{T}(\mathbf{y}-\mathbf{X}\boldsymbol{\theta})}{n-p} \tag{5-33}$$

where n is the number of elements in the error vector and p the number of parameters in the estimator. The quantity $n-p$ is also referred to as the *degrees of freedom of the residual*. Note the difference in the correction term of Eq. (5-12) with respect to Eq. (5-33), where the latter equation provides an unbiased estimate of the variance of the stochastic variable.

Analogously to the estimation of the covariance matrix of the residuals, the covariance matrix of the estimated parameters can be calculated with the help of the estimated variance $\hat{\sigma}^2$:

$$\text{Cov}\left\{\hat{\boldsymbol{\theta}}\right\} = \hat{\sigma}^2\left(\mathbf{X}^\mathsf{T}\mathbf{X}\right)^{-1} \tag{5-34}$$

The 95% confidence interval, for large sample sizes, of the estimated parameters is then given by:

$$\hat{\boldsymbol{\theta}}_c = \hat{\boldsymbol{\theta}} \pm 2\cdot\text{diag}\left(\text{Cov}\left\{\hat{\boldsymbol{\theta}}\right\}\right) \tag{5-35}$$

In the same fashion as the confidence interval for the estimated parameters, the confidence interval for the estimated output as estimator and confidence interval for the estimated output as predictor can be estimated. The first interpretation of the variance of the estimated output is a quantity to analyze the performance of the regression model on its training data. Its value can be found by:

$$y(i) = \hat{y}(i) \pm 2s\{\hat{y}(i)\} \tag{5-36}$$

where $s\{\cdot\}$ is the standard symbol for the standard deviation of the stochastic variable and the variance of the estimated output can be estimated by:

$$\text{Var}\{\hat{y}(i)\} = \hat{\sigma}^2\mathbf{x}^\mathsf{T}(i)\left(\mathbf{X}^\mathsf{T}\mathbf{X}\right)^{-1}\mathbf{x}(i) \tag{5-37}$$

Similarly, the variance of the predicted output is given as:

$$\text{Var}\{y-\hat{y}(i)\} = \hat{\sigma}^2\left(1+\mathbf{x}^\mathsf{T}(i)\left(\mathbf{X}^\mathsf{T}\mathbf{X}\right)^{-1}\mathbf{x}(i)\right) \tag{5-38}$$

In the case of a GLS estimate, the covariance matrix of the estimated parameters can be found in the same way as for the OLS case by also including the weights matrix, i.e. the inverse of the estimated covariance of the residuals:

$$\mathrm{Cov}\left\{\hat{\boldsymbol{\theta}}\right\}_{\mathrm{GLS}} = \sum_{i=1}^{N}\mathbf{x}(i)\sum_{j=1}^{N}\hat{\mathcal{R}}_{\varepsilon\varepsilon}(i-j)\mathbf{x}^{\mathsf{T}}(j) \tag{5-39}$$

In order to account for the inaccuracy of the estimated weights matrix, Klein & Morelli (2006) suggest the use of a sandwich estimator for a more robust estimate of the parameter covariance matrix:

$$\mathrm{Cov}\left\{\hat{\boldsymbol{\theta}}\right\}_{\mathrm{GLS}} = (\mathbf{X}^{\mathsf{T}}\mathbf{X})^{-1}\left(\sum_{i=1}^{N}\mathbf{x}(i)\sum_{j=1}^{N}\hat{\mathcal{R}}_{\varepsilon\varepsilon}(i-j)\mathbf{x}^{\mathsf{T}}(j)\right)(\mathbf{X}^{\mathsf{T}}\mathbf{X})^{-1} \tag{5-40}$$

More importantly, Grauer & Morelli state that for the identification of aerodynamic models, simplified version of Eq. (5-40) should not be used because they tend to underestimate the uncertainty of the estimates (Grauer & Morelli, 2014). The use of Eq. (5-40) is therefore recommended and can also be used in the estimation of the uncertainties for OLS.

Finally, as an additional tool to analyze the correlation of the estimated parameters, the correlation matrix can be calculated by normalizing the diagonal terms in the covariance matrix:

$$\mathrm{Corr}\left\{\hat{\boldsymbol{\theta}}\right\} = \begin{pmatrix} \frac{1}{s(\hat{\theta_1})} & 0 & \dots & 0 \\ 0 & \frac{1}{s(\hat{\theta_2})} & \dots & 0 \\ \vdots & \vdots & \ddots & \vdots \\ 0 & 0 & \dots & \frac{1}{s(\hat{\theta_p})} \end{pmatrix} \mathrm{Cov}\left\{\hat{\boldsymbol{\theta}}\right\} \begin{pmatrix} \frac{1}{s(\hat{\theta_1})} & 0 & \dots & 0 \\ 0 & \frac{1}{s(\hat{\theta_2})} & \dots & 0 \\ \vdots & \vdots & \ddots & \vdots \\ 0 & 0 & \dots & \frac{1}{s(\hat{\theta_p})} \end{pmatrix} \tag{5-41}$$

Generally, in addition to the statistical tools presented above, an inspection of the models residuals should be performed. Both visually and statistically. The developed equation for the determination of the residuals autocorrelation in Eq. (5-17) should again be assessed. For a completely uncorrelated population of residuals, the autocorrelation should remain between the 2 standard deviation bounds as the number of lags increases. The standard deviation, for large sample sizes, can be approximated by (Box & Jenkins, 1994):

$$s\left\{\hat{\mathcal{R}}_{\varepsilon\varepsilon}\right\} \approx \frac{\hat{\mathcal{R}}_{\varepsilon\varepsilon}(0)}{\sqrt{N}} \tag{5-42}$$

5-4-2 Hypothesis Testing

Once a least square routine is applied to a set of data with a predetermined model structure, the significance of the overall model can be tested with a so-called F-test. By applying this statistic, the selected model can be tested against the null hypothesis which is defined as:

$$H_0: \ \theta_1 = \theta_2 = \ldots = \theta_p = 0 \tag{5-43}$$

If the null hypothesis is rejected at a certain confidence level, it is safe to assume that one or more parameters in the model describe a reasonable part of the variance in the observed variables. Therefore, the model is said to be significant. The F-statistic itself can be calculated with:

$$F_0 = \frac{\boldsymbol{\theta}^\intercal \mathbf{X}^\intercal \mathbf{y} - N\overline{\mathbf{y}}^2}{p\hat{\sigma}^2} \tag{5-44}$$

The null hypothesis is rejected if $F_0 > F(\alpha, p, N-p)$ in which α denotes the selected significance level. Usually, the latter quantity is set to 0.05.

The Fisher Information matrix is defined as follows:

$$\mathbf{I}\left(\hat{\theta}\right) = -\mathbb{E}\left(\frac{\partial^2 \ln \mathbb{L}(\mathbf{y}|\hat{\theta})}{\partial \theta^2}\right) \tag{5-45}$$

where $\mathbb{L}\left(\mathbf{y}|\hat{\theta}\right)$ indicates the maximum likelihood value of $\mathbf{y}$ given the estimated set of parameters $\hat{\theta}$. A reasonable estimate of the covariance matrix of parameter $\hat{\theta}$, for large sample sizes, is given by the inverse of the Hessian matrix.

From asymptotic theory of maximum likelihood, the difference between the parameter estimation and some parameter of interest, say θ_0, approaches a normal distribution with zero mean. Normalization by the standard deviation should in that case result in a zero mean, unit variance distribution. This statistic is referred to as the Wald statistic and can be formulated as follows:

$$W = \frac{\hat{\theta} - \theta_0}{\sigma(\hat{\theta})} \sim \mathcal{N}(0, 1) \tag{5-46}$$

In most cases, the parameter of interest would be the zero vector because we want to test whether the estimated parameter differs from zero or not, hence whether the parameter is relevant. In the Wald test, the null hypothesis is rejected if the test statistic is larger than a pre-determined critical value: $W_n > z$. This critical value can be any value, however usually the value is an indication of the certainty level. Since the Wald test asymptotically converges to the χ^2-distribution, a confidence interval of, e.g. 95%, can be found by taking the inverse of the χ^2-distribution.

$$z = F^{-1}(1 - \alpha) \tag{5-47}$$

In an analogous fashion as the F-statistic for the overall model structure, the statistical significance of the individual parameters can be tested by the partial F-statistic. This statistic is used in model selection which will be further discussed in Section 5-5. The partial F-statistic can be calculated by:

$$F_0 = \frac{\hat{\boldsymbol{\theta}}^2}{\mathrm{Var}(\hat{\boldsymbol{\theta}})} \tag{5-48}$$

5-5 Model Structure Selection

The aforementioned methods for statistical analysis, see Section 5-4 and in particular Section 5-4-2, can also directly be applied in the process of model structure selection. By assuming an initial (linear) model structure, significant terms can be added until the regression equation is satisfactory. Several techniques for the selection of regression models have been developed, of which stepwise regression is considered as the preferred method (Klein, 1989). This method is a so called forward method because terms are added at each step. Alternatively, backward elimination can be used by removing terms from a full-term model.

5-5-1 Modified Stepwise Regression

The application of a forward stepwise regression method in aerospace applications (Klein et al., 1981) was adjusted to, as initial condition, always include the linear part of the baseline model as defined in Section 5-3. This modified stepwise approach (Mulder et al., 1994; Klein, 1989; Batterson & Klein, 1989) was successfully applied in numerous researches and works by testing the significance of each added parameter which are obtained from a pool of candidate regressors. Klein, Batterson and Murphy argue that models obtained from modified stepwise regression can determine regression models closer to the true physical model or with better prediction capabilities than stepwise regression without constraints and, in addition, the modified stepwise regression routine can directly be applied to large amplitude maneuvers (Klein et al., 1981). However, for this approach to work, the regression data should be partitioned according to the variables which influence the existence of non-linear terms in the aerodynamic model (Klein, 1989; Batterson & Klein, 1989).

In summary, the modified stepwise regression approach consists of the following steps:

1. Formulation of the initial model. For a modified stepwise approach, these models form the constraints as all linear terms included in the initial model should also be included in the final model. In addition, a pool of candidate regressors should be defined. Most commonly, this pool includes all linear, quadratic and terms with cross interaction, such as $\alpha\beta$.

2. Calculate the parameter estimate of the selected model structure through the normal equations. Note that for this step any regression routine can be used, however, in most cases OLS is applied.

3. Calculation of common statistical measures, such as the sum of squares, parameter covariance matrix and variance of the residuals.

4. With the metrics obtained from the previous step, the F-statistic for testing the relevance of the model can be calculated. In addition, the significance of each parameter can be tested separately with the partial F-test. Parameters that are found to be insignificant will be removed from the model.

5. The choice of new parameters to enter the model will be based on (1) the significance of the parameter to enter the model, where the selected parameter should pass the selected significance level and (2) the improvement of the models overall F-statistic, where the newly introduced parameter should improve the value of the corresponding metric.

In general, models that result from the aforementioned procedure often contain non-linear pure quadratic terms and terms with cross-interactions. These terms do not directly have a true physical meaning, however, it can be stated that these additional terms allow the model to resemble the given data more closely by reducing the model residuals to an uncorrelated random sequence. These properties make the modified stepwise regression an excellent tool to analyze and create an appropriate model structure for large-amplitude dynamic maneuvers (Klein et al., 1981).

5-5-2 Multivariate Orthogonal Functions

As alternative to the modified stepwise regression approach, Klein used a method to transform the set of regressors to the orthogonal domain (Klein, 1989). This method was later described and repeated by different authors to assess the influence of different regressors on the regression model (Lombaerts et al., 2010; Grauer & Morelli, 2014; Morelli, 2012). An additional benefit that follows from the transformation of the set of regressors to a set of orthogonal regressors is that data collinearity can be dealt with effectively. A more in depth description of data collinearity will be presented in the next section.

Different methods to obtain a set of orthogonal regressors exist. In practice, computer software often allows a relatively easy computation of the principal components of a regression matrix. The procedure used by Klein in (Klein, 1989) transforms the set of original regressors $\mathbf{X}$ to the orthogonal space by:

$$\mathbf{Z} = \mathbf{X}\mathbb{T} \tag{5-49}$$

where $\mathbb{T}$ is the transformation matrix from the ordinary to the orthogonal domain. The regression model now becomes:

$$\mathbf{y} = \mathbf{Z}\boldsymbol{\gamma} + \boldsymbol{\varepsilon} \tag{5-50}$$

Straightforward application of the earlier presented principles of least squares regression results in the following set of estimated parameters:

$$\hat{\boldsymbol{\gamma}} = \left(\mathbf{Z}^{\intercal}\mathbf{Z}\right)^{-1}\mathbf{Z}^{\intercal}\mathbf{y} \tag{5-51}$$

Regular statistical measures and procedures as described in Section 5-4 can be used to assess the performance of the estimated regression model. The estimated parameters $\hat{\boldsymbol{\gamma}}$ can be transformed back to the ordinary domain by again employing transformation matrix $\mathbb{T}$:

$$\hat{\boldsymbol{\theta}} = \mathbb{T}\hat{\boldsymbol{\gamma}} \tag{5-52}$$

The transformed set of regressors $\mathbf{Z}$ can, in principle, easily be obtained by using the `pca` routines in the Matlab computer software package. This matrix corresponds to the coefficients found from this routine. Transformation matrix $\mathbb{T}$ corresponds to the principal components score matrix. Note that this routine automatically centers the variables and orders then in the transformed regression matrix according to the size of the eigenvalue (decreasing). The latter corresponds to the the variance of the principal component.

The main advantage of this approach is that regressors can be tested for their significance independently from the model due to the orthogonal nature of the resulting set of regressors, where in the stepwise regression approaches the significance of the independent parameters can be tested, however, this is not independent of the model. From the above mentioned procedure, a simple threshold can be set to only include principal components that explain more than a preset amount of the total variance. Alternatively, Grauer & Morelli use an approach where we start with one principal component. Subsequently, principal components are added up until the point where the Predicted Square Error (PSE) attains a minimum. This number of principal components will be used in the transformation matrix. The PSE is defined as (Morelli, 2012):

$$\text{PSE} = \frac{1}{N}(\mathbf{y} - \hat{\mathbf{y}})^{\mathsf{T}}(\mathbf{y} - \hat{\mathbf{y}}) + \sigma^2_{\max}\frac{n}{N} \tag{5-53}$$

where n is the number of principal components and the maximum variance of the model fit error can be estimated by:

$$\sigma^2_{\max} = \frac{1}{N-1}\sum_{i=1}^{N}(y(i) - \overline{\mathbf{y}}) \tag{5-54}$$

The PSE in its current form is a convex function with a global minimum, allowing for a very straightforward selection of the number of principal components to be used in Principal Components Regression (PCR).

5-6 Data Collinearity

Using ordinary regression routines as described in Section 5-2 applied in the framework of aerodynamic model identification can often lead to badly scaled or singular matrices. As a result of these numerical deficiencies, the accuracy of the estimated set of parameters can reduce significantly. This problem, in most cases, is closely related to collinearity, a near linear dependency, in the given set of variables of the linear regression model.

Near linear dependencies in the regression matrix, i.e. amongst the the independent variables, are data problems which are often related to the model specification. For example, pitch rate q and the change in angle of attack over a unit time interval $d\alpha/dt = \dot{\alpha}$ are closely related and therefore simultaneous use of these variables in linear least squares regression often leads to ill conditioned design matrices.

The solution to these aforementioned problems can often be solved relatively easy by leaving out one of the correlated variables. However, this approach is not always tolerated, e.g. when a given fixed model structure is to be fit with a set of data. A more structural solution might be the use of PCR. By selecting the appropriate amount of principal components for the regression, the variance of the estimated parameters can be reduced. However, PCR is not an unbiased estimator since it trades off excessive variance of the OLS estimator for a slight increase in the bias of the parameter. The total sum of squares, which is the sum of the squared bias and variance, will be reduced as effect of this tradeoff, arguably, leading to a better approximation of the given data. Therefore, the accuracy of the parameter estimates in the case of data collinearity can be increased by the use of PCR.

5-7 Model Globalization

The earlier presented methods prove to be excellent tools in the identification of an aerodynamic model using the TSM. However, in most cases model identification is only required for local models, describing the dynamics only in a sub-space of the total state-space. In contrast to the last approach, the aerodynamic model that will be identified as part of this thesis must cover the whole flight envelope as denoted in the requirements.

Several methods exist for the creation of global aerodynamic models, however only a selection of these methods has shown to exercise sufficient approximation power over the whole domain. Over the last few years, a small collection of advanced techniques have been proposed and succesfully applied in the identification of a global aerodynamic model. Most notably, the global non-linear identification method with multivariate splines, introduced by De Visser (2009), show great theoretical potential. However, at the same time this method suffers from its increased complexity in terms of the theoretical basis w.r.t. methods such as presented in this paper. Therefore, a successful identification with this method requires perfect theoretical understanding of the applied concepts. Something that might not be possible within the given time frame.

Other methods, such as the identification of a global model with a neural network also show great potential (De Weerdt, Chu, & Mulder, 2005). However, neural networks have a complex, nontransparent and obscure internal structure. In addition, physical interpretation of the identified model coefficients is not possible. Therefore this method is less attractive for off-line models that will be used in future research endeavor into control algorithms.

In order to successfully use the proposed set of techniques summarized as the TSM, a method is sought after to identify a global model by using linear regression techniques. In general, the application of least squares to identify a global model lacks sufficient approximation power over the whole domain (De Visser et al., 2009). Especially when only considering the conventional linear model. Extension of the model structure, such as described in Section 5-5, with non-linear terms can already enhance the fit over the whole domain (Morelli, 2012; Grauer & Morelli, 2014). Grauer argues that the use of multivariate orthogonal functions can successfully be applied to a set of candidate regressors to efficiently identify a global model, however this approach requires a specific set of input maneuvers to be executed. In order to further increase the ability to successfully capture the aerodynamics over the whole flight envelope, different authors have suggested the identification of local models in so called hyperboxes, subspaces of the prevailing aerodynamic angle (De Weerdt et al., 2005; Klein, 1989; Van Oort et al., 2010).

The latter method shows the greatest potential for successful identification of a global model from flight test data, applied in combination with the TSM and within the given time frame. The selection of the number of subspaces and the appropriate model structure can be seen as the challenges of this method.

5-8 Conclusion

As second major part in the methodology of the Two Step Method, linear parameter estimation techniques play a significant role of importance. Many different techniques have been described in literature, however, the most used class of methods is the collection of least square methods. Ordinary least squares is the most basic type of least squares regression. However, for this approach to remain unbiased and efficient, the presented set of regression data must suffice to a number of conditions. Most importantly, the expected value of the residuals must be equal to zero and the residuals should be homoscedastic, indicating a stationary variance in the diagonal elements and very small correlation terms. In addition, the presented data set must contain sufficient excitation of the aircraft's dynamic states for a successful application of least-squares parameter estimation methods.

When the basic assumptions of OLS are violated, one must resort to a more appropriate method. In most cases, the use of a generalized least squares method suffices. However, in reality a priori information about the residuals covariance matrix is not available. In such cases, a hybrid method can be applied to estimate the latter quantity by OLS and subsequently using this information to for the weights matrix for GLS regression. This approach should be used with caution because if there are lagged dependent variables present in the regression matrix, the two-step GLS approach loses its optimality and regular OLS will be more efficient.

For the formulation of the aerodynamic model there is a general consensus in literature about the basic structure. In principle, the longitudinal and lateral motion can be decoupled resulting 6 equations to describe the forces and moments around the three reference axes. In general, for simulation design, identification of the parameters in the aircraft body axis is preferred because conversion to the stability axes requires all three acceleration components which greatly amplifies noise levels. The identification of an global aerodynamic model can be done with a collection of advanced identification methods. Despite their great potential, application of such methods is not straightforward and should also be possible within the given time. For this reason, the creation of an initial global model by the interpolation of multiple local models, identified in subspaces of the prevailing aerodynamic variable, is the preferred approach.

In general two different methods are available to automate the model structure selection. Modified stepwise regression assumes that the model always contains the linear terms and adds terms from a pool of candidate regressors if they pass a certain significance level. In addition, these terms should be uncorrelated from existing terms in the model. Alternatively, model terms can be chosen from a pool of candidate regressors by using an orthogonal basis functions approach. The advantage of this approach is that all regressors can be analyzed for their significance independently in contrast to the iterative stepwise regression method. Both methods should be used with caution as higher order terms and cross interactions increase the chances of ill conditioned regression matrices, indicative for data collinearity. For this problem, the orthogonal basis functions approach should be the most robust solution in theory.

Chapter 6

Conclusion

As a result of new aviation legislation, from 2019 on all air-carrier pilots are obliged to go through flight simulator-based stall recovery training. This implies that all aircraft dynamics models driving flight simulators must be updated to include accurate pre-stall, stall and post-stall dynamics. For this reason, the division of Control and Simulation has recently set up a task force to develop a new methodology for high-fidelity aircraft stall behavior modeling and simulation. This data is to be derived from flight test data from our Cessna Citation II laboratory aircraft and tested in our SIMONA simulator. At this moment, the C&S division uses a simulator model of the Cessna Citation known as the Delft University Aircraft Simulation and Analysis Tool (DASMAT) model as its baseline Citation aircraft model. This model does not include an accurate model for the aircraft's stall behavior. As part of this stall modeling research, a new high-fidelity flight simulation model of the Cessna Citation II laboratory aircraft will be developed, which will replace the current DASMAT model as baseline model.

In order to facilitate the upgrade of the old simulation framework, a preliminary feasibility study was presented in this report. Early analysis has indicated several problems with the current model of which the most important can be identified as follows: (1) the model suffers from the lack of an accurate mass and inertia simulation, (2) the model does not include an accurate landing gear problem, (3) the overall model structure of the simulation framework is obscure and outdated, (4) most importantly, the current simulation framework features a Cessna Citation I aerodynamic model, which is a mismatch from the current laboratory aircraft, the Cessna Citation II. Despite these deficiencies DASMAT forms an excellent basis to further build upon because it is in agreement with the general conventional simulation model structure and, in addition, its modularity allows for easy extension with future modules. The latter property should be retained at any cost. Furthermore, deficiencies were established within the engine model. However, this model forms its own collection of systems and subsystems. Above all, any improvement of the engine model would require an individual identification procedure which cannot be fit into the given time frame for this thesis assignment.

To streamline the upgrade process, the individual components of the DASMAT simulation framework were classified by their importance in the same process. By far the most important upgrade has to be made to the aerodynamic model that is implemented at current. This upgrade is classified as the only high priority upgrade. In addition, the integration of a mass model is highly desirable and should therefore be prioritized. Other blocks, such as the engine block, equations of motion and the observation model do not require too much work on their own. Currently these blocks, like all subsystems of DASMAT, are represented by a block-in-block structure and urgently require an upgrade to the new embedded Matlab function representation. The latter will be done as part of this thesis work.

The most urgent upgrade of the simulation framework comes in the form of the identification and implementation of a new aerodynamic model. The latter is to be done with a set of techniques referred to as system identification techniques. System identification is development of mathematical systems and equations from a set of measurement data. Therefore, the main objective of this work was formulated as follows: Design a high-fidelity simulation model of the Cessna Citation II aircraft, by the identification of an aerodynamic model from the provided experimental flight data, which is valid over the whole flight envelope and integrate this model into the upgraded or extended DASMAT simulation framework. The collection of such a dataset is out of the scope of this thesis, however, opportunities to collect new data may arise.

In literature, many different approaches have been described to identify such an aerodynamic model. However, most promising for application to the problem presented in this thesis is the Two-Step Method. This method effectively decomposes the non-linear parameter estimation problem into a non-linear flight path estimation problem and a linear parameter estimation problem.

Originally, the Kalman filter was introduced for application to problems defined in linear state space. It was not much later when an extension with effective local linearization allowed the application of the Kalman filter to non-linear equations. In first instance the Kalman filter was primitively meant as navigation filter, combining the information from different sensors to generate a state estimate with the highest degree of accuracy. The latter approach was also applied to offline state reconstruction problems, in order to generate an accurate state estimate. Over the past few years, many extensions to the popular Kalman filter were introduced. However, the (Iterated) Extended Kalman Filter can still be considered as the prime class. In theory, this filter suffers from a great lack of approximation power for moderately to highly non-linear systems as it uses a first order Taylor expansion to approximate the non-linear trajectory. For this reason, different methods of representing the stochastic properties of the system in question were sought after. For this reason the Unscented Kalman Filter was introduced.

The Unscented Kalman Filter uses a different method to approximate the stochastic properties of the non-linear system. Instead of a linearization approach, the formulation of a set of sigma points should in theory capture the statistics of the mean and covariance up to the third degree and higher. Therefore, from a theoretical perspective, the Unscented Kalman Filter would be well suited for applications to systems of non-linear nature.

In this report, a comparison has been made between the IEKF and the UKF when applied in the framework of a non-linear Cessna Citation I simulation model. This comparison was done in terms of performance, defined as the ability to reconstruct the real state and sensitivity to initial conditions. In addition, the theoretical prospects of both filter types should be taken into account. When comparing the average of a 50 run Monte Carlo simulation, the performance of both filter types is very similar. In some cases, such as the estimation of the sensor biases the UKF performs slightly better while the position components are better approximated by the IEKF. Some attention is also given to the performance of selected filters with the addition of Kalman smoother, which should theoretically lead to a smoother approximation of the true state. The latter class of backward recursive Kalman filters does not lead to a significant increase in the accuracy of the estimate. In contrast, in most cases the application of smoothers increases the difference between the true state and the state estimate.

In terms of sensitivity to initial conditions both filter types also show similar performance when applied to the Citation I model. In this context a remark should be given to the performance of the IEKF in cases with large noise intensity corruption of the data. The latter might lead to problems with the observability of the internal state. The UKF is less sensitive because of its different state representation. Theoretically the UKF should also give a better approximation when working with data corrupted by non-Gaussian noise.

Experimental flight data is often obtained from different instruments and therefore inherently misaligned due to differences in the sample rate of the measurements. A more structural solution to this problem was presented in the form of a multi-rate Kalman filter. However, in this report it was also shown that this type of filter does in most cases only lead to an improvement of the state estimate of which the sample rate is low. Other state estimates will deteriorate from such an approach and therefore resampling by interpolation offers an excellent alternative for offline flight path reconstruction.

In the last chapter of this report, a collection of linear parameter estimation methods for use in the second step of the Two-Step Method was presented. In cases where the basic assumptions for the Ordinary Least Squares estimator are violated, use can be made of the Generalized Least Squares method. In reality, a priori information about the residuals covariance matrix is not available, for this reason a hybrid two step method should be employed to obtain the latter matrix. This should be done with caution, as in some cases such estimates are less efficient than the standard OLS method.

In literature there is a general consent about the standardized linear structure of the aerodynamic model expressed in terms of the non-dimensional forces and moments. In most cases, this linear structure does not have enough approximation power over the whole domain. For this reason, a modified stepwise regression approach was proposed to come up with a higher accuracy model structure. Alternatively, one can resort to the orthogonal domain with the use of multivariate orthogonal basis functions to select a set of regressors from a candidate pool. When an appropriate model structure has been selected, globalization can be applied by identification of multiple locally defined models, identified in subspaces of the prevailing aerodynamic variable. This approach is well suited for the model to be identified as part of this thesis, since it can more easily be extended by a model for the stall and post-stall dynamics at higher angles of attack.

Altogether, with the methods discussed in this preliminary thesis, an aerodynamic model will be identified that will cover the regular, pre-stall flight envelope of the Cessna Citation II. When incorporated into the upgraded or extended DASMAT simulation framework, this model can successfully form the basis for future research endeavor into numerous fields.

Bibliography

Allerton, D. J. (2010). The impact of flight simulation in aerospace. *Aeronautical Journal*(3581), 747–756. Available from `http://aerosociety.com/News/Publications/Aero-Journal/Online/750/The-impact-of-flight-simulation-in-aerospace`

Armesto, L., Chroust, S., Vincze, M., & Tornero, J. (2004). Multi-rate fusion with vision and inertial sensors. *IEEE International Conference on Robotics and Automation, 2004. Proceedings. ICRA '04. 2004*, *1*, 193–199.

Armesto, L., Tornero, J., & Vincze, M. (2008). On multi-rate fusion for non-linear sampled-data systems: Application to a 6D tracking system. *Robotics and Autonomous Systems*, *56*(8), 706–715. Available from `http://www.sciencedirect.com/science/article/pii/S0921889007001698`

Baarspul, M. (1990). A review of flight simulation techniques. *Progress in Aerospace Sciences*, *27*(1), 1–120. Available from `http://www.sciencedirect.com/science/article/pii/0376042190900066`

Batterson, J. G., & Klein, V. (1989, apr). Partitioning of flight data for aerodynamic modeling of aircraft at high angles of attack. *Journal of Aircraft*, *26*(4), 334–339. Available from `http://dx.doi.org/10.2514/3.45765`

Bennis, R. J. M. (1998). *Non-linear State Estimation Techniques with Application to Dynamic Modelling of Angle of Attack Vane from Cessna Citation II Flight Data.* Unpublished master's thesis, Delft University of Technology, Delft.

Box, G. E. P., & Jenkins, G. M. (1994). *Time Series Analysis: Forecasting and Control* (Vol. Third). Available from `http://doi.wiley.com/10.1111/j.1467-9892.2009.00643.x`

Chowdhary, G., & Jategaonkar, R. (2010). Aerodynamic parameter estimation from flight data applying extended and unscented Kalman filter. *Aerospace Science and Technology*, *14*(2), 106–117. Available from `http://www.sciencedirect.com/science/article/pii/S1270963809000650`

Chu, Q. P., Mulder, J. A., & Van Woerkom, P. (1995, jun). Aircraft flight path reconstruction with nonlinear adaptive filters. In *American control conference, proceedings of the 1995* (Vol. 2, pp. 1196–1200 vol.2).

Chu, Q. P., Mulder, J. A., & Van Woerkom, P. T. L. M. (1996). Modified Recursive Maximum

Likelihood Adaptive Filter for Nonlinear Aircraft Flight-Path Reconstruction. *Journal of Guidance, Control, and Dynamics*, *19*(6), 1285–1295.

De Visser, C. C. (2011). *Global Nonlinear Model Identification with Multivariate Splines.* Unpublished doctoral dissertation, Delft University of Technology, Delft.

De Visser, C. C., Mulder, J. A., & Chu, Q. P. (2009). Global Nonlinear Aerodynamic Model Identification with Multivariate Splines. In *Aiaa atmospheric flight mechanics conference.* AIAA.

De Weerdt, E., Chu, Q. P., & Mulder, J. A. (2005, aug). Neural Network Aerodynamic Model Identification for Aerospace Reconfiguration. In *Aiaa guidance, navigation, and control conference and exhibit.* American Institute of Aeronautics and Astronautics. Available from `http://dx.doi.org/10.2514/6.2005-6448`

Dias, J. N. (2015). Unsteady and Post-Stall Model Identification Using Dynamic Stall Maneuvers. In *Aiaa atmospheric flight mechanics conference* (pp. 1–15).

Federal Aviation Administration. (2013). *Qualification, Service, and Use of Crewmembers and Aircraft Dispatchers* (Tech. Rep.). U.S. Department of Transportation. Available from `http://www.faa.gov/documentLibrary/media/Notice/N{\_}8900.241.pdf`

Grauer, J. A., & Morelli, E. A. (2014, jul). Generic Global Aerodynamic Model for Aircraft. *Journal of Aircraft*, *52*(1), 13–20. Available from `http://dx.doi.org/10.2514/1.C032888`

Julier, S. J., & Uhlmann, J. K. (1997). A New Extension of the Kalman Filter to Nonlinear Systems. *International Symposium for Aerospace Defense Sensing Simulutation and Controls*, *3*(2), 26. Available from `http://discovery.ucl.ac.uk/135543/`

Julier, S. J., & Uhlmann, J. K. (2004). Unscented filtering and nonlinear estimation. *Proceedings of the IEEE*, *92*(3), 401–422.

Kalman, R. E. (1960). A New Approach to Linear Filtering and Prediction Problems. *American Society of Mechanical Engineering - Journal of Basic Engineering*, *82*(Series D), 35–45. Available from `http://scholar.google.com/scholar?hl=en{\&}btnG=Search{\&}q=intitle:A+New+Approach+to+Linear+Filtering+and+Prediction+Problems{\#}0`

Klein, V. (1989). Estimation of aircraft aerodynamic parameters from flight data. *Progress in Aerospace Sciences*, *26*(1), 1–77. Available from `http://www.sciencedirect.com/science/article/pii/037604218990002X`

Klein, V., Batterson, J. G., & Murphy, P. C. (1981). *Determination of airplane model structure from flight data by using modified stepwise regression* (Tech. Rep.). Hampton: NASA Langley Research Center.

Klein, V., & Morelli, E. A. (2006). *Aircraft System Identification: Theory and Practice* (2nd ed.). Reston, VA: AIAA Education Series.

Klein, V., & Schiess, J. R. (1977). Compatibility check of measured aircraft responses using kinematic equations and extended Kalman filter. In *Technical report tn d-8514* (pp. 1–47). Washington D.C..

Kumar, R., & Ghosh, A. K. (2011). Parameter Estimation using Maximum Likelihood Method from Flight Data at High Angles of Attack. *International Journal of Mechanics, Aerospace, Industrial, Mechatronic and Manufacturing Engineering*, *5*(11), 2350–2355.

Laban, M. (1994). *On-Line Aircraft Aerodynamic Model Identification.* Ph.d. thesis, Delft University of Technology, Delft.

Lichota, P., & Lasek, M. (2013). Maximum likelihood estimation for identification of aircraft aerodynamic derivatives. *The Archive of Mechanical Engineering*, *LX*(2).

Ljung, L. (2002). System identification: theory for the user (second edition). *Automatica*, *38*(2), 375–378.

Lombaerts, T., Oort, E. V., Chu, Q. P., Mulder, J. A., & Joosten, D. (2010). Online Aerodynamic Model Structure Selection and Parameter Estimation for Fault Tolerant Control. *Journal of Guidance, Control, and Dynamics*, *33*(3), 707–723. Available from `http://arc.aiaa.org/doi/abs/10.2514/1.47256`

Lubbers, B. (2009). *A model of the Experimental Fly-By-Wire flight control system for the PH-LAB*. Unpublished master's thesis, Delft.

Maddala, G. S. (1971). Generalized Least Squares with an Estimated Variance Covariance Matrix. *Econometrica*, *39*(1), 23–33. Available from `http://www.jstor.org/stable/1909137`

Morelli, E. (2012, jan). Efficient Global Aerodynamic Modeling from Flight Data. In *50th aiaa aerospace sciences meeting including the new horizons forum and aerospace exposition.* American Institute of Aeronautics and Astronautics. Available from `http://dx.doi.org/10.2514/6.2012-1050`

Mulder, J. A. (1986). *Design and evaluation of dynamic flight test manoeuvres*. Unpublished doctoral dissertation, Delft.

Mulder, J. A., Baarspul, M., Breeman, J. H., Nieuwpoort, A. M. H., Verbaak, J. P. F., & Steeman, P. S. J. M. (1987). Determination of the mathematical model for the new Dutch government civil aviation flying school flight simulator. In *Society of flight test engineers, 18th annual symposium.* Amsterdam.

Mulder, J. A., Chu, Q. P., Sridhar, J. K., Breeman, J. H., & Laban, M. (1999). Non-linear aircraft flight path reconstruction review and new advances. *Progress in Aerospace Sciences*, *35*(7), 673–726. Available from `http://www.sciencedirect.com/science/article/pii/S0376042199000056`

Mulder, J. A., Sridhar, J. K., & Breeman, J. H. (1994). *Identification of Dynamic Systems-Applications to Aircraft Part 2: Nonlinear Analysis and Manoeuvre Design* (Vol. 3) (No. 2). Neuilly Sur Seine: North Atlantic Treaty Organisation.

Mulder, J. A., Van Staveren, W. H. J. J., & Van der Vaart, J. C. (2000). *Flight Dynamics (Lecture Notes): AE3-302*. Delft: TU Delft.

Pratt & Whitney Canada Incorporated. (1996). *JT15D Series Engines - Performance Estimation Program - User's Manual* (Tech. Rep.). Longueill, Quebec: Pratt & Whitney.

Rauch, H. E., Striebel, C. T., & Tung, F. (1965, aug). Maximum likelihood estimates of linear dynamic systems. *AIAA Journal*, *3*(8), 1445–1450. Available from `http://dx.doi.org/10.2514/3.3166`

Sarkka, S. (2008). Unscented Rauch Tung Striebel Smoother. *IEEE Transactions on Automatic Control*, *53*(3), 845–849.

Sibley, G., Sukhatme, G. S., & Matthies, L. H. (2006). The Iterated Sigma Point Kalman Filter with Applications to Long Range Stereo. *Rss*. Available from `http://robotics.usc.edu/publications/media/uploads/pubs/500.pdf`

Smyth, A., & Wu, M. (2007). Multi-rate Kalman filtering for the data fusion of displacement and acceleration response measurements in dynamic system monitoring. *Mechanical Systems and Signal Processing*, *21*(2), 706–723. Available from `http://linkinghub.elsevier.com/retrieve/pii/S0888327006000653`

Söderström, T., Ljung, L., & Gustavsson, I. (1978). A theoretical analysis of recursive identification methods. *Automatica*, *14*(3), 231–244.

Sontag, E. D. (1984). A concept of local observability. *Systems and Control Letters*, *5*(1), 41–47.

Stevens, B. L., & Lewis, F. L. (2003). *Aircraft Control and Simulation.* Available from `http://www.worldcat.org/oclc/51751879`

Strejc, V. (1983). Least Squares Parameter Estimation for Nonlinear Systems. *Automatica*, *16*, 535–550.

Teixeira, B. O. S., Tôrres, L. A. B., Iscold, P., & Aguirre, L. A. (2011). Flight path reconstruction - A comparison of nonlinear Kalman filter and smoother algorithms. *Aerospace Science and Technology*, *15*(1), 60–71. Available from `http://dx.doi.org/10.1016/j.ast.2010.07.005`

Van Der Linden, C. A. A. M. (1998). *DASMAT - Delft University Aircraft Simulation Model and Analysis Tool.* Delft: Delft University Press.

Van Der Merwe, R., & Wan, E. A. (2001). The square-root unscented Kalman filter for state and parameter-estimation. In *Acoustics, speech, and signal processing, 2001. proceedings. (icassp '01). 2001 ieee international conference on* (Vol. 6, pp. 3461–3464 vol.6).

Van Der Merwe, R., & Wan, E. A. (2004). Sigma-Point Kalman Filters for Integrated Navigation. In *Proceedings of the 60th annual meeting of the institute of navigation (ion)* (pp. 641–654). Available from `http://citeseerx.ist.psu.edu/viewdoc/download?doi=10.1.1.9.5753{\&}rep=rep1{\&}type=pdf`

Van Horssen, L. J. (2016). *Aerodynamic Stall Modeling for the Cessna Citation II based on Flight Test Data.* Unpublished master's thesis, Delft University of Technology.

Van Oort, E. R., Sonneveldt, L., Chu, Q. P., & Mulder, J. A. (2010). Full-Envelope Modular Adaptive Control of a Fighter Aircraft Using Orthogonal Least Squares. *Journal of Guidance, Control, and Dynamics*, *33*(5), 1461–1472. Available from `http://arc.aiaa.org/doi/abs/10.2514/1.48175`

Walcott, B. L., Corless, M. J., & Zak, S. H. (1987). Comparative study of non-linear state-observation techniques. *International Journal of Control*, *45*(6), 2109–2132. Available from `http://www.tandfonline.com/doi/abs/10.1080/00207178708933870`

Wan, E. A., & Van Der Merwe, R. (2002). The unscented Kalman filter for nonlinear estimation. *Adaptive Systems for Signal Processing, Communications, and Control Symposium 2000. AS-SPCC. The IEEE 2000*, 153–158. Available from `papers3://publication/uuid/94787C0B-195F-4748-9277-D391BB80EB69`

Zhan, R., & Wan, J. (2007). Iterated unscented Kalman filter for passive target tracking. *IEEE Transactions on Aerospace and Electronic Systems*, *43*(3), 1155–1163.

Part III

Preliminary Thesis - Appendices

Reference Frames

This appendix features an overview of the aircraft body fixed, stability and ECEF or navigation reference frames.

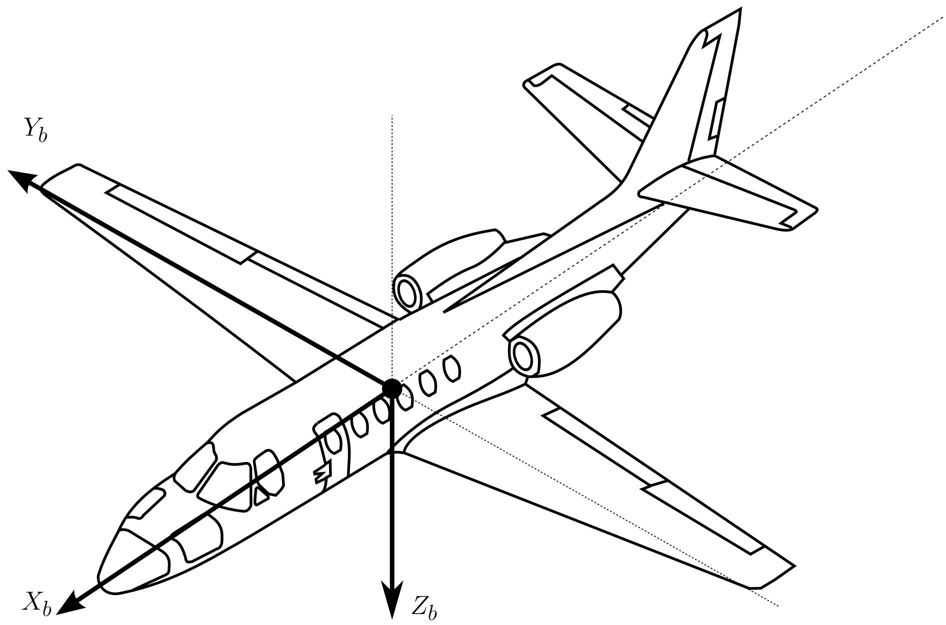

Figure 1: Overview of the orientation of the body fixed reference frame $\mathbb{F}_b$

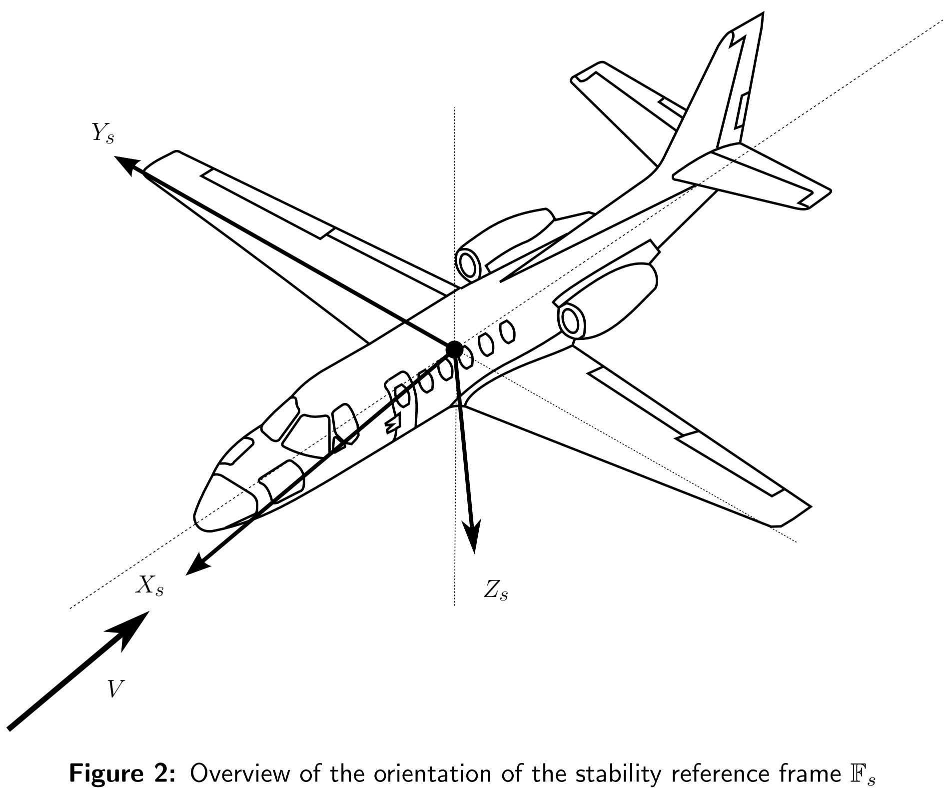

Figure 2: Overview of the orientation of the stability reference frame $\mathbb{F}_s$

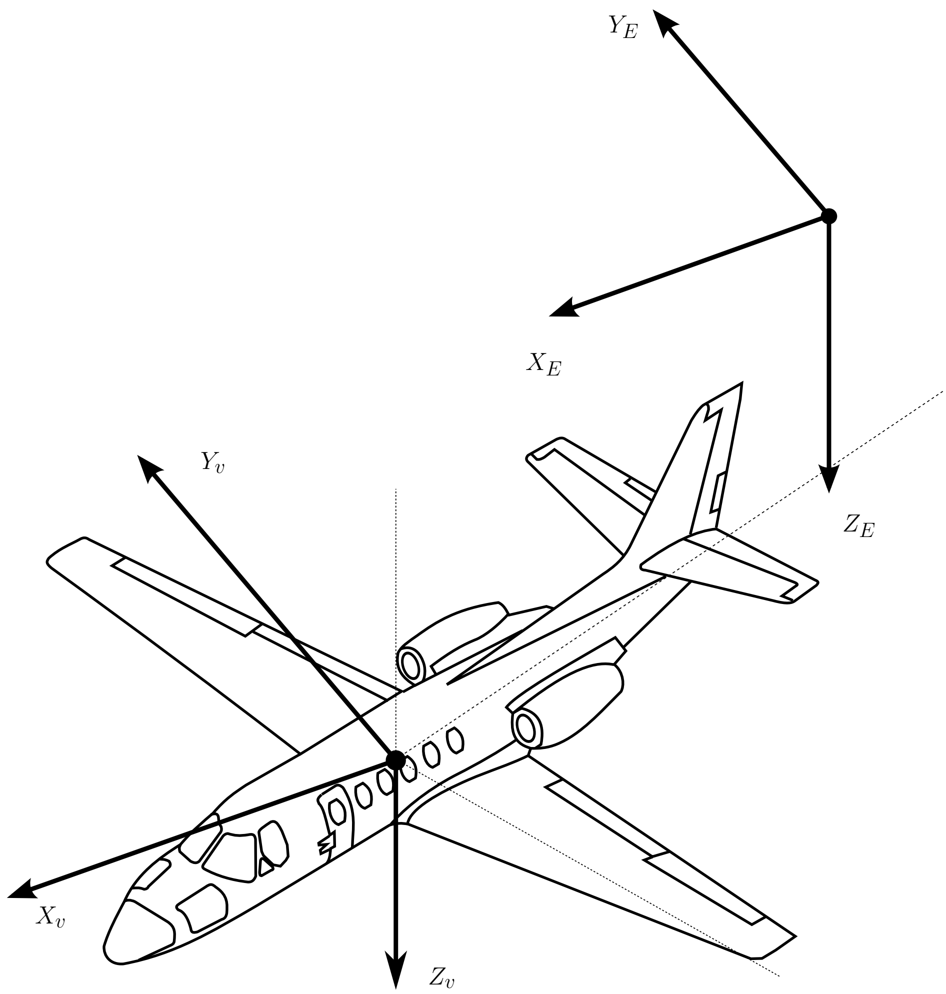

Figure 3: Overview of the orientation of the navigation or Earth Centered Earth Fixed (ECEF) reference frame $\mathbb{F}_E$

Sensor Bias Estimation

During this MSc research project, an a priori estimation of the sensor biases was made for use in the Kalman filter routines. Measurements were obtained from (1) a stationary and balanced ground measurement, and (2) in-flight measurements. The in-flight measurements - for e.g. the determination of the variance of the angle of attack signal - were obtained by choosing a relatively steady part during the flight, i.e. very limited variation in the corresponding measurement.

Measurement	Bias	Std	Unit	Instrument	Source
φ	-	4.4582×10^{-6}	deg	arinc/GPS	20151007_074445
λ	-	2.5609×10^{-6}	deg	arinc/GPS	20151007_074445
z	-	0.1869	m	arinc/Dadc1	20151007_074445
$\dot{z}$	-	0.0471×10^{-5}	m/s	arinc/Dadc1	20151007_074445
ϕ	-	0.0013	rad	arinc/Ahrs1	20150317_083328
θ	-	0.0019	rad	arinc/Ahrs1	20150317_083328
χ	-	0.0027	rad	arinc/Fms1	20150317_083328
V_{TAS}	-	0.2086×10^{-5}	m/s	arinc/Dadc1	20151007_074445
α	-	0.2086×10^{-5}	rad	analog/vane	20151007_074445
p	-1.15×10^{-5}	0.0013	rad/s	arinc/Ahrs1	20150317_083328
q	-2.1896×10^{-5}	5.6528×10^{-4}	rad/s	arinc/Ahrs1	20150317_083328
r	-3.0848×10^{-5}	2.2982×10^{-4}	rad/s	arinc/Ahrs1	20150317_083328
A_x	0.1253	0.0095	$\mathrm{m/s^2}$	arinc/Ahrs1	20150317_083328
A_y	0.1642	0.0247	$\mathrm{m/s^2}$	arinc/Ahrs1	20150317_083328
A_z	0.0306	0.0581	$\mathrm{m/s^2}$	arinc/Ahrs1	20150317_083328
δ_e	-	0.0011	rad	synchro	20150317_083328
δ_a	-	6.937×10^{-4}	rad	synchro	20150317_083328
δ_r	-	4.7028×10^{-4}	rad	synchro	20150317_083328

Table 1: An overview of the a priori estimation of the bias and standard deviation determined from smooth parts in the flight data.

Flight Test Cards

In this appendix the flight test cards that were made for the collection of new experimental flight test data during this thesis project are presented. Only a small selection of the test conditions as shown on these cards have been performed due to time restrictions. For future data collection, is is encouraged to collect data at the points specified on these test cards. More specifically, the current database has little data in altitude ranges FL50-FL80 and FL110-FL150, corresponding to test points 1-11 and 23-28. In addition, flight test data with flap, trim tab and gear measurements are scarce if not unavailable. Extra attention should be provided to these conditions for the extension/improvement of the current flight model.

TU Delft
Flight Department

FLIGHT TEST CARD

PROJECT	:	Design, Identification and Implementation of a High-Fidelity Cessna Citation II Flight Simulation Model
TEST CARD NUMBER	:	1a
SUBJECT	:	Model identification conditions
REFERENCE	:	
NOTES	:	
EST. DURATION OF TEST POINT	:	-- min
HAZARD CATEGORY	:	ROUTINE / ~~LOW~~ / ~~MEDIUM~~ / ~~HIGH~~

INITIAL CONDITIONS

ALT/FL :	>FL50-FL80<	ENGINE SETTING:	Level flight
IAS :	As required	FLAP SETTING :	As required
MACH :		LANDING GEAR :	As required
MASS :		OTHER :	AP/YD off
C.G. :			

EXPERIMENT PROCEDURE

#	Check	ALT/FL	IAS	Flap setting	Landing gear
1	☐	>FL50 - FL80<	120	0 degrees	Up
2	☐	>FL50 - FL80<	120	15 degrees	Up
3	☐	>FL50 - FL80<	120	40 degrees	Up
4	☐	>FL50 - FL80<	120	40 degrees	Down
5	☐	>FL50 - FL80<	160	0 degrees	Up
6	☐	>FL50 - FL80<	160	15 degrees	Up
7	☐	>FL50 - FL80<	160	40 degrees	Up
8	☐	>FL50 - FL80<	160	40 degrees	Down
9	☐	>FL50 - FL80<	200	0 degrees	Up
10	☐	>FL50 - FL80<	200	15 degrees	Up
11	☐	>FL50 - FL80<	250	0 degrees	Up

For each experimental condition, perform the series of identification inputs as indicated on card 2.

TU Delft Flight Department — **FLIGHT TEST CARD**

PROJECT	:	Design, Identification and Implementation of a High-Fidelity Cessna Citation II Flight Simulation Model
TEST CARD NUMBER	:	1b
SUBJECT	:	Model identification conditions
REFERENCE	:	
NOTES	:	
EST. DURATION OF TEST POINT	:	-- min
HAZARD CATEGORY	:	ROUTINE / ~~LOW~~ / ~~MEDIUM~~ / ~~HIGH~~

INITIAL CONDITIONS

ALT/FL	:	>FL80-FL110<	ENGINE SETTING	:	Level flight
IAS	:	As required	FLAP SETTING	:	As required
MACH	:		LANDING GEAR	:	As required
MASS	:		OTHER	:	AP/YD off
C.G.	:				

EXPERIMENT PROCEDURE

#	Check	ALT/FL	IAS	Flap setting	Landing gear
12	□	>FL80 - FL110<	130	0 degrees	Up
13	□	>FL80 - FL110<	130	15 degrees	Up
14	□	>FL80 - FL110<	130	40 degrees	Up
15	□	>FL80 - FL110<	130	40 degrees	Down
16	□	>FL80 - FL110<	160	0 degrees	Up
17	□	>FL80 - FL110<	160	15 degrees	Up
18	□	>FL80 - FL110<	160	40 degrees	Up
19	□	>FL80 - FL110<	160	40 degrees	Down
20	□	>FL80 - FL110<	200	0 degrees	Up
21	□	>FL80 - FL110<	200	15 degrees	Up
22	□	>FL80 - FL110<	250	0 degrees	Up

For each experimental condition, perform the series of identification inputs as indicated on card 2.

TU Delft Flight Department

FLIGHT TEST CARD

PROJECT	:	Design, Identification and Implementation of a High-Fidelity Cessna Citation II Flight Simulation Model
TEST CARD NUMBER	:	1c
SUBJECT	:	Model identification conditions
REFERENCE	:	
NOTES	:	
EST. DURATION OF TEST POINT	:	-- min
HAZARD CATEGORY	:	ROUTINE / ~~LOW~~ / ~~MEDIUM~~ / ~~HIGH~~

INITIAL CONDITIONS

ALT/FL	:	>FL110-FL150<	ENGINE SETTING	:	Level flight
IAS	:	As required	FLAP SETTING	:	As required
MACH	:		LANDING GEAR	:	As required
MASS	:		OTHER	:	AP/YD off
C.G.	:				

EXPERIMENT PROCEDURE

#	Check	ALT/FL	IAS	Flap setting	Landing gear
23	☐	>FL110 - FL150<	140	0 degrees	Up
24	☐	>FL110 - FL150<	140	15 degrees	Up
25	☐	>FL110 - FL150<	180	0 degrees	Up
26	☐	>FL110 - FL150<	180	15 degrees	Up
27	☐	>FL110 - FL150<	220	0 degrees	Up
28	☐	>FL110 - FL150<	250	0 degrees	Up

For each experimental condition, perform the series of identification inputs as indicated on card 2.

TU Delft
Flight Department

FLIGHT TEST CARD

PROJECT	:	Design, Identification and Implementation of a High-Fidelity Cessna Citation II Flight Simulation Model
TEST CARD NUMBER	:	2
SUBJECT	:	Model identification inputs
REFERENCE	:	
NOTES	:	
EST. DURATION OF TEST POINT	:	-- min
HAZARD CATEGORY	:	ROUTINE / ~~LOW~~ / ~~MEDIUM~~ / ~~HIGH~~

INITIAL CONDITIONS			
ALT/FL :	See 1a	ENGINE SETTING:	Level flight
IAS :		FLAP SETTING :	See 1a
MACH :		LANDING GEAR :	See 1a
MASS :		OTHER :	AP/YD off
C.G. :			

TEST PROCEDURE	REC. NRS
Safety pilot: 1. Perform 3211 maneuver on elevator (15 [s] total) 2. Perform 3211 maneuver on aileron (15 [s] total) 3. Perform 3211 maneuver on rudder (15 [s] total) FTE: 1. Make recording during maneuvers	

Simulation Framework Upgrade

As part of this thesis work, an upgraded simulation framework has been presented. In addition to the integration of a new aerodynamic model, as presented in accompanying paper, the individual components of the DASMAT simulation framework have been upgraded. In this appendix, a short overview of the new model is presented including some notes that can be used in further development of the new framework.

In Figure 4 an overview of the upgraded DASMAT framework is presented. As can be seen from this figure, changes have been made to the overall layout of the model by the addition of a mass model. After the equations of motion block, outputs are collected in a bus signal containing: (1) the state vector, (2) state derivative vector, (3) mass model vector and (4) a vector containing the forces and moments defined in the body frame.

The Airdata block, Aerodynamic model block, gravity block and equations of motion block have received full upgrades to be represented by Matlab function blocks. The Airdata block and Aerodynamic block are still shown as subsystems as these blocks contains more than one sub-system. In general, no changes have been made to the Engine model and Landing gear model. The only change required for these blocks was a conversion or the old state vector, i.e. V, α, β representation, to the new state vector, i.e. u, v, w representation.

Overall, the following additional changes have been made:

- Input vector for the control surface deflections is now aligned with the general aerospace definition, i.e. elements of the vector are now organized as δ_a, δ_e, $delta_r$.
- Airdata block does now contain a discrete wind gust model, Von Karman wind turbulence model and Wind Shear model (standard Matlab implementation). The turbulence and wind model parameters are initialized in the `initcit.m` script.
- The aerodynamic model block is designed to contain the base aerodynamic model and additional models, such as the stall model. The base aerodynamic model itself uses the `interp2` function to extract the aerodynamic parameters from the model look-up tables. These look-up tables have a fixed structure and are organized as depicted in Figure 5. Note that the dimension of the actual data table corresponds to the dimension of the altitude and Mach vectors. The dimension of the data table is $(m \times n \times k)$, where m is the length of the Mach vector, n is the length of the altitude vector and k is the number of parameters in the table.

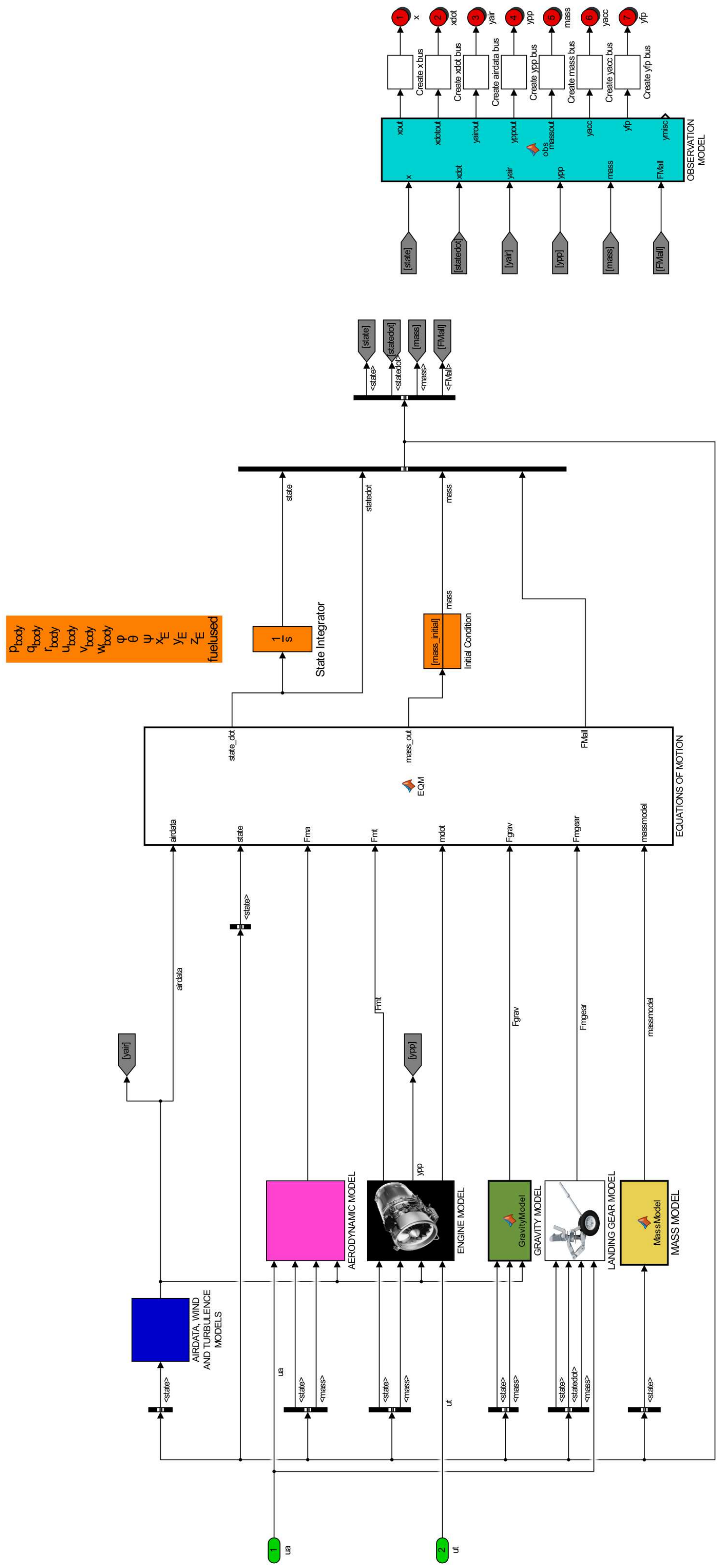

Figure 4: Overview of the upgraded simulation framework. Model inputs are shown in green and outputs are indicated by the red color.

C<X>table.mat

- Name .... Model name, e.g. N for the yaw moment
- Coeff .... Model coefficient names, e.g.
- Alt .... Altitude range corresponding to the table values.
- Mach .... Mach range corresponding to the table values.
- Data .... Actual data table

Figure 5: File structure of the Matlab aerodynamic model database file.

- The Environment input variable has been removed. Environmental variables are now initialized in the `initcit.m` script and loaded into the Matlab function blocks as masked variable. If any older application or template requires these inputs, they can easily be added to the framework and connected to a ground block to prevent errors.
- The mass model is initialized by the `initmass.m` script, also executed as part of the `initcit` routine. The mass model makes use of a structure containing entities such as the basic empty weight, passenger locations, passenger weights, basic empty weight inertia etc. This structure is automatically created and loaded into the mass model block. The output of the mass model block only contains the mass, cg location and elements of the inertia tensor.
- The observation function is now presented as a Matlab function block. Currently, the following outputs are produced: (1) state vector, (2) derivative state vector, (3) airdata vector, (4) engine state vector for both engines, (5) mass model output, (6) accelerations and load factor, (7) flight path information and (8) a misc vector. The latter vector allows for additional outputs to be created inside the observation model. Note however that a bus creator should be placed on the output of the Matlab function block.
- Trim has been moved to a pass-through block before the `ua` input. The trim simply consists of addition of the trim values to the current control surface deflection.
- Note that the currently implemented aerodynamic model is always defined in the center of gravity because of limitations during the identification process. For this reason, shifts in the cg cannot be simulated properly. It can be chosen to assume a fixed position for the definition of the forces and moments, allowing for the simulation of shifts in the cg. However, it should be noted that the fidelity of the forces and moments as predicted by the aerodynamic model is lost in that case.
- Model (mask) initialization is done by `initcit.m`. In this script, the following data and settings are created: (1) load aircraft and aux data, (2) initialize turbulence scales, gust settings, wind in ECEF frame etc., (3) load aerodynamic model databases/tables, (4) initialize aircraft trim, (5) load landing gear parameters.
- The folder structure of the Citation simulation model is presented in Figure 6

```
Main folder
├── acdata Name ........................ Folder containing aircraft and engine data
├── library Name  Folder containing C routines for the engine and landing gear model
├── massmodel .......................... Folder containing the mass model routines
├── modeltables ........................ Folder containing the model database files
├── gearparams ......................................... Gear parameters file
├── initcit ............................................ Citation initialization routine
├── initmass ........................... Citation mass model initialization routine
└── CitationMain.mdl ................................... Main Citation simulation model
```

Figure 6: Simulation framework folder structure.

Part IV

Paper - Appendices

Appendix

A. Model Parameter $(M - h)$ fit

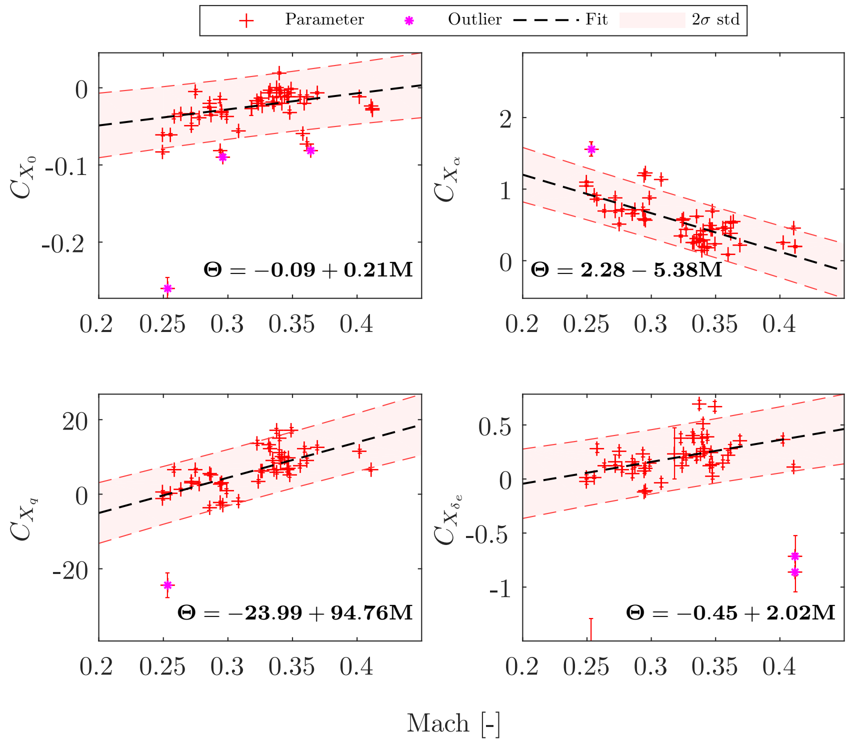

(a) C_X parameters versus M at an average altitude of 5000 m

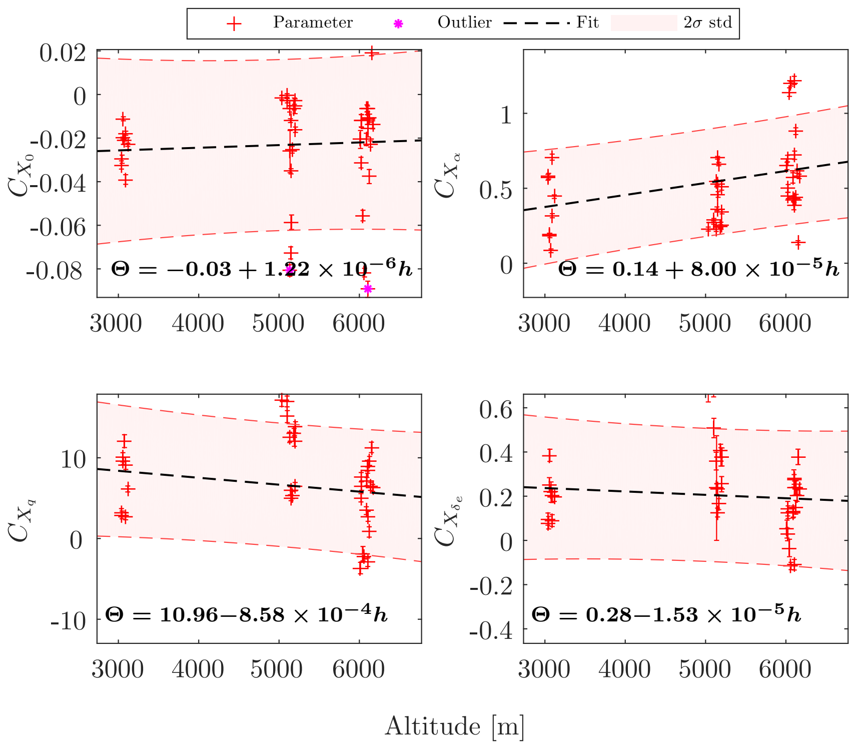

(b) C_X parameters versus h at an average Mach number of 0.32

Figure 12. Estimated parameters of the C_X model, obtained from a collection of 52 longitudinally induced δ_e 3-2-1-1 and hardover maneuvers with the error bars indicating the uncertainty of the estimate, plotted versus the Mach number M and altitude h together with the robust least squares fit and its corresponding 2σ confidence bounds on the predicted output.

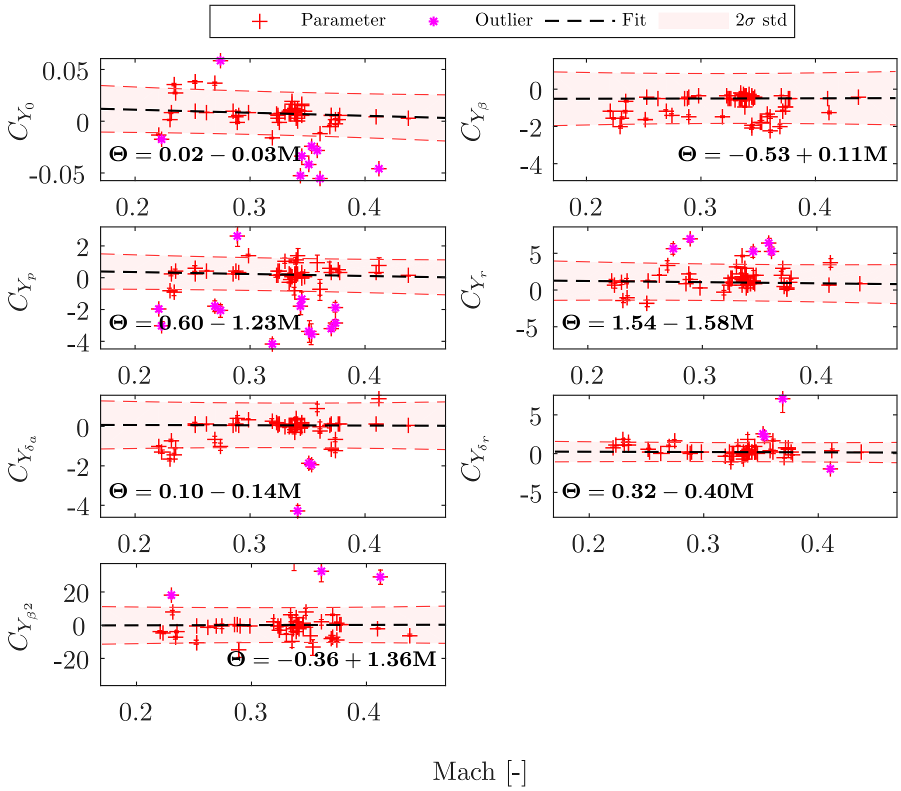

(a) C_Y parameters versus M at an average altitude of 5000 m

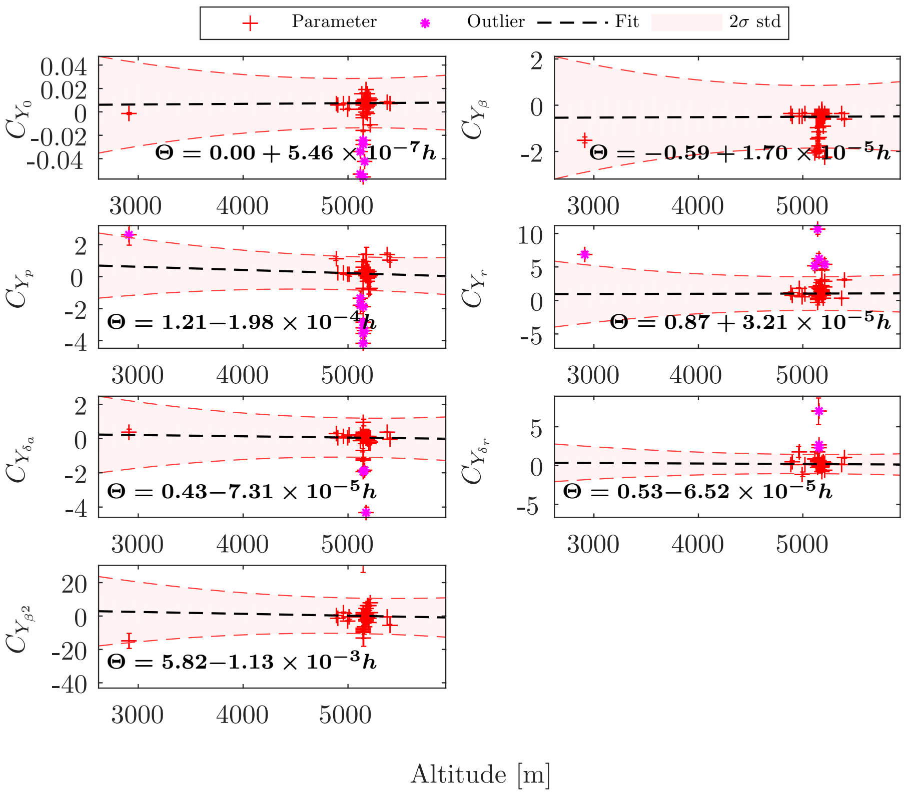

(b) C_Y parameters versus h at an average Mach number of 0.34

Figure 13. Estimated parameters of the C_Y model, obtained from a collection of 61 laterally induced δ_a and δ_r 3-2-1-1 and hardover maneuvers with the error bars indicating the uncertainty of the estimate, plotted versus the Mach number M and altitude h together with the robust least squares fit and its corresponding 2σ confidence bounds on the predicted output.

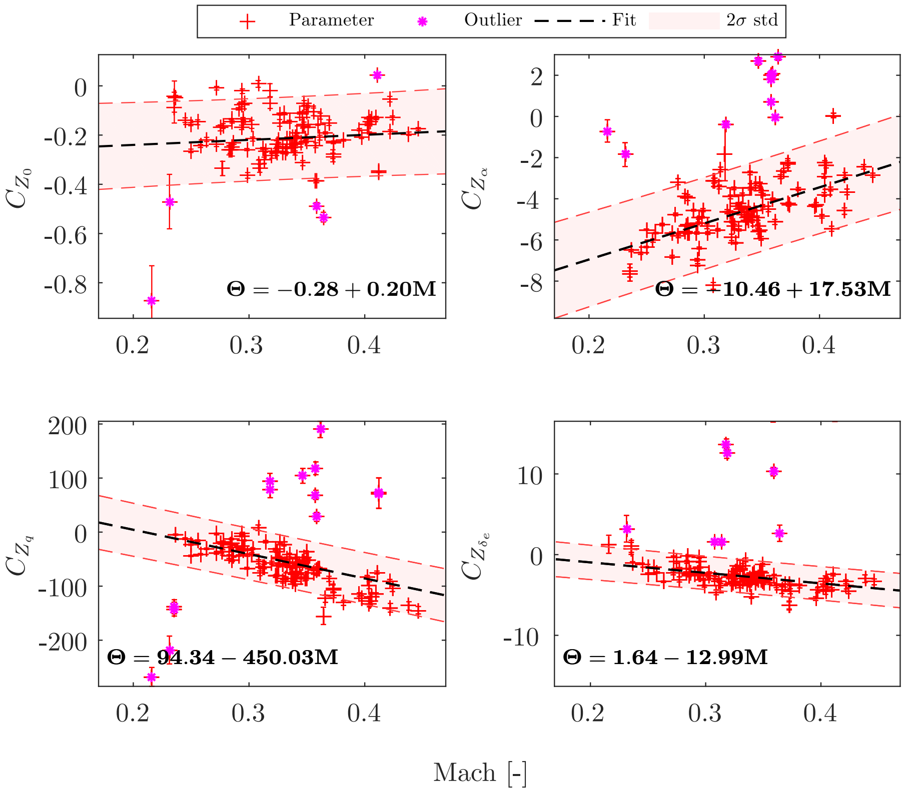

(a) C_Z parameters versus M at an average altitude of 5000 m

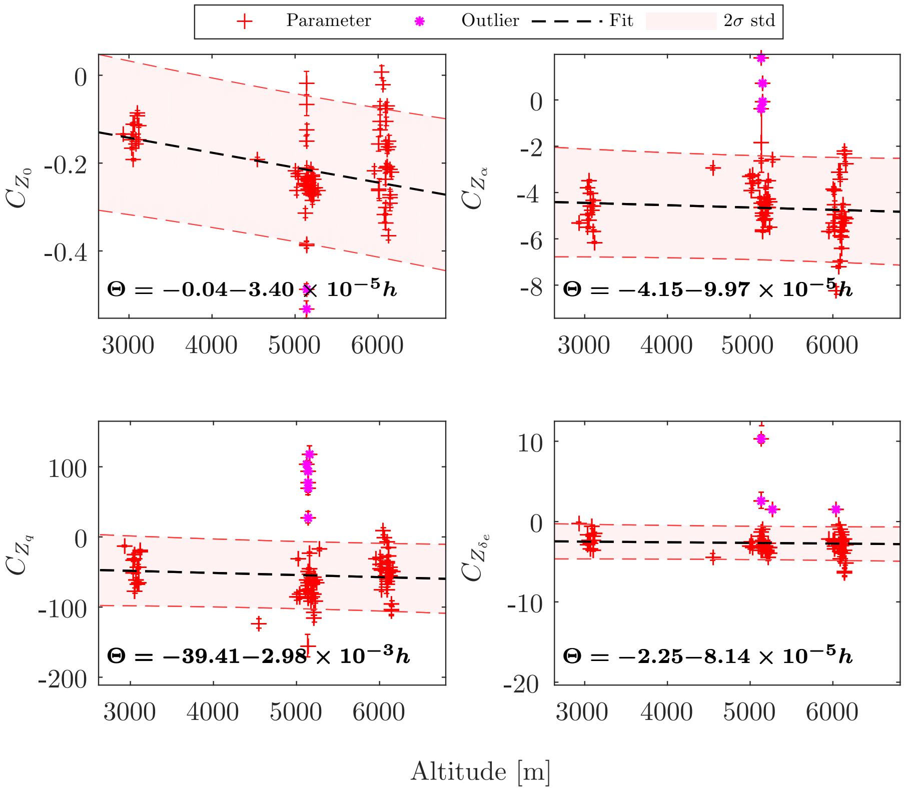

(b) C_Z parameters versus h at an average Mach number of 0.33

Figure 14. Estimated parameters of the C_Z model, obtained from a collection of 112 longitudinally induced δ_e 3-2-1-1 and hardover maneuvers with the error bars indicating the uncertainty of the estimate, plotted versus the Mach number M and altitude h together with the robust least squares fit and its corresponding 2σ confidence bounds on the predicted output.

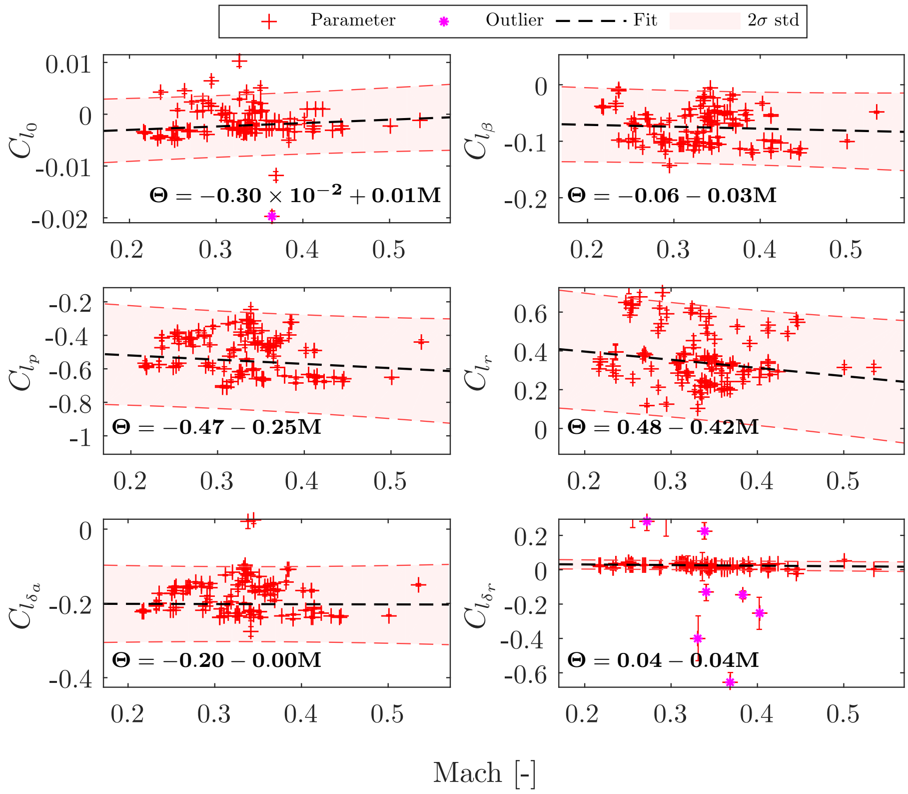

(a) C_l parameters versus M at an average altitude of 5100 m

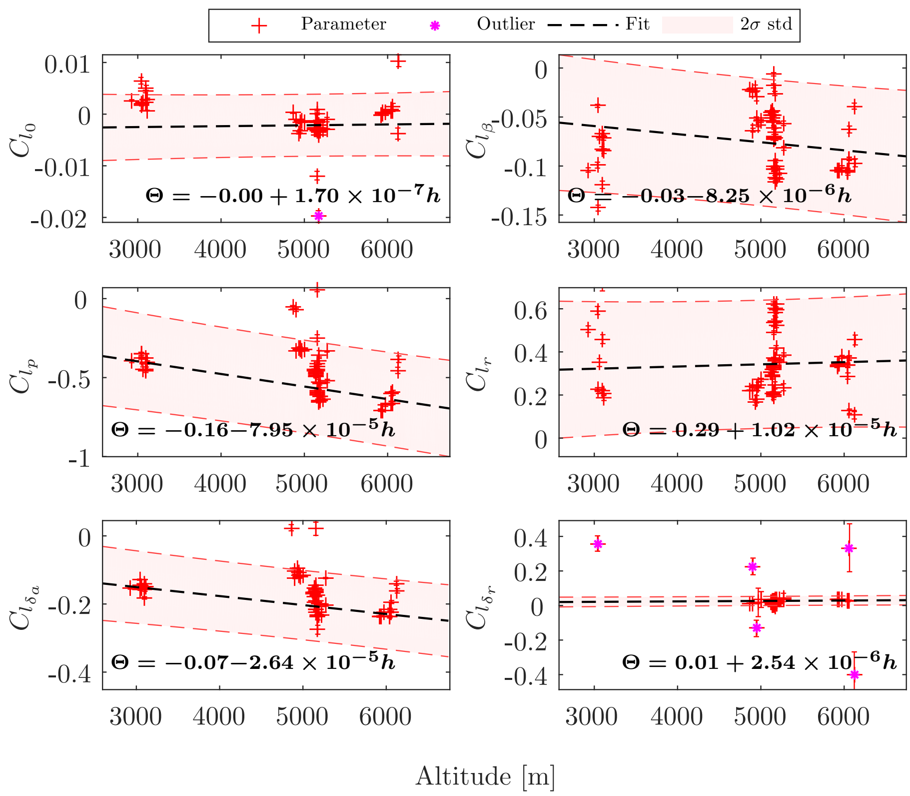

(b) C_l parameters versus h at an average Mach number of 0.33

Figure 15. Estimated parameters of the roll rate C_l model, obtained from a collection 107 of laterally induced δ_a and δ_r 3-2-1-1 and hardover maneuvers with the error bars indicating the uncertainty of the estimate, plotted versus the Mach number M and altitude h together with the robust least squares fit and its corresponding 2σ confidence bounds on the predicted output.

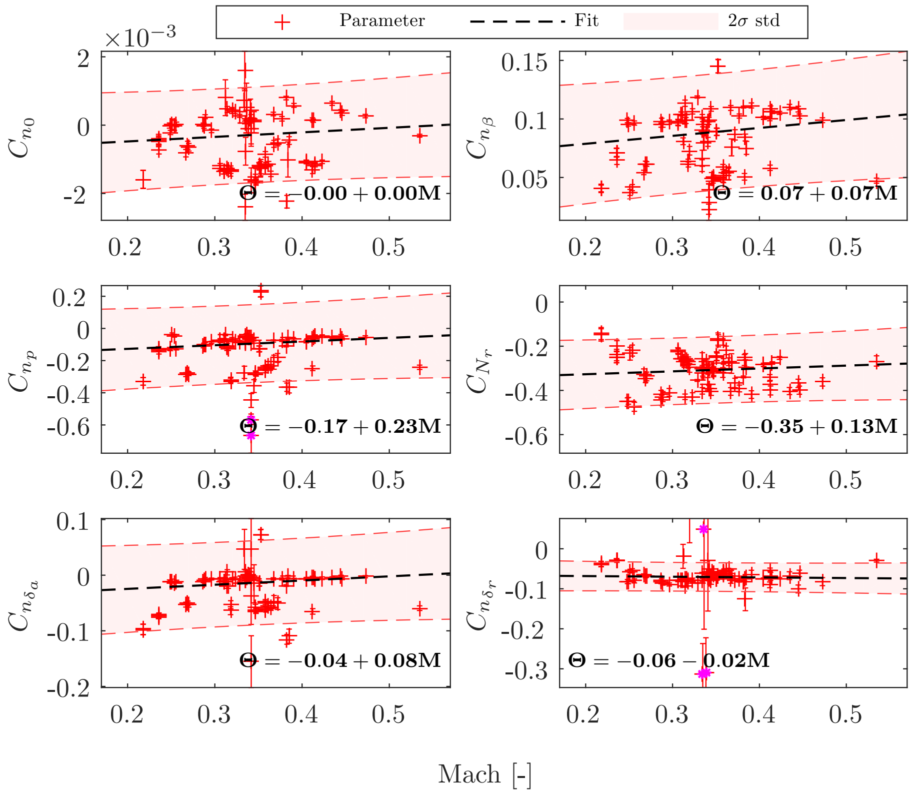

(a) C_n parameters versus M at an average altitude of 5100 m

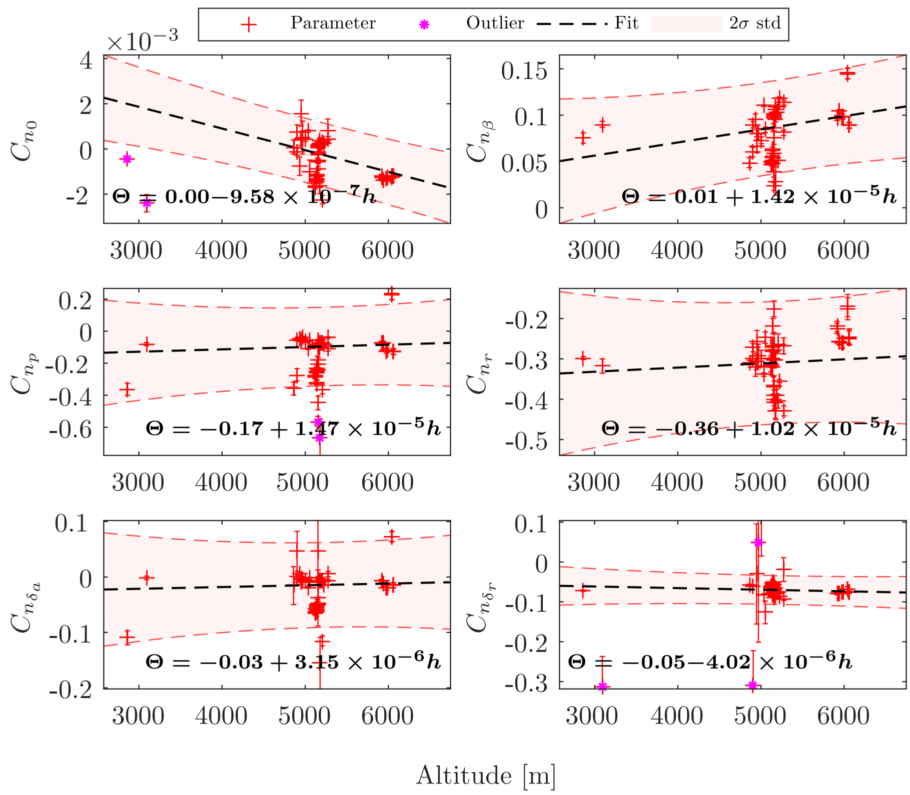

(b) C_n parameters versus h at an average Mach number of 0.33

Figure 16. Estimated parameters of the yaw rate C_n model, obtained from a collection 82 of laterally induced δ_a and δ_r 3-2-1-1 and hardover maneuvers with the error bars indicating the uncertainty of the estimate, plotted versus the Mach number M and altitude h together with the robust least squares fit and its corresponding 2σ confidence bounds on the predicted output.

B. Region of Validity

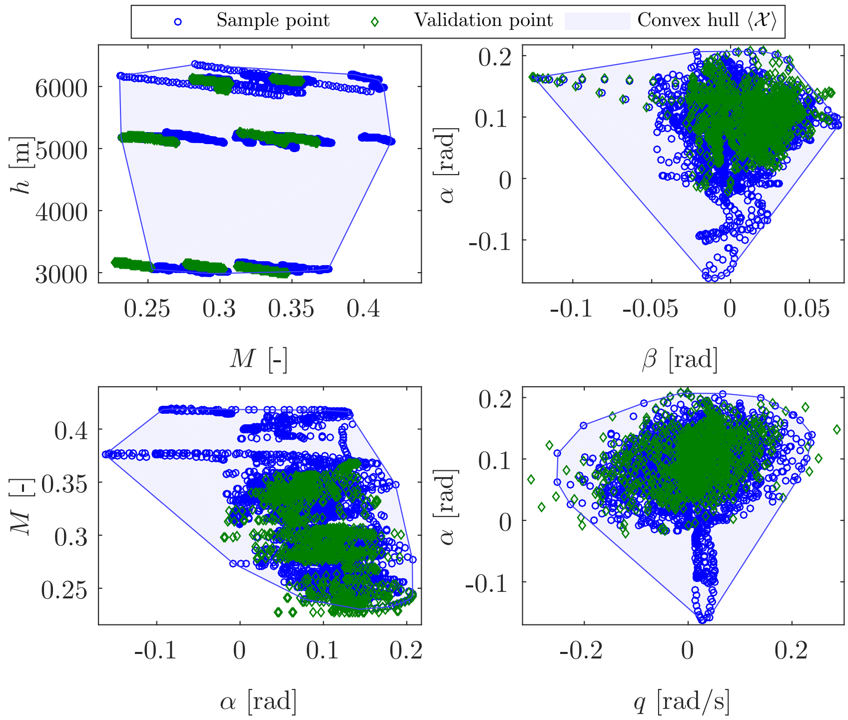

Figure 17. Sample point used in the identification of the C_X model together with its convex hull $\langle \mathcal{X} \rangle$ and the set of validation points.

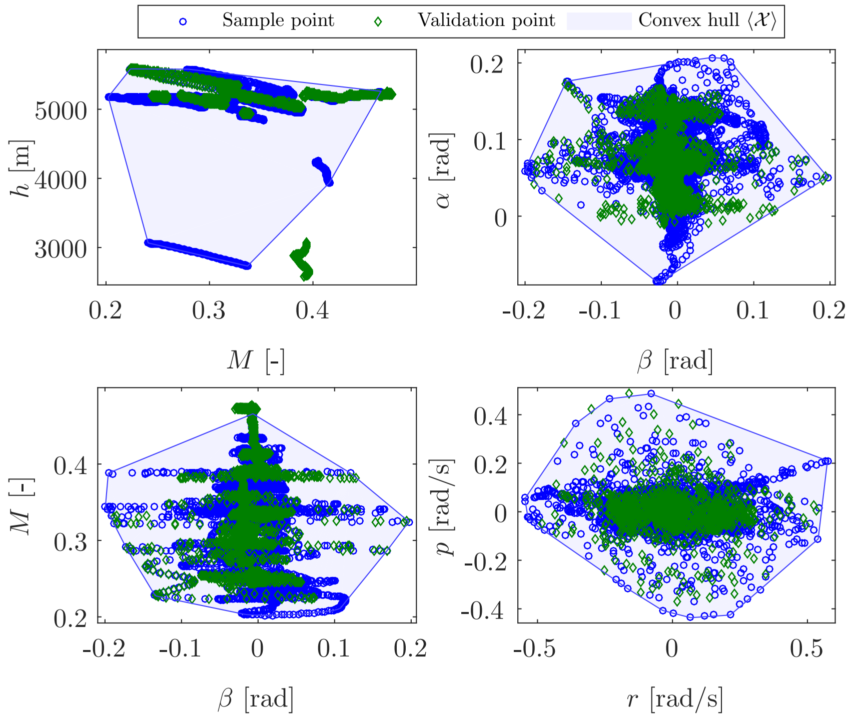

Figure 18. Sample point used in the identification of the C_Y model together with its convex hull $\langle \mathcal{X} \rangle$ and the set of validation points.

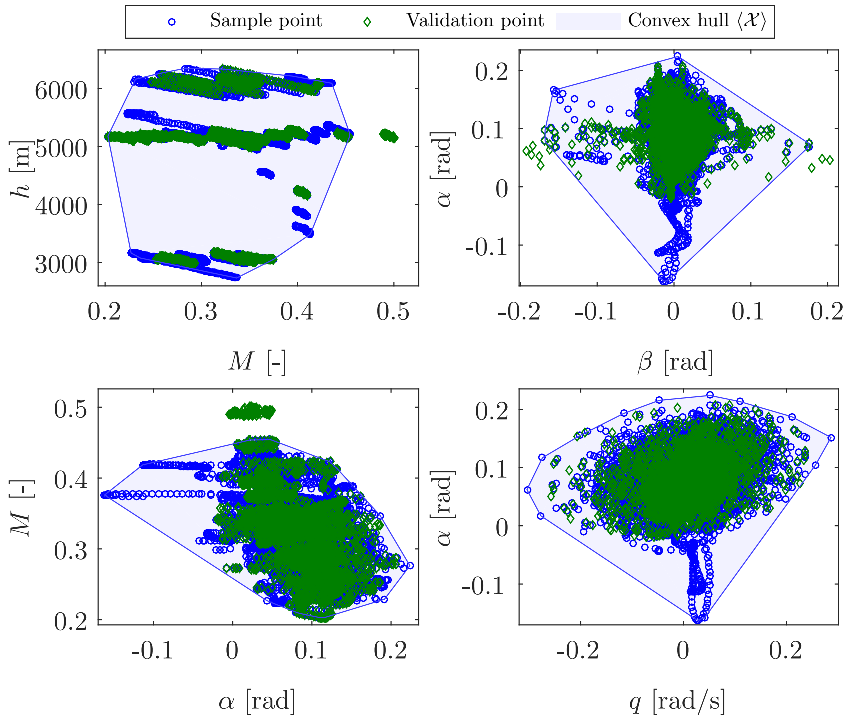

Figure 19. Sample point used in the identification of the C_Z model together with its convex hull $\langle\mathcal{X}\rangle$ and the set of validation points.

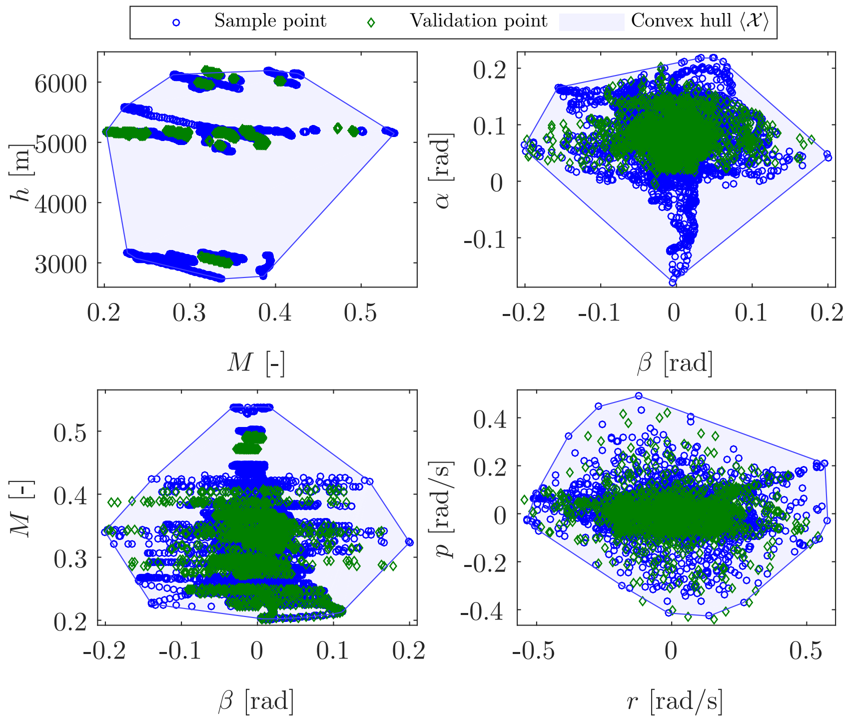

Figure 20. Sample point used in the identification of the C_l model together with its convex hull $\langle\mathcal{X}\rangle$ and the set of validation points.

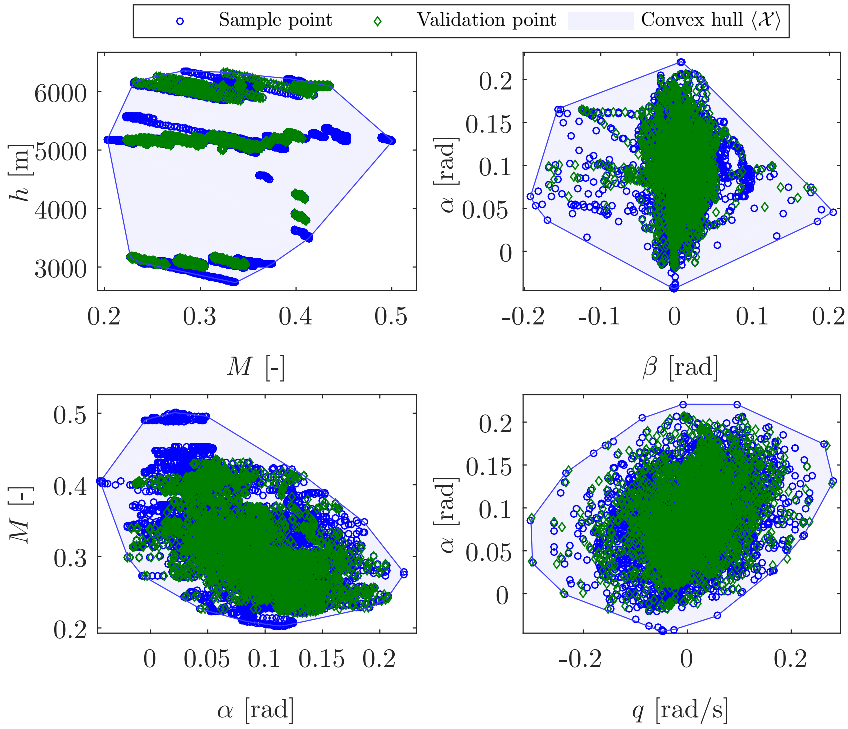

Figure 21. Sample point used in the identification of the C_m model together with its convex hull $\langle\mathcal{X}\rangle$ and the set of validation points.

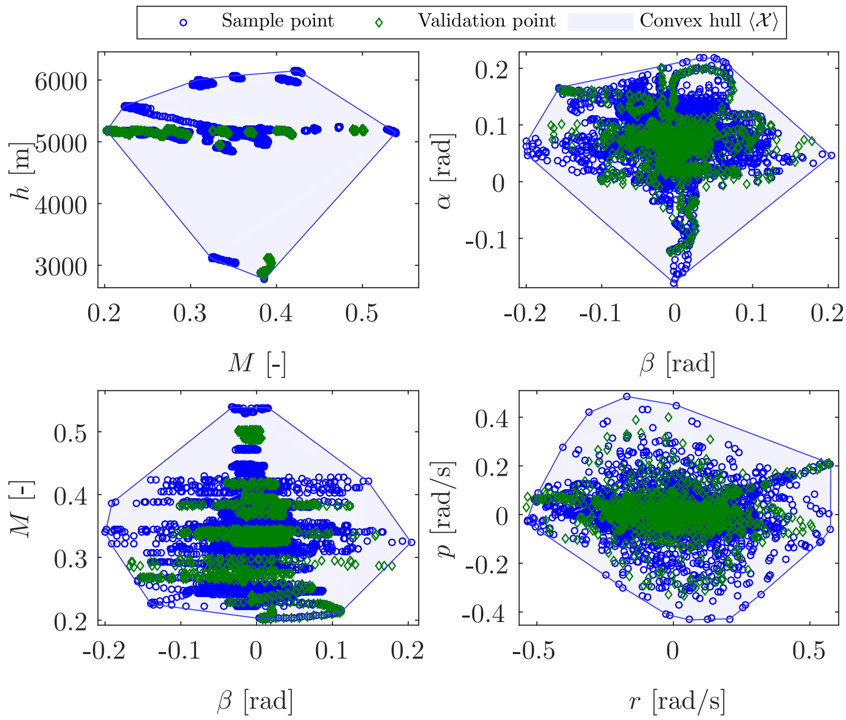

Figure 22. Sample point used in the identification of the C_n model together with its convex hull $\langle\mathcal{X}\rangle$ and the set of validation points.